UNIONE EUROPEA

UNIVERSITÀ ITALO FRANCESE | UNIVERSITÉ FRANCO ITALIENNE

ÉCOLE DOCTORALE UNIVERSITÉ PARIS-EST
Sciences, Ingénierie et Environnement

Università degli Studi di Catania

Ministero dell'Istruzione dell'Università e della Ricerca

Experimental analysis of the efficiency of carbon fiber anchors applied over CFRP to firebrick bonded joints

CAGGEGI CARMELO

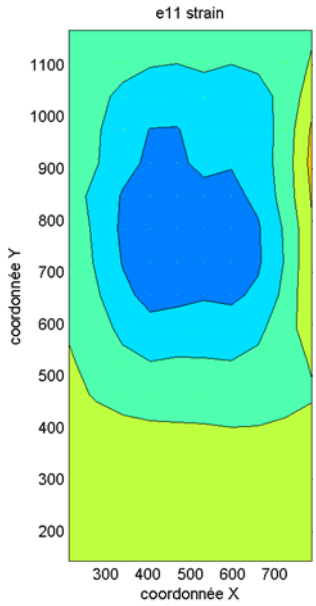

PHD SCHOOL ON "**INGEGNERIA STRUTTURALE E GEOTENICA**" - **XXV CICLO**

UNIVERSITY OF CATANIA (ITALY)

PHD SCHOOL ON "**SCIENCE, INGENIERIE ET ENVIRONNEMENT**"

UNIVERSITY PARIS-EST (FRANCE)

Experimental analysis of the efficiency of carbon fiber anchors applied over CFRP to firebrick bonded joints

CAGGEGI CARMELO

Italian Supervisor - University of Catania
Professor Massimo Cuomo

French Supervisor - University of Paris-Est Marne-La-Vallée
Professor Luc Chevalier

Others members of thesis group
Prof. Vincent Pensée (UPE MLV), Prof. Loredana Contrafatto (UNI CT)

PHD SCHOOL ON "**INGEGNERIA STRUTTURALE E GEOTENICA**" - **XXV CICLO**

UNIVERSITY OF CATANIA (ITALY)

PHD SCHOOL ON "**SCIENCE, INGENIERIE ET ENVIRONNEMENT**"

UNIVERSITY PARIS-EST (FRANCE)

Contents

Introduction

In these recent years, the strengthening of masonry building has known a massive use of CFRP sheets. Those composite materials glued on the elements to reinforce are exposed to prematurely debonding crisis due to a tension load which is much smaller than the tensile strength of the CFRP. A way to upgrade failure load of CFRP-to-support bonded joint is to reinforce the cohesion between the fibers and the support by the use of mechanicals anchors built with the same fibers of the composite and fastened in the support like “nails”. Research on the use of anchors for masonry supports has been limited and there are no experimental analyses related to the design and the placement of fiber anchors.

The aim of this thesis is to provide experimental data to quantify the efficiency of the carbon fiber anchors applied on a reinforced fire brick. This is a ground work to study CFRP to masonry bonded joint fastened by fiber “nails”. Specifically, the analysis of the displacement and the strain fields of the reinforced surface have been realized by means of Digital Image Correlation (DIC), an optical appealing method never used to study a FRP to support bonded joint fastened by FRP anchor.

This work is divided in five chapters. The first is devoted to a literature review about FRP properties, design parameters and reinforcement improvement technics (nails, U WRAPS). Experimental and numerical aspects are discussed.

In the second chapter, the experimental procedure is described and details about the project of the testing machine are addressed. Motivations and designs of the specimen’s configuration are presented.

The third chapter deals with general aspects about the digital image correlation technic.

Results and main considerations are presented in the fourth chapter.

Finally, the increase in resistance adducted by the FRP anchors is quantified defining the average peak of load registered in the reinforced configurations and the energy dissipated during the fracture processes. The several perspectives of this research work are presented at the end of the thesis.

Chapter 1

FRP reinforced systems: from debonding fracture to mechanical anchors

1. FRP reinforced systems: from debonding fracture to mechanical anchors

An analysis of the literature about the reinforcement of masonry structures by means of FRP (Fiber Reinforced Poymers) is proposed in this chapter. A description of the properties of the reinforcement (FRP) and of the support (masonry) is presented in the first part of this section. Subsequently the parameters and the design criterions of the straightened FRP systems are defined. After that, the attention is focused on the premature debonding failure of the systems FRP-to-support bonded joints. The final part of the chapter deals with the mechanicals anchors (FRP anchors and U Wraps) and with their capacity to improve the peak resistance of the straightened systems.

1.1 Materials

1.1.1 Mechanical property of FRP

The Fiber reinforced polymers, named briefly FRP, are composite materials constituted by reinforcing fibers embedded in a polymeric matrix. The fibers are responsible for carrying the load acting on the composite; the matrix has three functions to protect the fibers from the environment, to distribute the load and to link the composite to the support [1]. The FRP have heterogeneous and anisotropic properties and a prevalent linear elastic behavior up to failure in contrast to steel (yield behavior). In the field of civil engineering the fiber reinforced polymers could be made in factory (pre-impregnated fabric) or realized directly in the job site applying special resins over the dry fabric (non-impregnated fabric).

Three main types of fibers are used: glass (GFRP), aramid (AFRP) and carbon fibers (CFRP) (*fig. 1.a*). These latter are assembled in a filiform geometry, they are continuous and their diameter is in the range of 4 to 10 micrometers [2]. The mechanical properties of fibers have been shown in the *figure 1.b*. Among the three typologies already mentioned, the CFRP have the greatest values of maximal stress and the greatest value of stiffness. In the structural strengthening field the fibers are assembled in unidirectional, bidirectional or multiaxial fabrics. The *unidirectional* tissue is characterized by fibers all oriented in the direction of the length, the *bidirectional* fabric is made of an orthogonal weft-warp weaving and the *multiaxial* tissue is characterized by fibers oriented in different directions.

The matrix of FRP composites is commonly realized with thermoset resins. These latter are characterized by a low viscosity, good adhesive properties, a good resistance to chemical agents and

an absence of melting temperature. In the field of civil engineering the epoxy resin is commonly used; it has a good resistance to moisture, to chemical agents and excellent adhesive properties. The epoxy resin changes her mechanical properties at a temperature greatest of 60°C, this is an essential characteristic in the design project field.

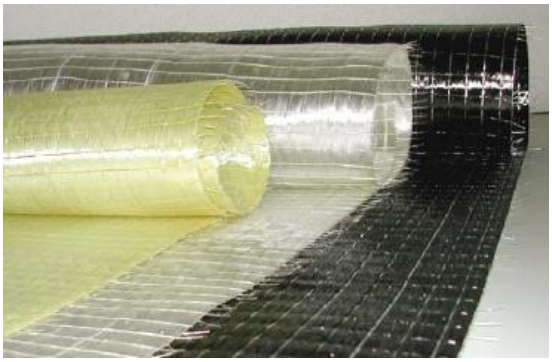

1.a Fabric fibers(aramidic, glass, carbon)

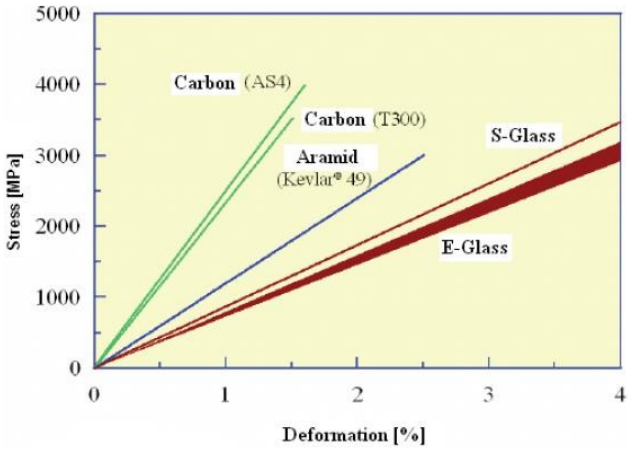

1.b Stress-strain diagram for different fibers [1]

	Young's modulus E	Tensile strength σ_r	Strain at failure ε_r	Coefficient of thermal expansion α	Density ρ
	[GPa]	[MPa]	[%]	$[10^{-6}\ ^\circ C^{-1}]$	$[g/cm^3]$
E-glass	70 – 80	2000 – 3500	3.5 – 4.5	5 – 5.4	2.5 – 2.6
S-glass	85 – 90	3500 – 4800	4.5 – 5.5	1.6 – 2.9	2.46 – 2.49
Carbon (high modulus)	390 – 760	2400 – 3400	0.5 – 0.8	-1.45	1.85 – 1.9
Carbon (high strength)	240 – 280	4100 – 5100	1.6 – 1.73	-0.6 – -0.9	1.75
Aramid	62 – 180	3600 – 3800	1.9 – 5.5	-2	1.44 – 1.47
Polymeric matrix	2.7 – 3.6	40 – 82	1.4 – 5.2	30 – 54	1.10 – 1.25
Steel	206	250 – 400 (yield) 350 – 600 (failure)	20 – 30	10.4	7.8

1.I Comparison *between the properties of FRP components and* steel [1]

In the table 1.I one can see a comparison between the property of fibers, matrix and steel.

The mechanical properties of FRP materials are due to the composite geometry (shape, thickness), fibers orientation (unidirectional, bidirectional or multiaxial fabric) and concentration. The composite does not have the same mechanical properties of the fibers, in fact the presence of the matrix lowers the level of the stress resistance (see *fig. 1.c and table 1.II*). For FRP materials characterized by unidirectional fibers the mechanical property of the composite may be estimate using the rule of mixtures written below.

$$E_{frp} = V_{fib}E_{fib} + (1 - V_{fib})E_m$$
$$f_{frp} \cong V_{fib}f_{fib} + (1 - V_{fib})f_m$$

Obviously the increase of fiber volumetric fraction improve the mechanical quality of the composite (*fig. 1.d*).

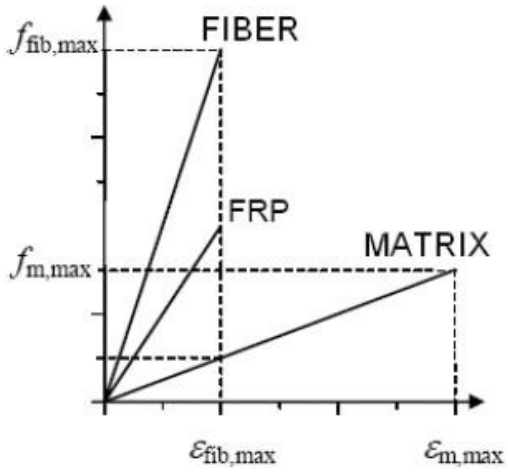

1.c Stress-strain diagram for fibers and matrix [1]

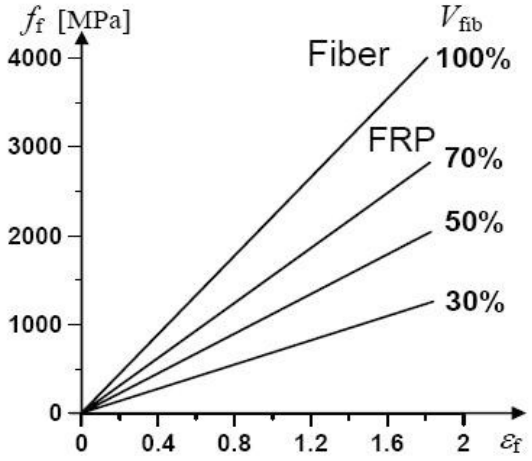

1.d Fibers and mechanical properties [1]

Pre-cured systems	Modulus of elasticity [GPa]		Ultimate strength [MPa]		Ultimate strain [%]	
	FRP	Fiber	FRP	Fiber	FRP	Fiber
	E_f	E_{fib}	f_f	f_{fib}	ε_{fu}	$\varepsilon_{fib,u}$
CFRP (low modulus)	160	210-230	2800	3500-4800	1.6	1.4-2.0
CFRP (high modulus)	300	350-500	1500	2500-3100	0.5	0.4-0.9

1.II CFRP and carbon fibers [1]

Analyses of graphic stress-strain of FRP rods (*fig. 1.e*) permit to compare properties of steel (traditional material used in civil engineering for his high tensile resistance) and those of FRP composites. Stiffness of FRP is smaller than that of steel. The behavior of steel is ductile, unlike the failure of FRP composite is fragile after an elastic stroke. The stress tensile limit of CFRP is more than five times higher than that of steel. Among the composites materials represented in the *figure 1.e* FRP made by carbon fibers has the highest value of stiffness.

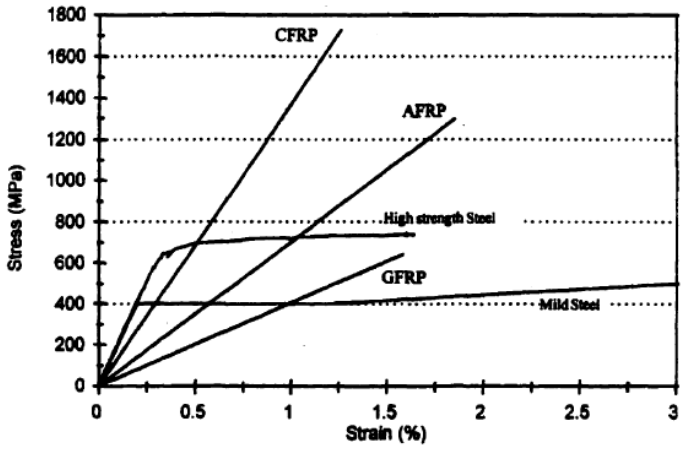

1.e Behavior of fibers rod [2]

1.1.2 Mechanical property of masonry

Traditional masonries are composed of prismatic blocks and mortar. The formers give the system mechanical resistance, the latter is applied among the blocks to distribute the load and to prepare the surface to apply others layers of prismatic elements. Normally the blocks could be naturals (stone) or artificial (fire brick, cinder block.). Each geographical territory is characterized by typical typologies of masonry since in each zone there are typical materials and typical construction techniques. The principal typologies of stone used in the civil engineering are: igneous rocks (granite, basalt, pumice, tuff…), metamorphic stone (marble…) and sedimentary stone (limestone, sandstones…). Instead, the main typologies of masonry are: the rubble masonry, the ashlar masonry, the slipform stone masonry, the dry set masonry, the solid brick work, etc (*fig. 1.f and 1.g*). Masonry characterized by rubble elements presents a big quantity of mortar and poorer mechanical quality than the ashlar masonry.

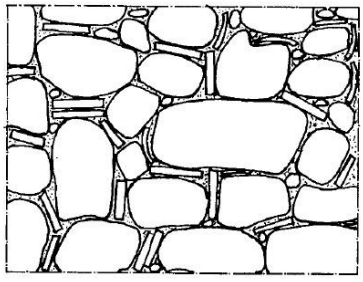

1.f Stone rubble masonry (territory of Catania) [3]

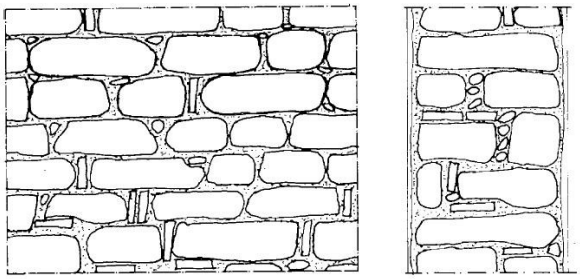

1.g Stone ashlar masonry (territory of Catania) [3]

The large field of wall typologies and materials make impossible a global and synthetic analysis of the masonries. The technical Italian law *D.M. 14 January 2008* [4] provide a classification of mortar types (*table 1.III*); the number of these classes (M2,5, M5…) corresponds to the compression strength in N/mm^2. In the same ministerial regulation, there is a table of the masonry compression strength values in relation to mortar quality and stone typologies (*table 1.IV*).

Classe	Tipo di malta	Composizione				
		Cemento	Calce aerea	Calce idraulica	Sabbia	Pozzolana
M 2,5	Idraulica	--	--	1	3	--
M 2,5	Pozzolanica	--	1	--	--	3
M 2,5	Bastarda	1	--	2	9	--
M 5	Bastarda	1	--	1	5	--
M 8	Cementizia	2	--	1	8	--
M 12	Cementizia	1	--	--	3	--

1.III Composition and classification of mortar [4]

Resistenza caratteristica a compressione f_{bk} dell'elemento	Tipo di malta			
	M15	M10	M5	M2,5
2,0	1,0	1,0	1,0	1,0
3,0	2,2	2,2	2,2	2,0
5,0	3,5	3,4	3,3	3,0
7,5	5,0	4,5	4,1	3,5
10,0	6,2	5,3	4,7	4,1
15,0	8,2	6,7	6,0	5,1
20,0	9,7	8,0	7,0	6,1
30,0	12,0	10,0	8,6	7,2
≥ 40,0	14,3	12,0	10,4	--

1.IV Masonry compressive strength fk [N/mm2] in relation to mortar class and stone resistance [4]

The compressive characteristic strength f_{bk} of the elements (first column of the *table 1.IV*) is defined above:

$$f_{bk} = 0{,}75\ x\ f_{bm} \tag{1.1}$$

Where:

f_{bm} *is the average value of the compressive strength of the stone element.*

Table 1.IV shows that the masonry *compressive characteristic strength* f_k is included between 1 MPa and 14,3 MPa.

Indeed the tensile resistance of masonry wall is approximately equal to 1/10 of f_k, for the safety this low value is frequently considered null by engineers.

Unlike FRP materials masonries have good permeability property and good fire resistance.

1.2 Strengthening design criteria, application and failure modes

The strengthening of civil structures by FRP consists to apply the composite over the support to reinforce (concrete, masonry…). In the framework of masonry building the use of the fiber reinforced polymer (laminates, sheets, grids and bars) is oriented to increase the capacity of each structural member as well as the global capacity of the structure [1]. Particularly the main reason that justify the use of FRP are:

- To carry the tensile stress within the structural members or between adjoining members
- To connect more structural members (orthogonal walls, walls and vault…)
- To stiffen the horizontal elements (vault, floor…)
- To limit the crack width

- To confine the columns to enhance their resistance

The application of FRP on the member to reinforce is carried out by adhesion or by means of mechanical anchorages devices. Often in the civil engineering field, the non-impregnated fabric (carbon , glass or aramid) is bonded directly over the support surface using epoxy resins. The results is the realization of the FRP composite directly “in situ”.
The adhesion between support and FRP is fundamental for the efficiency strength. Unlike concrete elements, masonries have commonly the external surfaces roughened, this is due to the presence of blocks and mortar. This surface configuration make necessary to apply a leveling mortar on the roughened layer. In synthesis the phases of application of a FRP strength system are:

- Clean the surface of application
- Apply, if necessary, a leveling mortar [1]
- Spread a layer of epoxy bi-component resin
- Spread the dry-fabric on the resin
- Spread another layer of epoxy resin on the fabric by a roller brush.

The roller brush is used to eliminate the empty air within the fabric and the resin. In figures *1.h* the photos of FRP application procedure carried out during reinforcement of the vaults of the church “Spirito Santo” in Nicolosi (CT-Italy).

fig. 1.h - Steps of FRP application (strengthening of the vaults of the church “Spirito Santo” in Nicolosi - CT): application on a leveling mortar of a layer of epoxy resin (photo 1), placing of the dry monodirectional glass fabric (photo 2), application by roller brush of a epoxy resin layer (photo 3)

The failure of the masonry reinforced by FRP could occur in one or in a mixture of the follows modality [1]:

- Excessive cracking in the wall (tensile stress)
- Crushing of masonry structural element

- Shear slip of masonry
- FRP rupture
- FRP debonding

Among these failure typologies, the debonding is one of the most critical because occurs at tension much smaller of tensile capacity of the composite. The study of this brittle modality of failure is the starting point of this thesis research.

1.3 The debonding crisis

1.3.1 Definitions

Debonding failure consists in the detachment of FRP from the support. It occurs with a brittle expansion of a crack between the reinforce and the substrate.

The fracture could be [1]: adhesive, cohesive, mixed (see *fig.1.i*). The adhesive fracture take place in the interface between adhesive and support material, it is characterized by a smooth surface. Frequently, it occurs when the application of the reinforce is inaccurate. The cohesive fracture take place inside the support, it is characterized by a rubble surface. In both sides of the crack opening is present the same material (concrete, mortar…). This kind of fracture is often noted when the debonding occurs. The mixed fracture is registered when both cohesive and adhesive failure happen. In this case, the crack surface is characterized by the coexistence of support and FRP composite materials.

fig 1.i - The main typologies of fracture (adhesive, cohesive, mixed) [1]

The debonding may occur in two main failure modes [1]: plate and debonding and intermediate crack debonding. The first failure type occurs when the detachment between FRP and support take place in the extremity of the reinforcement (*fig. 1.j*). Instead, the intermediate crack debonding take place in the proximity of the existing crack on the support (*fig. 1.k*). In this case, the presence of a stress concentration occurs to the development of the debonding. When on the reinforce are applied not only stresses in the direction of the fibers but also significant tensile stresses perpendicular to

the composite surface (peeling), the forces that can be transferred by the adhesive layer are reduced and the debonding occurs prematurely [1].

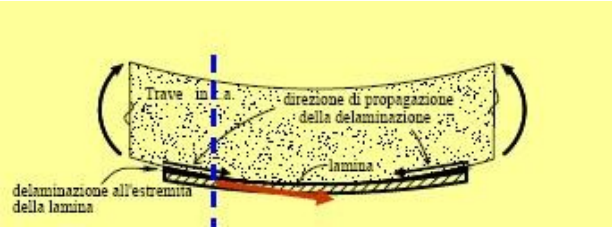

fig 1.j - Failure mode "plate and debonding"

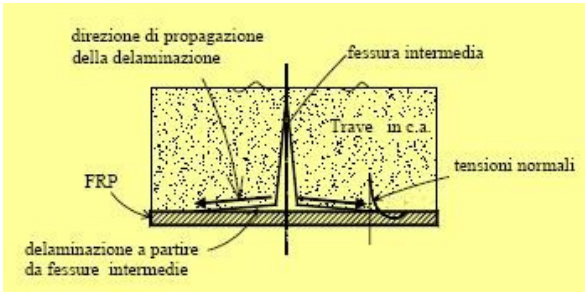

fig. 1.k - Failure mode "intermediate crack debonding"

The study of the debonding makes necessary to define some parameters: the fracture energy (Γ), the effective bond length (l_e) and the design bond strength (f_{dd}). In the simple case represented in the figure *1.l* are defined the geometric property of a simple reinforce.

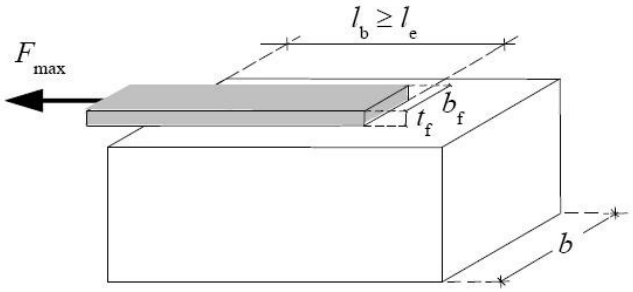

fig 1.l -Support reinforced by a FRP sheet [1]

The fracture energy Γ [J] is the quantity of energy dissipated during the debonding failure; it's equal to the area underlying the curve *displacement [mm] – Load [kN]* that describe a shear test.

In the design of a reinforcement is topic to calculate the ultimate value of the force that could be transferred from the FRP reinforcement to the support prior to FRP debonding, this force is named f_{mdd}.

Experimental and numerical studies show that an increase of the bond length l up to the length l_e cause an augment of the f_{mdd}; further increase of the bonded area doesn't increase the value of the force transferred. The length l_e is called *optimal bond length* [1] or *effective bond length* [5]. Therefore in the case of the simple block reinforced of *fig. 1.l* the strain stresses is transferred between the FRP and the support in a short area nearest to the applied load; the length of this bond area is l_e. When the load increase, in this zone occurs the apparition of cracks, at the same time, the stress transfer area is displaced to the unloaded side of reinforcement. This phenomenon justify that if $l > l_e$ the system have a residual ductility after the formation of the first crack (before the

debonding, the stress transfer zone has to move toward the extremity of the unloaded side). If $l = l_e$ the appearance of the first crack is simultaneous with the total debonding fracture. Yuan et al. [5] defined l_e as the value corresponding to 97% of the load carrying capacity if l is infinite.

To define the debonding parameters a lot of fracture mechanics based models starting from experimental results have been realized . Niedermaier R. in 1996 [5] studying the bond strength between a steel plate and a concrete support by means of a nonlinear fracture mechanics defined the relations of f_{dd}, l_e and Γ_f. Denoted Ep the Young modulus of composite, the ultimate bond load is given by:

$$\begin{aligned} &0{,}78 b_p \sqrt{2 G_f E_p t_p} \quad [N] \quad if \quad l \geq l_e \\ &0{,}78 b_p \sqrt{2 G_f E_p t_p}\, \frac{l}{l_e}\left(2 - \frac{l}{l_e}\right) \quad [N] \quad if \quad l \leq l_e \end{aligned} \qquad (I.1)$$

Where the effective bond length l_e is written as:

$$l_e = \sqrt{\frac{E_p t_f}{4 f_{ctm}}} \quad [mm] \qquad (1.3)$$

And G_f is the fracture energy:

$$G_f = c_f k_p^2 f_{ctm} \quad \frac{N\ mm}{mm^2} \qquad (1.4)$$

With c_f a constant determinate in a linear regression analysis using the results of double shear or similar tests, and K_p a geometrical factor defined by:

$$k_p = \sqrt{1{,}125 \frac{2 - \frac{b_p}{b_c}}{1 + \frac{b_p}{400}}} \qquad (1.5)$$

Where :

$t_p = thickness\ of\ composite \quad mm$

$b_p = widht\ \ of\ composite \quad mm$

$b_c = width\ of\ the\ concrete\ block \quad mm$

$c_f = constant\ determined\ in\ a\ linear\ regression\ analysis\ using\ the\ resuts\ of\ double\ shear\ or\ similar\ tests$

In these expressions the value of ultimate load is proportional to: the width of the bonded composite, the energy fracture, the stiffness of the composite and the thickness of the FRP. Instead the effective bond length is proportional to the stiffness and the thickness of the composite and inversely proportional to the strength tensile capacity of the concrete support. It's interesting to note that the value of G_f is connected to the ratio between b_p and b_c.

Neubauer U. and Rostàsy (1997) [5] studied the debonding problem by means of a serie of double shear tests on CFRP applied over a concrete support. They affirmed that, for both cohesive failure and adhesive failure, the shear-slip relationship may be represented by a bilinear model (*fig. 1.m*).

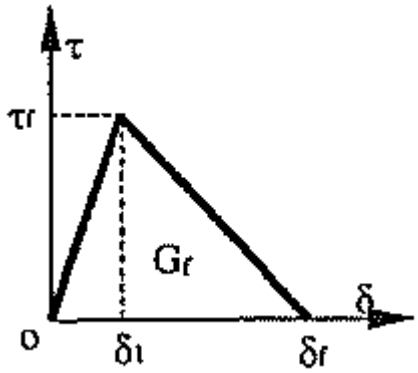

fig. 1.m - Shear-slip relationship model [5]

They defined an average value of c_f, corresponding to 0,204 [mm] and proposed the following new expressions of the parameters:

$$P_u = \begin{cases} 0{,}64 k_p b_p \sqrt{E_p t_p f_{ctm}} & se\ l \geq l_e \\ 0{,}64 k_p b_p \sqrt{E_p t_p f_{ctm}}\ \frac{l}{l_e}\ 2 - \frac{l}{l_e} & se\ l < l_e \end{cases} \quad (1.6)$$

$$G_f = c_f f_{ctm}\ \frac{N\ mm}{mm^2} \quad (1.7)$$

$$l_e = \frac{\sqrt{\frac{E_p t_p}{2 f_{ctm}}}}{} [mm]$$

(1.10)

In the equation (1.6) of P_u the value of G_f, present in (1.2), is replaced by $f_{ctm}k^2_p$. It's possible to underline that the value of the bond length of equation (1.10) is bigger than that of equation (1.5).

To design a reinforcement Neauber and Rostasy [5] proposed to use 75% of the ultimate bond strength.

The CNR DT 200/2004 [1] provides the following equations of design bond strength (f_{fdd}) and fracture energy (Γ_{fk}):

$$f_{fdd} = \frac{1}{\gamma_{f,d}\ \overline{\gamma_M}}\ \ \frac{\overline{2E_p\Gamma_{FK}}}{t_p}\ \ \frac{N}{mm^2} \tag{1.9}$$

$$\Gamma_{Fk} = c_1\ \ \overline{f_{mk}f_{mtm}}\ \ \frac{N}{mm} \tag{1.10}$$

Where $\boldsymbol{\gamma_{f,d}}$ is a partial factor depending on the FRP application, $\boldsymbol{\gamma_M}$ is a partial factor of the masonry, $\mathbf{c_1}$ is an experimental determined coefficient, $\mathbf{f_{mk}}$ is the masonry average compressive strength and $\mathbf{f_{mtm}}$ is the masonry average tensile strength.

1.3.2 Analytical considerations

The equation of the optimal anchor length (l_e) provided by the CNR [1] is the same than that of Neauber and Rostasy [5], eq. (1.8).

In the framework of industrial mechanic the adhesion problem has been much studied. In 2008 Jongsma J. [7] proposed a model to analyze the shear stress distribution in the adhesive layer of a "easy peel" system (*fig. 1.n*). This last is a type of closure for metal cans of aliment products, it consists in a foil material (*easy peel sealing*) bonded over a ring (*easy peal ring*) seamed on the top of the tin (*fig. 1.o*). When the closed can is sterilized, the product is heated and, consequently, it expands (*fig.1.p*).

fig. 1.n - Metal cans with easy peal system [7]

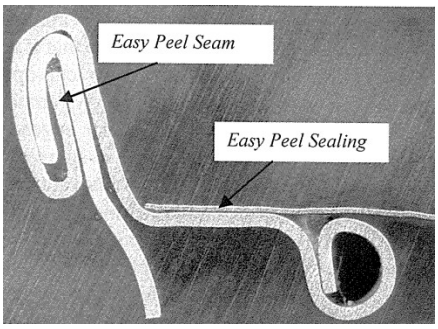

1.o Cross section of easy-peel ring [7]

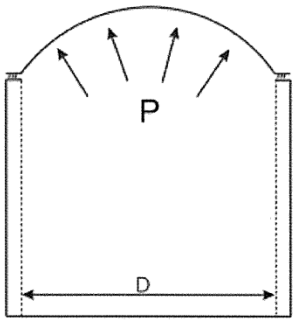

fig. 1.p - Expansion of a metal can during the sterilization [7]

During this process in the adhesive layer is developed a shear stress. To study this last Jongsma J. [7] realized an analytic elastic model. The boundary conditions of the debonding problem studied are presented in *figure 1.q*. The aluminum support is blocked in a extremity, upon this last are placed, in order, a stratum of adhesive and the aluminum easy peel.

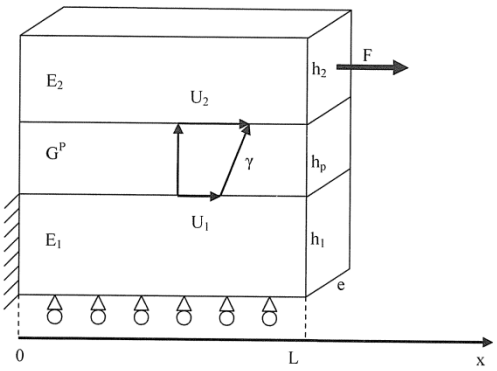

fig. 1.q - Schematic representation of simplified sealed zone (easy-peal) [7]

The value of the shear deformation γ(x) is directly obtained from the motion induced by the lower and upper metallic layers. Resolving the differential equations describing the equilibrium on the interfaces *support-adhesive* and *adhesive-easy peel sealing*, the shear deformation γ(x) is obtained as:

$$\gamma\ x\ = \frac{(u_2 - u_1)}{h_p} = \frac{1}{h_p} \frac{F}{E_1 h_1 E_2 h_2 \omega \sinh(\omega L)}\ E_1 h_1 \cosh\ \omega x\ + E_2 h_2 \cosh(\omega\ L - x\ ) \tag{1.11}$$

With:

$$\omega^2 = \frac{G^p}{h_p}\ \frac{E_1 h_1 + E_2 h_2}{E_1 h_1 E_2 h_2} \tag{1.12}$$

Where u_1 is the displacement in x-direction of the lower joint interface, u_2 is the displacement in x-direction of the upper joint interface, E_1 is the Young modulus of the lower aluminum part, E_2 is the Young modulus of the upper aluminum part, L is the seal width , G_p is the shear modulus of polymer joint, h_1 is the thickness of the lower aluminum part, h_2 is the thickness of the upper aluminum part, h_p is the thickness of polymer joint and F is the tensile force applied on upper aluminum part.

The results of Jongsma [7] confirm that the shear distribution is not homogeneous in the adhesive layer; there is a short area nearest to the applied load characterized by a stress concentration (the effective bond length). When the adhesive thickness (h_p) decrease the stress concentration is more remarkable (*fig. 1.r*). Jongsma affirm that this is a proof that the phenomenon of the heterogeneous shear stress distribution is a thin layer effect.

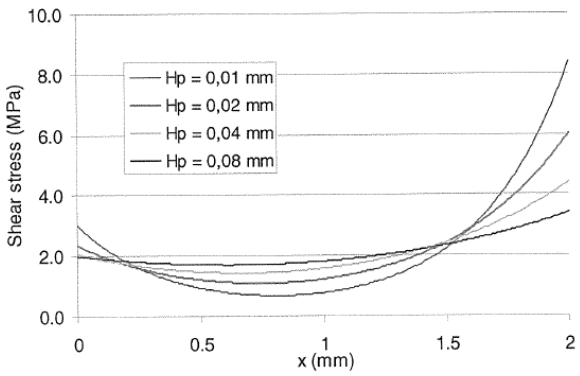

fig. 1.r - Shear stress distribution in the adhesive zone according to Jongsma analytic model for four different adhesive thickness [7]

Cottone and Giambanco (2010) [8] studied the stress transfer between a FRP to support bonded joint during a single shear pulling test. They modelised the composite reinforcement as an indefinitely elastic beam connected to a Winkler non-linear deformable foundation (*figures 1.s a,b*).

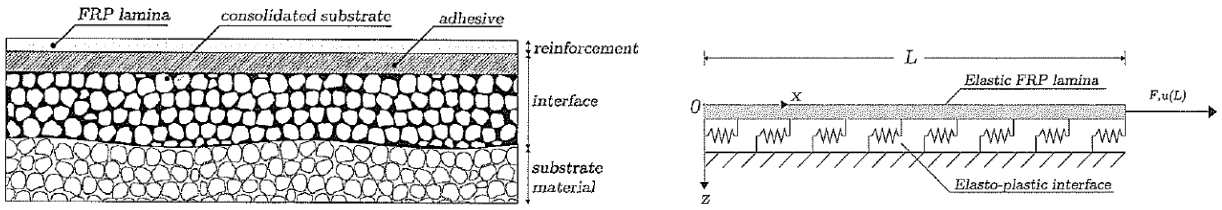

fig. 1.s - a) Physical schematization of the contact stratus ; b) Mechanical scheme adopted for the simulation of single shear pulling test by Cottone and Giambanco [8]

The interface layer is composed by two stratus: the thin film of adhesive and a layer of consolidated material of the substrate. They chosen this typologies of schematization because the cohesive fracture occurs a few millimeters under the interface "adhesive-support". In [8] the behavior of the FRP to the support interface is described by constitutive laws derived from elasto-plasticity theory with softening (*fig. 1.t*). The study permits to focalize the pure elastic response of the FRP-substrate system, the evolution of the elasto-plastic zone and the fracture propagation.

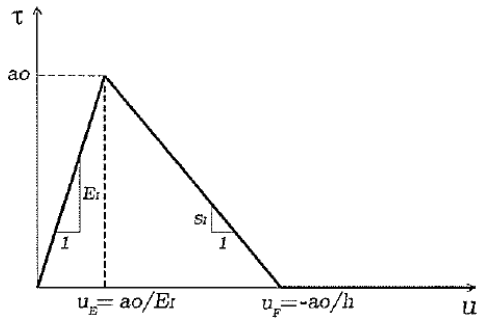

fig. 1.t - Bilinear bond-slip one-dimensional model [8]

During a single shear test, when the applied force F exceed the elastic limit F_E, the damage process takes place in the extremity loaded. In this experimental step, the interface can be divided in two parts; the portion of length ρ where an elasto-plastic damage occurs, and the remaining portion whose behavior is elastic (figure *1.u*).

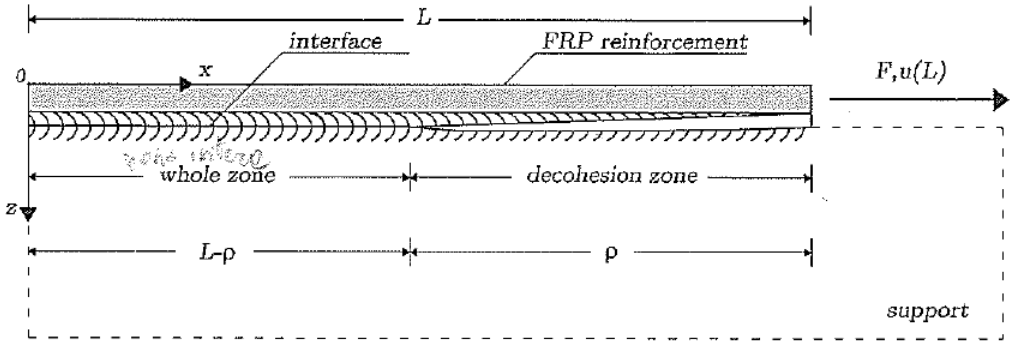

fig. 1.u - Schematic representation of the interface when Fe < F < FF (elastic whole zone and elasto-plastic decohesion zone) [8]

When the force F reach the value of F_U (ultimate fracture load) a crack appear in the extremity loaded of the FRP to support bonded joint. In this experimental step, in the interface there are a elastic whole zone, a elasto-plastic damaged zone and a cracked zone (*fig. 1.v*).

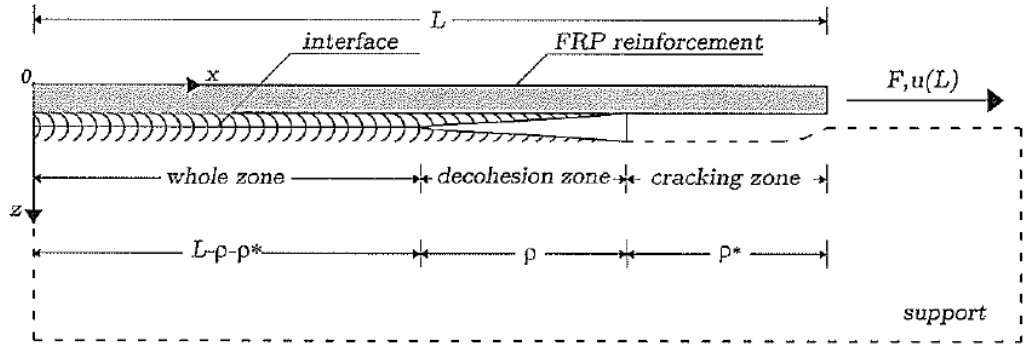

fig. 1.v - Schematic representation of the interface when u(L) > uF [8]

Cottone and Giambanco [8] define an equation to calculate the maximum extension of the elasto-plastic zone at the interface; the length ρ_i.

$$0 \leq \rho \leq \rho_i = \frac{\pi}{2} \frac{s_i b}{K_B}^{-\frac{1}{2}} \tag{1.13}$$

Where s_i is the interface softening modulus and K_B is the axial stiffness of the composite. The length ρ_i coincides with the effective bond length [8]. If the bond length L is smaller than ρ_i the

apparition of the first crack occurs simultaneously with the total debonding fracture. If L is bigger than ρ_i, after the first crack the elasto-plastic damage zone is displaced to the opposite direction of the applied load, this phenomenon happens without any increase of F. The advancement of the crack corresponding to a continuum displacement of the elasto-plastic zone to the unloaded end; when the value of $\rho = \rho_i$ and there is no more whole zone, the crack can't advance more and a total debonding occurs. In synthesis if $L < \rho_i$ a brittle failure take place. If $L > \rho_i$, more L is bigger than ρ_i more the ductility of the FRP to support bonded joint is increased.

1.3.3 Experimental and numerical study

In the literature studies many different experimental set-ups have been used to determine the FRP-to-concrete bond strength. A classification of the bond tests, with a clearly representation of the corresponding boundary condition is given by Yao et al. [6]. They defined the following five tests type: a) far end supported double-shear tests (FES); b) near end supported (NES) double-shear tests; c) far end supported (FES) single shear tests; d) near end supported (NES) single-shear tests; e) beam test; f) modified beam test (*figure 1.w*).

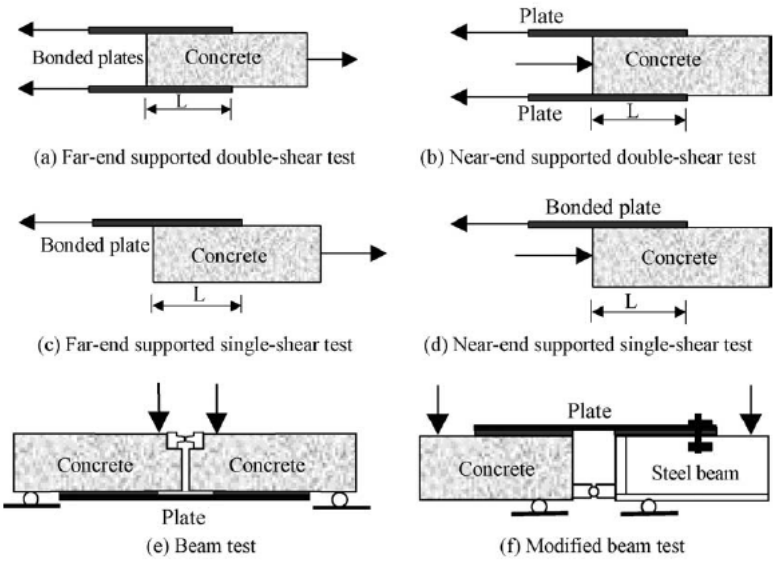

fig. 1.w - Classification of bond tests [6]

Numerical and experimental studies have shown that the different boundary condition can lead to significantly different test results. The double shear test and the single shear pull tests have been widely used for their simplicity. Yao et al. [6] realized an experimental study using a NES single-shear pull test. They affirm that this boundary condition permits to describe the stress state in the critical region of a beam when an intermediate crack-induced the debonding failure. Therefore, the

near end single-shear pull test is proposed to be a standard set-up for determining the FRP-to-concrete bond strength [6]. The experimental session conducted by Yao et al [6] consist in 72 shear tests on concrete prisms bonded with FRP strip. Different series of specimens was studied to analyze the follow factors: the bond length, the width ratio between the FRP strip and the concrete support (b_{frp}/b_c) and the offset (δ) in the load position (*fig. 1.x*).

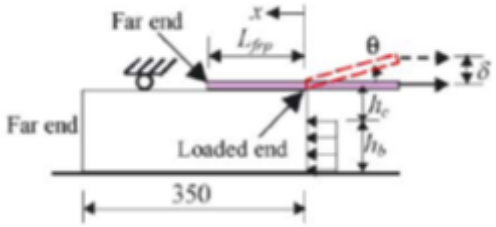

fig. 1.x - Specimen and boundary condition of Yao et al. experimental session [6]

The experiments confirm that the failure of the FRP reinforced systems occurs mainly with a cohesive fracture. Indeed, fifty-six out of the 72 specimens failed due to a debonding in concrete, eight specimens failed with an adhesive fracture and the remaining eight specimens failed in the concrete by detachment of a big angular prism (concrete prism failure, see *figures 1.y*).

fig. 1.y - Failure modes in the Yao et al. experimental session [6]

The adhesive fracture occurs only in the tests series prepared by an assistant with limited experience. The concrete prism failure takes place when the rate $b_{frp}/b_c \geq 0{,}8$. In the specimens characterized by a small bond length when the first crack take place in the loaded-end quickly occurs a brittle debonding failure. The *figure 1.z* shows the strain distribution in FRP during the test I-1 (specimen with L_{frp} = 75mm). Analyzing the image it is possible to note that the strain increase with the applied load and the stress transfer zone moves from the loaded side to the unloaded side. In the test I-16, executed over a specimen dissimilar from the specimen I-1 only for a larger bond length (L_{frp} = 190 mm), the first crack occurres at a similar load of the test I-1 but the propagation of the fracture have to achieve a farthest extremity. The displacement of the stress

transfer zone during the test is clear in the *figures 1.aa*. The figure proposed by Yao et al. [6] are realized using a normalized distance from loaded end (x/L_e), where L_e is the effective bond length defined by Chen [5].

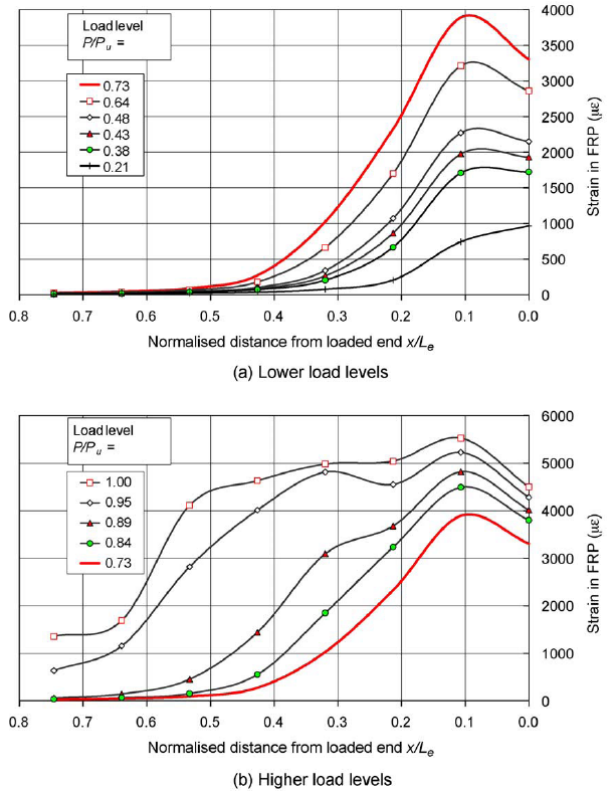

fig. 1.z - Strain distribution along the FRP, test I-1 of Yao and al. (L=75 mm) [6]

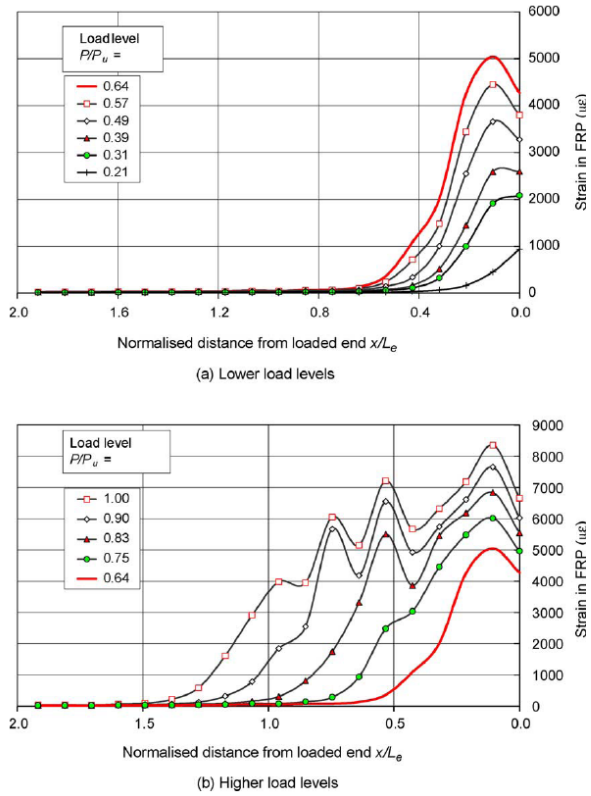

fig. 1.aa - Strain distribution along the FRP, test I-16 (L=190)

The Yao et al. [6] tests underline that an increase of the bond length not increase the load of the first crack but the ductility of the system. In this case the displacement of the effective bond length (stress transfer zone) through the whole FRP to concrete interface permits to delay the total debonding fracture.

Finally Yao et al. [6] found in their experiment that the existence of a loading offsets reduced the ultimate bond strength significantly only when the bond length is small.

Research on masonry-FRP systems is much more limited. Experimental studies by means of shear tests have been managed on brick (homogeneus support), pillar and masonry walls (heterogeneous support). Briccoli Bati S. and Fagone M. [10] made an experimental analysis using near end supported shear tests to value the collapse load of CFRP reinforce applied to a single brick specimens. The tests executed had a FRP width (b) varying from 10 to 100 mm and a length (l_b) varying from 10 to 240 mm. The image *1.bb* shows that the increase of the bond length leads to an

increase of the collapse load until the achievement of an effective bond length. The value of l_e is the abscissa of the point where the slope of the curves l_b-F_{max} become almost horizontal (*figure 1.bb*).

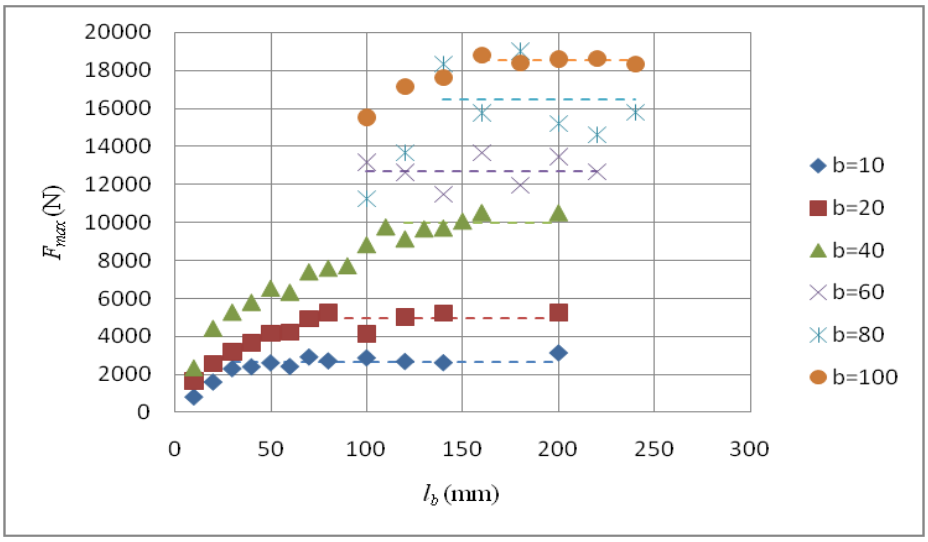

fig. 1.bb - Bond length and specific maximum load varying the FRP width (*a M. Fagone Cortesy*)

More the FRP width (*b*) is bigger, more the value of the collapse load increases. The main failure mode unregistered during the tests [10][11] is the cohesive fracture (*figures 1.cc*).

fig. 1.cc - Failure mode, NES double shear tests (a M. Fagone courtesy)

Another experimental analysis by NES double shear test on FRP to historic brick bonded joint has been executed by Capozzucca [12]. The reinforcements tested were been made by GFRP, CFRP and SRP (Steel reinforced polymer) with a width of 50 mm and a bond length of 250 mm. The historic brick have approximately dimension of 300x150x80 mm. The stress transfer advancement described in this work is coherent with the Yao et al. analysis [6] (*fig. 1.dd*).

Experimental and numerical studies show that most of failure modes in flexion of masonry walls reinforced by FRP systems are due to the extremity or to the intermediate debonding [13], [14].

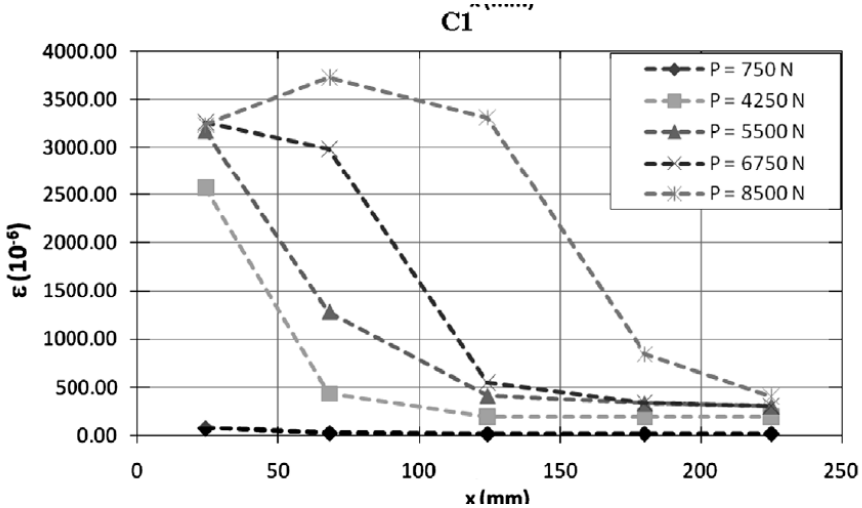

fig. 1.dd - Experimental strain values for the CFRP-to-historic brick bonded joint [12]

Fedele and Milani [9] studied the debonding failure of a masonry pillar reinforced with FRP by means of a damage continuum model. The masonry element is constituted by three standard bricks interposed by two mortar joints. Since the fracture occurs nearly in a cohesive manner Fedele and Milani [9] realized a numerical study with the assumption of perfect adhesion between the reinforcement and the underlying support. This hypothesis permits to take into account only the mechanical properties of the FRP and masonry constituents; the properties of the adhesive interface could be neglected. The constitutive law used to simulate the debonding is characterized by different isotropic damage variables in tension and compression. The mortar joints and the bricks are modeled independently; each material with his internal variables and his activation criteria.

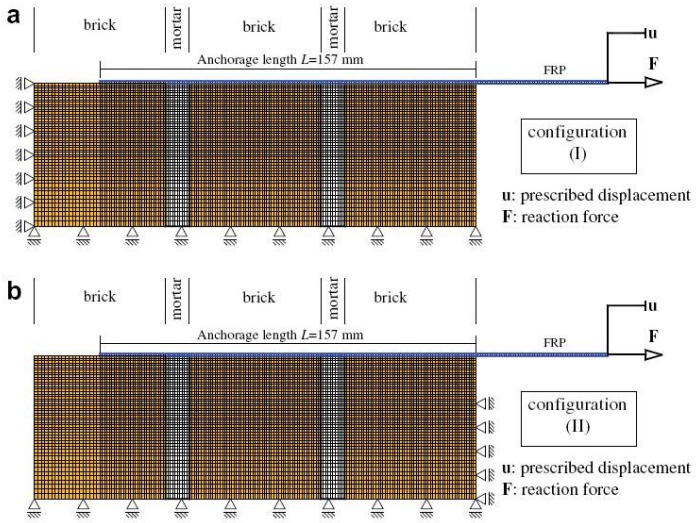

fig. 1.ee - Finite element discratization; configuration I (FES double shear test), configuration II (NES double shear test)

The numerical study simulate two different experimental boundary conditions; a FES double shear test (configuration I) and a NES double shear test (configuration II) [5] (*fig. 1.ee*). The fracture in the configuration (I) occurs close to the unloaded-end and the crack advancement starts in the left mortar joint (*figures 1.ff and 1.gg*).

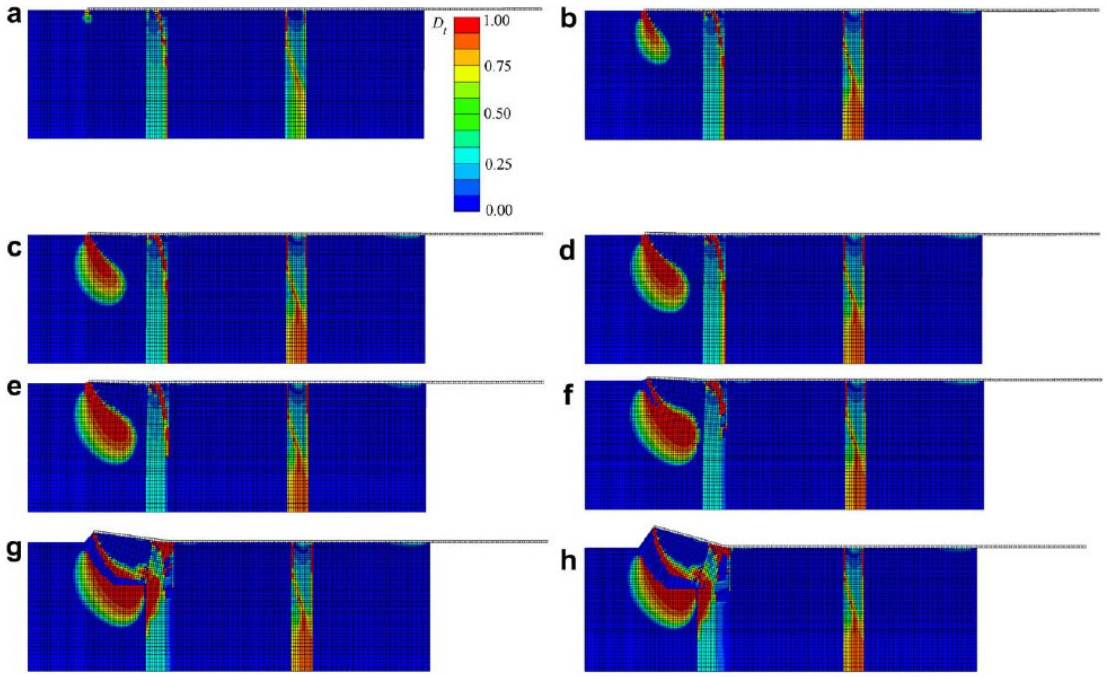

fig. 1.ff - Distribution of the damage in tension Dt for the numerical FES double shear test (configuration I)

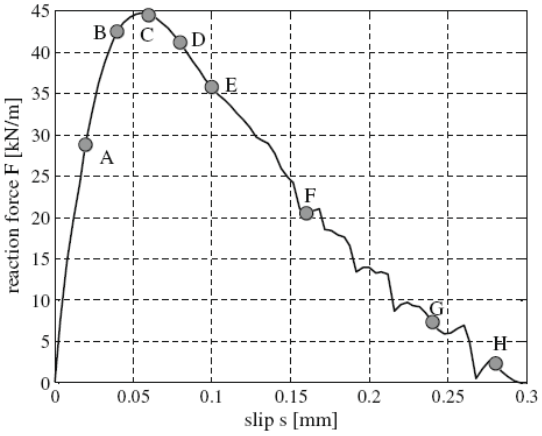

fig. 1.gg - Displacement-Load curve of the numerical FES double shear test; points A-H indicate the instants selected for the damage evolution of fig. 1.gg

In the configuration (II), the fracture advancement takes place in proximity of the loaded end and the crack advancement passes through all the bricks and mortar joints (*figures 1.hh and 1.ii*).

Comparing the images *1.gg* and *1.ii* is evident that the peak load for the NES double shear test is five times bigger than that for the FES double shear test; this is due to the different tensile stress distribution in the support. The presence of weak joints in the substrate, like mortar in masonry, could change the crack advancement mode in the debonding fracture.

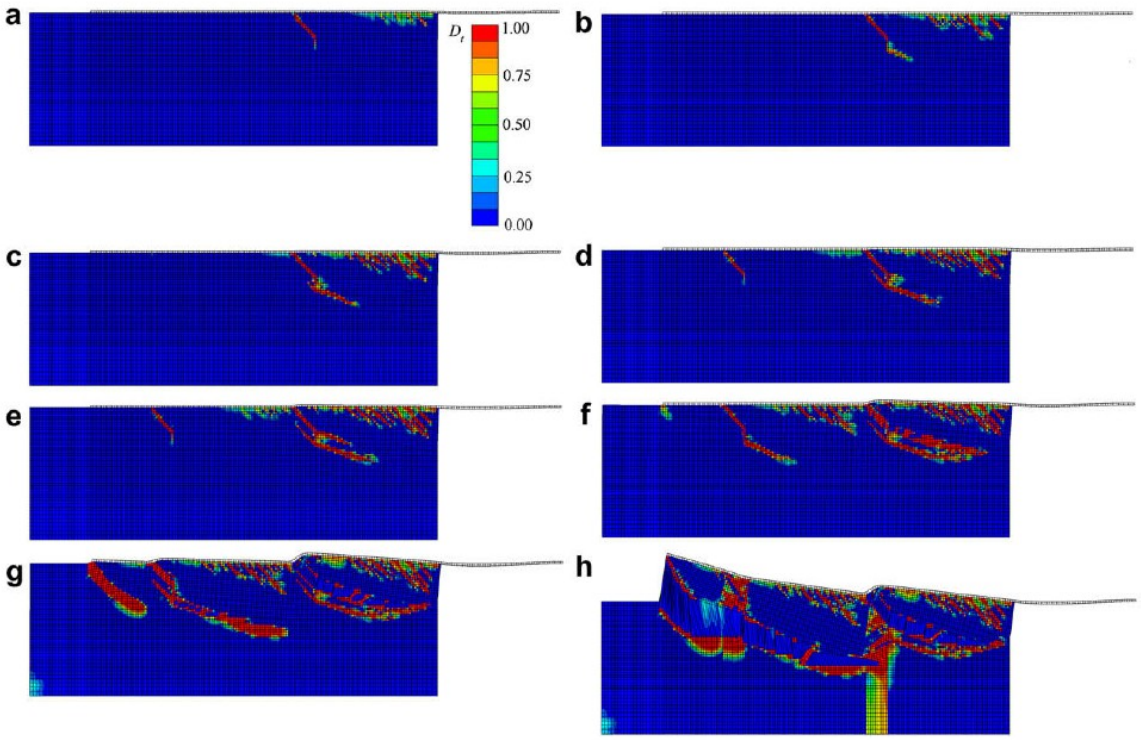

fig. 1.hh - Distribution of the damage in tension Dt for the numerical NES double shear test (configuration I)

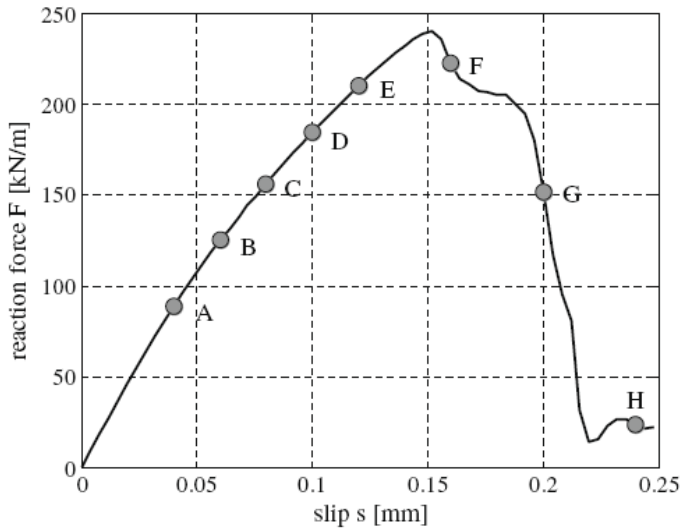

fig. 1.ii - Displacement-Load curve of the numerical NES double shear test; points A-H indicate the instants selected for the damage evolution of fig.1.hh

1.3.4 Debonding strength and masonry: a study case

The above literature review shows that the debonding between the composite and the support occurs earlier of the FRP fracture. To have an approximate estimation of the debonding strength of a FRP to masonry bonded joint, a simple study case is proposed below. Given a geometry configuration of simple shear test (values of b_{frp}, L_{frp}), the composite property (t_f, E_f, σ_f) and the support characteristics (Γ_{fk}, f_{bk}, f_{mk}, f_{mdm}), it has been calculated the value of l_e and f_{mdd} (when $L>l_e$). The calculus has been done using the normative design equation proposed by the Italian National Council of Research [1]. The value of l_e and f_{mdd} have been calculated for eight different typologies of masonry support, see table *1.IV* [4] considering a class of mortar M15. The partial factors ($\gamma_{f,d}$ and γ_M) have been chosen imaging a certified application of the FRP. The value of c_1 has been selected equal to 0,015 [1]. The results of the simple calculus are summarized in *table 1.V*. The optimal bond length (l_e) is inversely proportional to the specific fracture energy of the support (Γ_{fk}) (*fig. 1.jj*). Therefore a masonry with good cohesive properties, needs a optimal bond length shorter than a support of poor quality. In other words, when Γ_{fk} is high the stress transfer zone is reduced. Instead the design bond strength (f_{mdd}) is proportional to the specific fracture energy Γ_{fk} (*fig. 1.V*). As attended, a support characterized by good cohesive quality permit to increase the debonding strength of the reinforced FRP system.

Type	Masonry (M15)				FRP			FRP to masonry bonded joint				
	f_{bk} [N/mm^2]	f_{mk} [N/mm^2]	f_{mtm} [N/mm^2]	γ_M	Γ_{Fk}	E_f [N/mm^2]	t_f [mm]	σ_{lim} [N/mm^2]	l_b [mm]	c_1	γ_{fd}	l_e (mm)	f_{mdd} [N/mm^2]
I	2	1,2	0,12	2	0,01	270000	0,167	2700	450	0,015	1,2	433,45	79,94
II	3	2,2	0,22	2	0,01	270000	0,167	2700	450	0,015	1,2	320,12	108,24
III	5	3,5	0,35	2	0,02	270000	0,167	2700	450	0,015	1,2	253,80	136,53
IV	7,5	5	0,5	2	0,02	270000	0,167	2700	450	0,015	1,2	212,34	163,18
V	10	6,2	0,62	2	0,03	270000	0,167	2700	450	0,015	1,2	190,69	181,71
VI	15	8,2	0,82	2	0,04	270000	0,167	2700	450	0,015	1,2	165,81	208,98
VII	20	9,7	0,97	2	0,05	270000	0,167	2700	450	0,015	1,2	152,45	227,29
VIII	30	12	1,2	2	0,06	270000	0,167	2700	450	0,015	1,2	137,07	252,80

1.V Masonries and debonding strength

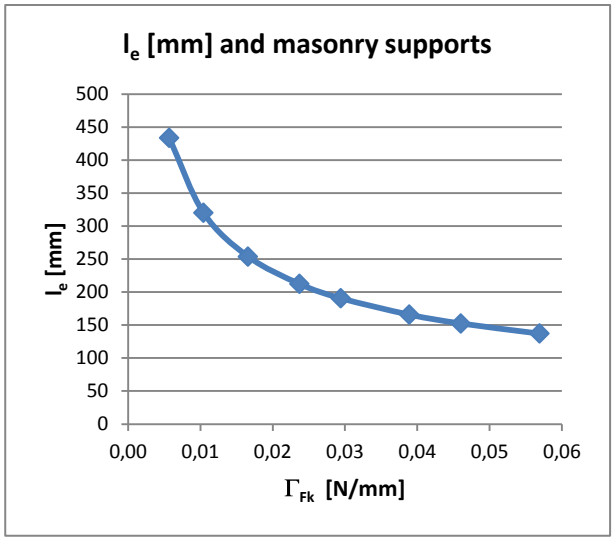

1.jj Optimal bond length (CNR) and masonries

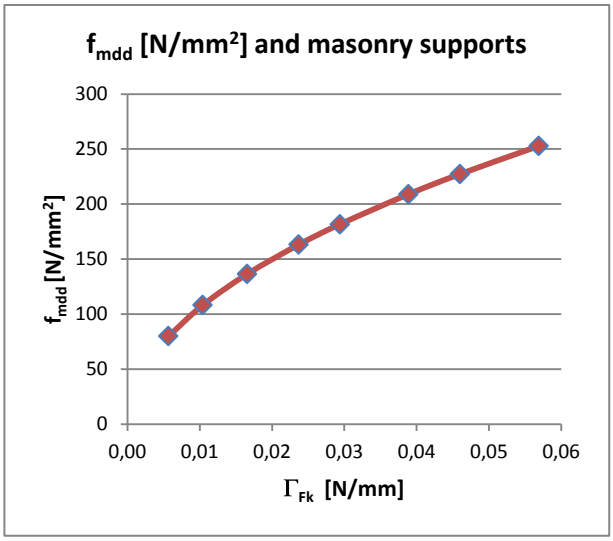

1.kk Design bond Strength (CNR) and masonries

The design bond strength (f_{mdd}) of the reinforced system with the better support quality (type VIII in table 1.V) is equal to 252, 8 MPa. This value is much smaller than the tensile resistance of the composite (σ_f=2700 MPa); only a little part of the high quality of the FRP is used. This thesis has been developed to increase the efficiency of the FRP reinforced systems.

1.4 Mechanicals anchors

A solution to increase the tension strength and the ductility of FRP reinforced systems as well is the use of "mechanical anchors" to joint support to composite sheet. In the framework of the reinforced concrete structure, some studies have been performed in the last years to define the typologies of anchors and the better configuration of application.

Ha lee and al. [15] executed a experimental study on the strengthening FRP systems fastened with steel nails. They utilized Near End Supported shear tests on concrete blocks, and flexural tests on reinforced concrete beams (*fig. 1.ll*). The composite applied over the concrete surface was a pultruded FRP strip characterized by hybrid carbon and glass fiber in a vinylester matrix (product named Safstrip). In the NES shear test session the FRP laminate (355 x 25 mm^2) has been applied directly on the concrete block (260 x 130 x 130 mm^3) without resin, and the adhesion between the support and the composite has been ensured only from one (conf. 1) or two (conf. 2) steel nails. Those lasts have a diameter of 3,5 mm (the same of the hole) and a length of 32 [mm].

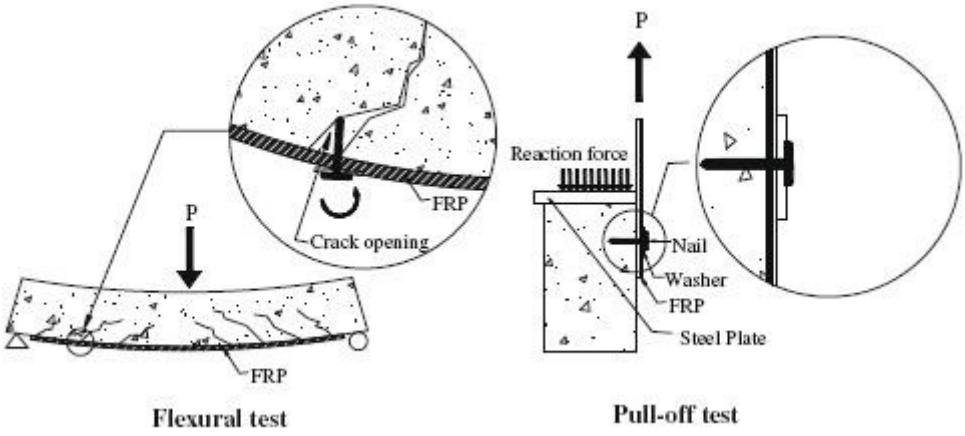

1.ll Boundary condition and failure of flexural tests and NES single shear test of Ha Lee et al. [15]

The average pull-off load for the configuration with two nails has been 11,7 kN, approximately twice that for one nail (6,10 kN). During the NES shear tests a bearing damage closeness the anchor occurs (*fig. 1.mm*). In the flexure beam test, the FRP laminate was fastened with more nails, always without the application of resin. The reinforced beam have an 35% increase of the ultimate moment when compared to the beams not strengthened. During the tests the nails rotated with a limited bearing failure of the FRP (*fig. 1.mm b,c*). The presence of the anchor acted as a crack initiator (*fig. 1.ll and 1.nn*). When the FRP strip slipped to the concrete, it remained linked to the support; the fasteners lead to a ductile flexural failure mode.

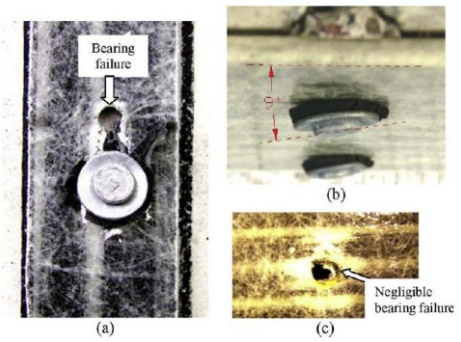

1.mm Nail and FRP interaction: a) extensive bearing failure (NES single shear test), b) nail rotation after flexure test, c) limited bearing failure after flexure test [15]

1.nn Crack and nails in a flexural test [15]

Other studies on the efficiency of the steel nails applied on FRP laminate exist in literature [16]. When the composite is realized directly in the job site applying special resin over a dry fabric and bonding the FRP on the support, other typologies of mechanical anchors are used. Among those the "U WRAPS" and the "fiber anchors" are the joint systems built by means of the same fibers

typologies of composite sheet (*see fig. 1.ll and fig. 1.pp*). The first system uses FRP strips applied over the reinforcement in different directions than the principal FRP [17], the second solution is similar to "nails" inserted in the strengthening system to connect mechanically the FRP sheet to the support.

fig. 1.oo- U WRAPS joint system *[17]*

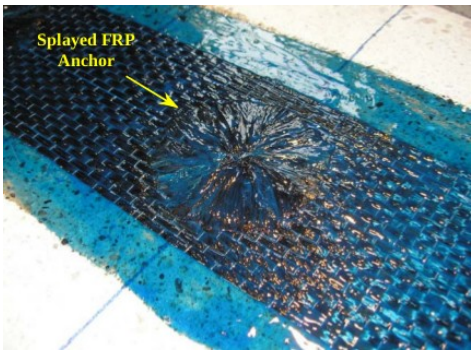

fig. 1.pp - Fiber Anchors joint system [Niemitz]

Orton *et al.* [18] made 40 experiments to test a reinforced concrete beam in bending with a preexisting crack at midspan. The beams was strengthened with CFRP without and with the addition of anchors joints (U WRAPS or fiber anchors). Orton et al. [18] is defined an indicator to define the efficiency of the CFRP material usage:

$$Efficiency = \frac{V_{LS}}{V_T} \quad \frac{T_{max}}{T_{cap}} \quad [\%] \tag{1.14}$$

Where V_{LS} is the volume of the longitudinal CFRP sheet, V_T is the total volume of CFRP, T_{cap} the tensile capacity of CFRP sheet, T_{max} the maximum measured tension in CFRP sheet and $\frac{T_{max}}{T_{cap}}$ the rate of the tensile capacity exploited.

In the Orton's specimens the value of T_{cap} was environ 130 kN. The beam strengthened by a FRP bonded joints, without mechanical anchorages, permits to exploit only 37 % of the tensile capacity of the sheet (efficiency = 37%) (*fig. 1.qq*). When two single layer U-Wraps were applied the $\frac{T_{max}}{T_{cap}}$ increase to 70% (efficiency = 21%). The application of two double layers U-Wraps permit to use 93% of the tensile capacity of the sheet, however the value of efficiency became 16 % due to the large use of CFRP material.

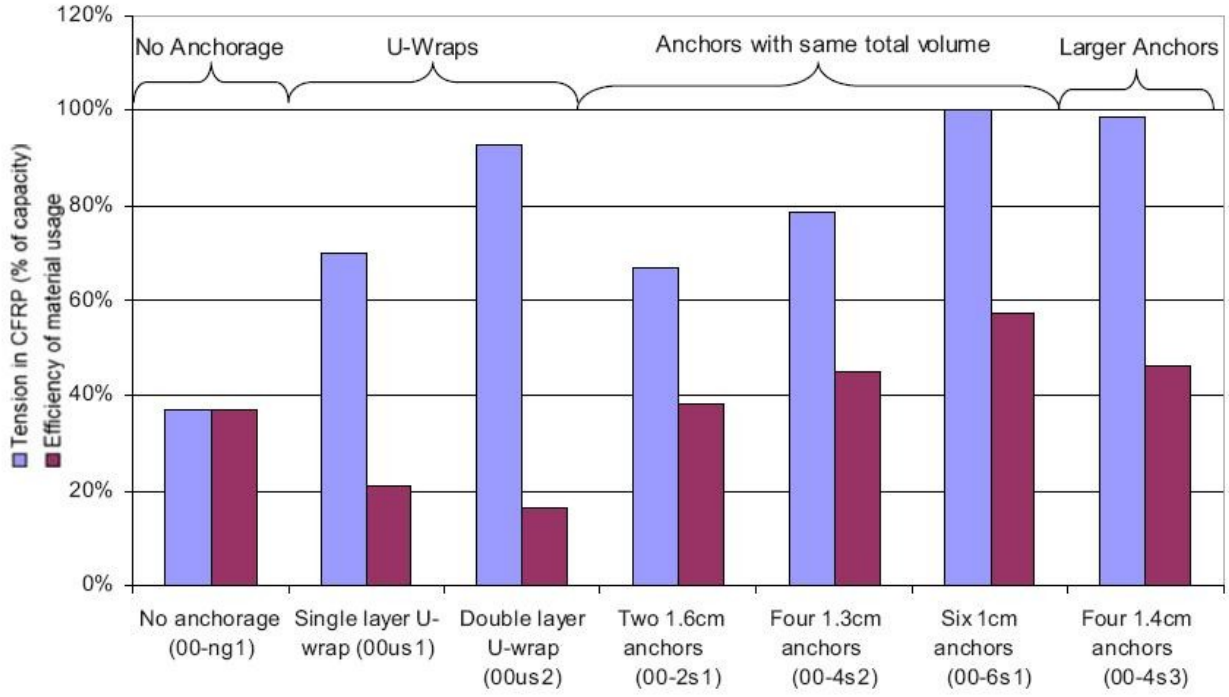

Fig. 1.qq - Percentage of the used CFRP sheet tensile capacity (in blue) and efficiency (in violet) of different configuration of reinforce [18]

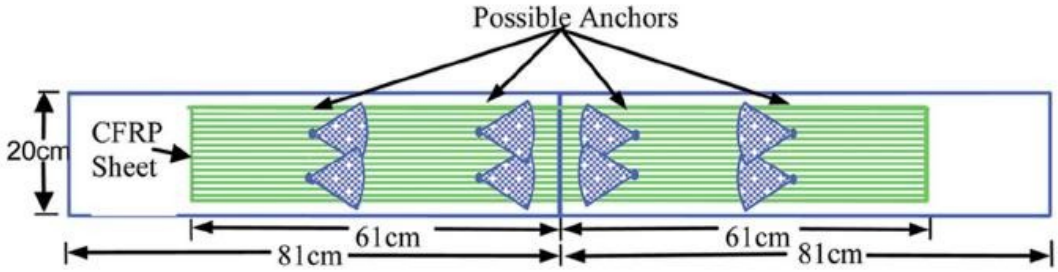

fig. 1.rr - Intrados of the cracked beam tested by Orton; they are visible the four anchors rows (two in each mid-span) [18]

When the FRP anchors are applied, they take place across the concrete blocks in aligned rows at 13 cm and 54 cm from the centerline of cracked beam. When two anchors of 1,6 cm diameter are applied in each mid-span row the 67 % of T_{cap} is exploit. The placing of four anchors (1,3 cm diameter), two in each mid-span row, increase the value of the tensile capacity used to 79% (efficiency = 44%). The better result has obtained applying six anchors of 1 cm diameter, three in each mid-span row, and reaching the CFRP sheet's full tensile capacity ($\frac{T_{max}}{T_{cap}} = 1$). In this case the value of the efficiency was 57%; the highest value registered, more high than the value obtained for the simple FRP to concrete bonded joints without mechanical anchors. It's simple to note that the

fiber anchors are more efficient than the U Wraps and permit to reduce the amount of CFRP material required to obtain a given strength.

fig 1.ss - Dry fiber anchor [20]

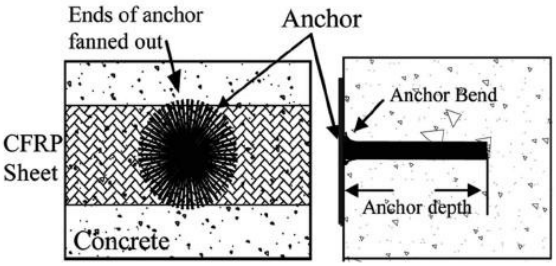

1.tt Fiber Anchor applied in a support (360° splay) [18]

The fibers anchors are built rolling a sheet of fiber's tissue (*fig. 1.ss*). The inferior part of this one is inserted through the composite strip, in an impregnated hole in the support (*fig. 1.uu*). The fibers at the top of anchor are spread over the FRP sheet like a fan shape. A layer of epoxy resin must be apply under and over the fan [18][19][20][21]. The studies of Kobayashi [18] about the stress transfer mechanism between the FRP sheet and the fan anchor define a fan opening angles limited to less than 90° to limit stress concentration [18][19][21]. However in the literature, a complete opening fan of 360° is considered [20]. The limit between the hole and the support must be rounded to reduce the stress concentration [22]; the fibers bending in this area has an important influence on the tensile capacity of the anchor.

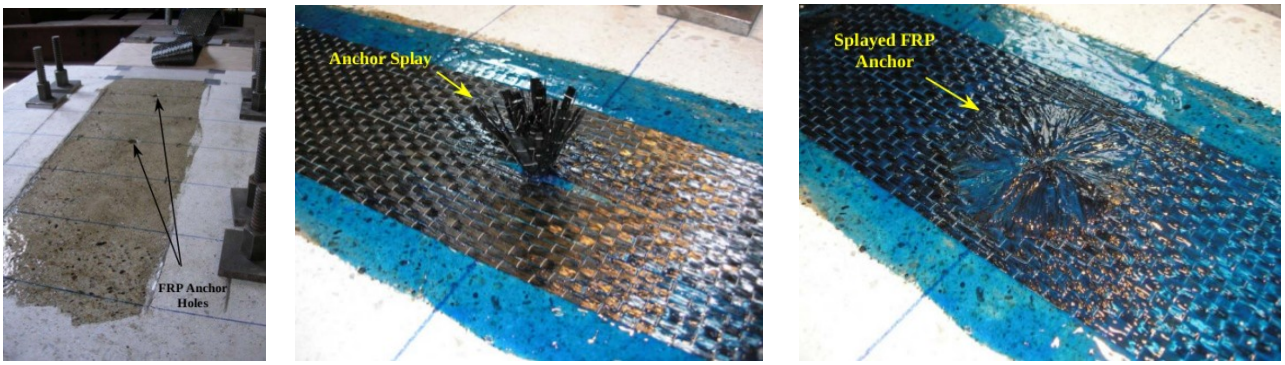

Fig. 1.uu - Some phases of the fiber anchors application process, I) Covering the support surface with primer after the realization of the anchors holes, II) Insertion of the anchor through the composite strip, III) fanning of the anchor splay [20]

Niemitz [20] studied the efficiency of carbon fiber anchors by means of 12 NES single shear tests on reinforced concrete blocks (dimensions of 101.6 x 86 x 32.2 cm^3) strengthened with CFRP sheet (*fig. 1.vv*). The Niemitz's anchors were applied dry in the support's holes filled approximately half

way with epoxy resin (*fig. 1.ss and 1.uu*). Without anchors and for a sheet of 12.7 cm wide and 76.2 cm long, the failure of strengthened system appeared for a tension equal to 46 % of the stress limit of the composite. When there are two anchors (each-one with a diameter of 1.3 cm and 360° fan diameter of 5.1 cm) placed longitudinally, the failure appeared at a tension equal to 68 % of the limit tension of the composite. The failure occurs with the local fracture of the fibers in the proximity of the first nail (load side), and with the debonding of the FRP sheet in the lateral sides of the reinforce (*fig. 1.ww*). When the two anchors are placed across the width of the sheet the ratio between the failure load of the reinforcement and the failure load of the composite in tension is equal to 71 % (*fig. 1.xx*). In this case the failure occurs in the same modality of the previous case but with more limited lateral debonding zones.

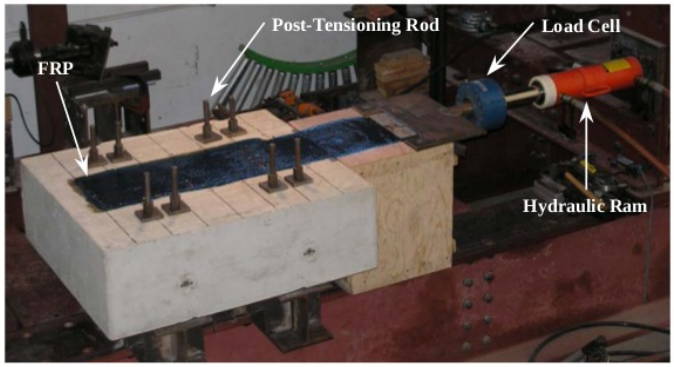

fig 1.vv - Specimen test setup of Niemitz [20]

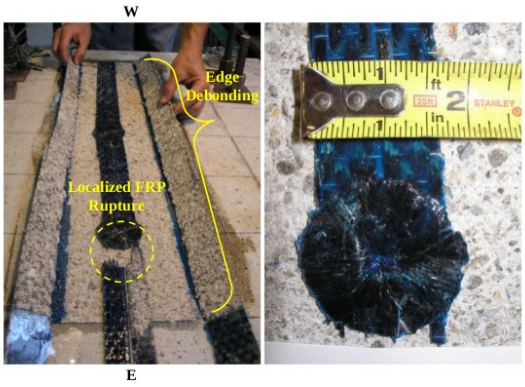

fig. 1.ww - Failure of the specimen with two anchors placed longitudinally [20]

For all tests the anchor length of 5.1 cm is enough to prevent the anchor pullout. Niemitz found that the overall effectiveness of FRP anchors is related to: the ratio between the anchor diameter and the fan diameter, the anchor spacing and the anchor depth. A larger fan diameter increases the force applied to the anchor; if the amount of fibers is not sufficient a shear failure of anchor is possible, indeed, this typology of failure has occurred in a test with an anchor diameter of 0,64 [cm] (*fig. 1.yy*). The most efficient disposition of anchors is across the width of the composite sheet. Spacing anchors longitudinally is convenient also to increase ductility of the system. It has been impossible, in the Niemitz's study [20], to record the peak stress values using a discrete number of strain gauges.

fig. 1.xx - Failure of the specimen with two anchors placed across the width of the sheet

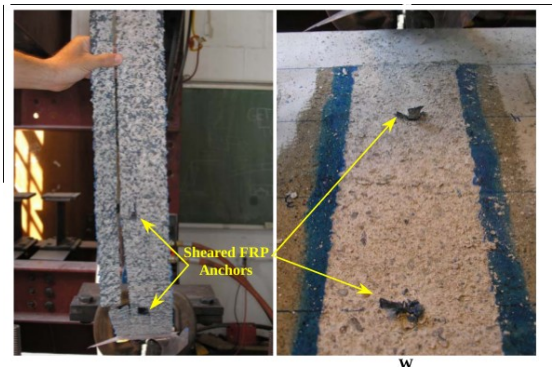

fig. 1.yy - Shear failure of the reinforced system with a small anchor diameter [20]

Zhang *et al.* [21] have studied the FRP anchors by means of 27 single shear tests on reinforced concrete blocks (40x20x20 cm^3) reinforced by FRP sheet (joint surface of width 5 cm and length 25 cm). They tested two typologies of anchors: dry and impregnated (*fig. 1.zz*). The second, more efficient, is made with an inferior extremity (dowel) of 2.5 cm pre-impregnated in the phase of rolling fiber tissue. For all the tested specimens the anchor length was equal to 4 cm and the anchor diameter to 1.2 cm.

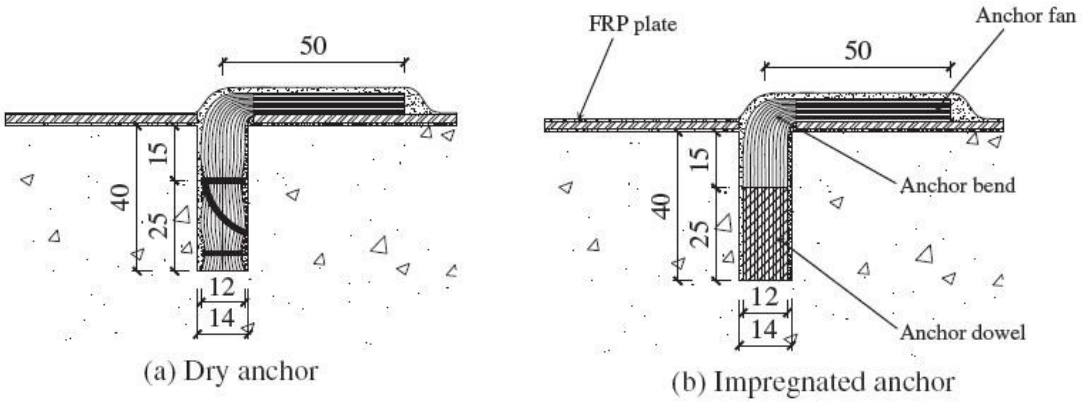

fig. 1.zz - Dry and impregnated anchors of Zhang et al. [21]

The anchor fan was oriented towards the direction of load (fan open of 60°) with a radius of 5 cm. Zhang *et al.* [21] schematized in five steps the generic load-slip response of FRP-to-concrete joints anchored tests (*fig. 1.aaa*). The first step is the linear stroke due to initial debonding of the sheet from the loaded bonded end propagated to the position of the anchor. The second step is another linear stroke (smaller slope than previous step) due to the contribution of the anchor. In the third step, the complete debonding of the plate brings a quick decreasing of the load. The fourth step is characterized by an improvement of the load due to the sliding of the roughened surfaces of the debonded plate and the concrete substrate. It is also due to the contribution of the tensile resistance

of anchor. In the fifth step the load reduced rapidly for anchor rupture failure and gradually for anchor pull-out. The average load peak (at the end of second step) of unanchored FRP-to-concrete control joints is 18 kN. The application of a dry anchor 200 (built rolling a fiber sheet of 200 mm) improves the load peak of 54%. The application of an impregnated fiber anchor 200 improves the load peak of 73%. Different design arrangements of impregnated fiber anchors are been studied in bending tests on FRP-strengthened reinforced concrete slabs [23].

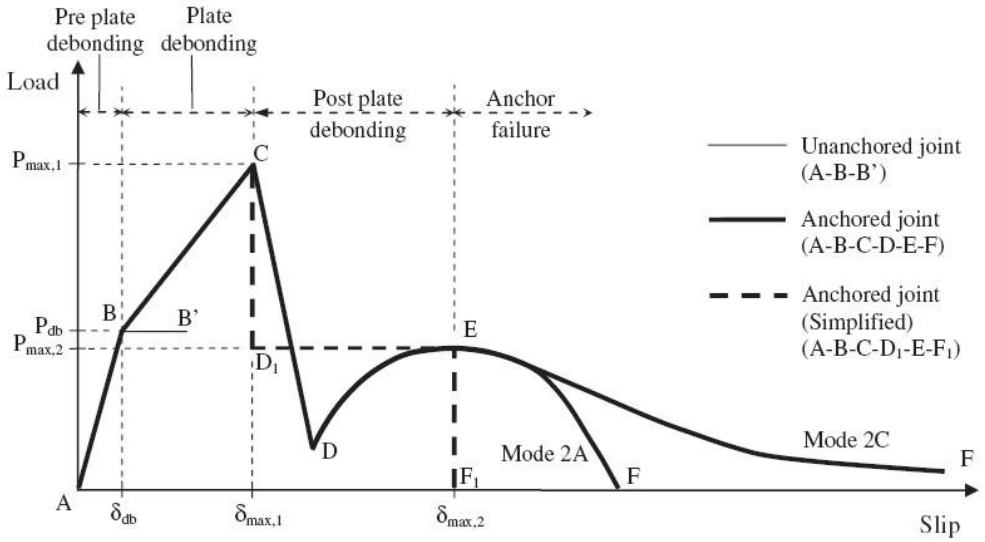

1.aaa - Load-slip response of FRP-to-concrete joints anchored tests [21]

Chapter 2

Experimental program

2 *Experimental Program*

Why realize a experimental study on the CFRP to fire brick bonded joints? What are the goals to achieve using the tests? Which are the problems connected with the test realization? How realize the experiments? In this chapter it has been answered to these questions. Herein, after a presentation of the motivations, goals and methodology of the experimental program (*par. 2.1*), a detailed description of the test setup is presented (*par. 2.2*).

The logical steps executed to project each particular of the experimental system have been: 1) focus the goals, 2) conception of the experimental device more efficiently, 3) design. This methodological process has been used to project the boundary condition, the specimen geometries, the anchor devices and the steel apparatus.

In the follows pages, defined the boundary condition more appropriate (*par. 2.2.1*), the geometry of the specimens is presented (*par. 2.2.2*). All materials used to prepare the sample are characterized and described. In particular the results of the compression tests on the fire bricks executed in Florence are shown. Moreover the properties of the CFRP components are presented in line with the technical sheet BASF. A particular attention is posed on the description of the carbon fiber anchors. All the phases of specimen realization are presented and commented.

Afterwards a description of the mechanical apparatus of the boundary conditions is presented. The Universal machine Deltalab of the ESIPE (Univ. Paris Est Marne La Vallée) laboratory is analyzed in paragraph 2.2.3. The mechanical systems created to lock the brick and to grip the fibers are presented in paragraph 2.2.4. The numerical studies executed to determine the better configuration of contrast are shown in the first part of this section. After that all the devices designed and realized are presented and commented. Moreover an experimental study of the stiffness of the new steel system is reported; in the same paragraph the results obtained have been compared with those of the numerical study. Afterwards the project and the devices of the steel grab system are described and commented. The paragraph 2.2.4 finish with a global geometrical representation of the boundary condition apparatus.

The paragraph 2.2.5 describes all the procedures necessary to prepare the test; the insertion of the reinforced fire brick inside the steel contrast, the gripping process of the fiber fabric, the alignment and the global assembling of the experimental system. The instrumentation applied on the apparatus is presented in paragraph 2.2.6 underlining the experimental data searched. Finally the test procedure is described.

2.1 Motivation, goals and methodology

In the field of the concrete structures a lot of studies exist on the use of FRP anchors systems. It has been demonstrate that this mechanical anchor typology increase the strength peak and the ductility of the reinforced elements. Moreover it is more efficient than the U-WRAPS method. Therefore, in the field of masonry, almost no study have been conducted on the FRP anchors. This lack of researches leads to an absence of scientific basis to define the correct design modality and anchor application methodologies; in this context the engineers employ the new joint technologies using only the proper experience or the FRP producer advices.

The experimental study proposed in this work has been designed to analyze the performance of mechanical anchors applied over CFRP straightened fire brick. This typologies of support has been chosen for the following motivations. Among the numerous different masonries, the "solid brick work" (see chapter 1) is the typology present in all the world with almost uniform characteristic, this happens for two reason: the fire brick of different territory have similar mechanical and geometrical characteristic (it is not the case of local stone) and the constructive technique used to build the walls is the same in all the regions (joints of mortar staggered). Moreover the fire brick structures are simple to realize. The use of this "classical" typology of masonry for the realization of the experimental tests could be "indicative" to evaluate the performance of FRP anchors on heterogeneous supports. The research program proposed is composed by three progressive steps:

- Near End Support single shear tests over CFRP straightened fire brick fastened with FRP anchors (brick + CFP sheet + anchor (s)
- Near End Support single shear tests over CFRP straightened pillars fastened with FRP anchors (pillars + CFP sheet + anchor (s)
- Flexural tests over CFRP straightened walls fastened with FRP anchors (wall + CFRP sheet + anchor (s)

The experimental study reported in this work is relative to the first research step. Specifically the **goals** of the test sessions have been:

a) Quantify the strength enhancement that CFRP anchors can provide to the strength capacity of the reinforcement
b) Study the efficiency of different design configuration varying the anchor fan angle, the anchor fan radius, the number and the placement of anchors
c) Observe the crack advancement and the failure modes of the FRP-to-firebrick system without and with the different anchor's configuration

d) Analyze and quantify the dissipation of energy during the crack advancement in each different design configuration
e) Obtain the strain field on the reinforced surface in each step of the load history using the Digital Image Correlation

To achieve these goals 72 Near End Supported shear tests divided in 6 typologies of specimens were managed. The design of the tests, the reinforced systems and the FRP anchors has been done after a detailed literature research. The experimental program has been realized in collaboration with the University of Firenze, Department of Construction. The "Fagone, Ranocchiai, Briccoli Bati" research group has believed interesting the proposition to study the FRP anchors and has made available his confirmed experience in the fields of masonry and FRP. The scope of the collaboration is join the French experience in the field of the Digital Image Correlation (DIC) with the Italian knowledge on the behavior of masonry structures reinforced by FRP and submitted to earthquakes. The tests have been made in parallel, in France and in Italy, to compare the results obtained with two different methodologies of strain analysis; the DIC in Paris and the use of traditional strain gauges in Firenze. The specimen preparation have been made in Firenze, after that the fifty percent of the samples was been sent in France. The tests in Paris have been done using the laboratory equipment of the University Paris-Est Marne-La-Vallée.

2.2 Experimental Setup

2.2.1 Boundary conditions

The experimental analyses have been done with series of Near End Supported single shear tests (*fig. 2.a*). This typology of boundary conditions reproduce a "intermediate crack debonding" [6]. As seen in the first chapter, the NES single shear tests are sample to reproduce and were been used in a lot of numerical and experimental literature studies [1][5][6][7][8][9][10][11][12][15][20][21]. The employ of a configuration test so affirmed has permitted to compare the experimental results obtained in this work with those of literature. Moreover the equation of the debonding parameters defined in literature are been obtained starting from shear hypothesis; the choice of similar boundary conditions make possible a cross-comparison between the normative and the experimental values of l_e, Γ and f_{mdd}.

The single shear tests (SST) have been preferred to the double shear test (DSS) because the slender thickness of the brick doesn't permit the application of the anchors in two symmetric surface of the block. Indeed, in the SST, the anchor system is applied only in one side of the fire brick and the support have a behavior more similar to that of the reality.

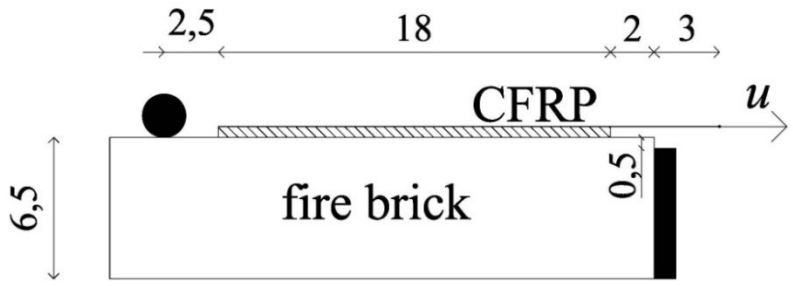

2.a Boundary conditions; NES single shear test, in black the steel lock. Measures are in [cm].

In the figure *2.a* the boundary condition chosen for the experimental tests are shown. The shear load is applied in the same side of the contrast; this last is placed at 0,5 [cm] from the brick corner. A steel cylinder is positioned close to the "far loaded end" to prevent a rotation of the brick. The load is applied the not bonded extremity of the composite.

2.2.2 Specimens

In this paragraph the features of the specimens are defined. In the first section properties of the materials used to make the samples are presented (fire bricks, the epoxy primer, the epoxy adhesive and the carbon fabric). Afterward the design motivations, the nomenclature and the geometry property of the specimens are described. Finally the realization procedure is reported.

2.2.2.1 Materials

2.2.2.1.1 Fire brick

The support of the reinforced system is realized with fire brick (12 x 25 x 6,5 cm^3) produced by *laterizi S. Marco (terreal Italia group)* and belonged to the commercial line "*classico*" (*fig.2.b*). The value of compressive strength of this material was obtained by means of 24 compression tests over cubes of 5x5x5 cm^3 executed in Firenze. These cubes have been cut out from 6 different fire bricks (*fig. 2.c and 2.d*). Since the production procedure give to the blocks different mechanical properties in each orthogonal orientation, the cubes obtained from the bricks have been tested in directions x, y, z.

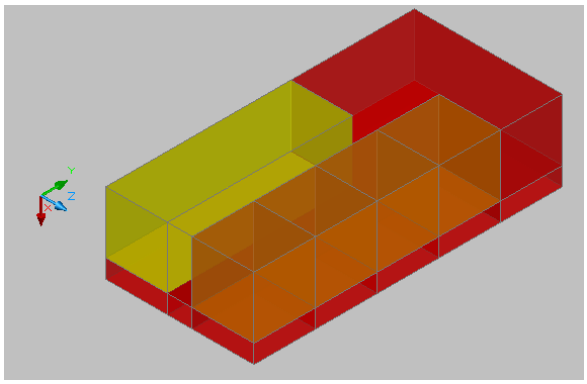

fig. 2.c - The subdivision of the firebrick to generate the cubic samples (compressive tests) and the parallelepiped specimen (Young modulus tests). It's shows also the reference axis.

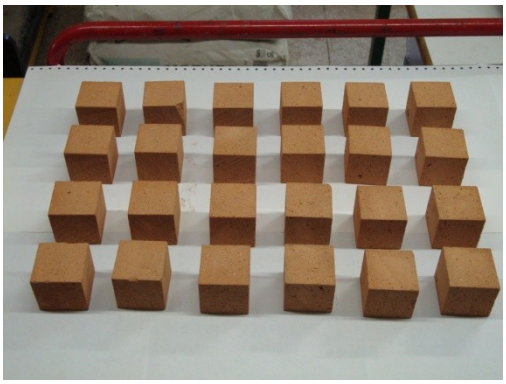

fig. 2.d - The 24 cubes tested in compression

The tests have been made using a compression testing machine characterized by a load cell of 150kN. Each cube to test has been posed on a steel support and loaded by means of a quadrangular compression plate; a steel sphere is interposed between this last and the load piston. Four displacement comparator was applied on the superior surface of the compression plate (*fig. 2.e*).

Figure 2.f shows the curve displacement-load for the three tests on the fire brick "1" in the directions x, y, z. The displacement in is the average of the values read by the four comparators. It's clear that the compression strength of the block are better in the direction of the clay input during the industrial missing in shape procedure.

fig. 2.e Compressive test over a cube

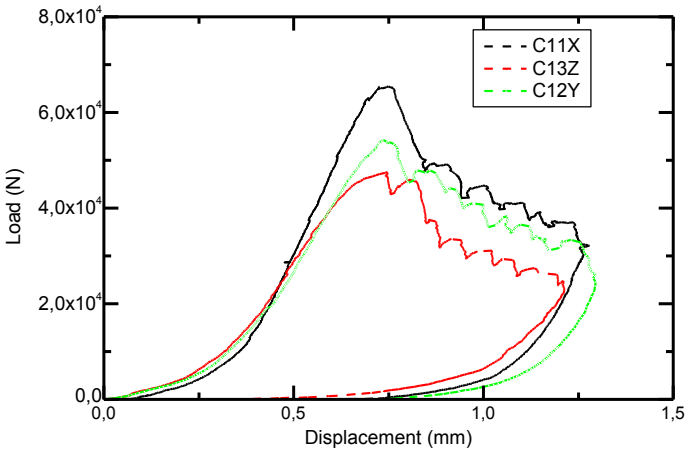

fig 2.f Graphes displacement-load for the compression tests over the firebrick 1(Fagone's datas)

The results are represented in *table 2.IV*; the average value of registered compressive strength is included between 18,22 [MPa] (direction z) and 22,18 [MPa] (direction x).

To obtain the Young Modulus six compression tests have been made over 6 parallelepiped specimens (5x5x15 cm^3) cut out from the same 6 fire bricks cited previously (*fig. 2.c*). Four comparators Ω were applied in the center of each lateral surface (5 x 15 cm^2) of the specimens (*fig. 2.g*). Reading the variation of the distance between the "foots" of the Ω, originally equal to 5 cm, it has been possible to calculate the strain value. The use of Ω comparators permit to obtain the strain field far than the boundary support. Known the strain field and the applied tension for each load step, the Young modulus is simple to obtain. In the stiffness tests the load is applied using the same procedure presented above for the compression test on cubes. In *figure 2.h* are shown the graphics displacement-load for the Young modulus compression tests. The mean value of the stiffness modulus E obtained is equal to 8814,66 [MPa] (*table 2.IV*).

fig. 2.g - Young modulus compression test

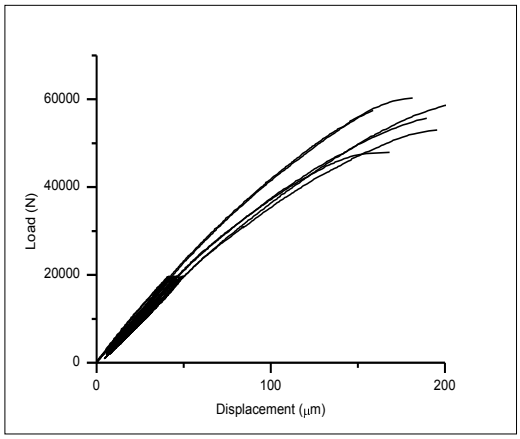

fig 2.h - Graphs displacement-load for the Young modulus compression tests

	load direction	mean value	st. dev.	coefficient of variation
		(MPa)	(MPa)	(%)
Compressive strength	x	22,18	2,00	9,02
	y	19,89	1,02	5,13
	z	18,22	1,35	7,40
Young modulus	y	8814,66	610,06	6,92

fig 2.IV - Compressive strength and Young modulus on a sample of six fire brick "S.Marco"

2.2.2.1.2 Epoxy resin primer

The epoxy resin primer used to improve adhesion between CFRP and support is named "MBRACE Primer" and is distributed by BASF [24]. This Primer is a two-part epoxy product and it is applied on the support before the adhesive. "MBRACE Primer" is a ready to use product with high adhesive and bond strength. Moreover it bonds to damp surface. T*able 2.V* shows the performance data of the product defined by the construction company. In *2.V* is possible to read the properties, 7 days after the primer application in an environment with a T=20°C, of the *bonding to concrete* σ_{BTC} (UNI EN 1542), the *direct tensile strength* σ_+ (ASTM D638), the *tensile modulus of elasticity* E_+ (ASTM D638), the *flexural tensile strength* σ_f (ASTM D790), the *compressive strength* σ_- (ASTM D695) and the *compressive modulus of elasticity* E_- (ASTM D695).

	σ_{BTM} [MPa]	σ_+ [MPa]	E_+ [MPa]	σ_f [MPa]	σ_- [MPa]	E_- [MPa]
MBRACE Primer	> 3,5	> 20	1200	> 35	> 40	1900

table 2.V - Performance data of "MBRACE primer"

The MBRACE Primer is supplied in packaging of ten liters (7,5 l of component A and 2,5 l of component B). The mixing ratio is 3 parts of A with 2 parts of B. The construction company recommended the application of only one layer of primer (environ 150 micron).

2.2.2.1.3 Epoxy resin adhesive

The epoxy resin adhesive used in the specimen construction is named "MBrace Adesivo" and it is distributed by BASF [25]. This saturant is applied over the still tacky Primer to bond the fiber fabric. The "MBrace Adhesive" must be applied below and upper the fiber tissue layer to guaranty the distribution of load and the protection of the composite from the environment. The resin adhesive is a two-part epoxy product with 100% solids content. It is a product "ready to use" with high adhesive and bond strength. Moreover, the low viscosity of "MBrace Adhesive" enables the use of a variety of fiber densities (glass, carbon, aramid). *Table 2.VI* shows the performance data of this epoxy adhesive defined by the construction company. The parameters presented in table *2.VI* are the same of that described in the paragraph 2.2.2.1.2 (properties 7 days after the saturant application in an environment with T=20°C).

	σ_{BTM} [Mpa]	σ_{+} [Mpa]	E_{+} [Mpa]	σ_{f} [Mpa]	σ_{-} [Mpa]	E_{-} [Mpa]
MBRACE Adesivo	> 3,5	> 25	3300	> 45	> 80	3100

table 2.VI - Performance data of "MBrace adhesive"

The "MBRACE adesivo" is supplied in packaging of ten liters (7,5 l of component A and 2,5 l of component B). The mixing ratio is 3 parts of A with 2 parts of B. The construction company recommended the application of one coat of MBrace adhesive on base substrate and one coat on the installed sheet.

2.2.2.1.4 Carbon fabric

The CFRP reinforcement is realized using a carbon unidirectional fabric named "MBRACE fibre CFRP" and distributed by BASF [26]. Fibers have the important role to carry the load acting on the composite. The principal characteristic of the "MBrace fibre CFRP" has been defined by the construction company; in the *table 2.VII* are shown the dry thickness *t*, the Young modulus *E* (ASTM D3039), the strain limit in tension ε_{lim+} (ASTM D3039) and the characteristic tensile strength (ASTM D3039). In this table it is important to underline that the properties are inherent the dry fabric and not the composite.

	t [mm]	*E [Mpa]*	ε_{lim+} *%*	f_{fk} *[Mpa]*
MBRACE fibre CFRP	*0,165*	*230000*	*> 1%*	*>1500*

table 2.VII - Geometrical and mechanical characteristic of "MBRACE fibre CFRP"

The carbon fabric is supplied in roll of 0,30 x 100 [m], and it is simple to cut by means of scissors or cutter. The construction company recommended the application of the fiber fabric on the surface while the adhesive is still wet.

2.2.2.2 Design of specimen's geometry

Seventy-two specimens have been made to execute the experimental session. The samples are divided in 6 different series; the nomenclature and the geometrical properties of each one is defined in *figure 2.j* and in *table 2.VIII*. From the name of each specimen it is possible to understand where the sample has been tested. If the first letter of the name is "T" the specimen was tried in Paris ("Trou" is the French for hole), instead if the epithet start with a "F" the sample was tested in Firenze ("Foro" is the Italian for hole). The second character of the nomenclature corresponds to the

number of anchors applied. The successive number present in the name defined the radius of the anchor in [mm]. The next character of the nomenclature underline the fan anchor opening; if it's "O" the fan is splayed with an angle of 360°, instead if it's a "V" the fan is splayed with an angle of 75° (*table 2.VIII*). The last number of the specimen's name correspond to the sample piece of each series. For example: the specimen T1_40_O_5 has been tested in French and it's characterized by: 1 anchor, 40 mm of fan radius and 360° opening fan angle; it is the fifth of the series.

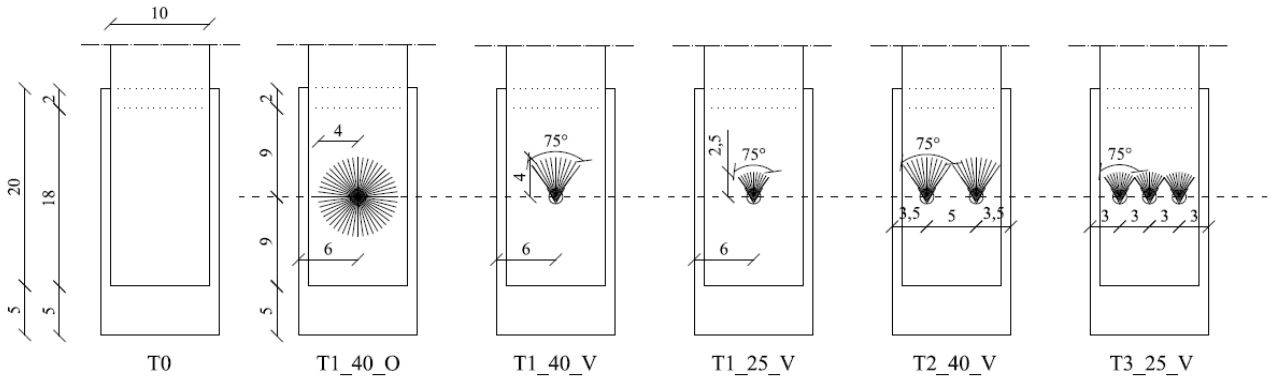

fig 2.j - The six typologies of specimen tested

number of anchors	fan radius (mm)	fan angle (degree)	specimens name*	number of specimens
1	40	360	T1_40_O_n	6
			F1_40_O_n	6
		75	T1_40_V_n	6
			F1_40_V_n	6
	25		T1_25_V_n	6
			F1_25_V_n	6
2	40		T2_40_V_n	6
			F2_40_V_n	6
3	25		T3_25_V_n	6
			F3_25_V_n	6

fig. 2.VIII - Geometrical property of the samples

The twelve FRP-to-fire brick bonded joints specimen of series F(T)0 are the specimens of reference made to know the behavior of the reinforced system without fiber anchors. The CFRP bond length (l) and the composite sheet width (b) chosen for the reference samples are equal for all specimens.

The bond length (l) has been designed to be longer than the optimal bond length defined by the CNR DT200/2004 [1]. This choice was made to analyze the advancement of the crack during the debonding failure [8][10][12][6][5]. Taking into account proprieties of the composite and of the support, it has been calculated the value of l_e using the equation (1.8). The Young modulus of the CFRP (E_p) is equal to the value of the Young modulus of the fabric (E_f) by a reduction coefficient defined by the CNR (α_{fe}=0,9) for the system impregnated in situ. The compressive strength (f_{bm}) of the fire brick is considered equal to the compressive strength in direction x measured during the

Firenze characterization tests. To obtain the characteristic value of compressive strength $f_{mk,}$ f_{bm} has been multiplied by the reduction coefficient 0,75 [4]. The masonry average tensile strength (f_{mtm}); since unless specific data is available, it has been assumed equal to $0{,}10f_{mk}$. The thickness (t_p) of the composite has been considered equal to 0,17 [mm].

$$l_e = \sqrt{\frac{E_p t_p}{2 f_{mtm}}} = \sqrt{\frac{0{,}9\times230000\ \times0{,}17}{2\times(0{,}75\times22{,}18\times0{,}10)}} = 102{,}85\ [mm] \tag{2.1}$$

Therefore the optimal bond length (l_e) is about equal to 10,3 [cm] and the bond length (l) of the specimen has been designed to be more longer (18 [cm]).

$$10{,}30\ \ cm\ = \boldsymbol{l_e} < l = 18\ [cm]$$

The width of the reinforcement was designed equal to 10 [cm] to permit the allocation of one or more anchors. In the Near End Supported side the carbon fabric is not attached to the support for a length of 2 [cm]. This particularity has been provided to space the bonded zone to the steel lock and to avoid a premature corner fracture. In the far end supported side the reinforcement is not present for a 5 [cm] length to permit the contact of the steel cylinder (see the boundary condition defined above). The geometrical properties of the reference specimens are shown in *figure 2.k*.

All remaining specimens are characterized by the presence of anchor (s); to avoid a transversal fracture due to the presence of a nail of 5 cm in depth a fire brick of 6,5 [cm] in thickness, all the samples with anchors have a support constituted by two bricks glued together (*fig. 2.l*).

The specimens of series T1_40_O have been achieved to measure the improvement in strength due to one anchor with angle fan of 360° and fan radius of 40 mm (*fig. 2.l*). The "nail" is applied in the center of the CFRP bonded surface; it is posed in the terminal part of the optimal bonded length. The anchor has a section of 1,2 [cm] and it has been inserted in a hole of 1,4 [cm] in diameter and 5 [cm] in depth; the values of anchor section, hole diameter and anchor depth have been maintained constants for all the specimens with fasteners.

The series T(F)1_40_V has been realized to evaluate the fan angle influence (*fig. 2.m*). The specimens of this group have the same features of the T(F)1_40_O except the fan angle of 75°. The comparison between the results of these series has permitted to evaluate the behavior of the reinforced system when the fibers are splayed in all direction (360° angle fan) and when the fibers are splayed only in the main direction of load (75° angle fan). It is important to underline that in the

first case the bonded surface between the sheet and the fan anchor is equal to 48,92 [cm^2] and in the second case it's equal to 10,19 [cm^2].

The series T(F)1_25_V is characterized by a fan radius of 25 mm (*fig. 2.n*). The specimen of this group have the fibers splayed only in the load direction with a 75° angle fan. The comparison between the results of series T(F)1_25_V and T(F)1_40_V permits to evaluate the influence of the fan radius. In this group the bonded surface fan anchor-sheet is equal to 3,81 [cm^2].

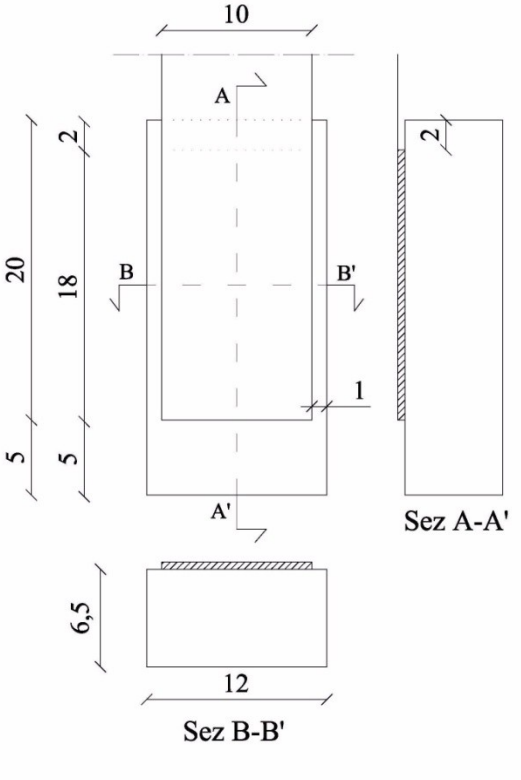

fig. 2.k - Specimen of series T(F)0

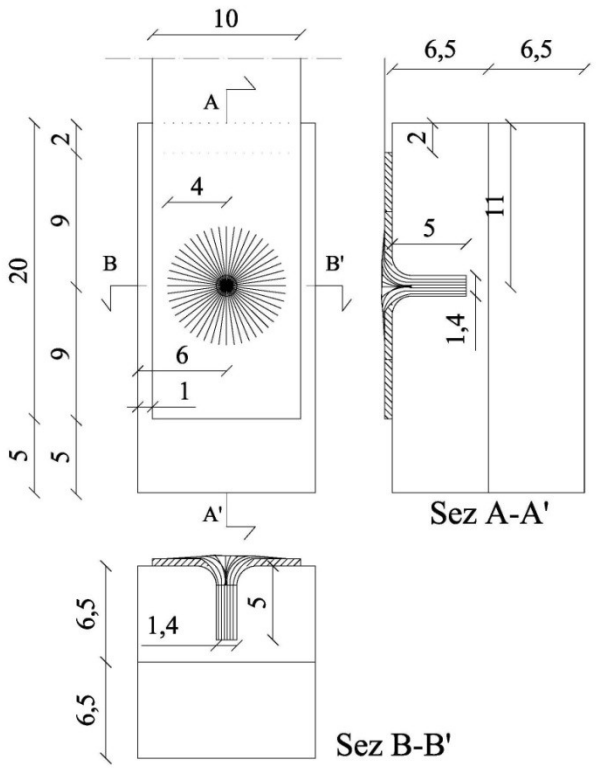

fig. 2.l - Specimen of series T(F)1_40_O

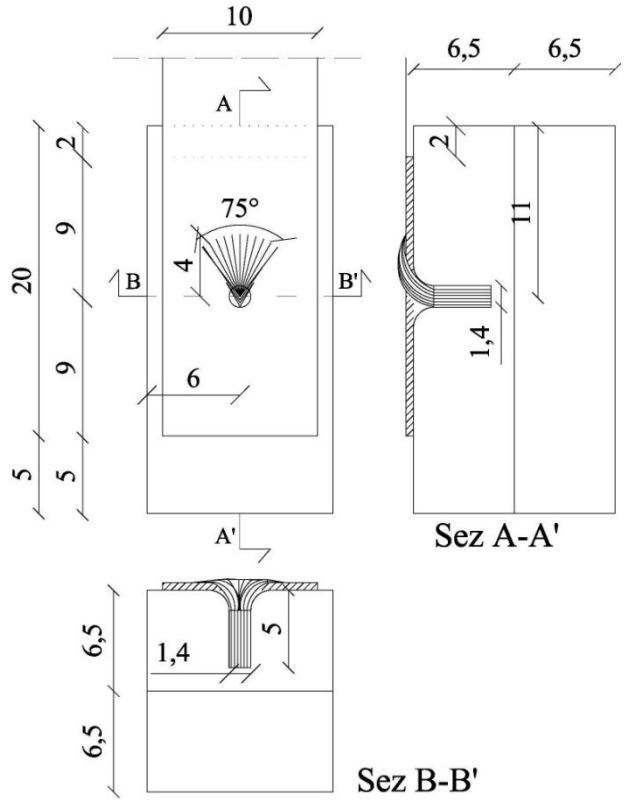

fig. 2.m - Specimen of series T(F)1_40_V

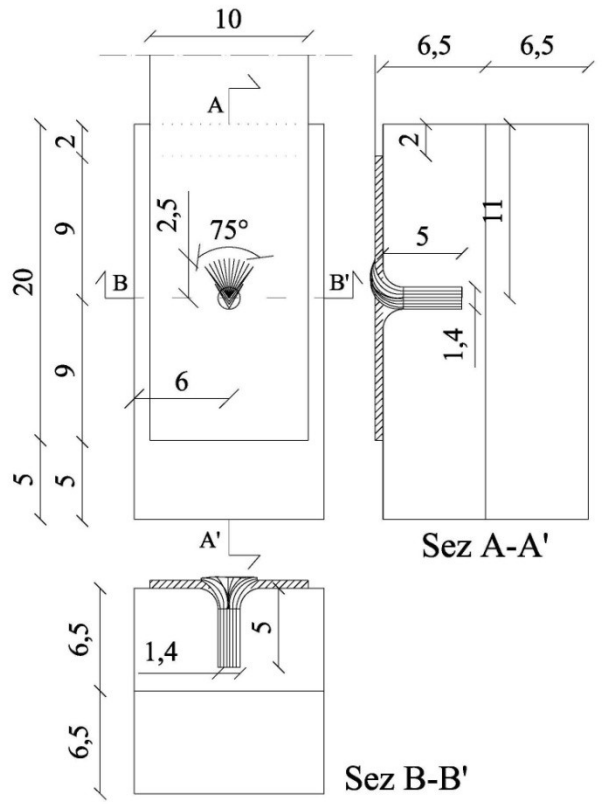

fig. 2.n - Specimen of series T(F)1_25_V

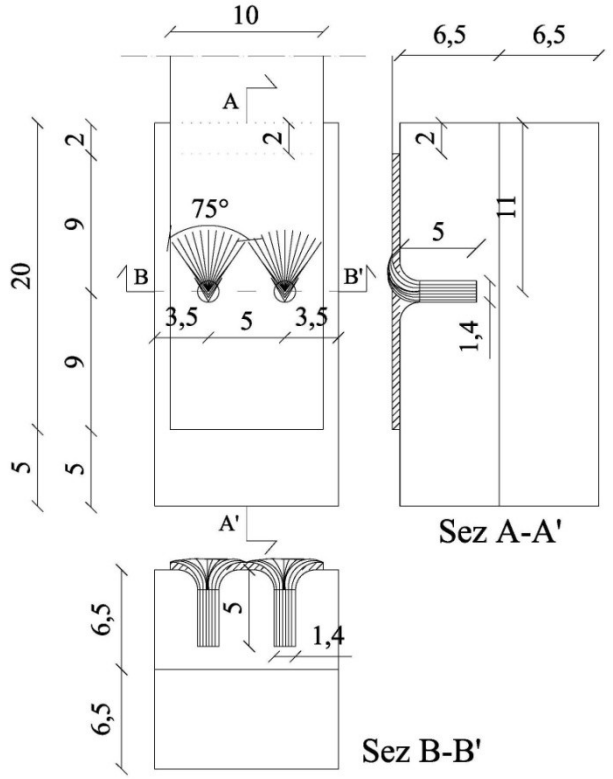

fig. 2.o - Specimen of series T(F)2_40_V

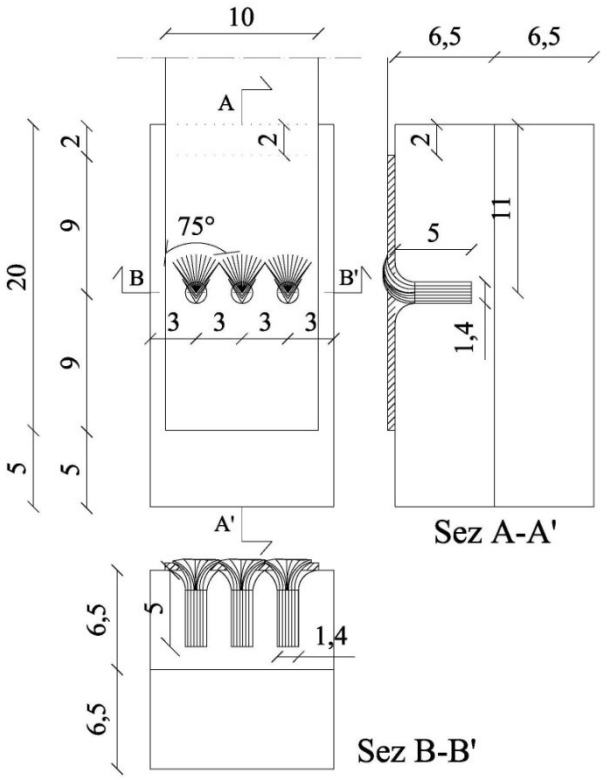

fig. 2.p - Specimen of series T(F)3_25_V

The series T(F)2_40_V has been carried out to study the efficiency of two fibers anchors posed in the same transversal line (*fig. 2.o*). The "nails" have a fan radius of 40 mm and an angle fan of 75° with fan fibers directed to the load versus. The bonded area "fan-sheet" is equal to 20,38 [cm^2]. The two anchor fan cover all the width of the CFRP.

The last series, the T(F)3_40_V, is characterized by three anchors posed in the same line along the width of CFRP. This group of specimens has been tested to measures the influence of the number of anchors. Those last have a fan radius equal to 25 [mm] and a fan angle equal to 75°. The overall bonded area between fans and sheet is 11,43 [cm^2]. The three anchors fans cover all the width of the CFRP.

2.2.2.3 Anchor details

The fibers anchors have been made with the best design characteristics defined in the literature studies in order to proceed to measures for the maximal improvement of stress capacity of reinforced system. Therefore, we assume that the behavior of anchors in concrete support is similar to that of anchors in firebrick support so that the anchor typology used in the present experimental session has been the one defined from Zhang et al. [21] "*impregnated anchor*". The anchor's depth was chosen equal to 5 cm to avoid pull out crisis, since in the Niemitz [20]experimental session a similar anchorage "profundity" was sufficient to keep off the release of the "nail".

The "nail" has been built by rolling a 200 mm strip to prevent the anchor shear crisis [21]. The fan anchor has been limited to less than 90° to limit stress concentration in all series of specimen except one. It has been chosen a fan opening angle of 75° because it permits to cover, with two (r = 40 mm) or three (r=25 mm) anchors placed in parallel, the whole width of FRP sheet. The sharp limit of the anchor's hole has been rounded to prevent strain concentration as recommended by ACI440(2002) [22].

Two anchors typologies have been realized; the first is characterized by a fan radius of 40 [mm] and the second by a fan radius of 25 [mm]. Since the anchor depth is equal to 50 [mm], the strips used to make the nails have dimension of 200x90 mm^2 for the anchor of the first configuration (50+40 mm), and of 200x75 mm^2 for the anchors of the second configuration (50+25mm). The 200 mm width is cut in the direction perpendicular to the fiber orientation (*fig. 2.q*).

The realization process of the CFRP anchors is constituted by the follow steps [21]:1) to cut the necessary carbon fabric strips (*fig. 2.q*), 2) to impregnate the epoxy resin in the inferior side of tissue cut (*fig. 2.r*), 3) to roll the tissue in the width direction (*fig. 2.s*), 4) to insert the dowel in a

pre-formed hole (12 mm of diameter) in a polystyrene mould (*fig. 2.t*), 5) to remove the anchor from the mould after minimum one day (*fig. 2.u*).

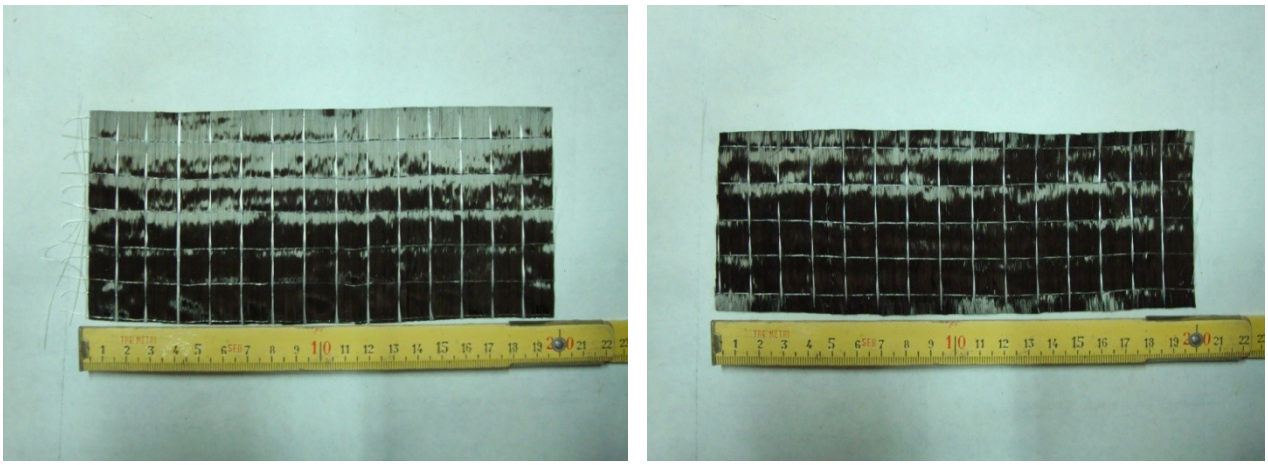

figures 2.q - The 200 mm carbon strips used to realize the two typologies of anchors; 200x90 mm2 for the first type and 200x75 mm2 for the second one

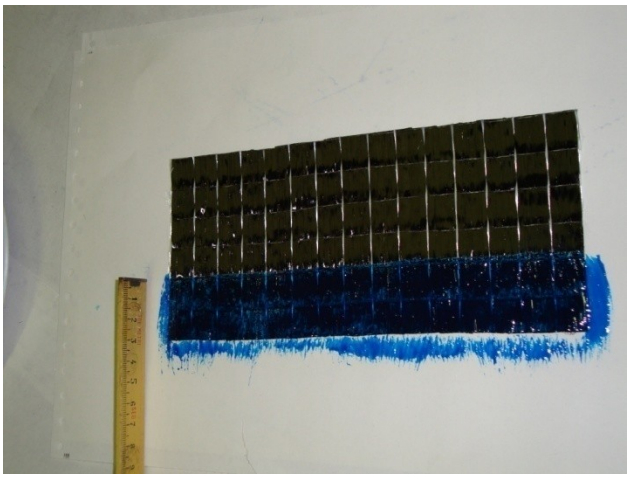

fig. 2.r - Impregnation with epoxy resin of the lower part of the carbon fabric

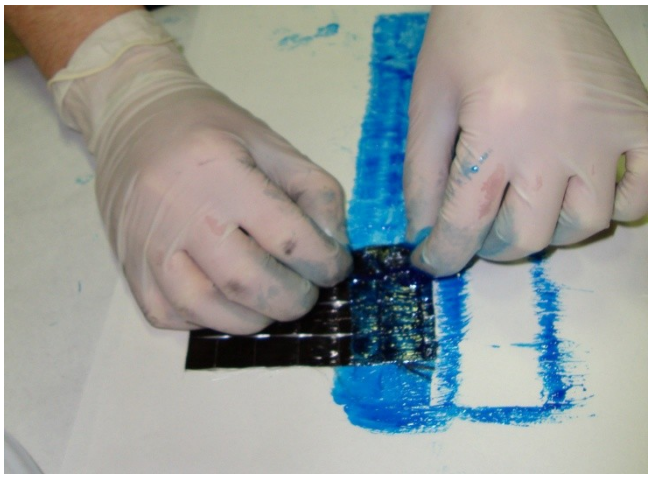

fig. 2.s - The carbon strip during the roll up phase

fig. 2.t - The anchor dowels inserted in the polystyrene mould

fig. 2.u - The impregnated anchor realized; on the right the anchor ready to be insert in the fire brick

2.2.2.4 Specimen construction details

The installation procedure of the FRP-to-firebrick bonded joint reinforced with anchors is defined by the following steps:

1) drill the hole in the fire brick (*fig. 2.v*)
2) round the hole's corner to a 13 mm radius
3) bond a second brick below the holed support (*fig. 2.w*)
4) to clean the cavity and the surface's of firebrick (fig. 2.x)
5) to fill the hole with epoxy (*fig. 2.y*)
5) to insert the anchor (*fig. 2.z*)
6) to apply the primer and the epoxy resin over the surface of firebrick to reinforce (*fig. 2.aa*)
7) to lay the sheet on the epoxy resin allowing the passage of the anchor through the unidirectional fibers (*fig. 2.bb*)
8) to apply the epoxy resin on the composite sheet (*fig. 2.cc*)
9) to splay the anchor fan over the sheet (*fig. 2.dd and 2.ff*)
10) to apply the epoxy resin over the fan anchor (*fig. 2.ee*)

fig. 2.v - The three typologies of support with anchor holes

fig. 2.w - The support constituted by two glued bricks

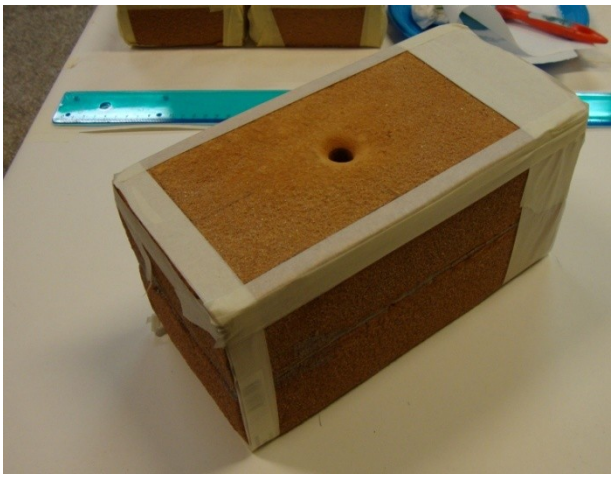

fig. 2.x - The fire brick ready to be reinforced

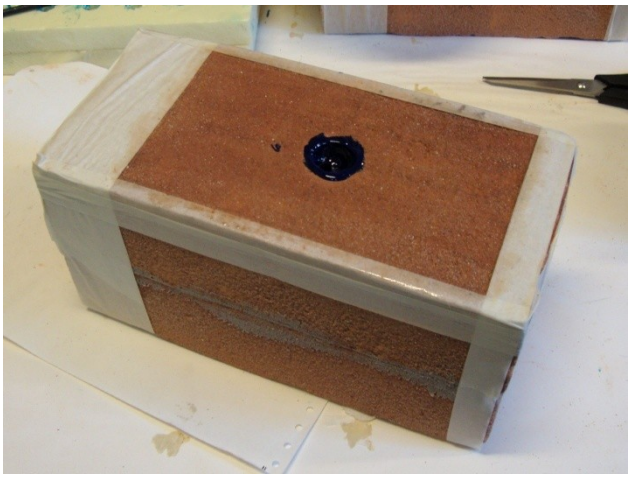

fig 2.y - Hole filled with epoxy resin

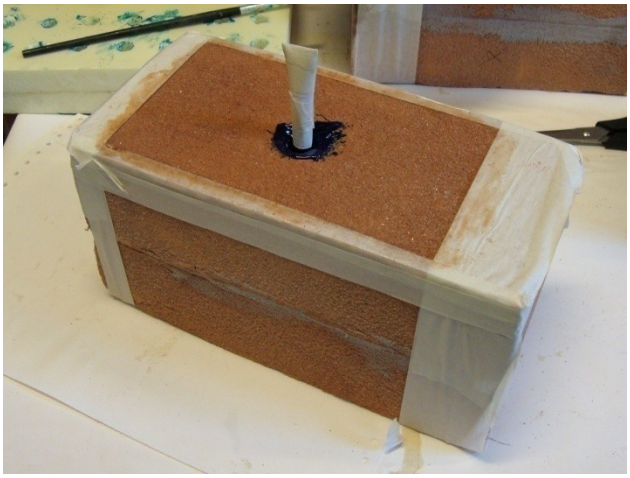

fig. 2.z - A impregnate anchor inserted in a hole support

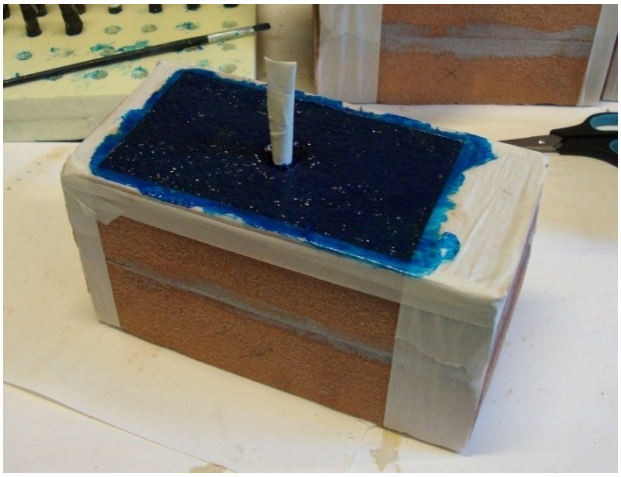

fig. 2.aa - Fire brick surface covered by epoxy resin

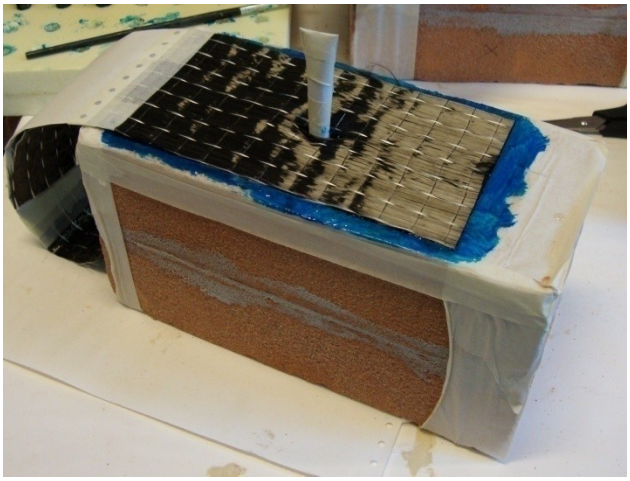

fig. 2.bb - The carbon fabric applied over the first layer of epoxy resin; the anchor pass through the unidirectional fibers

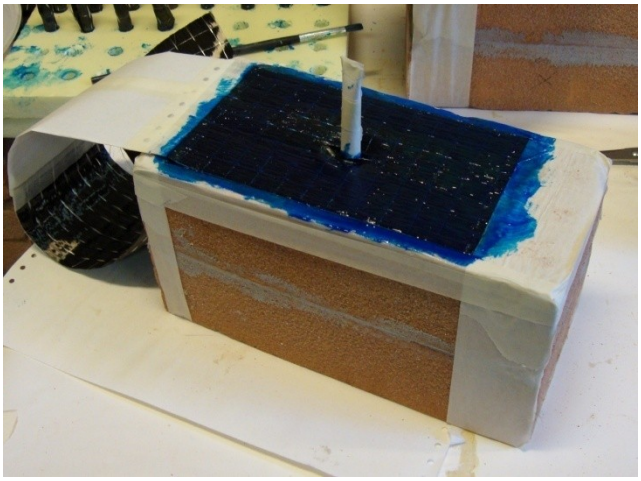

fig. 2.cc - The epoxy resin applied on the carbon fabric

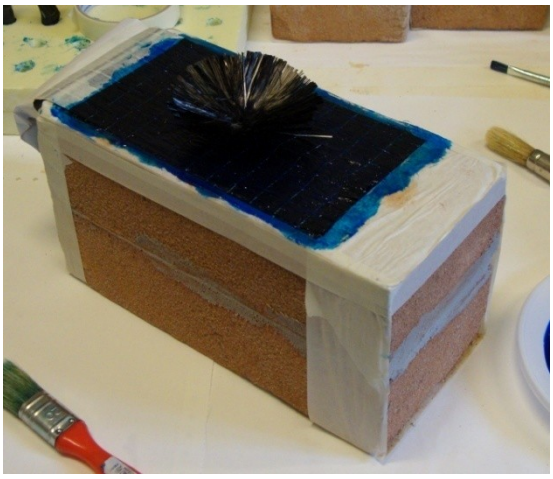

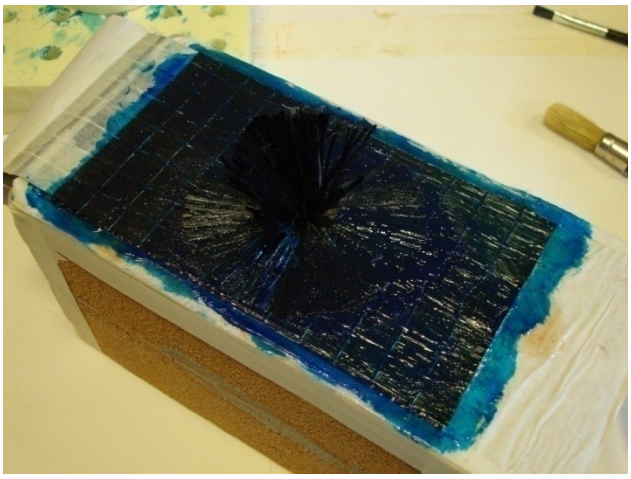

figures 2.dd - Two step of the splay procedure of the fan anchor

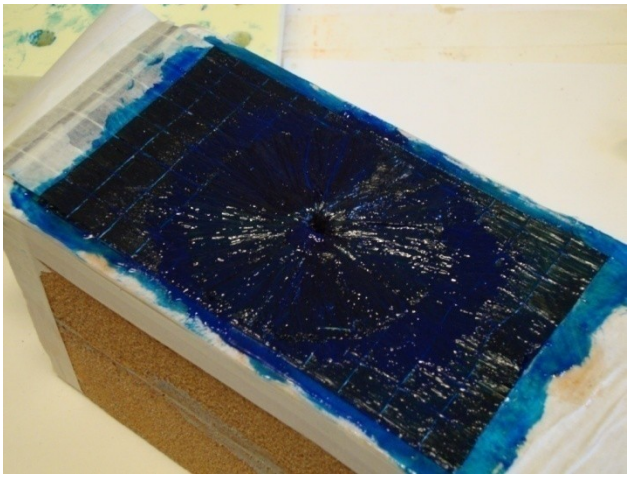

fig. 2.ee - Epoxy resin applied on the fan anchor splayed

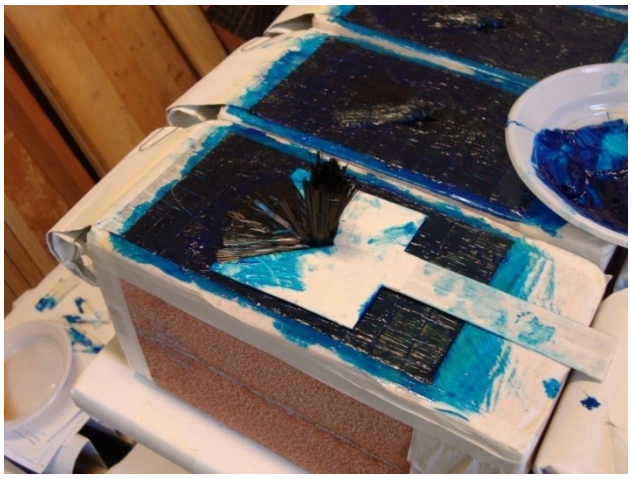

fig. 2.ff - The procedure to splay the fan anchor with 75°angle

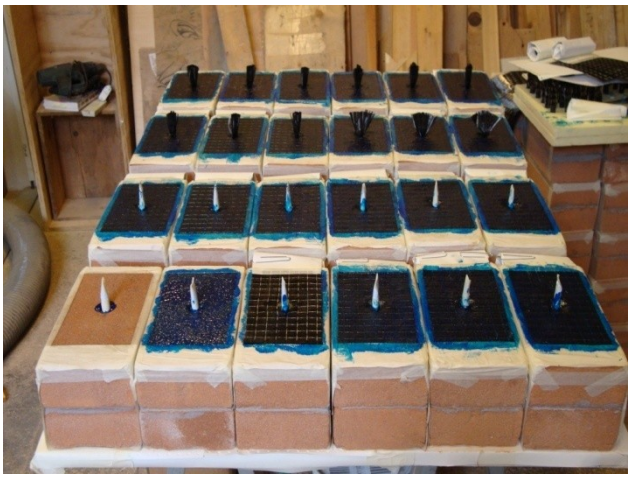

figures. 2.gg - The high number of specimens during the preparation procedure

2.2.3 *Universal machine*

The machine used to apply the load during the tests is the "Universal Machine EM550" produced by DELTALAB (France). It is a design electro-mechanical testing machine with a 50 [kN] capacity in traction and compression. The EM550 is connected to a PC provided of a specific software "*deltalab*" to control, acquire and analyze data. The universal machine is composed by a support, two columns, a cross-head and a movable traverse (*fig. 2.hh*). This last can move up and down among the columns. The load cell take place in the center of the inferior traverse surface, defining the load axis. In the support surface six bolt joints are present around and in proximity of the load axis (*fig. 2.ii*). The column spacing is 42 [cm].

fig. 2.hh - The universal machine EM550 DELTALAB

fig. 2.ii - Detail of the universal machine (load cell and bolts joints)

2.2.4 *Mechanical systems to contrast the brick and to grip the fibers*

The boundary conditions of the Near Ended Supported single shear test have been reproduced in France and in Italy with different steel systems. Hereunder the description of the apparatus realized in Paris. Particularly this steel system have been made up in the mechanical laboratory of ESIPE in the University Marne-La-Vallée Paris-Est. In the design phases particular attention has been posed to construct a simple, versatile and compatible apparatus with the universal machine. The system must be "simple" to make easy, accurate and fast the test procedure. It must be "versatile" to make

possible his future reuse in the next experimental sessions (NES single shear test on masonry pillars, 3D DIC).

2.2.4.1 Steel lock

2.2.4.1.1 Design; hypothesis and FEM studies

The apparatus that lock the brick has been made up in steel. The design of this one has been affected by the technical and geometrical properties of the universal machine. In particular, the steel system could be linked to the support only in correspondence of the six bolt joints of *figure 2.ii*. Moreover the reinforced face of the specimens must be collocated in the same plane that contain the load axis of the machine.

The steel lock must carry out the follows tasks:

- To apply the boundary condition defined in *figure 2.a*
- To define physically the plane where the load is applied; it's necessary to simplify the correct placement of the specimens
- To permit the insertion of specimens characterized by different size without lose the original alignment of the system.
- To be adequate to realize the test sessions on the fire brick and on the masonry pillar supports.
- To be sufficiently rigid
- To not hide the reinforced and the laterals surface of the sample to permit the realization of photos (Digital Image Correlation).

A steel plate of 1,5 [cm] thickness, bolted to the universal machine, function as the base of the apparatus; on this one the other steel elements are fastened. The load plane is defined by a metallic cylinder (*fig. 2.jj*); the extremities of this one are built-on two steel supports. The cylinder act as the linear lock to the rotation of fire brick; to reduce the friction contact it is smooth and it could rotate around its own axis. To make simple the placement of the specimen in the correct alignment, the cylinder should not move during all the experimental tests; it represent the correct line where the reinforced face of the specimen must be leaned. To reproduce the surface fix designed in *figure 2.a* a steel element, geometrically similar to a Z, is fastened on the metallic base plate (*fig. 2.kk*). To permit the insertion of specimens characterized by different sizes, the "Z box" can move back and forth; if necessary it can be removed and replaced.

The length of the cylinder and the width of the Z steel element permit to test specimens 25 [cm] in large, 27 [cm] in high and 15 [cm] in thick. The sessions on fire bricks and masonry pillars can be carried out using the same apparatus.

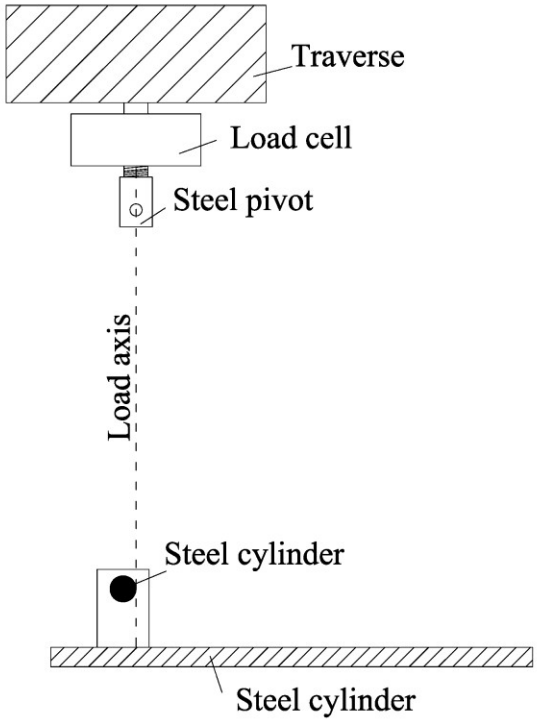

fig 2.jj - Cross section design 1; placement of the cylinder

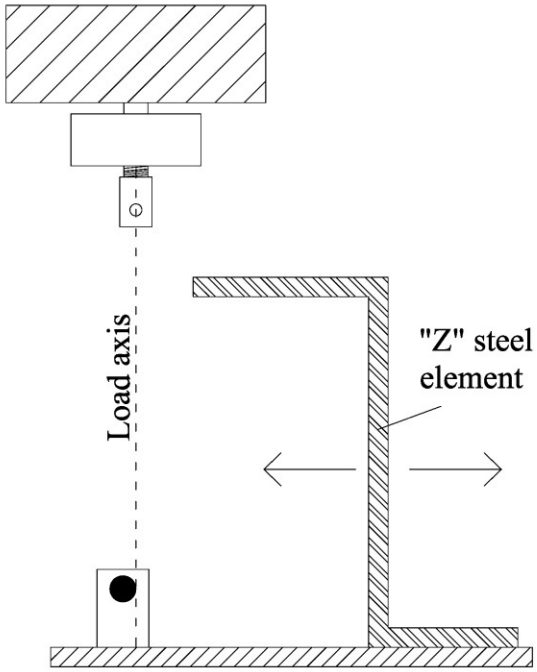

fig 2.kk - Cross section design 2; placement of "Z" element

The strength capacity of different "Z box" typologies have been tested using numerical analysis FEM (Finite Element Method). The material used to make up the apparatus is the steel "E24" (S235 of the Europeans norms); the property of this last are presented in *table 2.IX* [28][29].

Property at 20°C	ρ [kg/m^3]	E [Mpa]	ν	σ_y [Mpa]	σ_u [Mpa]
Steel E24 (S235)	7825	212000	0,28	170-235	340-510

table 2.IX - Mechanical property of the steel "E24" (S235) [28][29]

The preliminary numerical study (case 1) concerned the simple configuration of lock "Z" reproduced in the geometrical cross-section of *figure 2.ll* and in the 3D representation of *figure 2.mm*.

In the case 1 the 3D mesh (*fig. 2.mm*) of the steel element is characterized by the follows properties:

- It is subdivided in 22862 tetrahedrons
- The function shape of the elements is quadratic (9 nodes on each tetrahedron)

The mechanical properties of the solid are assigned equal to those of steel E24 (*table 2.IX*).

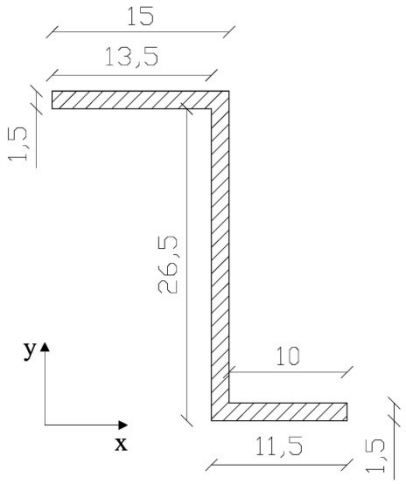

fig 2.ll - Cross section of "Z" contrast and referential axis in case 1

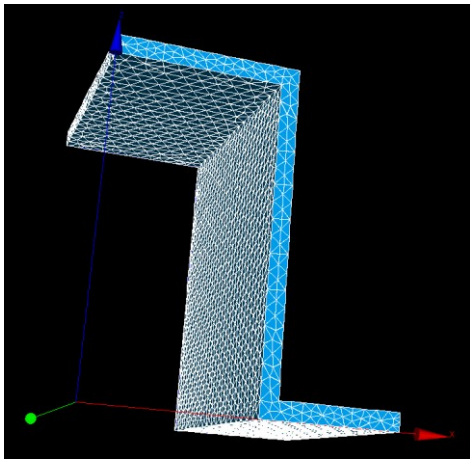

fig. 2.mm - 3D mesh of case 1

The boundary conditions that characterize the case 1 are described follow:

- A surface load L_s [MPa] is applied in the plane "A" on the direction y (*fig. 2.nn*). The stress L_s is equal to the maximum capacity of the Universal machine (50kN) divided by the surface of application (135 x 250 mm^2).

$$L_s = \frac{50000}{135 \times 250} = \frac{50000}{33750} = 1{,}48 \quad MPa$$

- The displacements of the surface "B" (*fig.2.oo*) are blocked.

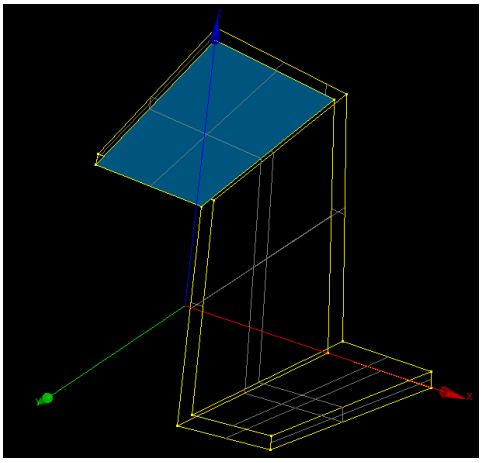

fig. 2.nn - The surface of load "A"

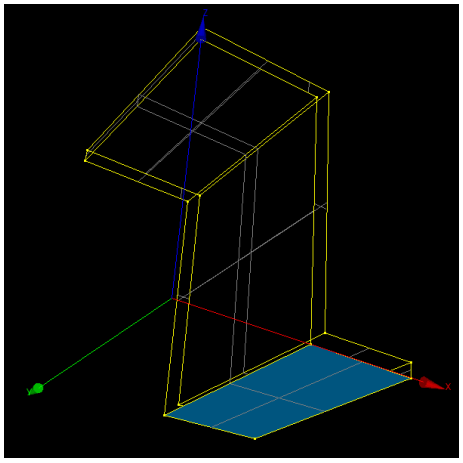

fig. 2.oo - The bonded surface "B"

Calculus have been made using Code_Aster where the material is assumed to exhibit an elastic behavior. The figure of the deformed shape (*fig. 2.pp*) and the images relative to the Van Mises

stresses σ_{id} (*fig.2.qq*) have been obtained by means of *Salome-Meca*. The maximum stress value considered admissible in this design study is the yield stress of steel E24 multiplied for a reduction coefficient equal to 0,9.

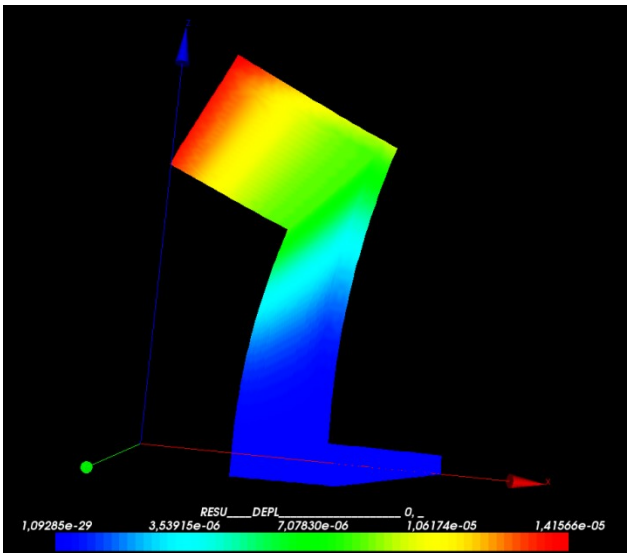

fig. 2.pp - The deformed shape of case 1

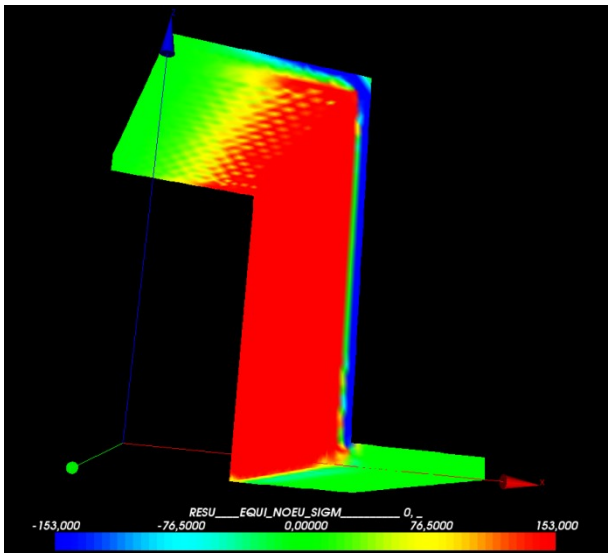

fig.2.qq - The Van Mises Stress; in dark red the zone where $\sigma_{id} > \sigma_{amm}$ and in dark blue the zone where $\sigma_{id} < -\sigma_{amm}$

$$\sigma_{amm} = \sigma_{yE24} \times 0{,}9 = 170 \times 0{,}9 = 153\ [MPa]$$

In the *image 2.qq* zones in red are the areas where $\sigma_{id} > \sigma_{amm}$ and in blue areas where $\sigma_{id} < -\sigma_{amm}$. It is evident that the system proposed in "*case 1*" require a reinforce.

The second step of the design process was to fasten in both the lateral sides of the Z element a steel plate. This last has been projected to not hide the lateral views of the specimen during the test. Moreover the steel reinforce plates are not linked to the "fix" late of the base but only to the Z "removable" element. The efficiency of this configuration of steel contrast, case 2 (*fig. 2.rr*), has been tested with a numerical analysis. The 3D mesh realized for this purpose is reproduced in *figure 2.ss*. The mesh is constituted by:

- 83332 tetrahedrons
- The function shape of the elements is quadratic (9 nodes each tetrahedron)

In this test the material's mechanical properties and the boundary conditions are equal to that assigned in "case 1". Therefore in the surface A (*fig. 2.tt*) has been applied a load L_s of 1,48 [MPa]

in the direction y and the surface B (*fig. 2.uu*) has been blocked imposing DX=DY=DZ=0. The behavior of the material has been supposed elastic (att. B).

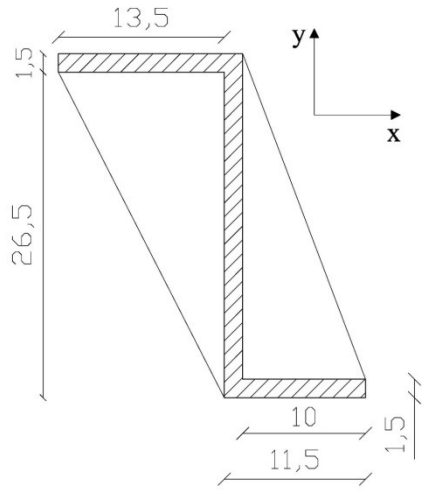

fig. 2.rr - Cross-section of the steel element in "case 2"

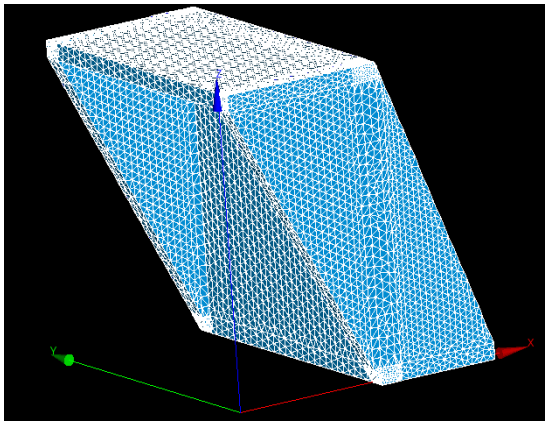

fig. 2.ss - Cross-section of the steel element in "case 2"

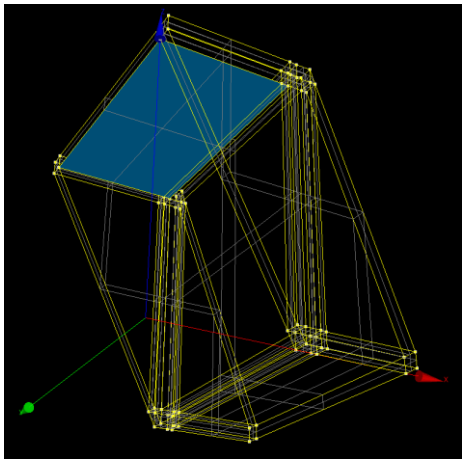

fig. 2.tt - The surface A in case 2

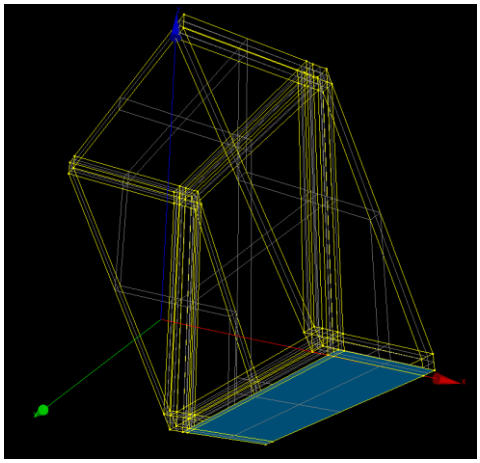

fig. 2.uu - The surface B in case 2

The deformed shape (*fig. 2.vv*) and the Van Mises stress distribution (*fig. 2.ww*) are shown herein. Results are sufficient to demonstrate that under the condition of case 2 the block element Z, reinforced with the steel lateral plates, preserve the elastic behavior. Indeed in *fig. 2.ww* there are not zones with $\sigma_{id} > \sigma_{amm}$ (dark red zones) and with $\sigma_{id} < -\sigma_{amm}$ (dark blue zones). However the steel block apparatus has been designed to be used for more typologies of specimen sizes and the numerical studies presented above reproduce only the cases when the contact surface between the specimen and the steel element is equal to the "surface A" (*fig. 2.nn* and *2.tt*). To understand if the

steel machine is sufficiently stiffen to resist to the worst load conditions, another case has been study (*case 3*). In this one the maximum load (50 kN) has been applied in direction y on the border of the steel contrast (*fig. 2.xx*) for a line 120 [mm] length; this case reproduce the extreme contingency when the sample is a fire brick (surface of contact 120x65 [mm^2]) characterized by imperfections that lead to a linear contact.

$$L_l = linear\ load = \frac{50000}{120} = 416{,}67\ \ \frac{N}{mm}$$

The Cross section, the 3D mesh, the material properties and the bonded surface B of the case 3 are the same to those of case 2 (fig. *2.rr, 2.ss, 2.uu*). The deformed shape (*fig. 2.yy*) and the Van Mises stresses distribution (*fig. 2.zz*) of case 3 has been obtained considering a elastic behavior of the "Z box".

Figure *2.zz* shows that the σ_{amm} is overcome by the σ_{id} in the top zone of the steel contrast plate and in the internal sides of the lateral steel reinforces (zones in dark red). In the same image, the dark blue zones underline the overcoming of the compressive admissible strength ($-\sigma_{amm}$).

To avoid the steel yielding in this critical zone a further steel plate 1,5 [cm] thick has been fastened on the superior extremity of the "*Z box*" (*fig. 2.aaa*). This configuration of steel contrast with the boundary condition of case 3 has been tested in case 4. The 3D mesh realized to study this case is presented in *fig. 2.bbb*. The mesh has been done by 55719 tetrahedrons characterized by a quadratic function shape.

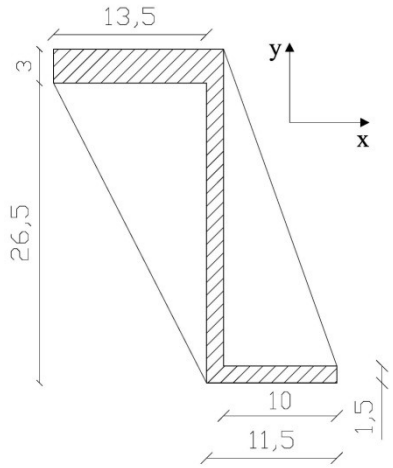

2.aaa - Cross-over section of case 4

2.bbb - 3D mesh representation of case 4

The material properties (E, v) and the boundary condition (L_l , bonded surface B) of the case 4 are the same as those of case 3. The deformed shape and the Van Mises stress distribution of case 4 are presented in figures *2.ccc* and *2.ddd*.

The image of the σ_{id} distribution shown that the geometry of the Z steel contrast analyzed in case 4 is sufficiently rigid to avoid the yielding of the metal material. In the submittal central part of the steel contrast and the internal superior sides of the lateral reinforces the values of σ_{id} (Van Mises criterion) are close but not exceeding the σ_{amm}.

The numerical analysis executed have permitted to validate that the steel contrast configuration of case 4 is the more appropriate to reproduce the boundary condition of fig. *fig. 2.a*.

Finally, the steel apparatus designed is composed by:

- a support steel plate bolted on the universal machine
- a steel smooth cylinder linked to support plate
- a steel element (with a "Z" shape) bolted on the support plate. It has the same geometrical property of the configuration reproduced in case 4 (*fig. 2.aaa*).

[mm] ***Deformed Shape*** / ***Van Mises Stress Distribution*** ***[MPa]***

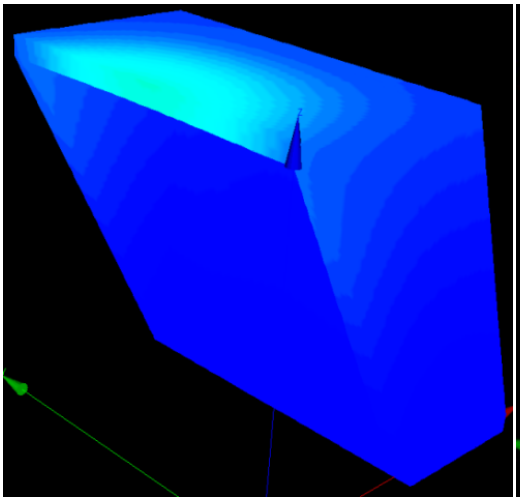

fig. 2.vv - Deformed shape of case 2

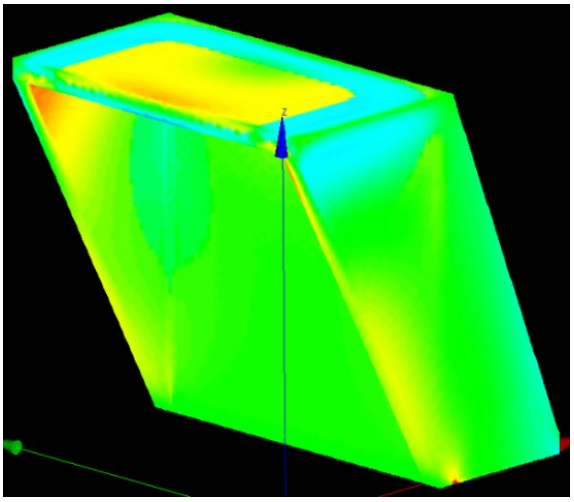

fig. 2.ww - Van Mises stress distribution of case

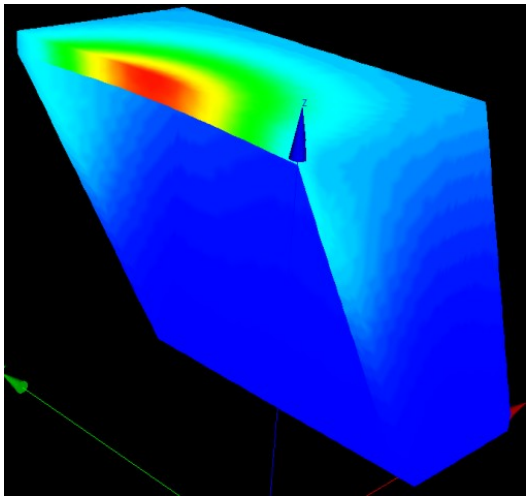

fig. 2.yy - Deformed shape of case 3

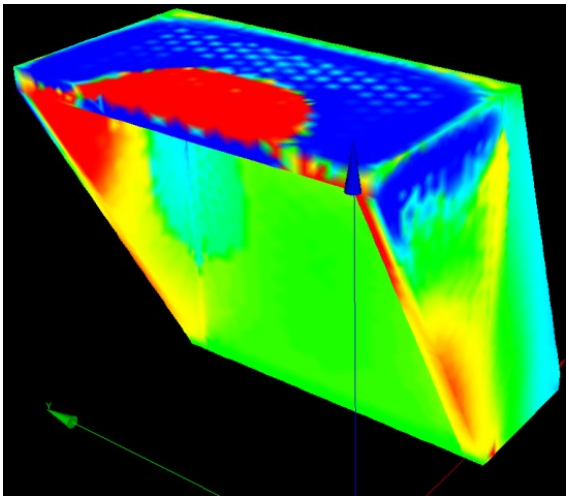

fig. 2.zz - Van Mises stresses distribution of case 3

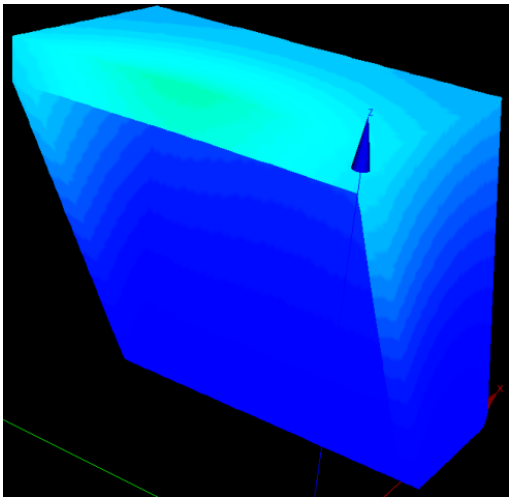

fig. 2.ccc - Deformed shape of case 4

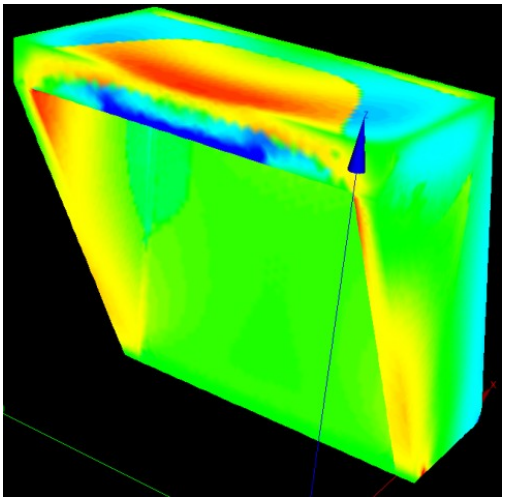

fig. 2.ddd - Van Mises stress distribution of case 4

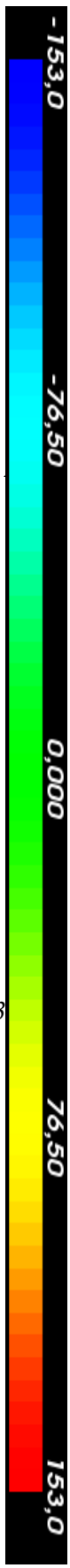

2.2.4.1.2 - Realization process

To actualize the design described in the previous paragraph several devices were adopted. The apparatus is assembled by 10 different pieces. All the pieces are connected by bolt steel joints. The bolts used are made in steel A2 with a diameter of 8 [mm] and 10 [mm] (*table 2.X*).

The cylinder is made in steel and it's built in two steel supports (*fig. 2.fff*). These last are fastened to the steel plate and they could be displaced unscrewing bolt joints. This particular permit to study in the future also the cases with a offset in the load axis position [6].

The steel Z element is fastened on the support plate; two linear openings in the base of the "Z box" function as "rails" to displace back and forth the movable apparatus (*fig. 2.ggg*). To fix the steel Z element it's simply necessary to tighten the bolts that cross the support and the openings (*fig. 2.hhh*).

The superior plate of 3 cm in thickness designed has been realized overlapping two 1,5 [cm] plate, both fastened to the lateral steel reinforces (*fig. 2.iii*). These last have been realized in an industrial factory (*fig. 2.jjj*).

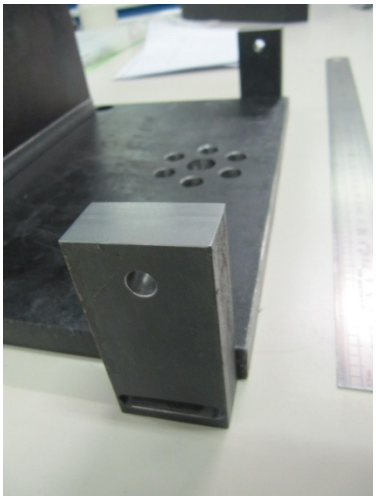

fig. 2.fff - The smooth steel cylinder built in the supports

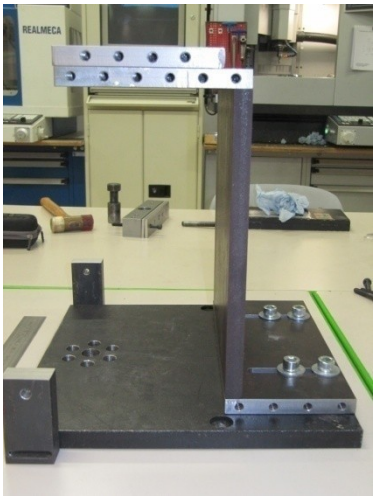

fig. 2.ggg - The linear openings ("rails") present in the base of the Z element

fig. 2.hhh - The bolt joints between the steel support and the Z box.

fig. 2.iii - The two 1,5 [cm] plates overlapped to reinforce the contrast

figures 2.jjj - The lateral reinforces of the "Z box"

2.2.4.1.3 - Stiffness test

The stiffness of the steel apparatus has been measured during a laboratory test that reproduce a experimental load history. The load has been applied to the steel contrast using the superior surface of a laboratory tongs (fig. *2.kkk*); this choice has permitted to realize the test without the making of others pieces. The surface of charge is equal to 40x90 mm^2 and it's almost identical to the submittal surface of the fire brick specimen (120x65 mm^2). The load has been applied increasing the charge of 1 kN at each step, for ten steps.

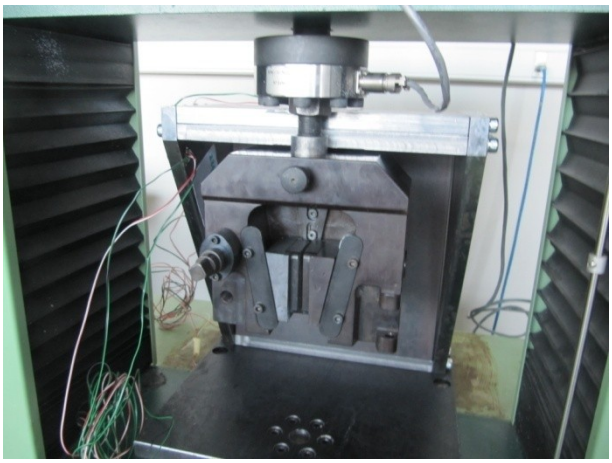

fig. 2.kkk - Boundary conditions of the stiffness test

Two strain gauge rosettes were been used to measure the strain in the more loaded zones of the apparatus; the location and the direction of the strain gouges has been defined using the numerical analysis (red zone in *fig. 2.ddd*). More specifically the rosettes are bonded onto the contrast steel plate (strain gauges 1) and onto the internal side of the lateral steel reinforce (strain gauges 2) (*fig. 2.lll*).

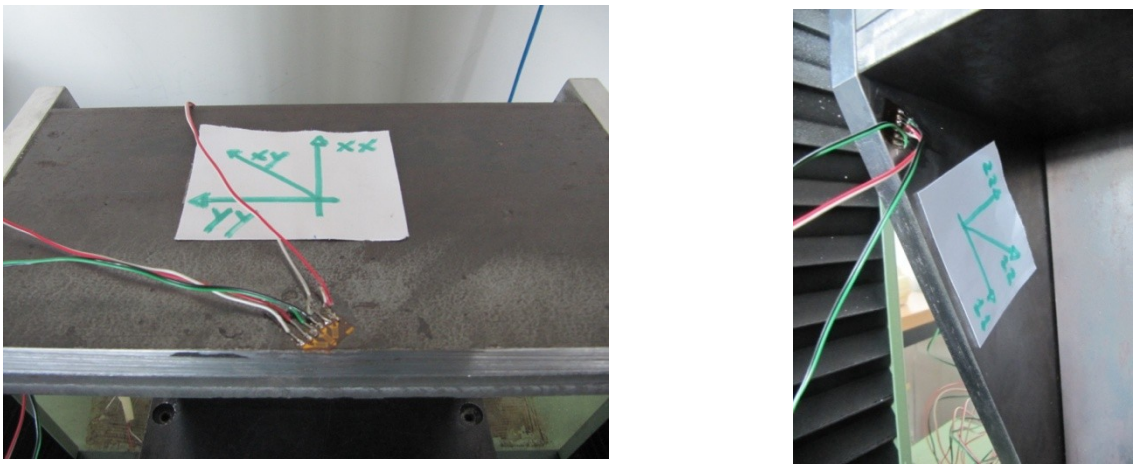

fig. 2.lll - The strain gauge rosettes applied on the critical points of the apparatus. In the images are framed on the left the gauges 1 and on the right the gauges 2. Moreover the name of the axis is shown

From each rosette it has been obtained the value e_x, e_y and e_{xy}. To obtain the strains the follows equations have been used.

$$\varepsilon_{xx} = e_x \,, \quad \varepsilon_{yy} = e_y \,, \quad \varepsilon_{xy} = e_{xy} - \frac{1}{2}\ e_{xx} + e_{yy} \tag{2.2}$$

The value of ε_{zz} is obtained using the Lamé coefficients (μ,λ):

$$\varepsilon_{zz} = -\frac{\mu}{2\mu+\lambda}\ \varepsilon_{xx} + \varepsilon_{yy} \tag{2.3}$$

Known the strain values, the tensor of stress could be obtained using the follows constitutive equations:

$$\sigma_{xx} = \lambda\ \varepsilon_{xx} + \varepsilon_{yy} + \varepsilon_{zz}\ + 2\mu\varepsilon_{xx} \quad (2.4)$$
$$\sigma_{yy} = \lambda\ \varepsilon_{xx} + \varepsilon_{yy} + \varepsilon_{zz}\ + 2\mu\varepsilon_{yy}$$
$$\sigma_{yx} = \lambda\ \varepsilon_{xx} + \varepsilon_{yy} + \varepsilon_{zz}\ + 2\mu\varepsilon_{yx}$$
$$\sigma_{zz} = \sigma_{zx} = \sigma_{zy} = 0$$

The value of σ_{zz} is equal to zero because the strain gauges is bonded upon a no charged surface. Using the tensor stress components is possible to calculate the Van Mises Stresses (σ_{id}).

The Van Mises stress σ_{id}, obtained for 10 kN load, has been multiplied by 5 and compared with the σ_{amm} to verify that the admissible stress of the apparatus is not reached even when the universal machine apply his maximum load (50kN).

The strain and the stresses values obtained in the stiffness test are shown in the *tables 2.XI* and *2.XII*.

	Strain gauges 1							[MPa]	[MPa]	[MPa]	[MPa]
L [kN]	1_e_{yy}	2_e_{xy}	3_e_{xx}	ε_{yy}	ε_{yx}	ε_{xx}	ε_{zz}	σ_{yy}	σ_{yx}	σ_{xx}	σ_{id}
1	0,00000018	0,00000015	-0,00000007	0,00000018	0,000000095	-0,00000007	-3,36111E-08	0,04	0,02	0,00	**0,06**
2	0,00000037	0,00000032	-0,00000016	0,00000037	0,000000215	-0,00000016	-6,41667E-08	0,08	0,05	-0,01	**0,12**
3	0,00000057	0,00000049	-0,00000025	0,00000057	0,00000033	-0,00000025	-9,77778E-08	0,12	0,08	-0,02	**0,19**
4	0,00000077	0,00000067	-0,00000034	0,00000077	0,000000455	-0,00000034	-1,31389E-07	0,16	0,11	-0,02	**0,25**
5	0,00000098	0,00000085	-0,00000044	0,00000098	0,00000058	-0,00000044	-0,000000165	0,20	0,14	-0,03	**0,32**
6	0,0000012	0,000001	-0,00000053	0,0000012	0,000000665	-0,00000053	-2,04722E-07	0,25	0,16	-0,04	**0,39**
7	0,00000138	0,00000117	-0,00000062	0,00000138	0,00000079	-0,00000062	-2,32222E-07	0,28	0,19	-0,05	**0,45**
8	0,00000156	0,00000132	-0,00000071	0,00000156	0,000000895	-0,00000071	-2,59722E-07	0,32	0,21	-0,06	**0,51**
9	0,00000177	0,00000147	-0,00000081	0,00000177	0,00000099	-0,00000081	-2,93333E-07	0,36	0,23	-0,06	**0,57**
10	0,00000196	0,00000162	-0,00000091	0,00000196	0,000001095	-0,00000091	-3,20833E-07	0,40	0,26	-0,07	**0,63**

table 2.XI - The strain and stress values calculated using the strain gauges 1

Strain gouge 2							[MPa]	[MPa]	[MPa]	[MPa]
e_{11}	e_{12}	e_{22}	ε_{yy}	ε_{yx}	ε_{xx}	ε_{zz}	σ_{yy}	σ_{yx}	σ_{xx}	σ_{id}
0,0000012	0,0000006	-0,0000008	0,0000012	0,0000004	-0,0000008	-1,22E-07	0,23	0,10	-0,10	**0,34**
0,0000028	0,0000013	-0,0000015	0,0000028	0,00000065	-0,0000015	-3,97E-07	0,56	0,20	-0,15	**0,74**
0,0000044	0,0000022	-0,0000022	0,0000044	0,0000011	-0,0000022	-6,72E-07	0,89	0,34	-0,20	**1,17**
0,000006	0,0000029	-0,000003	0,000006	0,0000014	-0,000003	-9,17E-07	1,21	0,45	-0,28	**1,58**
0,0000076	0,0000036	-0,0000037	0,0000076	0,00000165	-0,0000037	-1,19E-06	1,54	0,56	-0,33	**1,98**
0,0000093	0,0000044	-0,0000045	0,0000093	0,000002	-0,0000045	-1,47E-06	1,89	0,68	-0,39	**2,42**
0,0000109	0,0000052	-0,0000053	0,0000109	0,0000024	-0,0000053	-1,71E-06	2,22	0,81	-0,47	**2,85**
0,0000125	0,0000058	-0,000006	0,0000125	0,00000255	-0,000006	-1,99E-06	2,55	0,90	-0,52	**3,24**
0,0000141	0,0000066	-0,0000066	0,0000141	0,00000285	-0,0000066	-2,29E-06	2,88	1,02	-0,54	**3,65**
0,0000156	0,0000071	-0,0000074	0,0000156	0,000003	-0,0000074	-2,51E-06	3,18	1,10	-0,63	**4,02**

table 2.XII - The strain and stress values calculated using the strain gauges 2

The graphics Load-σ_{id} presented herein (*fig. 2.mmm*) underline that the stresses increase linearly with the applied load. The stresses measured by the strain gauges 1 at L=10 [kN] are almost ten times smaller than those of strain gauges 2. Moreover the σ_{id} at 50 kN obtained in the two analyzed points are much smaller than the σ_{amm}.

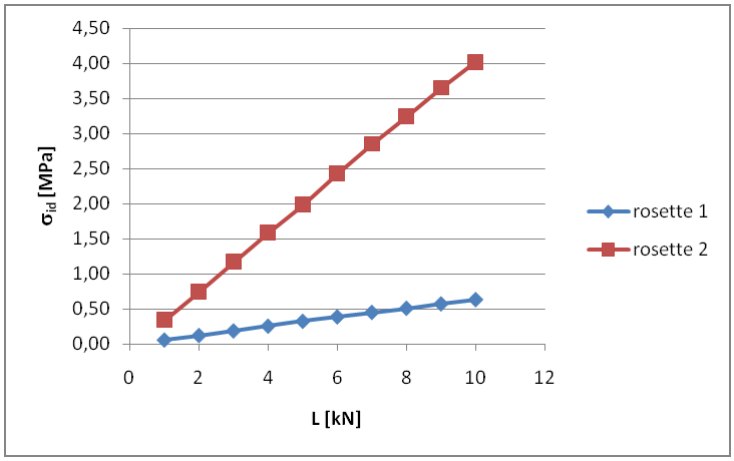

fig. 2.mmm - The graphic L - σ_{id} (Load – Van Mises stress) obtained in the point 1and 2

The stresses values calculated by means of the stiffness test have the same sign of those of numerical analysis (case 4) but a different order of magnitude. The reasons that could justify these results are:

- The apparatus is composite of more steel piece jointed by bolts. The numerical study has been made considering a monolithic element in steel.

- In the numerical case 4, the load is applied in the extreme border of the steel contrast; in the stiffness test the charge is distributed on a surface.
- The boundary condition supposed in the numerical study are not perfectly identically to the real condition. Moreover the universal machine don't give a rigid support under the surface B.
- The strain gauges rosette 1 is bonded onto the superior of the two contrast plates 1,5 [cm] thick (*fig. 2.iii*). This particular should be empathized because the load is applied in the inferior plate and the two steel elements are only overlapped and fastened to the lateral reinforces.

2.2.4.2 The steel tongs

A steel system has been designed to pick up the carbon fabric and to applied the load on the specimens. Some considerations have been taken into account for the project:

- The carbon tissue is constituted by unidirectional fibers difficult to grip
- The fabric free extremity of each specimen must be assembled in the grab system before the test and removed after the experiment.
- The roughness on the surface of brick could cause a non perfectly alignment between the surface of CFRP and the carbon fabric grabbed. This distortion may cause a peeling stress concentration.

Therefore the mechanical apparatus designed must carry out the follows task:

- Grab the carbon fabric avoiding any slipping
- Connect the load cell to the carbon fabric
- Place the carbon fabric in one of the sheaf of planes with axis the "load axis".
- Simplify and speed the experimental phases of assembly and disassembly.
- Permit a rotation of the grab system around the load axis to reduce the peeling stress concentration.

The solution adopted to grab the fibers is bond the carbon fabric around a steel plate and connect this last to the load cell using two metallic jaws.

The steel plate used to bond the fibers is not a simply parallelepiped (*fig. 2.nnn and 2.ooo*), it has an external perimeter of 110x90 [mm] and a thickness of 5 [mm]. In his bigger surface a slot of 5x10 [mm^2] is present. Moreover in one side of the plate a grove of 5x10 [mm^2] by 1 [mm] of thickness has been realized. One perimeter border of the plate, and one side of the slot have been rounded.

The steel plate just described has named “@” because the fiber fabric rounding the metallic element generate a shape similar to the symbol @.

fig. 2.nnn - The steel plate @; planes and cross section

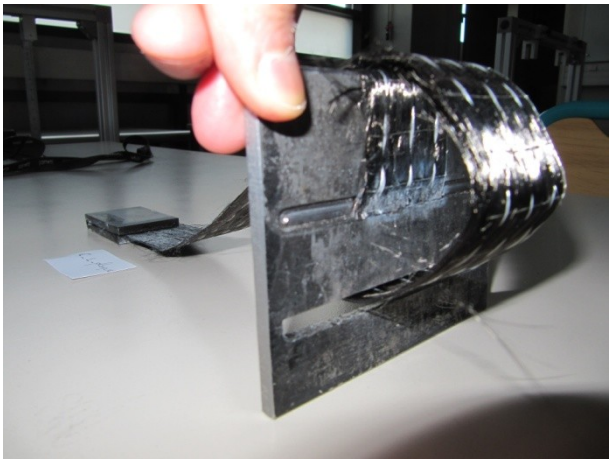

fig. 2.ooo - The steel plate @

The @ plate is blocked by two movable jaws realized in steel. These ones are bolted symmetrically to two metallic elements placed in the center longitudinal plane of the apparatus and connected to a horizontal steel parallelepiped (*fig. 2.ppp and 2.qqq*). This last is directly fastened to the load cell by a steel pivot. This cylindrical element is free to turn around its own axis.
The mechanical apparatus described above has two plane of symmetry, longitudinal and transversal, that intersect a point crossed by the load axis. The carbon fabric is collocated in the longitudinal plane.
The use of the @ plate permits to place the carbon tissue in the correct plane easily and quickly. All the adhesive procedures not interest the steel apparatus but only the movables plates. This device has permitted to assemble the grab dispositive with simple actions; moreover the realization of 4 @ plates has permitted to prepare more specimen in the same time.
The rotational degree of freedom of the load pivot has been provided to reduce the peeling stress concentration.

fig. 2.ppp - The horizontal piece realized to join the jaws to the

fig. 2.qqq - The steel tongs disassemble

The grab system is composed by 16 steel pieces. All the joints of the apparatus have been done by bolts.

2.2.4.3 Test machine; a global view

The test machine is composed by two part realized using an assemblage of steel pieces;

- a lock system
- a grab system

The *figure 2.sss* shows a frontal and a lateral view of the mechanical system achieved to reproduce Near End Single shear tests (*fig. 2.a*).

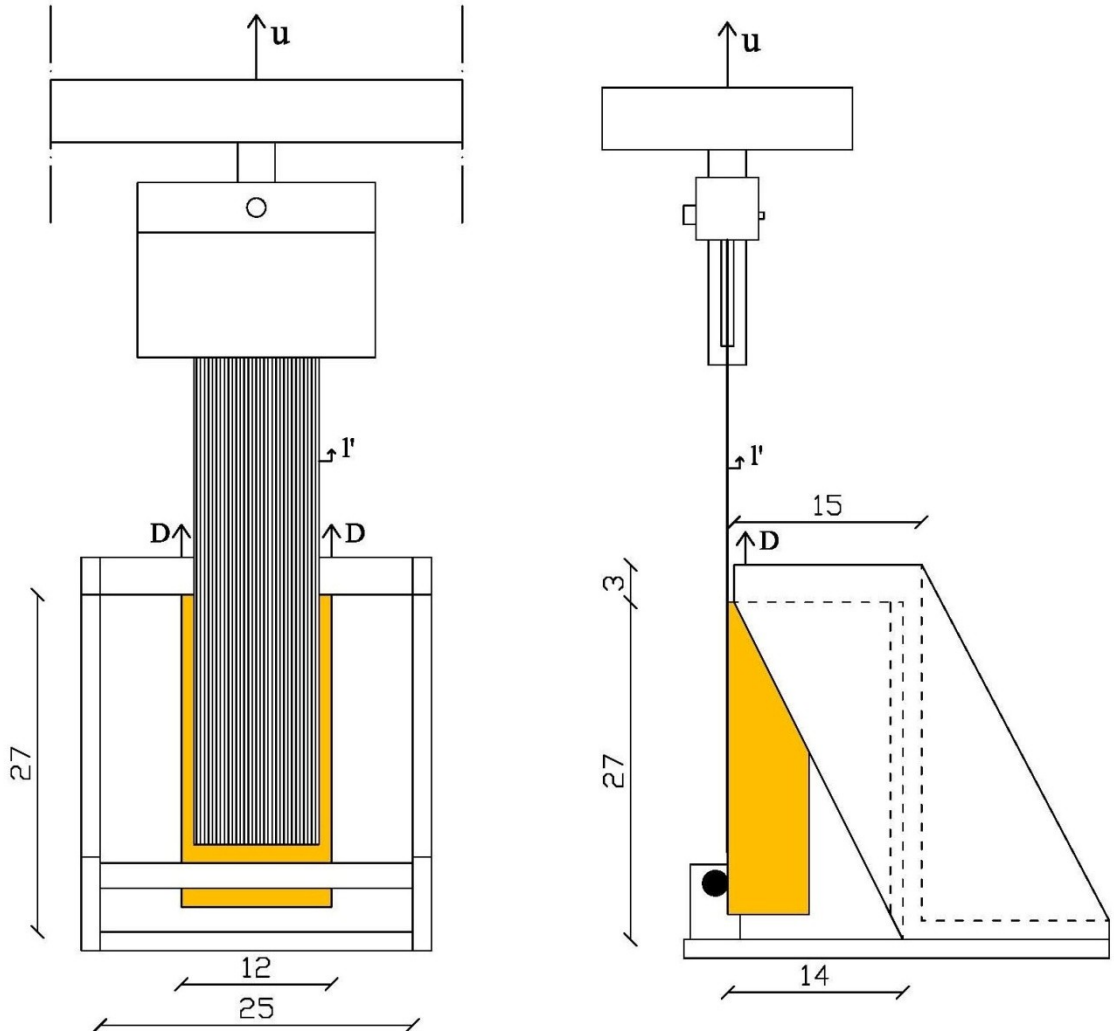

fig. 2.sss - Frontal and lateral view of the mechanical system realized (measures in [cm])

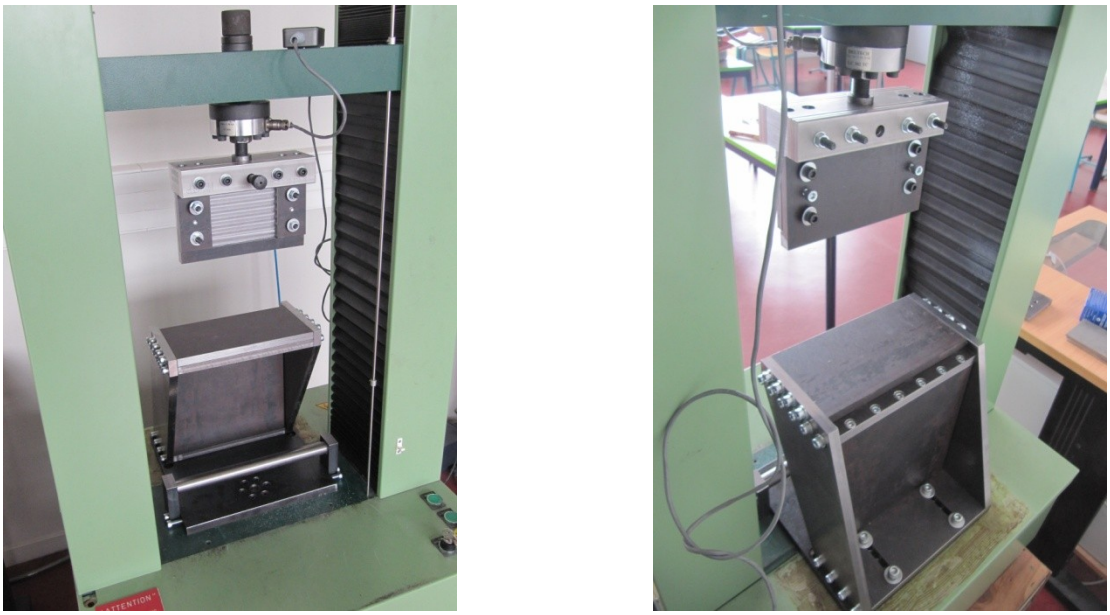

fig. 2.ttt - The steel apparatus assembled in the universal machine

2.2.5 Specimen installation

The specimen is posed in the suitable position, ready to be tested, using a fixed procedure. The phases and the devices used during the preparation and placement of the samples are described in the following.

In the first step of preparation, the dry extremity of the fiber fabric is rolled and bonded around the steel plate @. It's important to underline that the specimens has been made with a longer carbon fabric (around 75 cm); only 18 cm of this last are bonded to the fire brick (CFRP). This particularity is important because the rolling process around the plate "@" require a long strip. Indeed, the free extremity of the carbon fabric was passed inside the slot of the plate, turned around the perimeter blunt border of @ and bonded inside the grove present on the steel surface by a quick-setting glue (phase 1 of *fig.2.uuu*). After the fixation of the carbon fiber extremity, an epoxy resin is applied on the surface of the plate and the fabric is stretched and posed on the support. This process occurs rounding and bonding the fibers on the plate and on the fabric itself (*fig.2.uuu*). Finished the gluing phases the specimen connected with "his" plate was left in a particular position to have the drying of the adhesive with a perfect overlap of the fabric to the steel support. Specifically a simple device was been conceived to blocked the plate without touching the wet surface of adhesive; the fire brick was placed on a table, the plate was laid on the lateral corner of the table blocked and stretched by a belt (*fig. 2.vvv*). All the specimens were tested minimum twenty four hours after the gluing of the tissue on the steel plate @. The epoxy resin used in this step is named "Sikadur 300" and it's a 2-components impregnation resin produced by Sika [30].

When the specimen is bonded to the plate @, it is ready to be placed inside the steel apparatus. As mentioned previously, in this experimental session specimens of two size have been tested: the first typology has dimensions 250x120x65 [mm^3] (single fire-brick) and the second one has dimensions 250x120x130 [mm^3] (two fire-brick bonded together). The specimens of small size (series T0) were been inserted in the steel apparatus without any displacement of the "Z" steel element. In this case, to place the movable lock at the correct distance from the cylinder (140 mm) a template of 140x200x100 [mm^3] has been utilized (*fig. 2.www*). After that the specimen was insert in the space between the cylinder and the Z box.

To insert the specimens of big size it was necessary to unscrew 3 of the 4 bolts that fasten the Z lock with the support steel plate and displace the box as shown in *figure 2.xxx*. After placing of the sample the element of lock is reassembled, the distance of 140 [mm] between the Z and the cylinder is assured by the use of two templates of 70x140x40 [mm^3] (*fig. 2.yyy*).

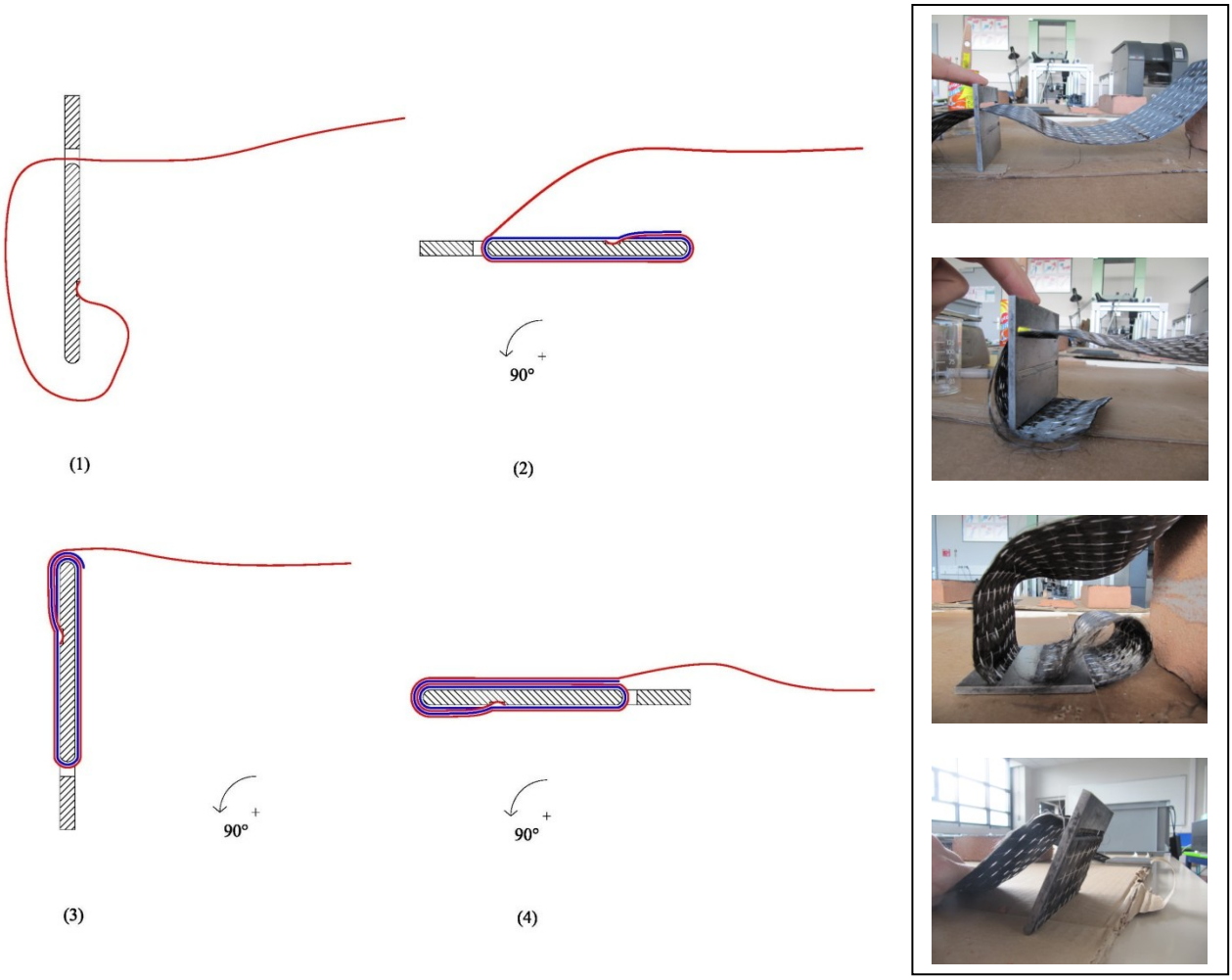

fig. 2.uuu - The fiber carbon to steel plate @ bonded phase; in red the fiber fabric and in blue the adhesive layer. On the right some photos of the procedure.

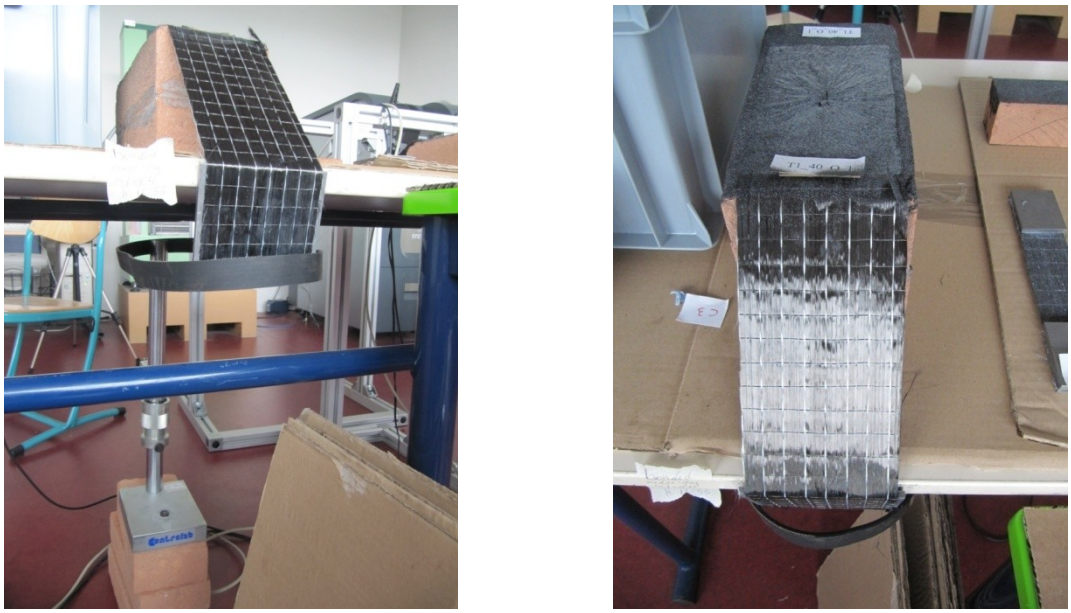

fig. 2.vvv - The device to stretch the fibers and block the plate without touch the adhesive

fig. 2.www - The alignment of the Z box with the template of 140x200x100 (cases T0)

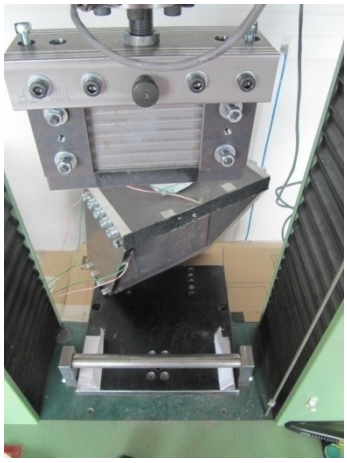

fig. 2.xxx - The alignment procedure of the Z box during the insertion of big size specimens

It's important to underline that the internal face of the cylinder is in perfect alignment with the load plane (*fig. 2.www*); to simplify the correct placing of this element a design 1:1 with the trace of the load plane is bonded on the surface of the steel support plate. The cylinder has been aligned to the trace before the starting of the experimental session; his position has been maintained fixed during all the tests.

After insertion of the specimen between the locks, the reinforced face of the fire brick was propped on the central part of the steel cylinder (*fig.2.yyy*).

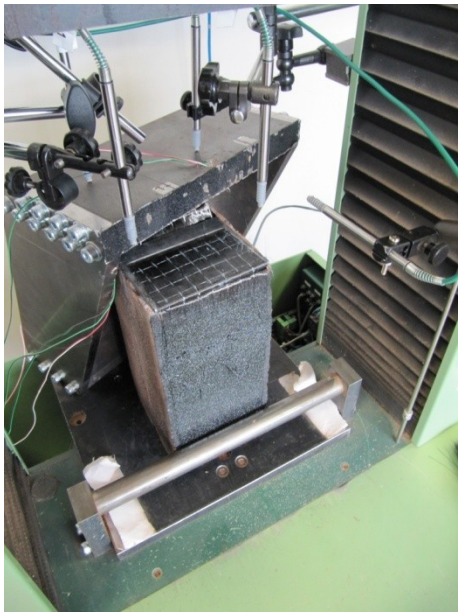

figures 2.yyy - The insertion of the specimen inside the contrast apparatus (photo on the left) and the reassembling of the Z steel contrast using the two templates 70x140x40)

The installation of the steel plate @ inside the grab system is the next phase of the procedure. To allocate the element @ inside the grab one jaw is disassembled (*fig. 2.zzz*); the other create a cavity where the plate is to place (*fig. 2.aaaa*). After the collocation of the steel plate the grab system is assembled again (*fig. 2.bbbb*).

During the last phase of the specimen placement the traverse of the universal machine is raised and, consequently, the grab system pick up the carbon fabric. When the sample touches the horizontal steel contrast the displacement of the traverse is stopped. Particular attention has been done to place the specimen in the correct position, with a distance between the fibers and the lock border of 5 [mm] (*fig. 2.cccc*). An image of the specimen placed in the test apparatus is shown in *figure 2.dddd*.

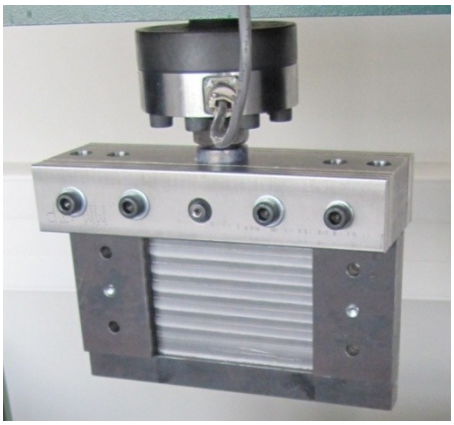

fig. 2.zzz - The configuration of the grab system disassembled

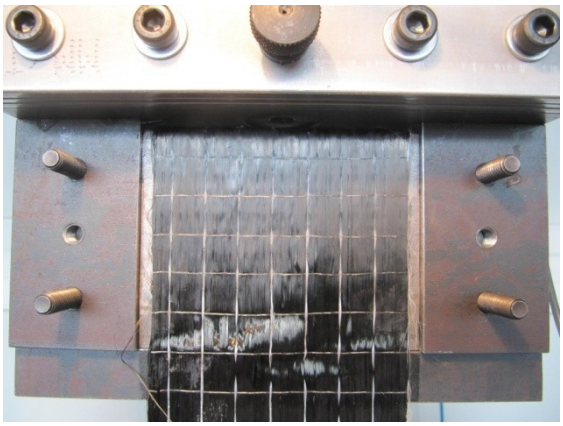

fig. 2.aaaa - The steel plate @ inserted in the jaws cavity

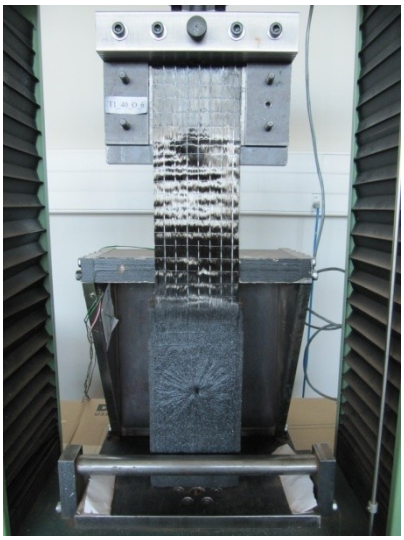

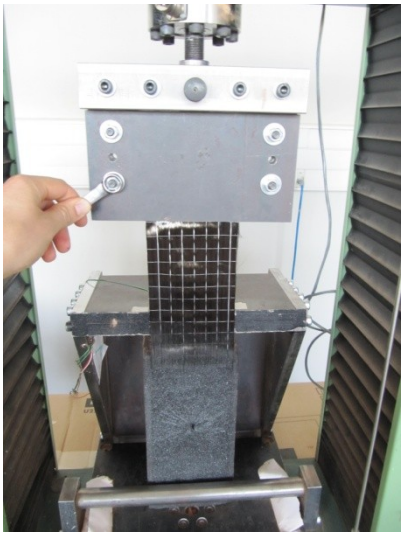

Figures 2.bbbb - The steel grab reassembling and the @ plate clamping; three steps of the procedure

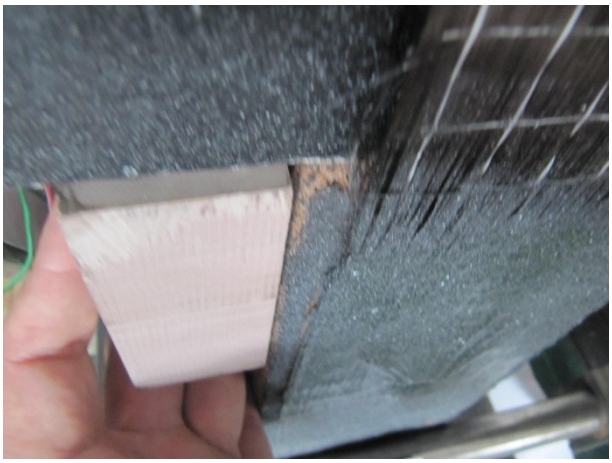

fig. 2.cccc - The template used to verify the 5[mm] distance between the fiber and the border of contrast

fig. 2.dddd - The specimen placed in the apparatus of test

2.2.6 Test procedure; instrumentation and load history

The instrumentation posed on the universal machine is composed by a load cell of 50 kN and a displacement transducer. The first one permits to quantify the load apply to the system, the second one measure the displacement of the traverse.

A set of comparators is posed over the submittal surface of the steel lock Z to evaluate the displacement related to the stiffness of the metallic system (*fig. 2.eeee*).

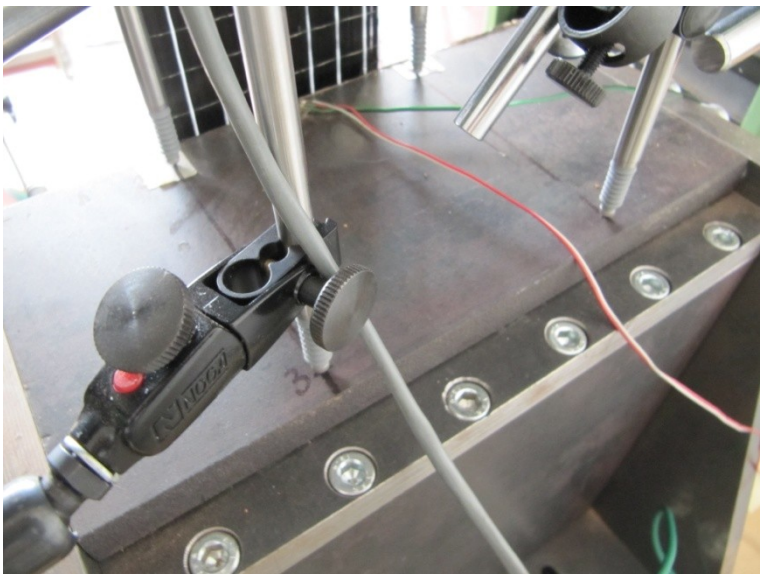

fig. 2.eeee - The comparators displaced on the steel contrast

A digital photo camera is positioned in front of the reinforced face of the specimen, at environ 1,20 [m], to take the necessary pictures to calculate the displacement and strain fields on the CFRP surface (Digital Image Correlation) (*fig. 2.ffff*).

The reinforced surface of all the samples is characterized by a white texture over a black paint cover; the details related to this pretreatment (motivations and technical procedure) are described in the Chapter 3 on the Digital Image Correlation. More devices have been developed to regulate the light in the test zone; specifically a screened system has been designed to augment the contrast of the white texture.

A digital video camera has been placed close the specimen to film the crack advancement and the sample failure from a 45° view (a lateral and a frontal face of the specimen have been framed) (*fig. 2.ffff*). The film of each test permit to define the failure mode and to register the noisy connected to the energy dissipation during the crack advancement. A foil of Plexiglas has been interposed between the video camera and the specimen to avoid a damage of the lens during the fragile failure of the reinforced fire bricks (*fig. 2.hhhh*).

figures 2.ffff - Photo and video camera placement during the tests

fig. 2.hhhh - The Plexiglas foil interposed between the video camera and the specimen

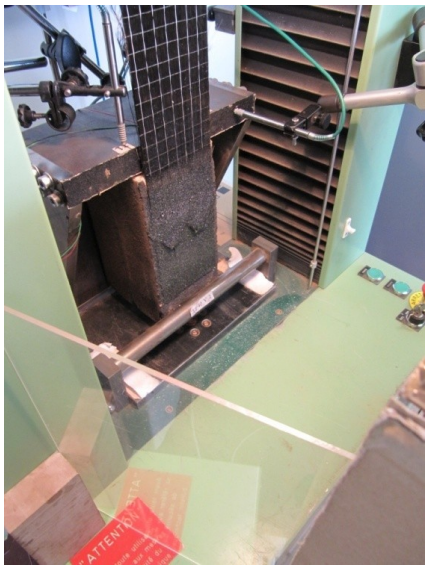

fig. 2.iiii - The cover used to eliminate the reflections on the Plexiglas surface

During the test the load has been applied displacing the traverse of the universal machine at a constant rate of 0,2 mm/min (*fig. 2.jjjj*). A succession of load steps of Δu=0,2 [mm] have been applied. Between the steps a delay of 0,5 [min] has been provided to take photos and to read the values from the comparators. The universal machine Deltalab register the value of the traverse displacement [mm] and the load apply to the system [kN] at each second [s] of test. The video camera film the experiment from the start of load story to the finish.

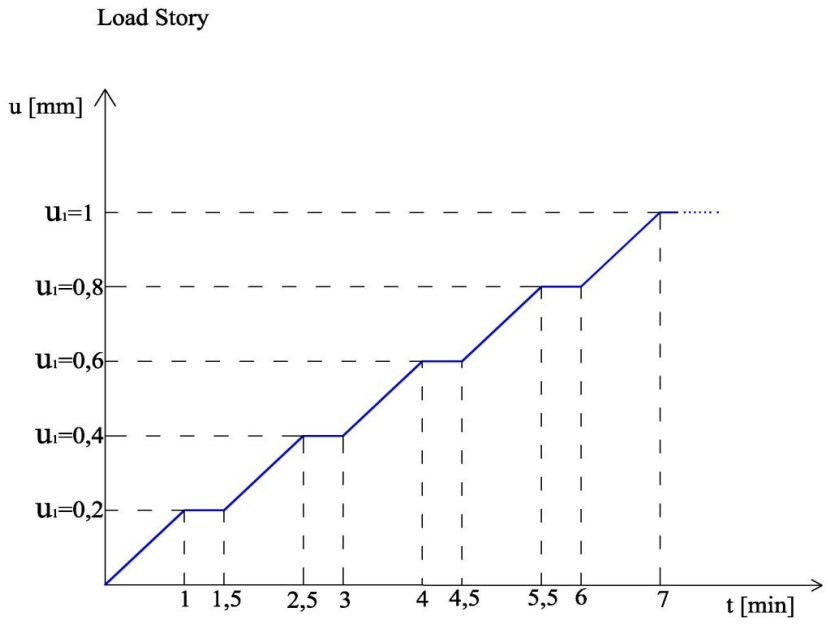

fig. 2.jjjj - The load story in a graph time – traverse displacement

During the crack advancement, denounced by a high damage noise, additional photos have been made. To collocate in the time the name of these photos a PC screen recording software has been used. This one frame the desktop of the computer where the photo saving operations occur juxtaposed a test video timer (*fig. 2.kkkk*).

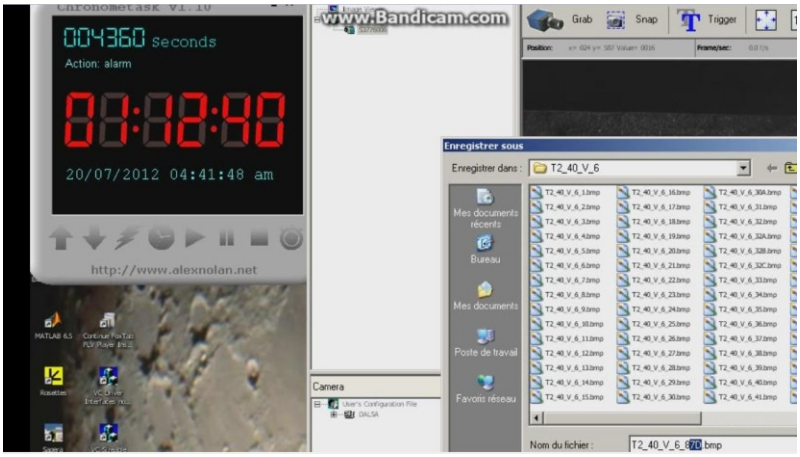

fig. 2.kkkk - A frame of the desktop during the PC screen recording; in the left side the timer and in the right side the photo camera software

Schematically during the tests have been registered:

- L [kN] - for each second of test (software DELTALAB)
- u [mm] – for each second of test (software DELTALAB)

- digital photo by "…"(file *.jpeg) – for each delay of load (software camera)

- digital photos by "…" (file *.jpeg) – during the last phases of the crack advancement, between the delay (software camera)

- PC screen recording (file *.MPG) – during the last phases of the crack advancement, between the delay (software Bandicam)

- D [mm] – displacement of the steel contrast (comparators)

- Film video (file *.MPG) – during all the test, from start to finish (video camera)

- photos by normal photo camera (file*.jpeg) – during all the test procedure

Chapter 3

The strain field analysis by Digital Image Correlation

3 The strain field analysis by Digital Image Correlation

The Digital Image Correlation (DIC) is an appealing Optical methodology developed in the eighties to estimate the displacement and strain fields. This chapter presents the motivation that justifies the use of this technique in the framework of the Civil engineering and, specifically, in the NES single shear test session carried out in this research study. A general description of the principles and of the method and advantages of the DIC is presented in the *paragraph 3.1*. Subsequently the technical characteristics of the CCD cameras and the constitutive properties of the digital photos are exposed (*par. 3.2*). The description of the DIC method and the discussion about the algorithm used in the thesis experimental studies are presented in *paragraphs 3.3* and *3.4*. After, the procedure to carry out the necessary speckle pattern onto the sample surface is shown (par. 3.5). The speckle pattern onto the firebrick reinforced specimen, the position of the CCD camera, the light exposition and the CORRELI parameters to use for the NES single shear test have been defined by a study case (*par. 3.6*). Specifically, several traction tests on rubber strips have been implemented to study the quality of the displacement and strain fields obtained by DIC. The last paragraph, the *3.7*, defines the procedure and the parameters used in the NES single shear test session to carry out the digital image correlation.

3.1 A optical measurement technique to study the 2D displacement and strain field

Usually, to estimate the two-dimensional strain fields of specimens subjected to applied load, strain gauges are glued onto the surface of the samples. When the object is deformed the gauges permit to measure an electrical resistance change; multiplying this last by a specifically gauge factor it's possible to quantify the strain. The traditional methodology just described consent to obtain only local value of deformation. The strain gauges could be attached only on flat and smooth surface.

In the last decades, to study the strain fields, a new method based on the optical measurement techniques has been developed; the Digital Image Correlation (DIC) [31][33]. This technique has been used frequently in the mechanical laboratory and, only in recent years, some application have been realized in the Civil engineering framework [34][40][41][42].

The digital image correlation permits to calculate the displacement field of the surface of interest matching pictures taken during the test. The photos must be realized by a Charge-Coupled Device (CCD) camera. The digital images carry out by this instrument are constituted by a chessboard of squares (pixels), each one characterized by a monochromatic color. Before the test, the surface of interest must be treated with paint cover to realize a "texture" (speckle) of clean-cut chromatic points. Each photo used for the digital image correlation corresponds to an applied load. The displacement field could be calculated matching the photos using a cross-correlation function that

can be solved in physical space or in Fourier space [35][36][37][39]. In the last years different approaches were been developed to identify the displacement field comparing two different digital images; within those a finite element approach has been adopted by Besnard G. et al. [38].

The use of the DIC leads to several advantages: 1) It permits to obtain the displacement and strain field. 2) All the surface of interest covered by the chromatic texture could be analyzed. This particular is fundamental when the zone of the strain and damage localization is not known a priori and the single measurement devices (strain gauges, extensometer…) are difficult to positioned [39]. 3) The displacement field of heterogeneous surface could be obtained (for example the displacement between the CFRP sheet and the closer brick surface). 3) It permits to find the displacement between points that do not belong to the same surface (the displacement between the splay anchor and the CFRP sheet). 4) Having the photo camera instrumentation, the displacement and strain field analyze is very cheap.

Several studies have been realized applying the Digital Image Correlation in the shear test of CFRP to concrete bonded joint. Corr et al. (2006) [40] carried out an experimental study by NES single shear test using the DIC to analyze the displacement and the strain field over the reinforced surface of the specimens. The study was executed with cross correlation between each one of the photos taken during the loading phases and the reference picture taken in the unloaded phase. In [40] the relation (3.1) has been used to calculate the bond stress $\tau(x)$. In this last the strain values obtained by DIC are used.

$$\tau\ x\ = \frac{E_{CFRP} A_{CFRP}\ \varepsilon_{i+1} - \varepsilon_i}{b_{FRP} \Delta x} \tag{3.1}$$

Where:

E_{CFRP} = Young modulus of the composite

A_{CFRP} = Cross sectional area of the composite

b_{FRP} = the CFRP width sheet

Δx = the distance between the zone (i+1) and i

The (3.1) requires some assumption; the support is rigid in comparison to the reinforcement and the CFRP has an elastic behavior. The photos used for the correlation have been taken with a period of 1 second between each image. The results obtained by Corr et al. shown the displacement of the stress transfer zone from the loaded side to the unloaded side (*fig. 3.a*).

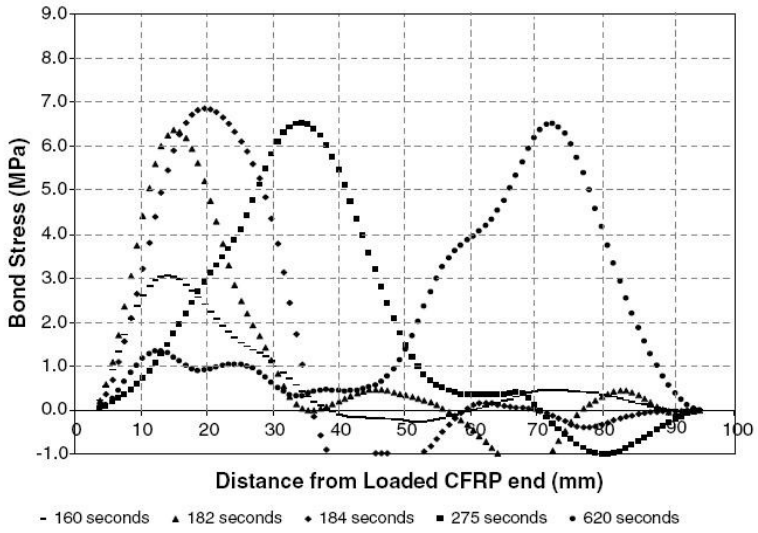

fig. 3.a - The bond stress distribution in four load step. The values of stresses are relative to the centerline of the CFRP sheet [40].

Carloni et al. [41] carried out an experimental study to obtain the through-thickness strains in the concrete reinforced by FRP during three NES single shear tests. To measure the strain below the composite layer, the traditional direct-shear configuration has been modified bonding the FRP close the boundary lateral corner of the reinforced surface (*fig. 3.b*). In [41], the Digital Image Correlation has been used to study the strain field onto the lateral side of the specimen. Since the thickness of the composite is insignificant in regard of the depth of the concrete block a layer of sponge 25 mm in thickness has been attached on the FRP; the displacement of this layer has been simple to measure and identical to those of the composite. A digital camera of 1280x1024 pixels has been used to take photos at regular intervals during the test. Before the experiment, the lateral surface of the specimen (concrete, composite and sponge) has been sprayed uniformly with white paint and stained by a speckle of black spots. The tests shown that the region of concrete support through the thickness of the sample involved in the stress transfer phenomenon is approximately 15 [mm] (*fig. 3.c*). Moreover the strain distribution below the FRP is similar to the one obtained from the analysis of the composite's surface. Carloni et al. conclude that the study of the fracture properties of the interface can be conducted by measuring the strain field on the surface of the FRP.

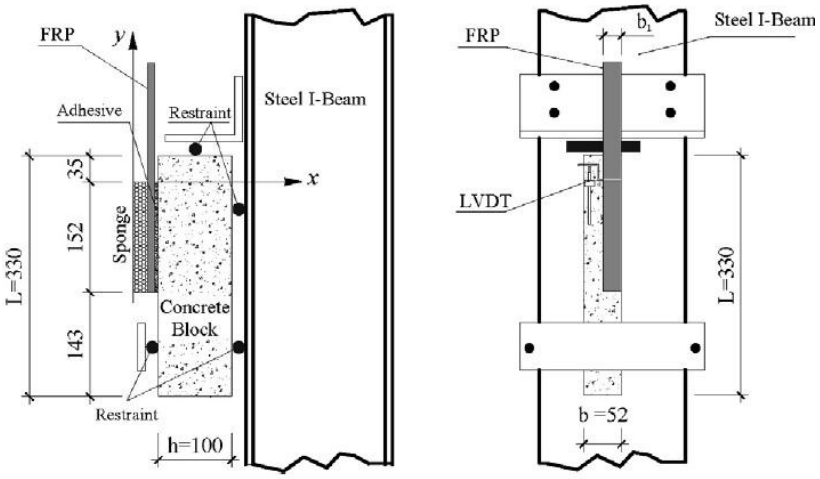

fig. 3.b - The "modified" NES single shear test executed by Carloni et al.[41].

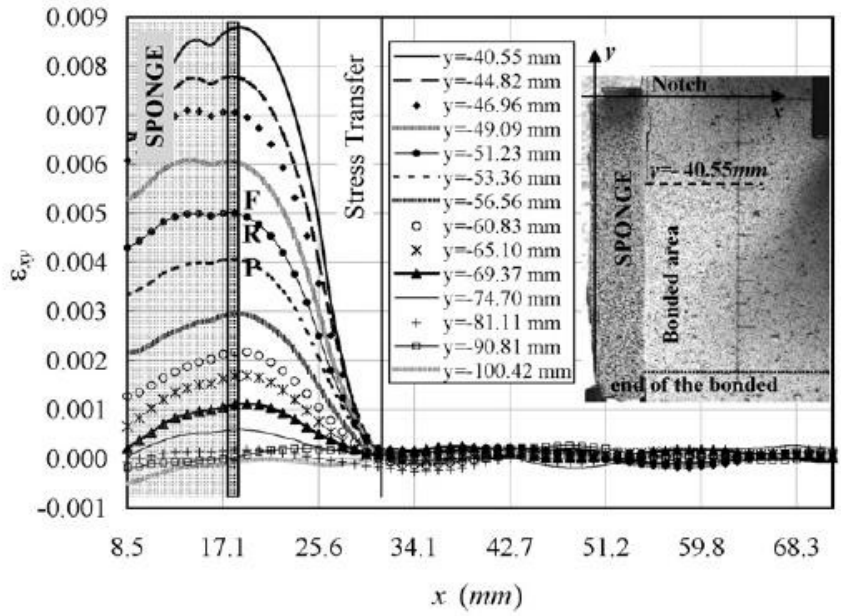

fig. 3.c - Shear strain ε_{xy} at different value of y (load step successive to the apparition of first crack)[41]

Some other studies on the FRP to concrete bonded joint have been realized using the Digital Image Correlation [42] [43].

It is believed that the performance of the digital image correlation are appropriate to study the two dimensional displacement and strain field of the FRP to firebrick bonded joint fastened with FRP anchor and subjected to NES single shear test. The choice of this optical measurement techniques permit to achieve the follows advantages:

1) The displacement and the strain values could be obtained for all the area of the reinforced surface and not only in some points (strain gauges…).
2) The displacement and the strain values onto the splay anchor could be obtained

3) Detailed analyzis of the strain concentration close the anchor could be carry out
4) The displacement and the strain fields on the specimen could be obtained after the achievement of the cohesive debonding of the sheet and the activation of the FRP splay anchor (see the load-slip response of *fig. 1.aaa*); while the brittle fracture could lead to the detachment of the strain gauges from the support.

The strain fields of the 36 specimens tested in Paris has been studied by Digital Image Correlation. The deformation values calculated during the 36 experiments managed in Florence have been obtained using strain gauges. Designs of the strain gauges dispositions adopted in Italy are reported in *figure 3.d*.

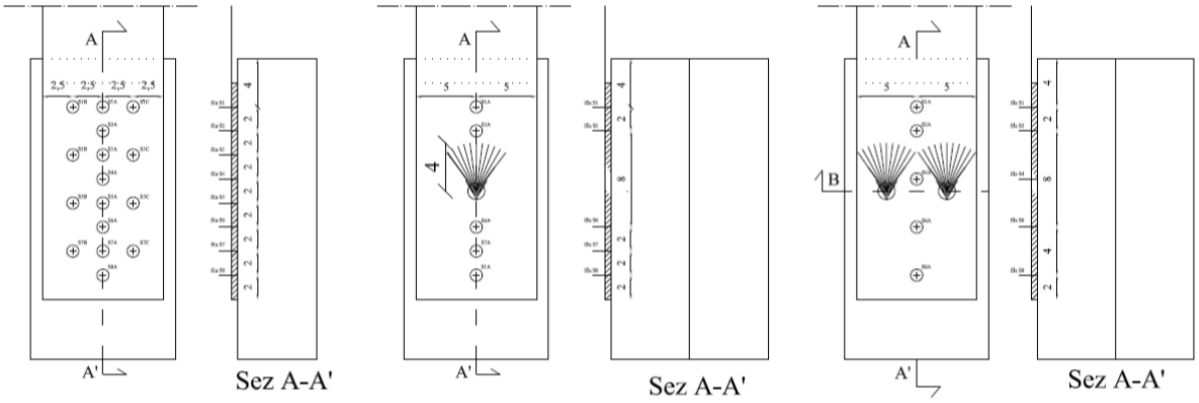

fig. 3.d - Disposition of the strain gauges adopted in Florence for the series F0, F1_40_V and F2_40_V

3.2 The CCD camera and the digital photos

The Charge Coupled Device (CCD) is a chip made in silicon designed in 1970 [44]. It is composed by an array of sensitive squares (pixels); each one stores the charge like a potential well. Therefore when the light falls on the surface of the semiconductor, each pixel registers a value of electrical charge [45]. In the CCD camera the image is projected by lens on the sensitive silicon surface and it is converted in an array of charge values. The computers can read the charge information stocked in each pixel and convert it to a intensity value. An important quality of the Charge Coupled Devices is the high speed process of recording and clearing the information detected in the pixels.

This very brief presentation of the CCD camera permits to understand that the digital images, realized with this device are intensity signals. The digital images are bi-dimensional grid, each cell of coordinate (x,y) correspond to a pixel characterized by a specifically intensity value. For the grayscale digital images the intensity values range from 0 to 255 (*fig. 3.e*). The colors of this scale change gradually from black (value 0) to white (value 255).

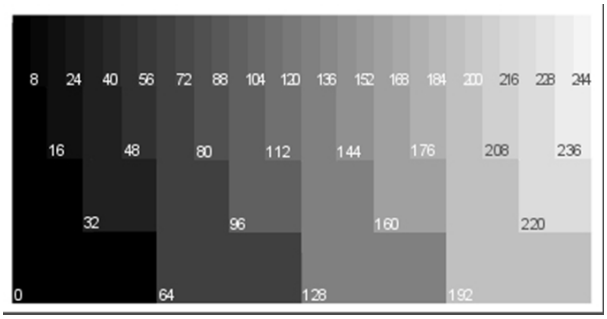

fig. 3.e - The gray level scale

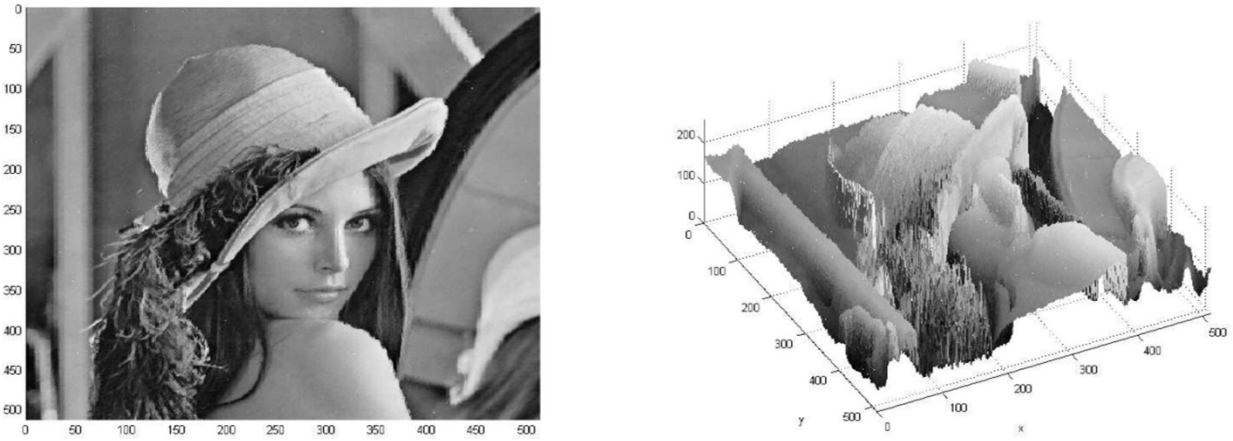

fig. 3.f - A digital image and the relative 3D graphic "x-y-gray level"

Finally, each digital image could be represented like a matrix of numbers; this possibility permits a large range of processing application on photos that were impossible to carry out with the analogical technology. The Digital Image Correlation exploits these CCD camera performances.

3.3 The digital image correlation method

The displacement field of a deformed image with respect to a reference image is obtained by the DIC matching more sub-regions. The standard approach described below uses a correlation function [36]. To simplify the explanation of the DIC process two one-dimensional signals have been correlated herein; the signal f(x), that represent the zone of interest (ZOI) of the reference image, and the signal g(x), that represent the displaced configuration of the same zone. The f(x) is constituted by five pixels (*fig. 3.g*); all the squares are black (grey level = 0) except the second, which is white (grey level = 255). The signal g(x) describes the same interest zone after a displacement u (fig. 3.h).

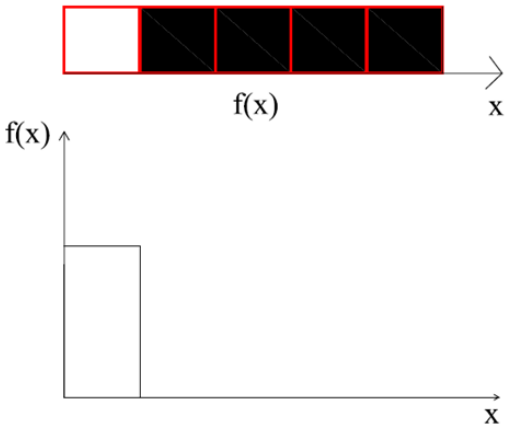

fig. 3.g - The signal f(x) and the graphic "x-f(x)"The "modified" NES single shear test executed by Carloni et al.[41].

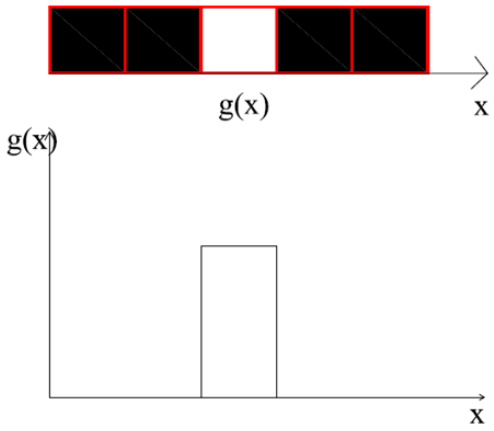

fig. 3.h - The signal g(x) and the graphic "x-g(x)"The "modified" NES single shear test executed by Carloni et al.[41].

It's possible to write:

$$g\ x\ = f\ x-u\ + b(x) \tag{3.2}$$

Namely, the signal g(x) is equal to the shifted copy f(x-u) of the reference signal f(x) summed with a random noise b(x). This last is due to the deformations and the optical measurements that modify lightly the speckle pattern. Changes in the ambient light during the test can also cause this noise. The value of the shift "u" is obtained using the cross correlation function h(δ) reported follow:

$$h\ \delta\ =\ g * f\ \ \delta\ =\ \int_{-\infty}^{+\infty} g\ x\ f\ x-\delta\ dx \tag{3.3}$$

The value of δ that maximize the cross correlation product $g * f\ \ \delta$ is the shift estimation value "u". If b(x) is nauth, like in the example proposed, the estimation is perfect.

Taking into account the mono-dimensional images f(x) and g(x) presented above, a simple example of the cross correlation procedure is proposed follow (*fig. 3.i*). Increasing the value of the tentative shift δ the function h(δ) varies. The maximum value of the cross correlation product is obtained when the tentative δ makes that the f(x) overlap perfectly the g(x). In the example proposed the h(δ) is maximized by $\delta=\delta_4$ (*fig. 3.j*).

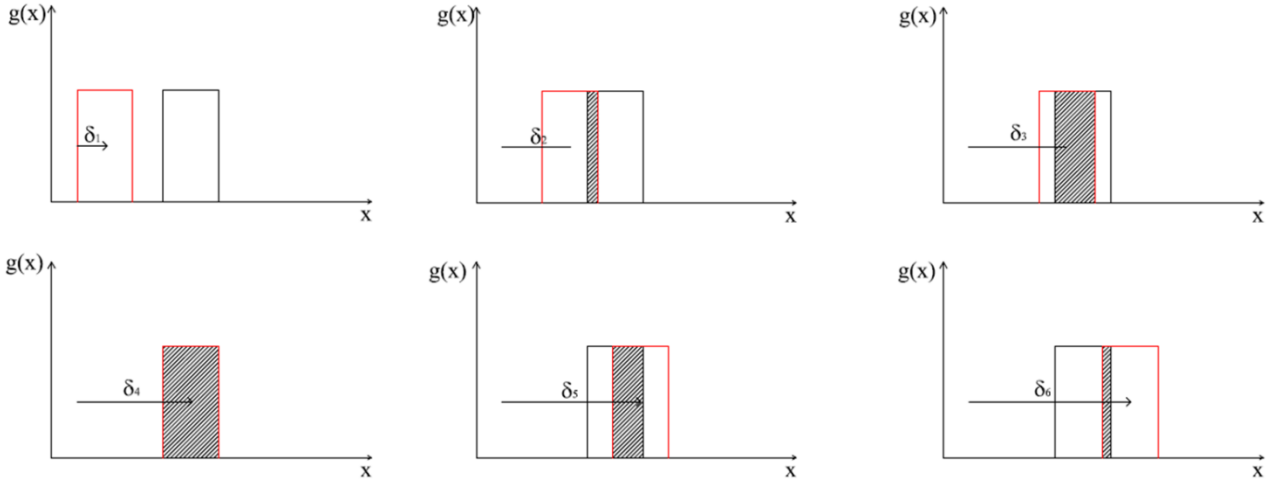

fig. 3.i - Example of cross –correlation process; the f(x) displaced by different value of tentative δ (in red).

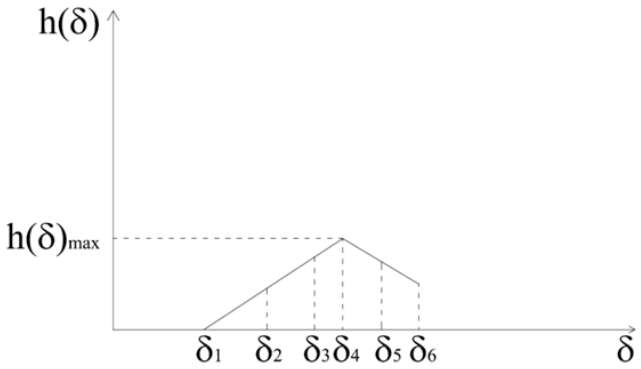

fig. 3.j - Example of cross-correlation process; the function h(δ).

The computation of h(δ) can be executed either in the Fourier space, by using an FFT, or in the original space [36].

If the images are bi-dimensional the same process of correlation is executed. In this case the signals will be f(x,y) and g(x,y) and the displacement of the sub-region of interest have a component in the x and y directions. In the figure is represented a signal f(x,y) with highlighted a zone of 10x10 pixels.

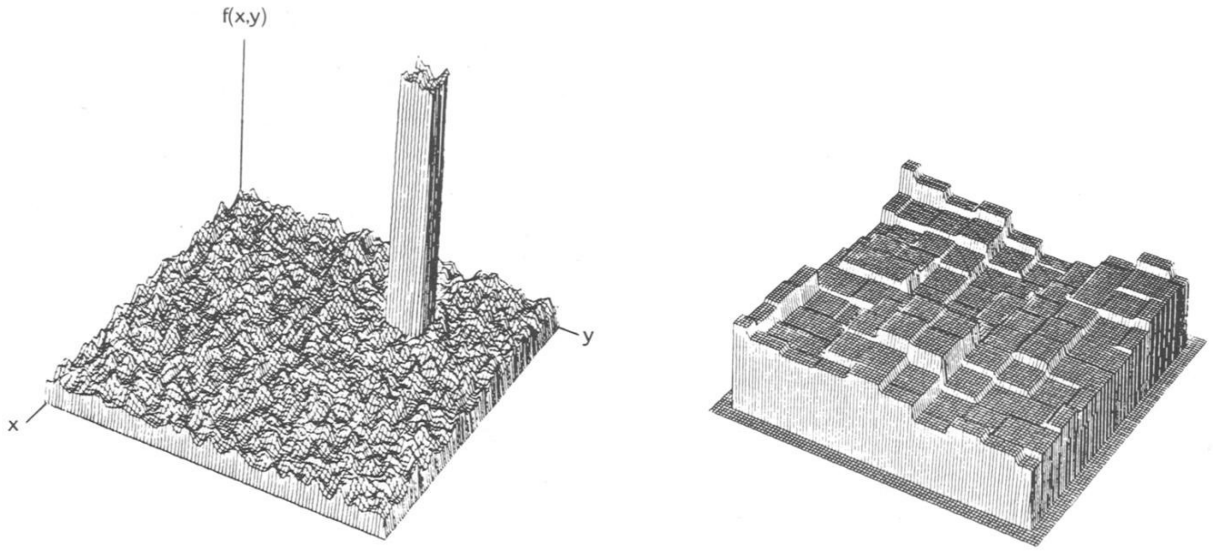

fig. 3.k - A bi-dimensional signal. In the left side the f(x,y) signal is represented. In the right side the zone of 10x10 pixels, highlighted in the left image, is zoomed. [33]

3.4 The correlation algorithm CORRELIGD to study the two dimensional-signals

The correlation algorithm CORRELI^{GD} has been used to compute the displacement and strain field upon the reinforced surface of the specimens. The software version used has been developed by a research group of LMT-Cachan [35][36][37]. The algorithm is based on a multi-scale approach to increase the efficiency of the correlation process. The computation method to manage the correlation between two signals is presented as follow; a "reference" image f(x,y) and a "deformed" image g(x,y) are taken. The first step of the process is define a region of interest (ROI) in the photo; this one represents f(x,y). After that, a zone of size 2^p x 2^p pixels^2 inscribed in the ROI and centered in the reference image is defined; the same region is considered in the deformed image. A first correlation is computed by a FFT to obtain the average displacement U_0 and V_0 that maximize the cross-correlation product between the ROIs of the signals f(x,y) and g(x,y). Found these values, the ROI of the deformed image is moved onto the ROI of the reference image displacing its center of U_0 and V_0. The following step is to choose the parameter *s* that defines the size of the sub-regions. These sub-regions are named Zone Of Interest (ZOI) and have a dimension equal to 2^s x 2^s pixel^2. The value of parameter *s* is smaller than *p*. Afterwards another parameter is chosen, the shift d*x* between two consecutive ZOIs (dx=dy). The centers of the Zone of Interests, defined by the parameters *s* and *dx,* form a grid. Each ZOI of the reference signal is cross-correlated with the corresponding zone of the deformed signal. A FFT correlation give the value of the additional in-plane displacement ΔU and ΔV for each ZOI. The displacements of the nodes of the grid, are equal to the value of U_0 and V_0 plus the ΔU and ΔV relative to each ZOI. By determining the maximum

of a parabolic interpolation of the correlation function, a sub-pixel correction of the displacement is obtained by finding the values δU and δV. The total displacement of a generic node "i" will be equal to:

$$U_{ZOI\,i} = U_0 + \Delta U_{ZOI\,i} + \delta U_{ZOI\,i} \quad (3.4)$$

$$V_{ZOI\,i} = V_0 + \Delta V_{ZOI\,i} + \delta V_{ZOI\,i} \quad (3.5)$$

To reduce the errors more iteration could be realized to reached a convergence criterion. The precision of the algorithm method is of the order of 2/100 pixel for the displacement and 10^{-4} for the strain measurements. After the computation of the displacement field the strain field is obtained using simple derivations with respect to the nodes coordinates. Because the displacement field is known discretely at a finite number of node, derivation is source of noise on the strain field representation: a smoothing step is generally useful to obtain an accurate strain field.

3.5 The speckle onto the observed surface

The performances of the Digital Image Correlation are related to the grey level characteristic of the pixels array. Specifically, the better results are obtained when local gray level fluctuations are present in the images to correlate [34]. Usually, to obtain this optimal pixel characteristic, a texture is realized on the observed surface. First, we cover the surface of a homogeneous paint which is then overlapped by a random speckle pattern of matt. To generate a high contrast the support cover is black and the speckle is white (or inversely) [34][36][41][42]. This choice permits to maximize the fluctuation of the gray levels in closer pixels (black=0 and white=255). Therefore the goal of the paint pretreatment is to simplify the production of high contrast images; namely photos with very dark shadows and very bright highlights. In this framework a very important attention is paid to the light that illuminates the observed surface.

In the experimental session of this thesis the homogeneous cover is carried out by spraying a black paint on the reinforced surface. This last has been overlapped by a speckle pattern made with a white spray paint. The methodology used to realize the texture has already been used in the laboratory of MSME.

3.6 A preliminary case study: rubber in traction

The concepts shown above underline that the quality of the Digital Image Correlation is connected to several factors combined with each other; the speckle morphology, the photographical setup, the scale [mm]/[pixel] the parameters of the software CORRELI. The execution of a preliminary study case has permitted to become familiar with the DIC optical measurement technique by setting, moreover, the parameters to use in the NES single shear test.

The preliminary study has been carried out using several traction tests on rubber strips. The test apparatus used to stretch the rubber is the same projected for the NES shear test (*fig.3.l*). The latex bands have a width equal to that of specimen's carbon fabric (10 [cm]) and a length of 120 [cm]. The strip is inserted in the apparatus by passing one of its extremities within the steel cylinder and the support steel plate; both ends of the rubber band are bonded to two steel plates and inserted inside the steel "tongs" (*fig. 3.l*).

fig. 3.l - The traction test on rubber. Boundary conditions and photos of the test apparatus

Before the texture is achieved onto the strips surface, more exercises of speckle execution have been carried out on cardboard sized 12x40 [cm^2]. This training phase has permitted to acquire the manual skills and to define the technical device necessary to realize the texture.

Two texture typologies (*fig. 3.m*) have been accomplished using a simple procedure. First a black cover is splayed on the surface of interest, after that, minimum 24 hours later, a cloud of white paint is generated on the sample by directing the spray upward; the white drop falling on the black

surface generate a texture. The speckle pattern achieved is more sensible to the modality of spraying of white paint; little modification of the spray direction allow to more different size of spots on the surface of interest. The typologies of speckle pattern analyzed in the rubber tests are realized using technical device simple to reproduces. The first kind of texture is characterized by the size of the spots that are very different from one to another. The second one is featured by more homogeneous spot sizes.

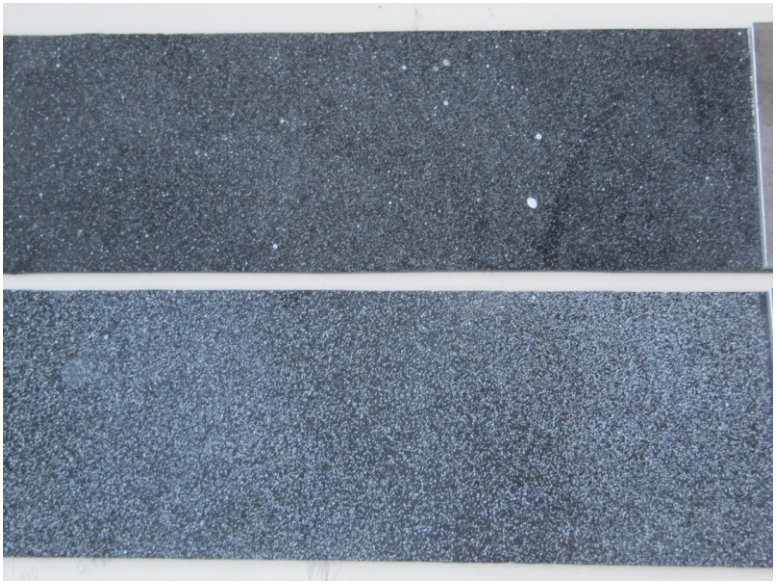

fig. 3.m - The two configurations of speckle: above the texture S1 (heterogeneous size spots), below the texture S2 (homogeneous size spots)

A CCD camera has been used has been placed in front of the specimen at a distance of 120 [cm] (fig. 3.n). To produce high contrast photos a lamp has been allocated close the studied surface (*fig. 3.n*).

fig. 3.n - The camera and the rubber test

The pictures taken have a size of 1360x1024 [pixel^2]. Two hypothesis of camera orientation have been tested, O1 and O2; the frame is 1360x1024 [pixel^2] in the first one and 1024x1360 [pixel^2] in the second one (camera rotate of 90°). To obtain the side length in [mm] of the pixel's square a "scale ratio" (R_z) has been calculated. This last is equal to the ratio between the rubber width in [mm] and the same measure in [pixel].

$$R_Z = \frac{Rubber\ Width\ [mm]}{Rubber\ Width\ [pixel]} = \frac{100\ [mm]}{x\ [pixel]}$$

The Region Of Interest (ROI) of the rubber surface has dimensions 70x200 [mm^2]. Obviously, if the camera "zoom in" the rubber, the ratio R_Z decrease and the number of pixels that describe the speckle increase.

The rubber tests have been carried out to answer the next questions.

- Which is the best configuration of speckle pattern (homogeneous or heterogeneous)?
- Fixed the speckle pattern, which is the more efficient ratio [mm]/[pixel]?
- Fixed the speckle pattern and the ratio [mm]/[pixel], which are the Digital Image Correlation parameters that allow the most efficient analysis?

The experiments have been carried out applying imposed displacements to the extremities of the rubber strip inserted in the steel tongs. The history of the load applied on the specimen is composed by 4 steps of imposed displacement (step of Δu=1 mm); after each one a delay of 30 [s] has been performed to block the displacement traverse and to have time to take frontal pictures.

The Deltalab machine given the value of the Force [N] applied on the rubber during the test. Known the cross section of the latex bands, 660 [mm^2], is simple to obtain the stress σ [N/mm^2].

More tests have been carried out applying the same loading history described above but modifying: the specimen analyzed (with heterogeneous and homogenous size spot), the orientation of DDC camera (frame of 1360x1024 or 1024x1360 [pixel^2]), the zoom of ROI, the size of ZOI, the shift between the ZOI, the number of iterations.

The strain field obtained by DIC has been used to find the experimental Young modulus of the rubber; this last has been compared with the literature value.

The displacement and strain field obtained by the correlations of image have been compared with than of the analytical solutions. In the tests executed, it has been possible underline that the quality

of results is maximized when a good combination between size of speckle, ratio R_Z and size of ZOI is adopted.

The experiments showed that the heterogenic speckle pattern lead to displacement and strain field characterized by local noise restricted to the bigger white spots. Increasing the ZOI size the magnitude of the concentrated noises decreases but still exist. In the tests executed, the texture characterized by spots of size almost homogeneous leads to displacement and strain field considerably less affected by local noises. The results obtained permit to affirm that the homogeneous speckle pattern is more efficiency than the heterogeneous.

If the frame is 1360x1024 the value of x is … [pixels], Rz is equal to …, and the ROI is defined by ….x….[pixel^2]. When the frame is 1024x1360 is possible "zoom in" the rubber surface; in this case R_Z is equal to …, and the ROI is defined by …x…[pixel^2]. In this experimental session the better results have been obtained by means of the second typology of frame; the speckle pattern considered permit to obtain good results realizing images with factor R_z equal approximately …..

The best results (optimal case) have been obtained analyzing digital photo with a R_Z=… of homogeneous speckle pattern and utilizing the follows DIC parameters:

ZOI size = 128 [pixel]
dx = 32 [pixels]
n. iterations = 6

The contour representation of the components D1 and D2 of the displacement field obtained using this optimal combination of parameters is reproduced in *figures 3.o and 3.p* for each load step.

The contour representation of the components ε11 and ε22 of the strain field is presented in *figures 3.q* and *3.r* for each load step.

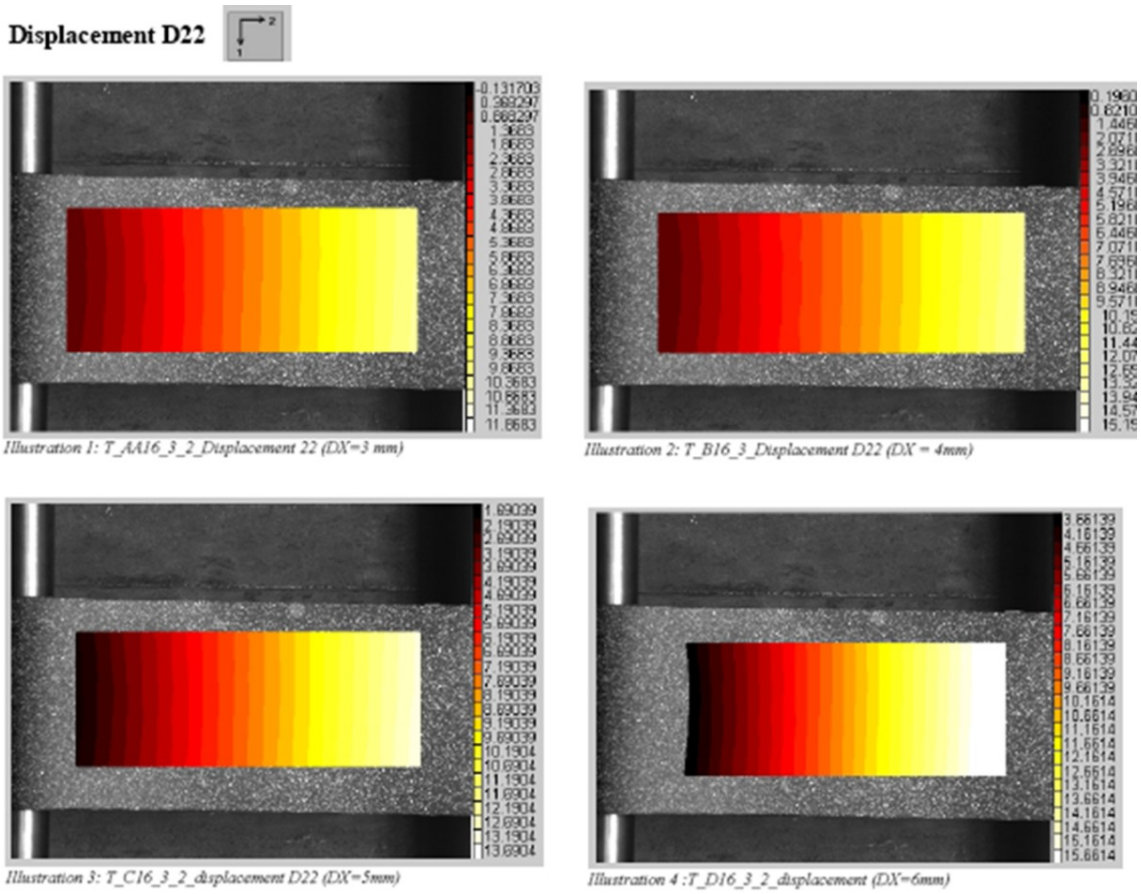

fig. 3.o -The contour representation of the displacement field (D2) in the optimal case for each load step. In the upper part are reproduced the reference axis.

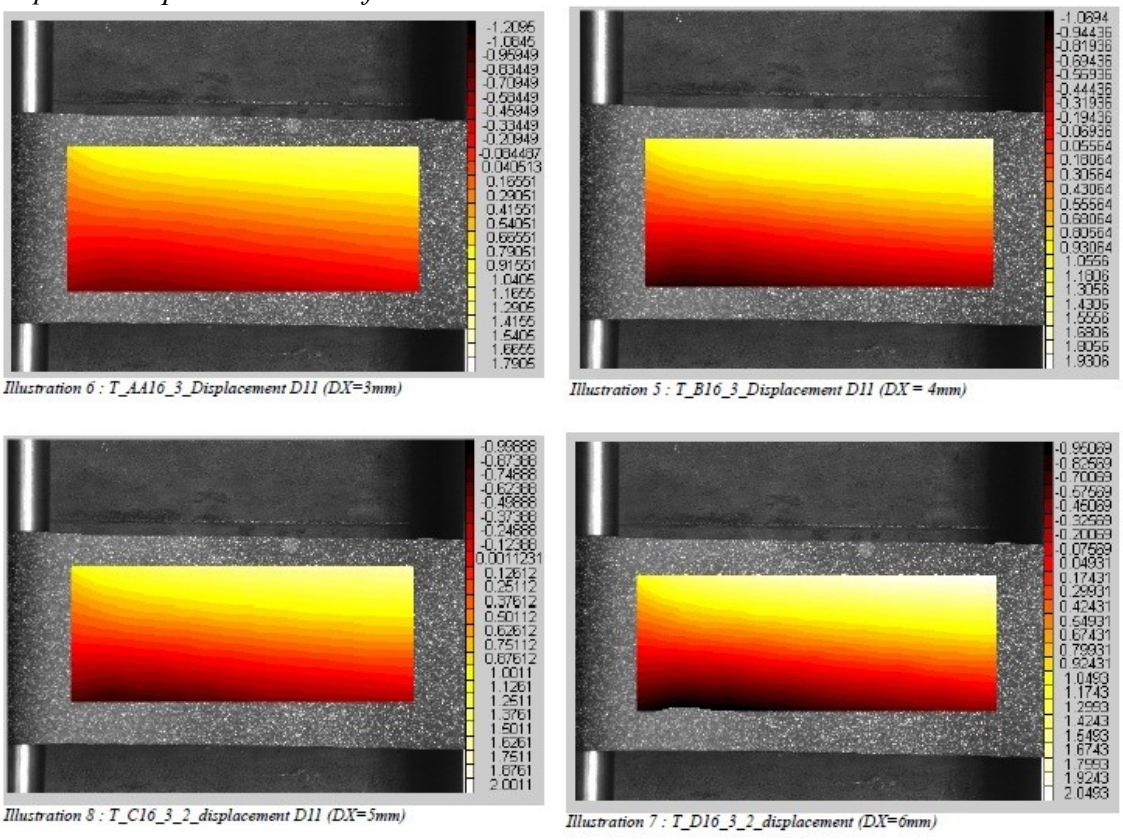

fig. 3.p - The contour representation of the displacement field (D1) in the optimal case for each load step.

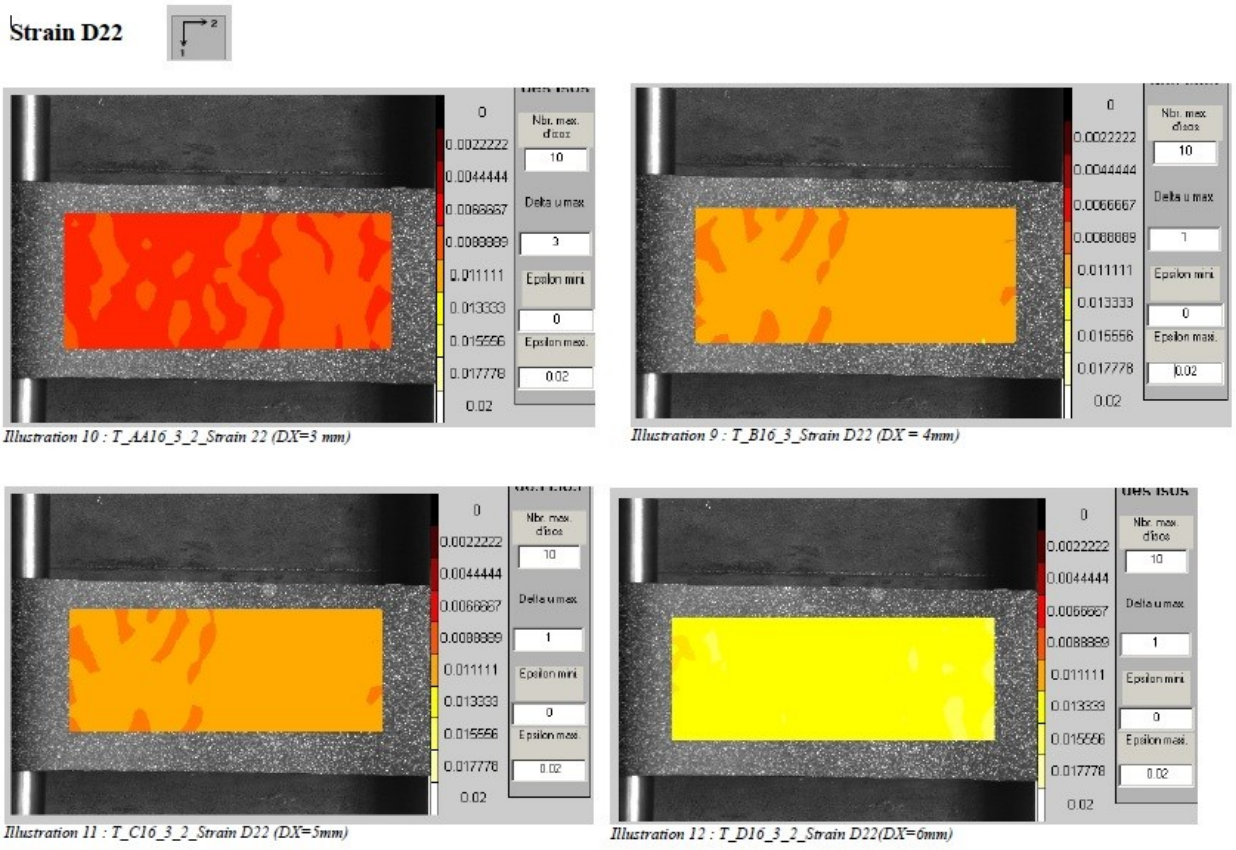

fig. 3.q - The contour representation of the strain field (ε_{22}) in the optimal case for each load step. In the upper part are reproduced the reference axis.

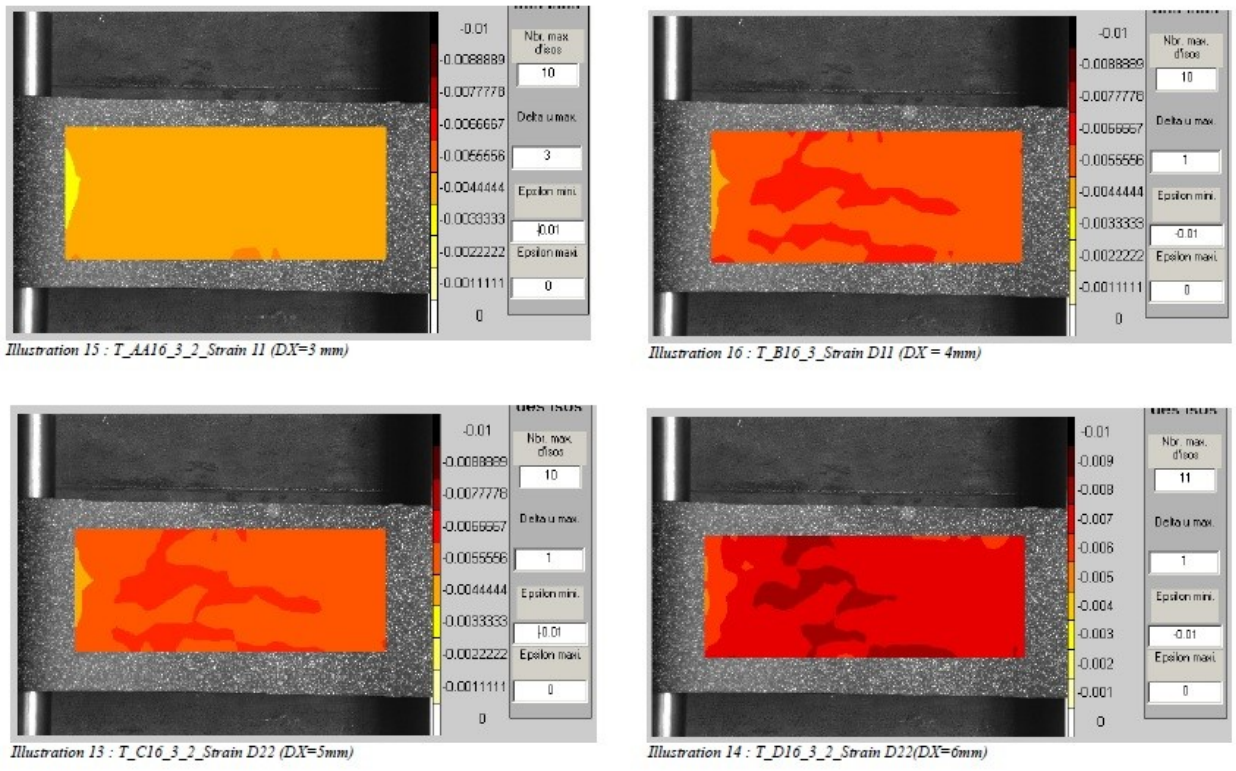

fig. 3.r - *The contout representation of the strain field (ε_{11}) in the optimal case for each load step.*

In the graph presented in *figure 3.s* the curve ε-σ [MPa] is shown where ε is obtained using the digital image correlation. The Young modulus obtained is equal to 0,008 [MPa]. This value matches perfectly with the rubber properties found in literature [46].

fig. 3.s - *The curve ε–σ obtained using the DIC analyze.*

3.7 The CFRP to fire brick bonded NES shear test and the Digital Image Correlation

During the NES single shear tests, the bidimensional displacement and strain fields of the firebrick reinforced surface have been obtained using Digital Image Correlation.
The speckle pattern onto the surface of interest has been drawn on the FRP surface, reproducing the homogeneous size spots tested in the rubber experimental session (*fig. 3.t*).

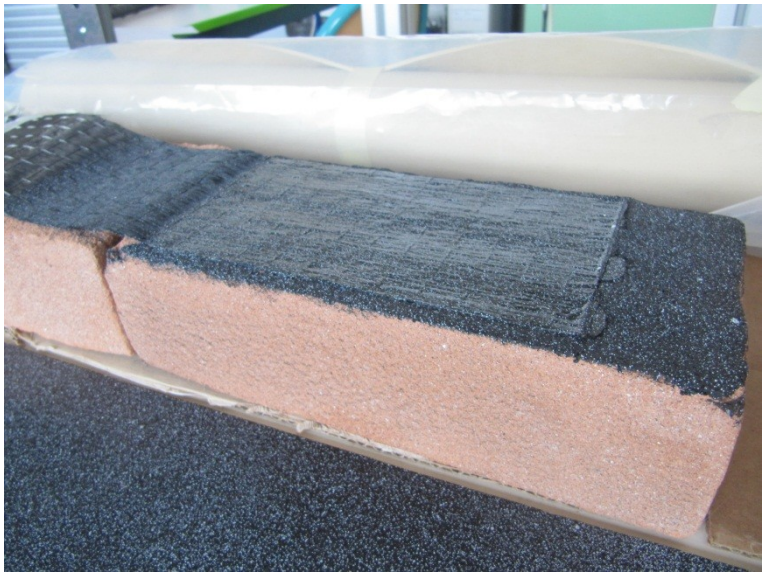

fig. 3.t - The speckle pattern onto the reinforced surface. The fire-brick specimen is drawn near the rubber sample characterized by homogeneous size spots.

During the NES single shear tests the digital images have been taken using a frame of 1024x1360 pixels. The value of R_z of reinforced fire brick images is approximately equal to the one chosen for an accurate representation of the strain field with the rubber study.
Unlike the rubber strip surface, the CFRP is bright and reflects the lights. This characteristic generates several problems connected to the impossibility to good quality pictures in full ambient light. The impossibility to close windows of the open space laboratory has forced to shadow the surface of the specimen from the direct lights using some devices; an aluminum frame covered by

more cardboards and blankets has been assembled between the camera and the specimen (*fig. 3.u*). The images of a CFRP surface before and after the assembling of the shadow device are presented in *figures 3.v* and 3.w.

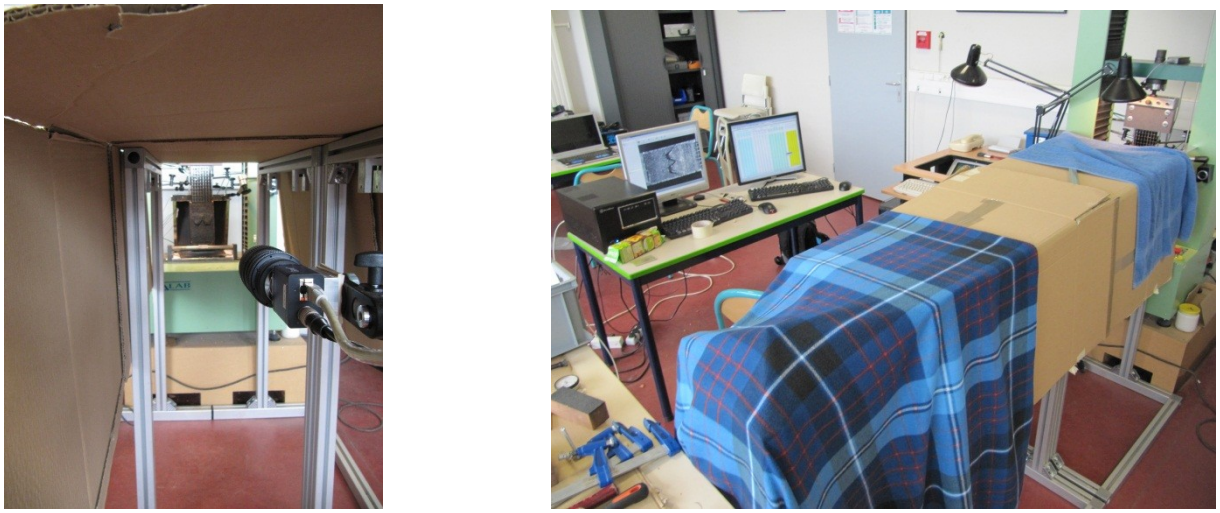

fig. 3.u - The devices used to overshadow the specimen

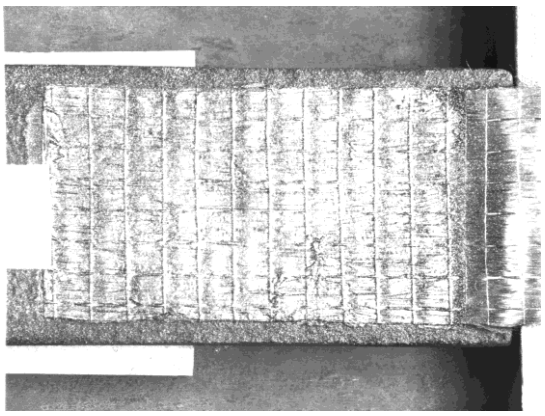

fig. 3.v - The bright CFRP surface

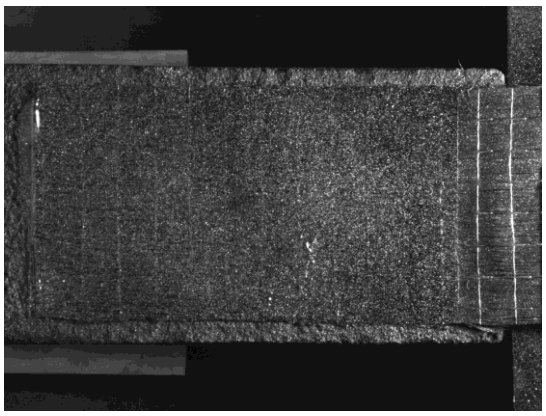

fig. 3.w - The bright CFRP surface shadowed by the cardboards devices

The CORRELI parameters chosen to execute the digital image correlations have been defined according to the optimal case studied in the rubber test session. Almost in all analysis the ZOI=128 and dx = 64.

Chapter 4

Experimental Results

4 Experimental Results

4.1 Results overview

The results presented in this chapter have been obtained processing the measures of the instrumental setup.

The values acquired in the experimental analysis for each specimen are listed follow:

- The load corresponding to the imposed displacement (graphs U-L)
- The definition of more phenomenological phases (elastic behavior – crack advancement – debonding – anchor loading – anchor failure)
- The peaks of load registered (P_1, P_2, P_3)
- The energy dissipated during the test ($\Delta\Gamma$, Γ_{end})
- The fracture mode (cohesive, adhesive, mixed,…)
- The bi-dimensional displacement and strain fields onto the reinforced side of the specimen (u and ε)

The consideration carried out during the processing of instrumental measures, the treatment procedure and the nomenclature of the results are presented in the next subparagraphs.

4.1.1 The displacement-load graphs, the peaks and the dissipated energy

The analyze of *Displacement–Load* graph (U-L) permits to collect many information about the failure phases of the reinforced system. The characteristic graph U-L obtained in the NES single shear test is shown in *figure 4.a.* In this representation, the linear strake AB corresponds to the elastic behavior of the firebrick support. A first load peak (**P_1**) is registered in B when the first crack appear in the extremity loaded of the FRP to support bonded joint. The strake B'C describe the crack advancement phase, in C the total debonding fracture occurs. The load value registered in this point, named P_2, corresponds to the maximum load peak obtained during the test. If no anchor are fastened to the composite sheet the test finish when **P_2** is achieved by the total detachment of the CFRP reinforcement and the simultaneously fall to zero of the load. The experimental study shown that the presence of "CFRP nail" gives to the reinforced system, after the load fall in C, a residual resistance and a new phase of loading (stroke DE). In E a failure of the system *CFRP sheet – CFRP anchor* occurs and, achieved the peak **P_3**, the load drops again.

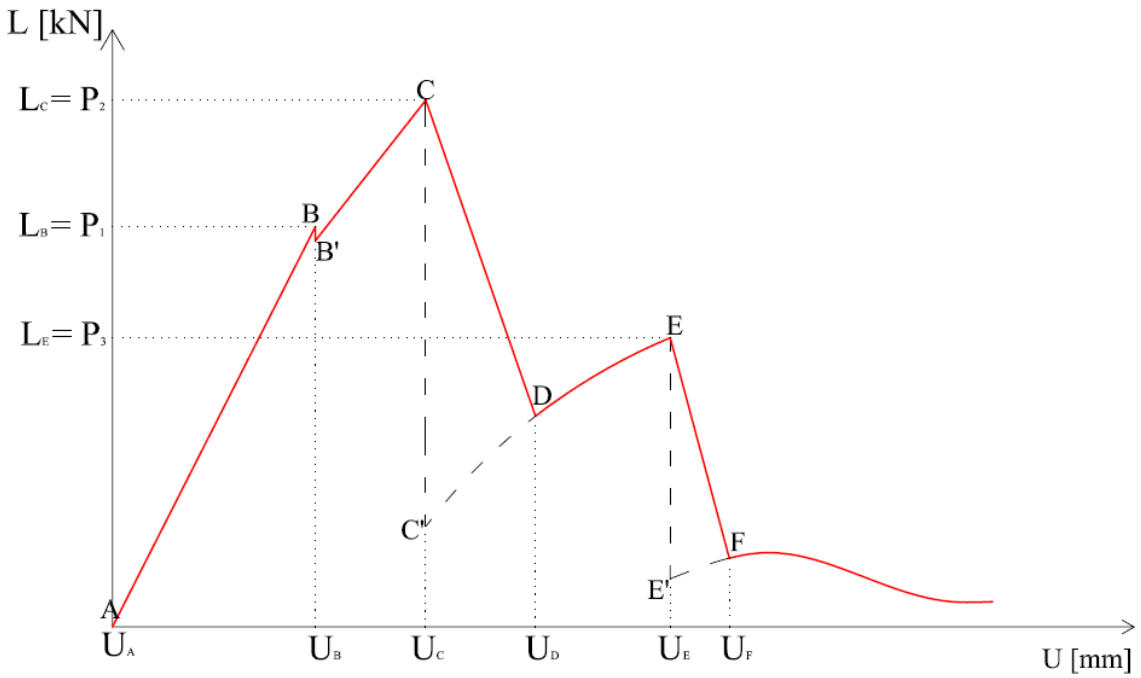

Fig. 4.a - The characteristic graph U [mm] – L [kN]

fig. 4.b - The specimen during three test phases; in the left an image of the sample during the crack advancement (strokes BC), in the center a photo of the specimen after the total debonding fracture (strokes DE), finally, in the right a figure of the anchor detached from the CFRP sheet after the achievement of the P3.

The value U is the imposed displacement applied to the specimen. It is equal to:

$$U = u - D \tag{4.1}$$

As previously described in *par. 2.2.6*, *u* is the displacement of the traverse, and D is the displacement of the steel lock. The displacement u increase linearly with the time during all the test (*fig. 4.c*). Instead the value of D increase linearly with the time until the achievement of the debonding failure (*fig. 4.c*); in this instant the load fall due to the spring back of the steel apparatus and a partial drop of D. According to these consideration, the linear increase of the displacement U during the time knows a jump at the debonding failure instant (*fig. 4.c*).

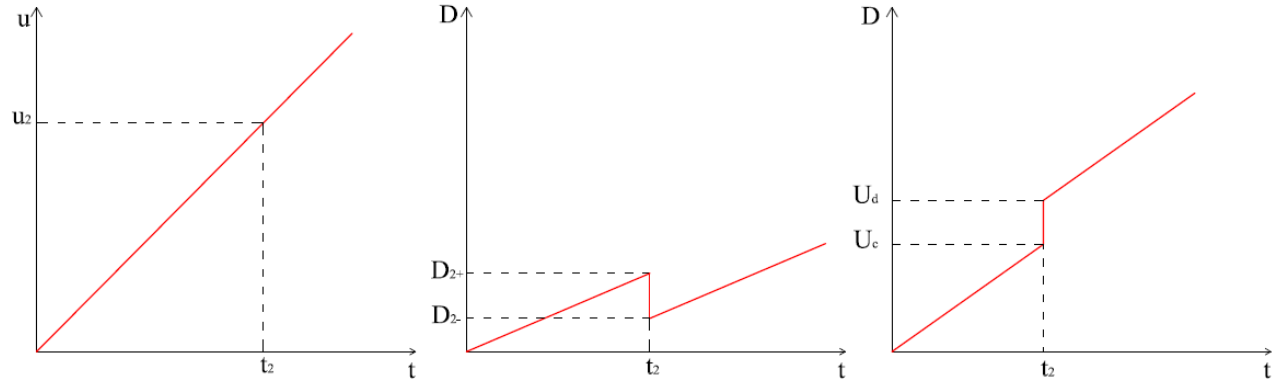

fig. 4.c - The graphs u-t, D-t and U-t

The graphs displacement-load are presented above (*fig. 4.d*). In the case of diagram u-L, when the load peak P_2 is reached an almost vertical drop is registered. By regarding the graph D-L it's simple to note that, achieved the peak P_2, an elastic return of the steel lock occurs; instantly the value of D_{2-} drops to D_{2+} (the nomenclatures $_{2-}$ and $_{2+}$ define the instant before and after the debonding failure). In the diagram U-L, when the peak P_2 is reached an inclined stroke describes the load fall. This slope is due to the spring back of the steel lock.

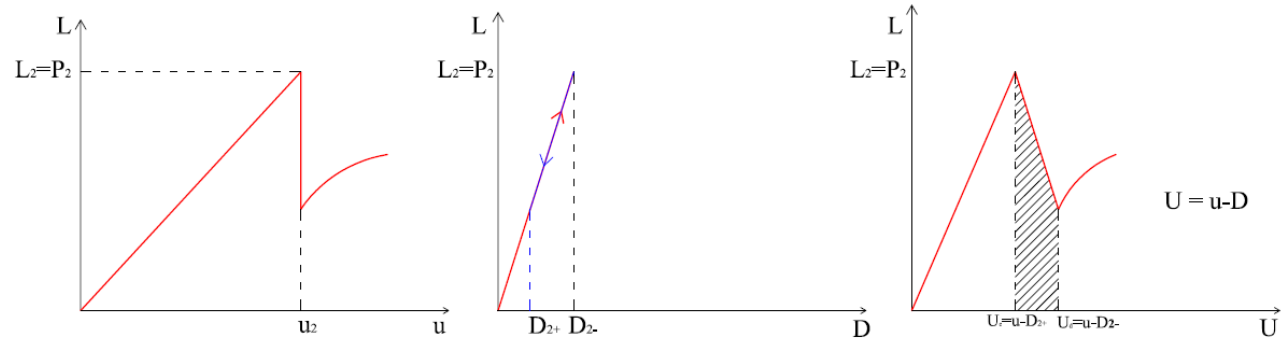

fig. 4.d - The graphs u-L, D-L and U-L

The energy necessary to lead to failure the reinforced system is an important parameter to measure the efficiency of the different reinforcement typologies. This dissipated energy, named Γ and measured in [J], is equal to the area underlying the U-L curve. Specifically, the total value Γ has been subdivided in 4 shares. The low dissipation of energy due to the friction between the inferior

and superior surfaces of the fracture, registered after the anchor fail, has been neglecting. The four energy shares are listed and defined below.

– $\Delta\Gamma_1$ is the amount of energy necessary to generate the first crack. It is equal to the area underlying the stroke AB (*fig.4.e*)

–$\Delta\Gamma_2$ is the amount of energy dissipated during the crack advancement phase, until the total debonding of FRP to fire brick reinforced system. It is equal to the area underlying the stroke BC (*fig. 4.e*).

–$\Delta\Gamma_i$ is the amount of energy dissipated during the load fall and the instantly spring back of the steel lock. The assumption made to quantify this $\Delta\Gamma$ is that the drop of D is so fast that the instrumentation setup is incapable to register it. A vertical drop, defined by stroke CC', and a next loading step, descripted by stroke C'D have been suggested. Since the impossibility to know exactly the slope of stroke C'D only a maximal value of $\Delta\Gamma_{imax}$ has been calculated; it is equal to the area of the rectangle whit vertex U_C - U_D - D - D' (*fig.4.e*).

–$\Delta\Gamma_3$ is the amount of energy dissipated during the fiber anchor loading phase. It is equal to the area underlying the stroke DE (*fig. 4.e*).

To compare the energy dissipated by the specimens of different series the *global value of energy* Γ_{END} has been defined. Obviously in the specimens of series T0 the third component of the sum is equal to 0.

$$\Gamma_{END} = \Delta\Gamma_1+\Delta\Gamma_2+\Delta\Gamma_3 \qquad (4.2)$$

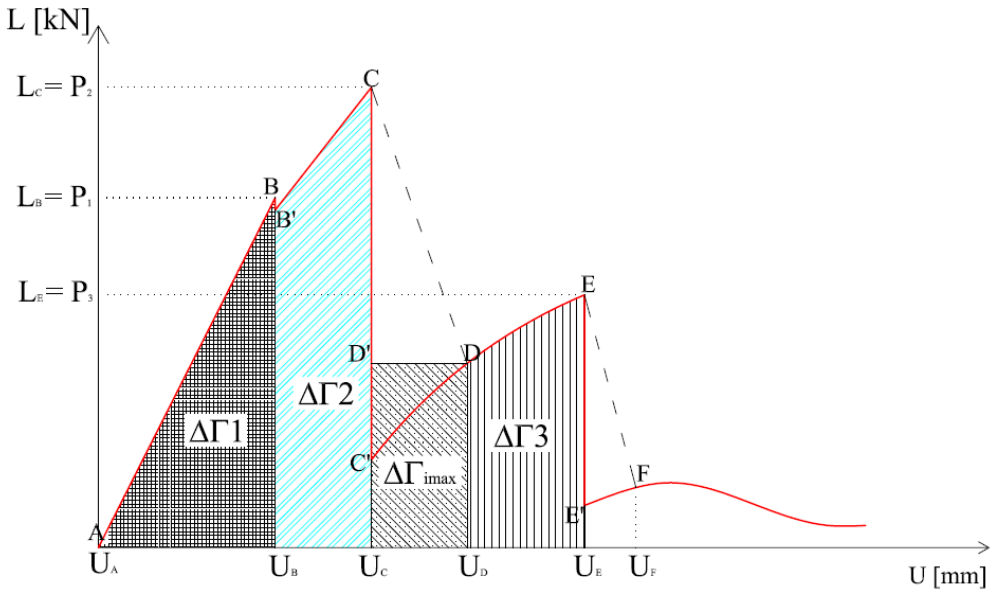

fig. 4.e - The graph U-L and the dissipated energy shares

4.1.2 *Failure modes and fracture definitions*

The achievement of the peaks is followed by a fracture development. In this experimental study several fracture typologies have been registered. To permit an easier lecture of the results, the nomenclature used in the chapter to define the rupture modality is presented herein.

The *cohesive fracture* (**CF**) , the *adhesive fracture* (**AF**) and the *mixed fracture* (**MF**) have been already presented in the first chapter (par. 1.3.1) [3].

The *prismatic failure* (**PF**) is characterized by the development of a fracture at few centimeters of depth inside the fire brick [6]. In this phenomenon a prismatic part of the support, bounded or connected by anchors to the composite sheet, is removed from the fire brick. The experiments shown that the approximates dimensions of the prism are 4 to 5 [cm] thickness, 12 [cm] width and 20 [cm] length. The prismatic failure takes place in a brittle manner and cause the instantly fall to 0 of the load.

The *Debonding Splay Anchor* (**DSA**) occurs when a delamination between CFRP sheet and splay anchor is registered. The detachment of the fan anchor permit a consistent slip of the sheet and generate a load drop.

The *Pull Out of the Nail* (**PON**) is a failure modality characterized by the total exit of the anchor from the support; the experimental session shown that the exit of the carbon nail leads to several prismatic fracture.

4.1.3 *Strain field analyze*

The displacement and strain fields of several load steps are shown in the result sheets. A graph U-D of each experiment permits to collocate in the time, the photos related to the fields presented. The image of reference corresponds to the frontal photo of the sample subjected to an applied displacement of 0,4 [mm]. The image related to the instant 0 of test is not suitable to be signal of reference because, during the first step of time history, substantial displacements due to the imperfection of the sample could generate same noises in the results. The displacement and strain fields presented in the outcome sheets are related to some photos taken during the crack advancement phase (stroke B'C) and to a photo taken after the total debonding fracture (stroke DE).

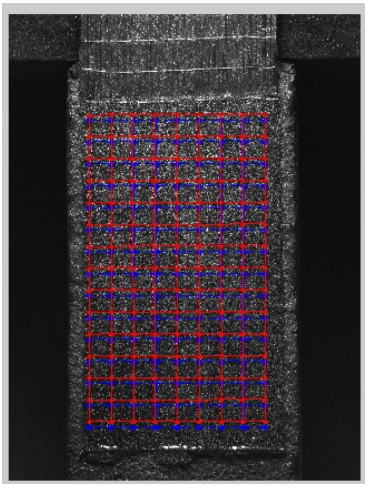

fig. 4.k - The grid realized onto the Region Of Interest

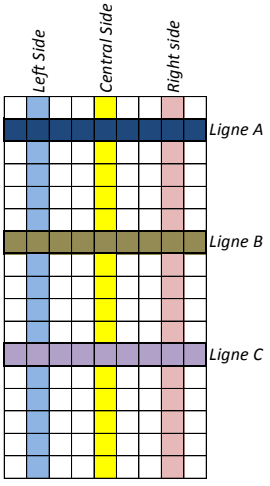

fig. 4.l - The matrix of values and the principals lines and columns

As explained in chapter 3, by using DIC the values of displacements and strains are obtained for all nodes of a geometrical grid (*fig. 4.k*). This last is defined by the correlation parameters (*par. 3.4*). The values of *u* and ε are stocked in a matrix composed by *n* lines and *m* columns (*fig. 4.l*). Each line n corresponds to an ordinate y, likewise each column n corresponds to a coordinate x. The graphs of the strain field are realized showing the values ε_{xx} and ε_{yy} of three principal lines (lines A, B and C) and three principal column (central, side left and side right). The strain increment during the test is underlined by presenting in the graphs the values obtained in more correlations. The displacement and strain fields of several photos are presented below using chromatic representation.

4.2 Result sheets

4.2.1 Series T0

The NES single shear tests executed on specimens T0 shown a uniform behavior of the samples. The *figure 4.m* collects the curves U-L obtained testing all the specimens of the series. The slope of the first stroke AB shown that the CFRP to fire brick systems *T0* have almost the same stiffness. In all the experiments the behavior of the sample during the application of the load history was the same; the underlined values cited herein are "average value". Achieved a peak P_1 (10,05 kN) a first fracture occurs in the loaded side of the specimen; after that, a crack started to advance from loaded to unloaded direction until the attainment of P_2 (12,36 kN). Achieved this peak value a brittle fracture was registered. The energy dissipated during the test has been evaluated computing the underlying surface of each curve. In *figure 4.n* is shown a bar graphs of the dissipated energy. The necessary energy to achieve the fracture in B is on average equal to 8,89 J. In all the crack advancement phases (stroke B'C) 6,75 J was dissipated. The value of Γ_{END} consumed to achieve the debonding failure was on average 18,77 J.

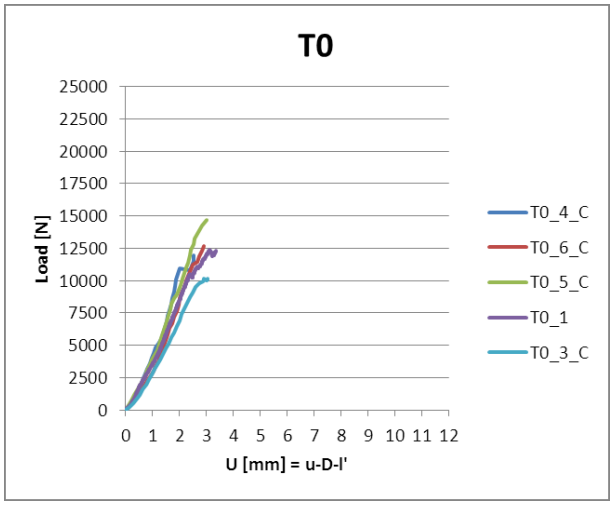

4.m - The curves U-L registered during test of series T0

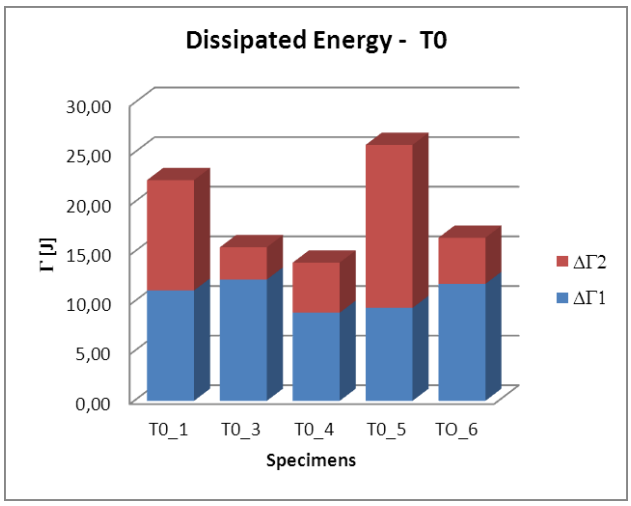

4.n The energy dissipated during the tests of series T0

The numerical values of peaks and delta energy are presented in *table 4.I.*

	u_1	P_1 [kN]	$\Delta\Gamma_1$ [kNmm]	u_2	P_2 [kN]	$\Delta\Gamma_2$ [kNmm]
T0_1	2,38	10,51	11,12	3,36	12,28	11,12
T0_3	2,72	9,82	12,22	3,05	10,14	3,25
T0_4	2,00	10,98	8,88	2,53	11,92	5,05
T0_5	1,89	8,95	9,36	3,00	14,69	16,42
T0_6	2,50	11,25	11,78	2,89	12,70	4,65
Average	1,91	10,05	8,89	2,47	12,36	6,75

fig. 4.I - Peaks and energy registered during the tests of series T0

Four of the six specimens tested in series T0 failed by cohesive fracture inside the fire brick. The cracks observed interest a layer under the CFRP of thickness 3-8 mm. The fractures developed during the stroke B'C subdivided the support in more blocks with a shape of "rib".

One of the specimen tested failed with a mixed fracture characterized by superficial and deep cracks. In all the experiments of series T0 a prism of support, with the approximates dimensions of 1,5 cm thickness and 5 cm length, was removed with the bonded CFRP sheet in the brittle failure. Several photos of the samples T0 after the test are presented in *figure 4.o*. The *table 4.I* attributes a failure mode to each sample.

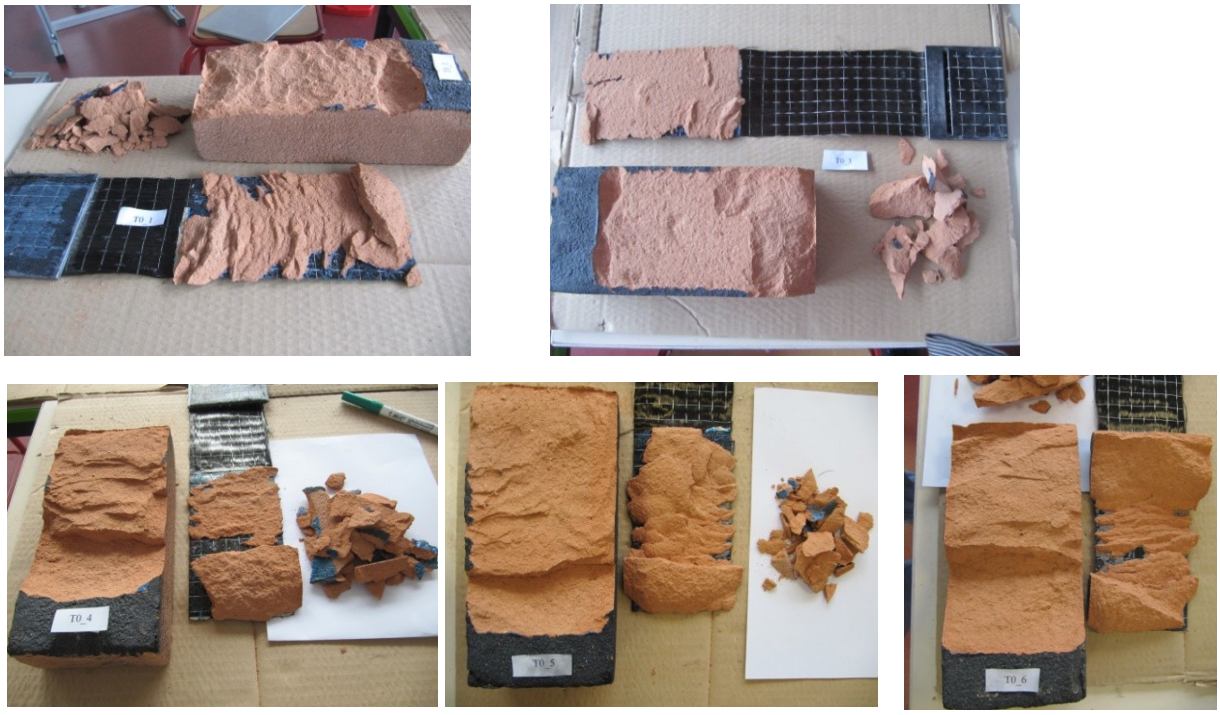

fig. 4.o - The samples of series T0 after the test execution (in order T0_1, T0_3, T0_4, T0_5, T0_6)

Specimen	*Fracture in C*
T0_1	*CF*
T0_3	*MF*
T0_4	*CF*
T0_5	*CF*
T0_6	*CF*

tab. 4.II - The failure modes of specimens T0

The strain fields of a representative specimen T0 is presented below (specimen T0_1). These results have been obtained by digital image correlation matching several photos with a reference image. The strain value presented herein are relative to some instants of the crack advancement process

(*fig. 4.p*) to shown the displacement of the strain transfer zone. The digital image correlation has been realized using a region of interest composed by a grid of square ZOI (127x127 pixel²) composed by 11 columns and 17 lines. The graph of figure 4.q shown the values of the strain ε_{yy} (same direction of the load) in the central column for eight different instant of load (tab. 4.III).

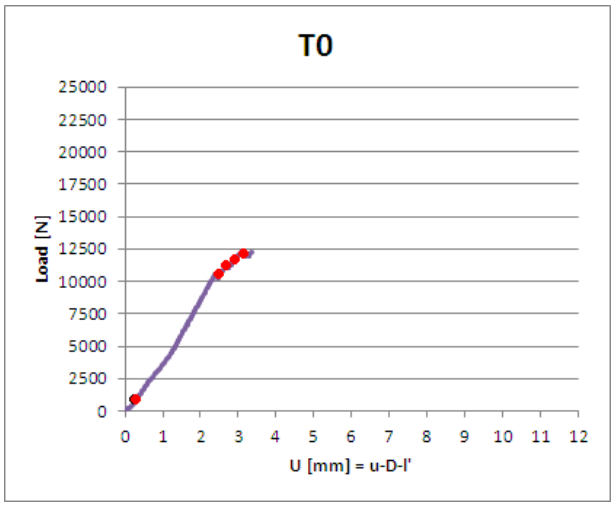

L [N]	*Photo*
1882	*6*
10670	*38*
10970	*39*
11210	*40*
12010	*43*
12040	*44*
12110	*44bis*
12210	*44quinque*

4.p - *The graph U-L of specimen T0_1 with the localization of the photos used to realize the chromatically representation of strain.*

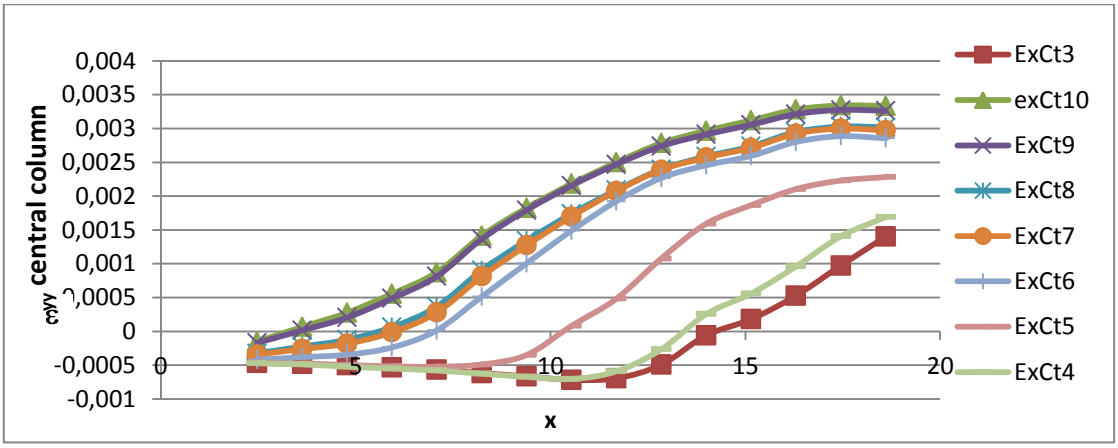

4.q - *The graphs x[mm]-□yy of several instant of load history (the results are referred to the central line)*

The *figure 4.q* describe the increment and the displacement of the strain transfer zone from the loaded to the unloaded side. This strain field evolution agree with the literature graph of strain presented in the first chapter (*figg. 1.z, 1.aa and 1.dd*).

The chromatic representation of *fig. 4.r* show the ε_{yy} field in four steps of charge. In the images it's evident the displacement of the strain transfer zone. The images remark a high concentration of strain in the left side; exactly the same side where the brittle failure export more support material (fig. 4.o). The images related to the ε_{xx} show that during the application of the load a contraction of the CFRP sheet in the x direction happen.

DIC _ Strain ε_{yy} (after "lissage")

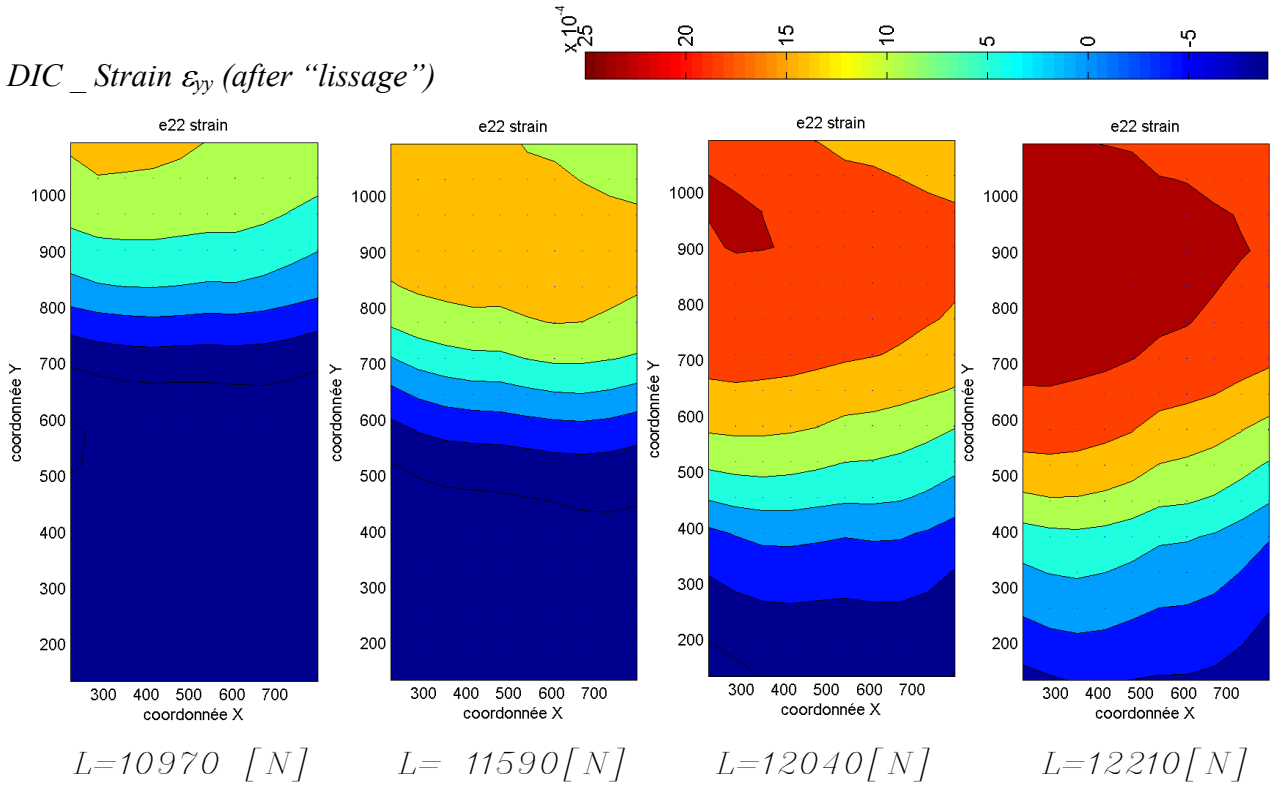

fig. 4.r - The strain εyy of four step of test T0_1 obtained by Digital $_{Image}$ Correlation

DIC _ Strain ε_{xx} (after "lissage")

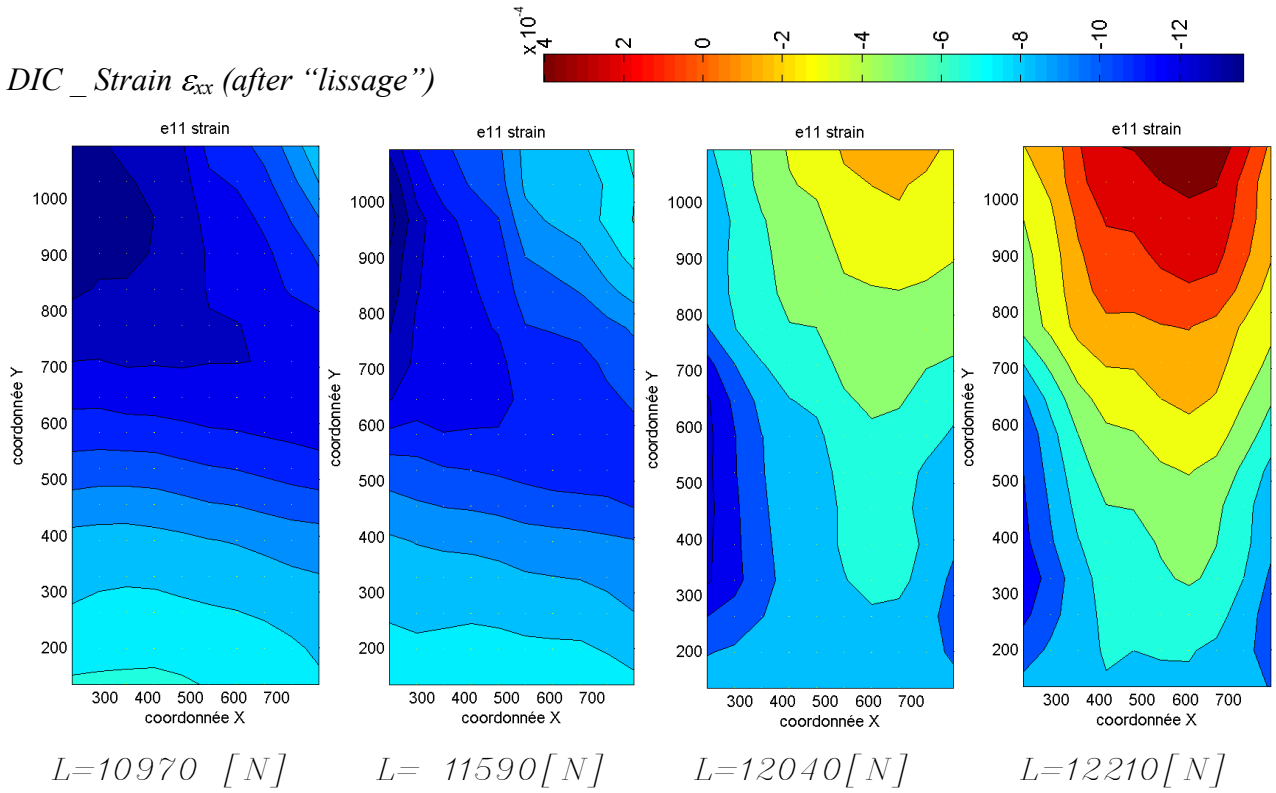

fig. 4.s - The strain εxx of four step of test T0_1 obtained by Digital $_{Image}$ Correlation

4.2.2 Series T1_25_V

All the specimens of series T1_25_V present an experimental behavior under shear loading similar to that exposed in the *fig. 4.a*. As well as in series T0 analyzed above, during the tests a first peak P_1 and a second peak P_2 were registered. After the achievement of this second one, a brittle debonding failure between the CFRP sheet and the fire brick support occurred. In the series T1_25_V the totally fall of the load, subsequent to the achievement of P_2, is avoided by the anchor (*fig. 4.t*). After the debonding, it remains inserted inside the support and bonded to the surface of the composite sheet. The anchor permits a new increase of load until peak P_3. When this value was reached the debonding of the CFRP sheet from the anchor splay occurred. Only in the test T1_25_V_4 this typology of failure was registered in the same time of the cohesive brittle fracture occurred in C (*fig. 4.a*). It is important to underline that the average of value P_2 registered in this series is equal to 15,56 kN; it's 25% higher than the value registered in series T0.

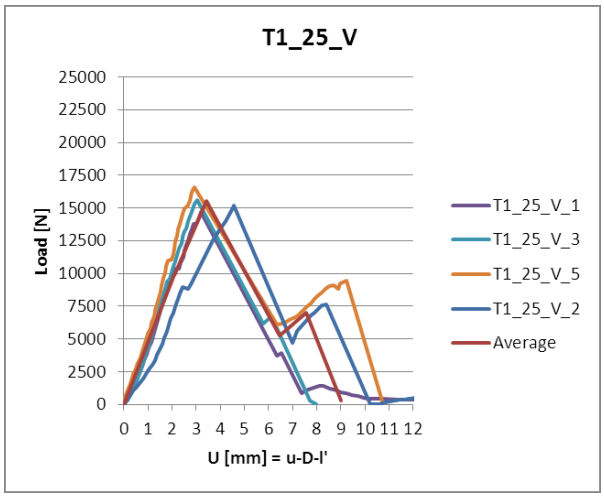

fig. 4.t - The curves U-L registered during test of series T1_25_V

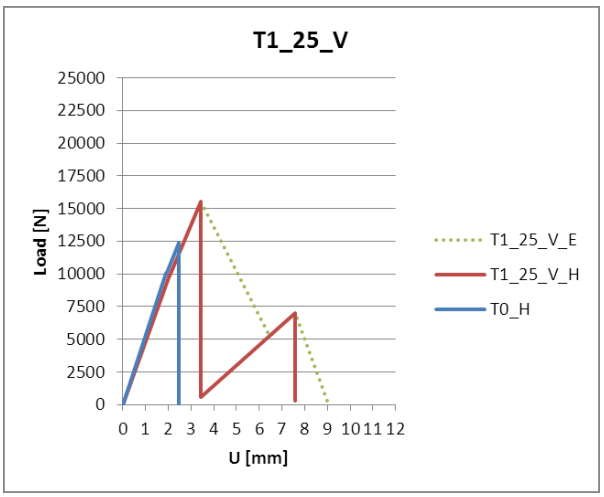

fig. 4.u - The master curve of specimens T1_25_V compared with that of T0; in dotted the experimental master curve, in red the MC

The graph U-L shown that the slope of stroke AB is almost equal for all the specimens; therefore all the samples T1_25_V present the same stiffness properties. The curve of sample T1_25_V_2 is not perfectly overlapped to the others because during this test a different steel apparatus clamping was utilized. The "master curve" MC presented in *fig.4.u* interpolate all the curves represented in *fig. 4.t*. Comparing the MC of the series T1_25_V and T0 it's shown that the stiffness of the CFRP to fire brick reinforced systems is the same "with" or "without" anchor. The dissipated energy during the tests, subdivided in the portions ($\Delta\Gamma_1$, $\Delta\Gamma_2$, $\Delta\Gamma_{imax}$, $\Delta\Gamma_3$), is represented in the bar graph of *fig. 4.v*. The average energy Γ_{end} is equal to 34,93 J; it's 86,11 % higher than that of T0.

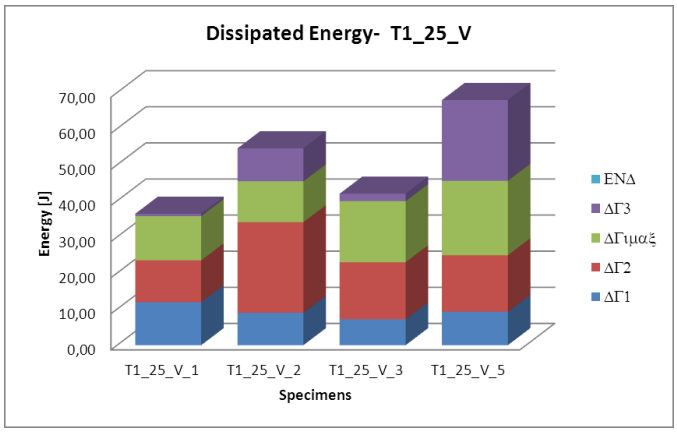

fig. 4.v - The energy dissipated during the tests of series T1_25_V

The *table 4.V* collect all the numerical values of peaks and energy.

	U_1	P_1 [kN]	$\Delta\Gamma_1$ [J]	U_2	P_2 [kN]	$\Delta\Gamma_2$ [J]	Γ_{imax_1}	U_3	P_3	$\Delta\Gamma_3$ [J]
T1_25_V_1	2,29	10,53	11,93	3,20	14,89	11,56	12,25	6,52	4,07	0,69
T1_25_V_2	2,43	8,99	8,97	4,57	15,18	25,11	11,32	8,39	7,65	9,14
T1_25_V_3	1,78	9,36	7,14	3,05	15,61	15,85	16,92	6,10	6,74	2,07
T1_25_V_5	1,81	10,96	9,25	2,95	16,56	15,65	20,64	9,23	9,42	22,37
average	2,08	9,96	9,32	3,44	15,56	17,04	15,28	7,56	6,97	8,57

fig.4.IV - Peaks and energy registered during the tests of series T1_25_V

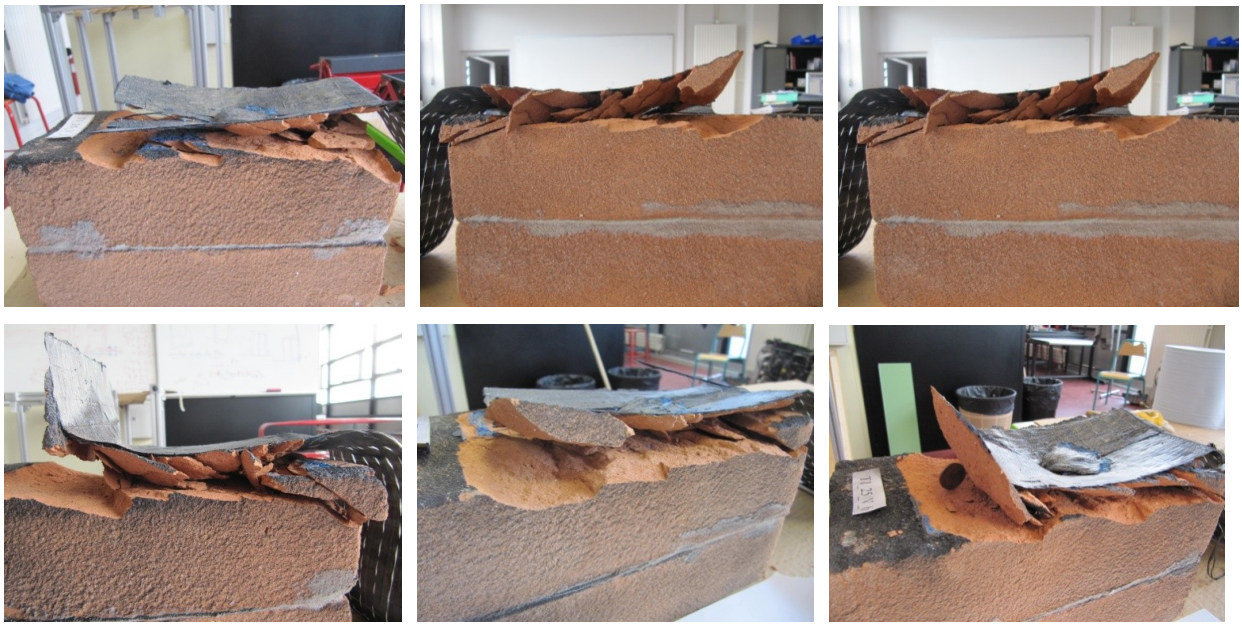

fig. 4.w - *The samples of series T0 after the test execution (in order T1_25_V_1, T1_25_V_2, T1_25_V_3, T1_25_V_4, T1_25_V_5, T1_25_V_6)*

Two principal failures interest the specimens (fig. 4.w); the debonding in point C, and the anchor failure in E (*fig. 4.a*). In the point C a cohesive fracture was observed in all tests; it was characterized by deep cracks in a layer of 5-8 mm tick under the CFRP sheet. As well as in series T0 a prism was removed by the CFRP from the unloaded end. The anchor failures of all the tests occurred by a brittle debonding between the sheet and the spray anchor (*table 4.V*).

Specimen	*Fracture in C*	*Fracture in E*
T1_25_V_1	CF	DSA
T1_25_V_2	CF	DSA
T1_25_V_3	CF	DSA
T1_25_V_4	CF - CSA	-
T1_25_V_5	CF	DSA
T1_25_V_6	CF	DSA

Table 4.V - The failure modes of specimens T1_25_V

The strain field of a representative specimen of series T1_25_V is analyzed herein. The sample studied below is the T1_25_V_5. The strain values have been obtained by DIC matching the photos localized in the graph U-L (*fig. 4.x*) whit a reference signal (photo at u=0,04 mm). The graph that represented the variation of the strain ε_{xx} during the increase of the load is shown if *fig. 4.y*. The value of deformations in this image are relative to the central column. Also in this case the displacement of the strain zone from the loaded side to the unloaded side is registered. The presence of the anchor are denounced by the bump of the curves in correspondence to y=90 mm (ordinate of the anchor). This last is due to the shadow generated by the anchor splay volume.

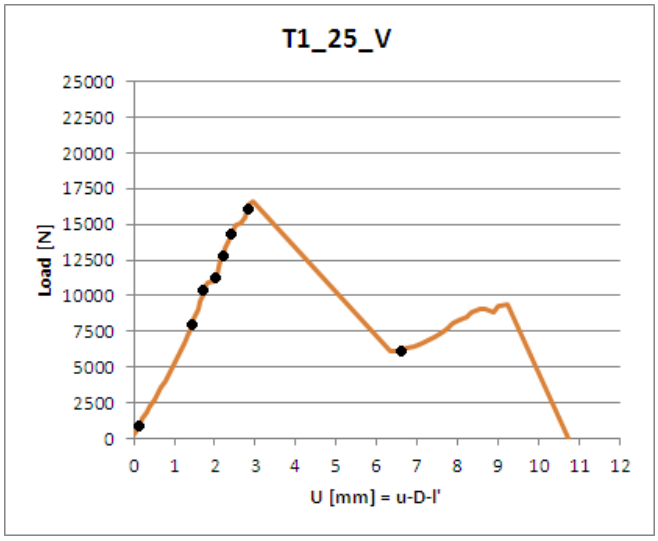

STEP DIC	L [N]	photo
refe	1020	2
1	7790	27
2	10600	36
3	11130	39
4	13010	45
5	14760	50
6	15990	54
7	5700	58

fig. 4.x - The graph U-L with the localization of the photos used for the DIC

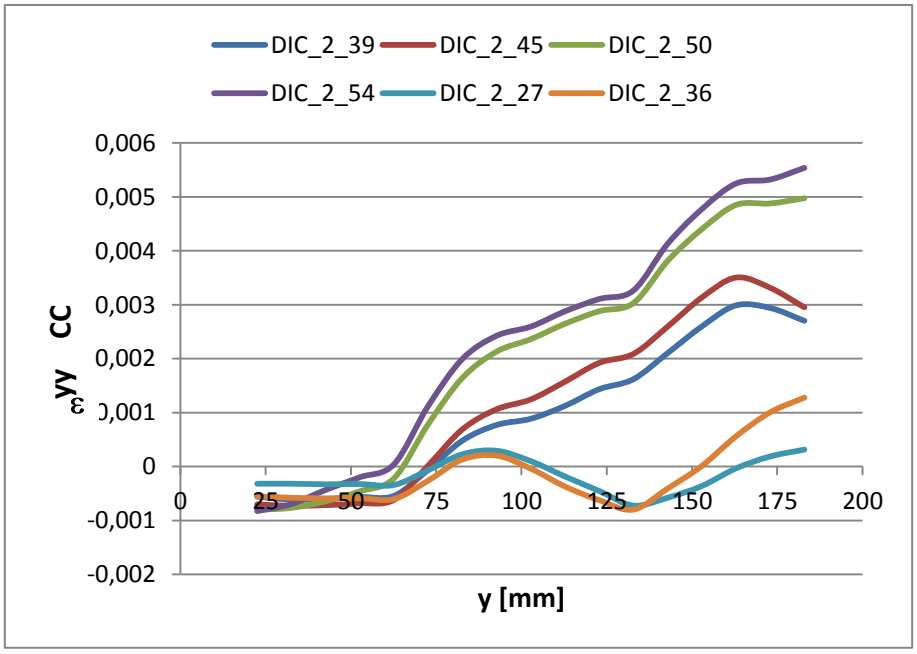

fig. 4.y - The graphs y[mm]-□yy of several instant of load history (the results are referred to the central line)

The chromatic representations of the strain fields ε_{yy} and ε_{xx}, corresponding to four load steps, are presented herein. The figure 4.z shown that the anchor obstruct the advancement of the strain "front". The ε_{xx} fields shown that a restriction of the CFRP sheet occur during the test versus the nail placement.

DIC _ Strain ε_{yy} (after "lissage")

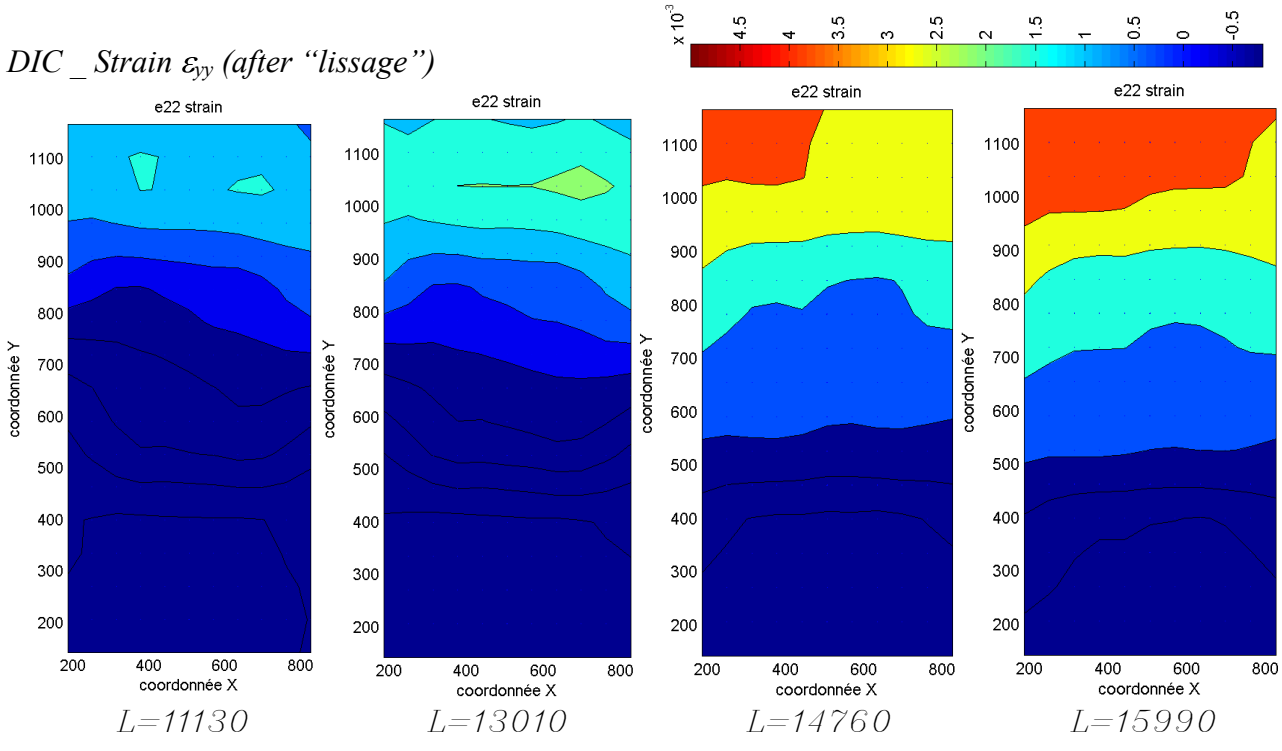

fig. 4.z - The strain εyy of four step of test T1_25_V_5 obtained by Digital $_{Image}$ Correlation

DIC _ Strain ε_{xx} (after "lissage")

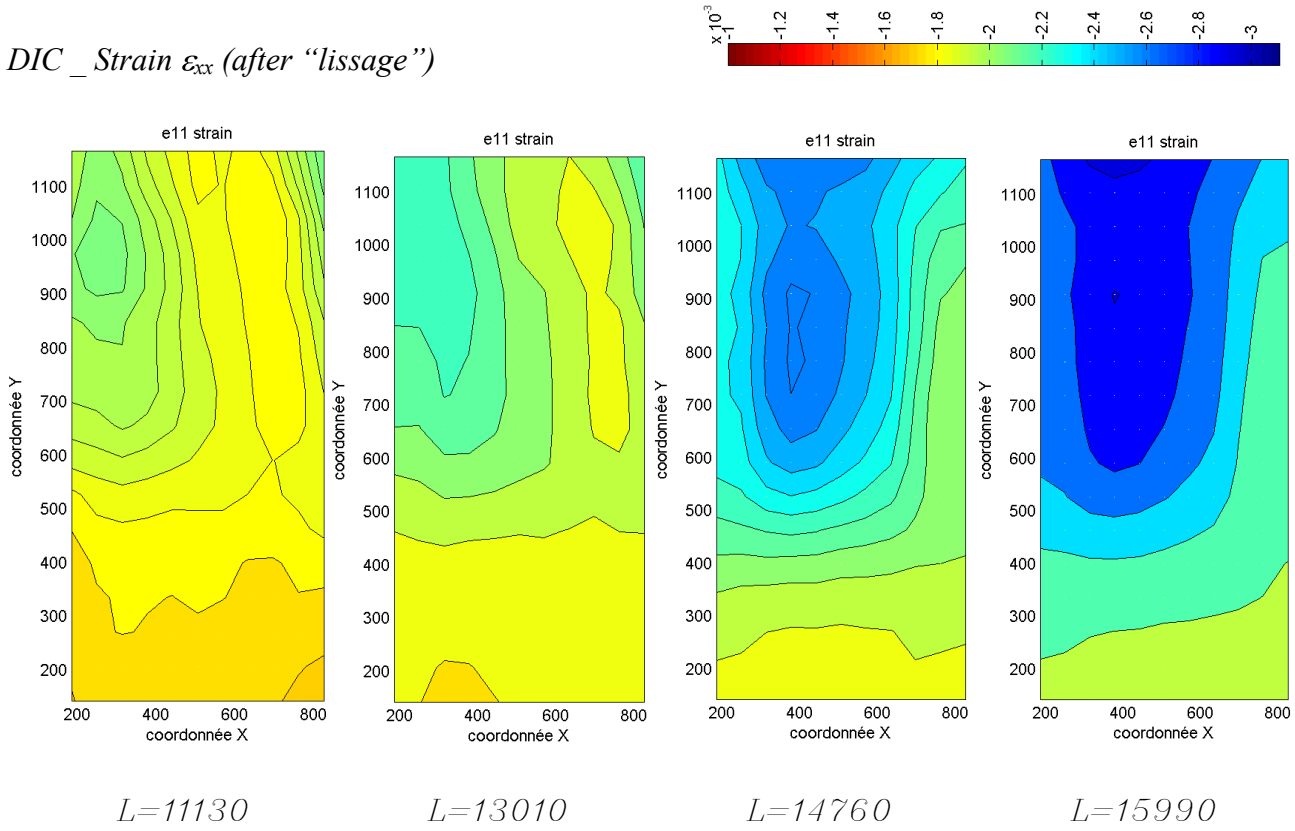

fig. 4.aa - The strain ε_{xx} of four step of test T1_25_V_5 obtained by Digital Image Correlation

4.2.3 Series T1_40_O

All the specimens of series T1_40_0, except one, are characterized by a test curve U-L (*fig. 4.t*) similar to that of *fig. 4.a*. The average values of the peaks P_1, P_2 and P_3 are respectively 10,89 kN, 15.62 kN and 7,80 kN. The average peak P_2 registered during the series T1_40_0 is 26,39% bigger than that noticed in tests T0. Only the test T1_40_O_2 not presents a loading anchor phase after the achievement of P_2. The master curve MC presented in *figure 4.dd* has been realized by interpolation of the T1_40_O experimental curves neglecting the sample T1_40_O_2.

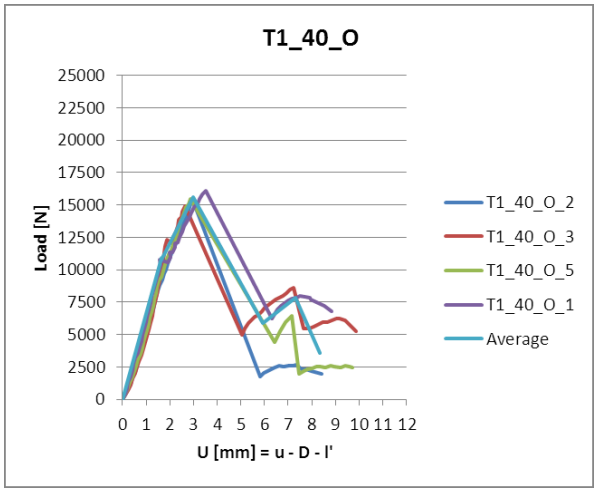

fig. 4.cc - The curves U-L registered during test of series T1_40_O

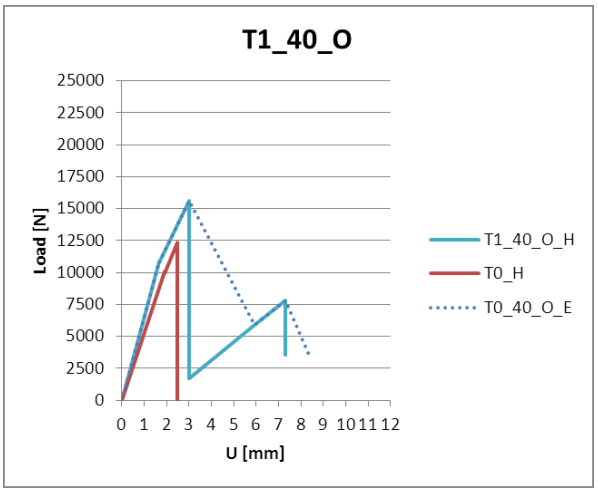

fig. 4.dd - The master curve of specimens T1_40_O compared with that of T0; in dotted the experimental master curve, in red the MC

The stroke slopes AB of the several tests represented in *figures 4.cc* show that the specimens T1_40_O are characterized by the same stiffness properties. Furthermore, the comparison of master curves *(fig. 4.dd)* demonstrates that the samples T1_40_O and TO have in common the same value of stiffness. The values of dissipated energy portions are plotted in the *figure 4.ee* using bar graphs.

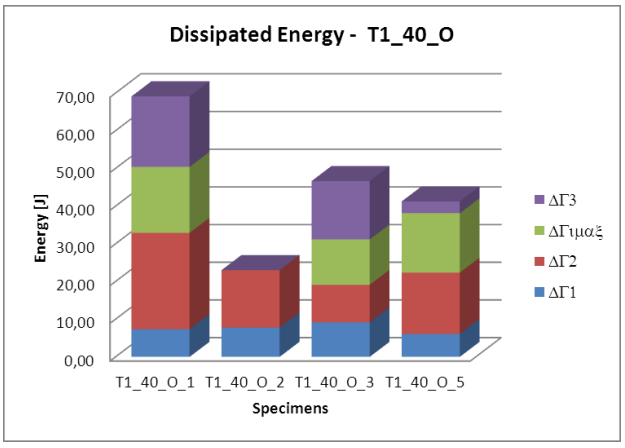

fig. 4.ee - The energy dissipated during the tests of series T1_40_O

The *table 4.VI* collects all the numerical values of peaks and energy.

	U_1	P_1 [kN]	$\Delta\Gamma_1$ [J]	U_2	P_2 [kN]	$\Delta\Gamma_2$ [J]	Γ_{imax_1}	U_3	P_3	$\Delta\Gamma_3$ [J]
T1_40_O_1	1,56	11,19	7,34	3,52	16,52	25,55	17,51	7,50	8,40	18,70
T1_40_O_2	1,75	9,75	7,77	2,97	15,45	15,25	NO	NO	NO	NO
T1_40_O_3	1,87	12,30	9,15	2,63	14,88	9,97	12,04	7,22	8,60	15,50
T1_40_O_5	1,54	9,18	6,10	2,86	15,46	16,24	15,78	7,14	6,41	3,11
average	1,66	10,89	7,53	3,00	15,62	17,25	15,11	7,29	7,80	12,44

tab. 4.VI - Peaks and energy registered during the tests of series T1_40_O

The failures mode observed when the peak P_2 was achieved are the cohesive fracture and the mixed fracture (*fig. 4.ff*). This last has been manifested only in the test T1_40_O_2, confirming the hypothesis that a peeling load component was developed during the experiment. The experiments show that the debonding of 360° splay anchor occurs in a ductile manner. When the peak P3 was achieved, approximately 150° of the opening anchor fan was detached from the support (*fig. 4.gg*). This splay's parties had the same direction of the applied load. After the load fall registered in E a residual resistance was recorded; this last is due to the remaining bonded part of the splay anchor and to the friction between the faces of fracture. In this phases, the application of load allows to a progressive debonding of the fan anchor and to the opening of the CFRP sheet in correspondence to the central longitudinal axis (*fig. 4.hh*).

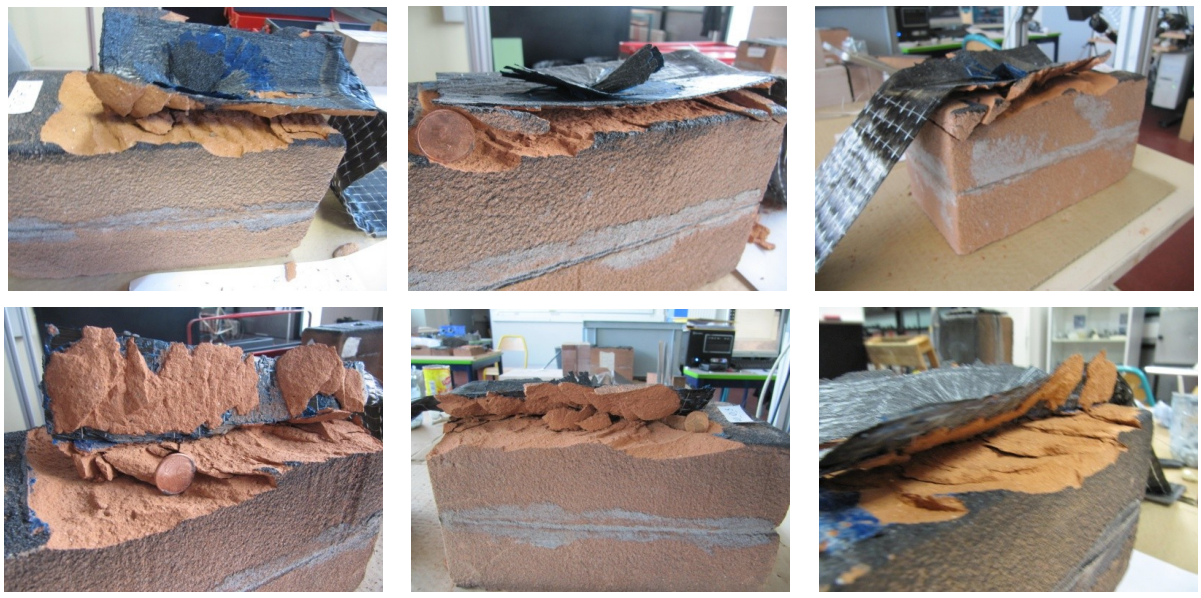

fig. 4.ff - The samples of series T0 after the test (in order T1_40_O_1, T1_40_O_2, T1_40_O_3, T1_40_O_4, T1_40_O_5, T1_40_O_6)

Specimen	*Fracture in C*	*Fracture in E*
T1_40_O_1	CF	DSA
T1_40_O_2	MF+DSA	-
T1_40_O_3	CF	DSA
T1_40_O_4	CF	DSA
T1_40_O_5	CF	DSA
T1_40_O_6	CF	DSA

Tab 4.VII - The failure modes of specimens T1_40_O

fig. 4.gg - The specimen T1_40_O_2 after the achievement of the peak P3

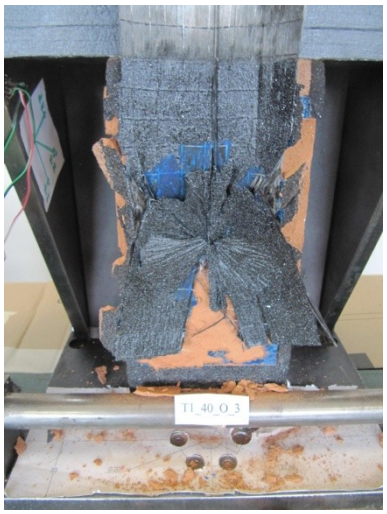

fig. 4.hh - The specimen T1_40_O_3 during the post P3 phases

The strain field computed by DIC shown that during the test the deformed zone moves from the loaded to the unloaded side. The anchor allow to a concentration of stress and deformation in the surface within the anchor and the loaded side. In the *par.4.2.3.1* a results sheet shown the displacement and strain field obtained in the indicative case of specimen T1_25_V_5.

4.2.4 Series T1_40_V

The curves U-L of the tests T1_40_V are represented in *fig. 4.ii*. The graphs are similar to that presented in the precedents paragraphs on CFRP reinforced fire brick fastened with one anchor. After a first stroke AB, achieved the value P_1, the crack advance from the loaded to unloaded side. Reached the value P_2, a load fall and a successive anchor loading phases permits to achieve the peak P_3. The average values of P_1, P_2 and P_3 registered during the tests are respectively 9.78, 16.13 and 10.10 kN. The curves of tests T1_40_V_1 and T1_40_V_2 shown that the total anchor debonding failure occurred by two delamination steps (*figures 4.kk*). The average load P_2 is 30,54% bigger than that of T0.

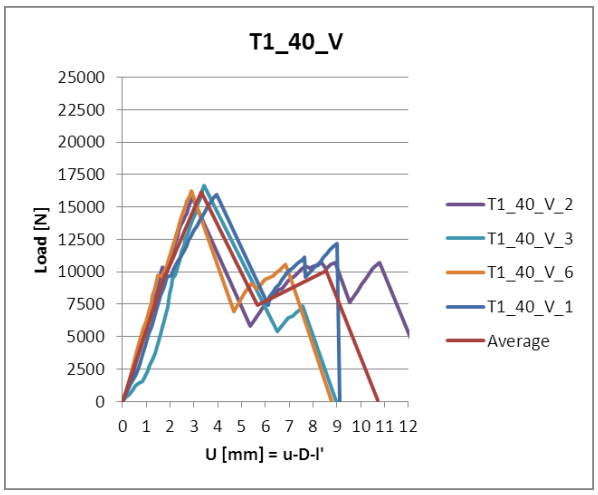

fig. 4.ii - The curves U-L registered during test of series T1_40_V

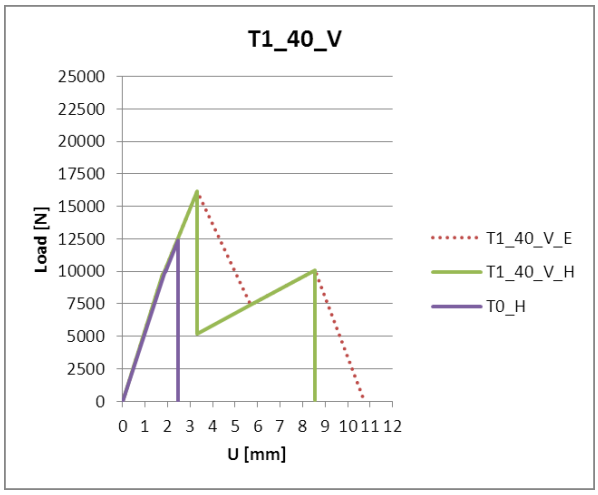

fig. 4.jj - The master curve of specimens T1_40_V compared with that of T0; in dotted the experimental master curve, in red the MC

As well as in the precedent series the stroke slopes AB of the tests (*fig.4.ii)* shows that the specimens T1_40_V are characterized by the same stiffness properties K. Furthermore the comparison of master curves *(fig.4.jj)* demonstrate, that the samples T1_40_O and TO have in common the same K.

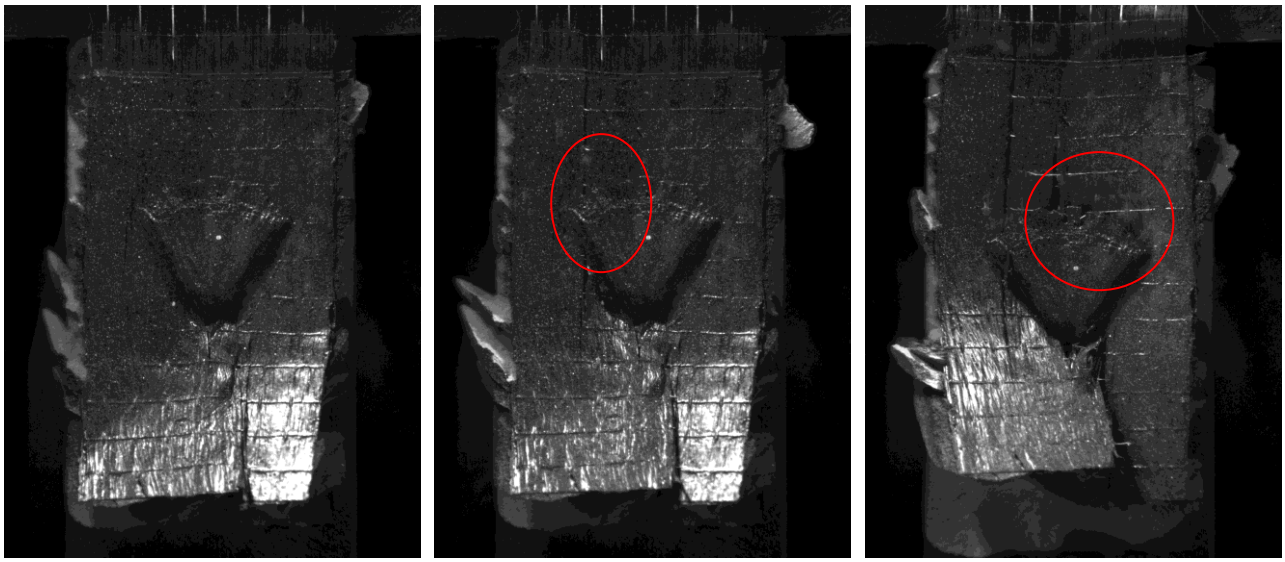

fig. 4.kk - Two frontal image of the specimen T1_40_V_1. At left the first partial fan debonding is shown, at right the photo of the specimen surface after the total delamination (second step)

The energy dissipated during the tests is reported in the bar graphs of *figure 4.ll*. The average value of Γ_{end} is equal to 51,53 [J]. It's 174 % more higher than the average Γ_{End} measured in series T0. The *table 4.VIII* collects all the numerical values of peaks and energy.

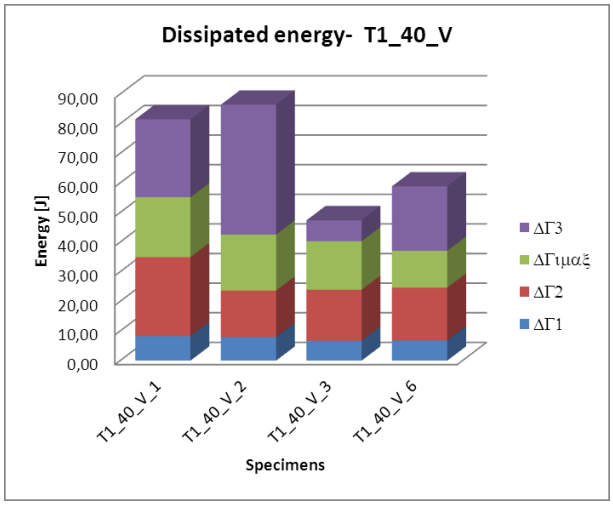

fig. 4.ll - The energy dissipated during the tests of series T1_40_V

	U_1	P_1 [kN]	$\Delta\Gamma_1$ [J]	U_2	P_2 [kN]	$\Delta\Gamma_2$ [J]	Γ_{imax_1}	U_3	P_3	$\Delta\Gamma_3$ [J]
T1_40_V_1	1,87	9,58	8,24	3,96	15,95	26,68	20,26	9,14	11,92	26,30
T1_40_V_2	1,68	10,38	7,96	2,92	15,72	15,68	18,91	10,77	10,71	43,87
T1_40_V_3	2,10	9,44	6,70	3,43	16,64	17,24	16,38	7,58	7,34	7,05
T1_40_V_6	1,48	9,72	6,85	2,90	16,22	17,80	12,46	6,76	10,44	21,74
average	1,78	9,78	7,44	3,30	16,13	19,35	17,00	8,56	10,10	24,74

tab. 4.VIII - Peaks and energy registered during the tests of series T1_40_V

Several modality of failure has been observed during the tests (*fig. 4.mm* and *tab. 4.IX*). The experiments T1_40_V_1, T1_40_V_3 and T1_40_V_6 have been characterized by a cohesive fracture in C and an anchor splay debonding in E. The specimen T1_40_V_2 failed by a Mixed Failure in C and a Pull Out of Nail (PON) in E. In this test the anchor was released from the support breaking the fire brick in few prisms. The specimen T1_40_V_4 known a fall of load in C due to a contemporary cohesive and anchor splay debonding fracture. The sample T1_40_V_5 fail in C with a prismatic failure, in this case no debonding has been registered.

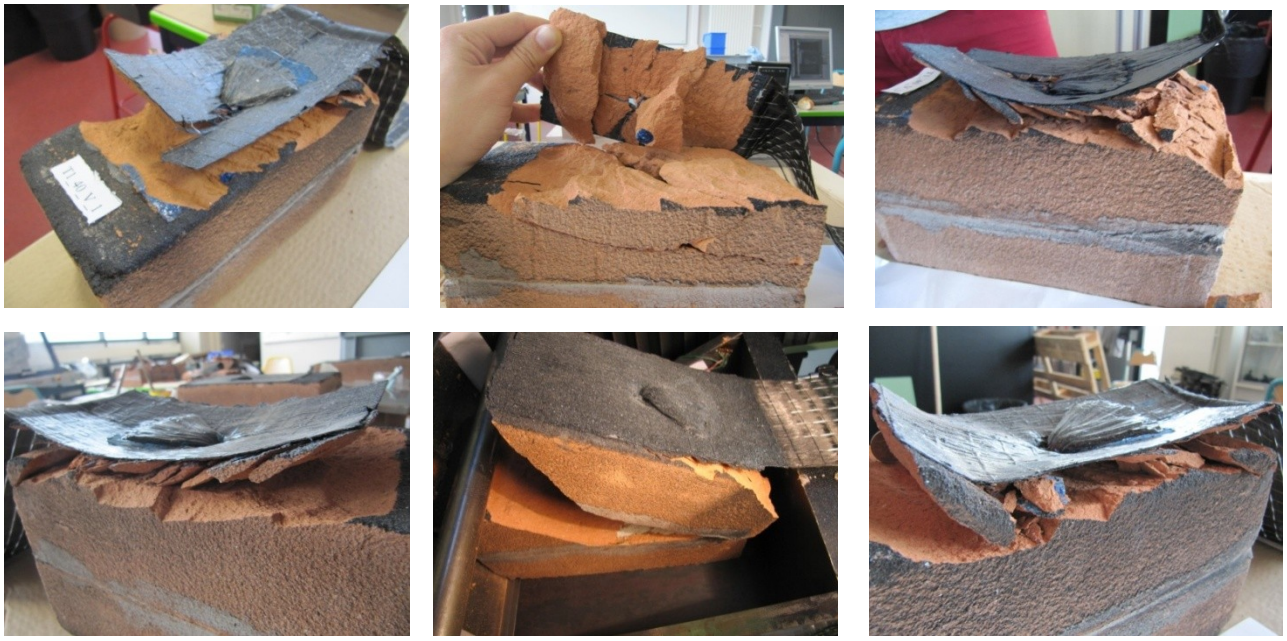

fig. 4.mm - The samples of series T0 after the test (in order T1_40_V_1, T1_40_V_2, T1_40_V_3, T1_40_V_4, T1_40_V_5, T1_40_V_6)

Specimen	*Fracture in C*	*Fracture in E*
T1_40_V_1	CF	DSA
T1_40_V_2	MF	PON
T1_40_V_3	CF	DSA
T1_40_V_4	CF - DSA	-
T1_40_V_5	PF	-
T1_40_V_6	CF	DSA

tab. 4.IX - The failure modes of specimens T1_40_V

The DIC shown that during the test, the deformed zone moves from the loaded to the unloaded side. The anchor allows to a concentration of stress and deformation in the surface within the fan and the loaded side. In the *par.4.2.4.1* a results sheet shown the displacement and strain field obtained in the indicative case of specimen T1_40_V_6.

T1_40_V_6

Specimen's imperfections:
Not remarkable

Speckle pattern quality:
Homogeneous size spot. Good quality

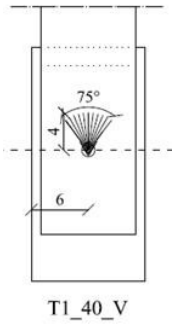

Alignment in the steel apparatus:
Optimal

Light:
Natural light

Remarks:
The test has been realized rounding the carbon fabric in the @ plate. A set of comparator has been used to control the displacement of the steel lock

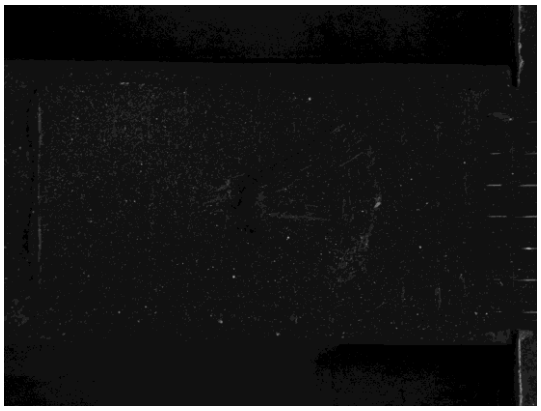

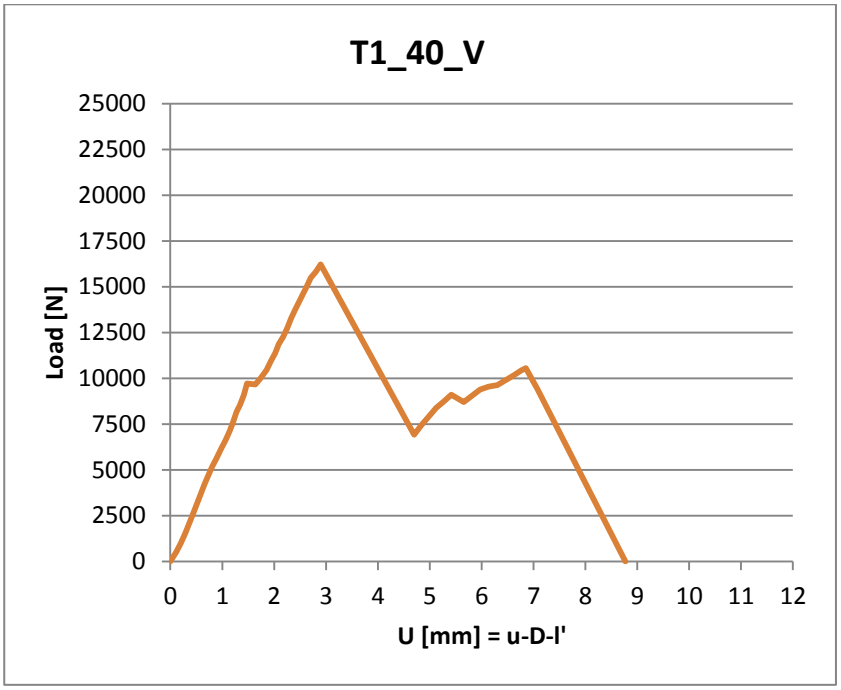

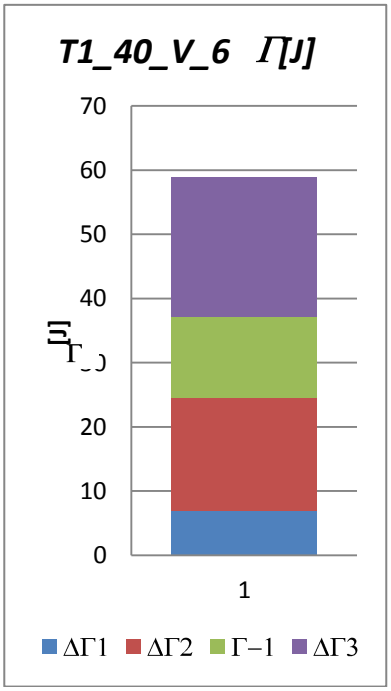

U_1	P_1 [kN]	$\Delta\Gamma_1$ [J]	U_2	P2 [kN]	$\Delta\Gamma_2$ [J]	Γ_{imax_1}	U_3	P_3	$\Delta\Gamma_3$ [J]
1,48	9,72	6,85	2,90	16,22	17,80	12,46	6,76	10,44	21,74

Specimen	*Fracture in C*	*Fracture in E*
T1_40_V_6	CF	DSA

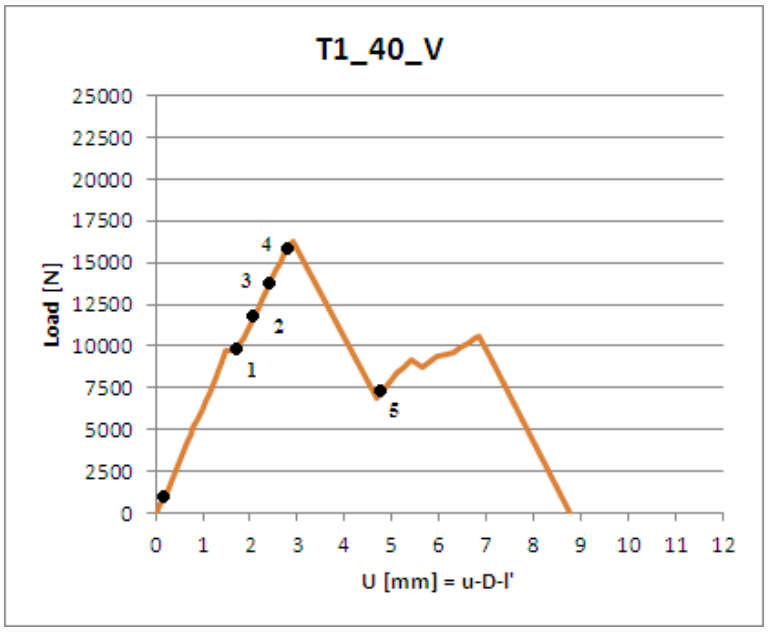

STEP DIC	L [N]	photo
refe	1000	2
1	9680	31
2	11880	38
3	13750	44
4	15830	52
5	6930	54

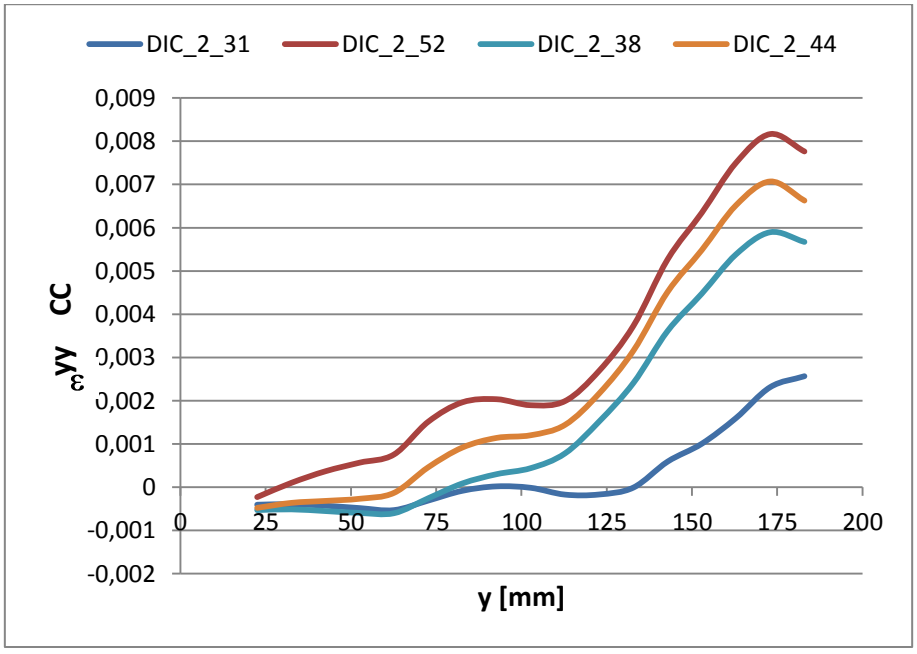

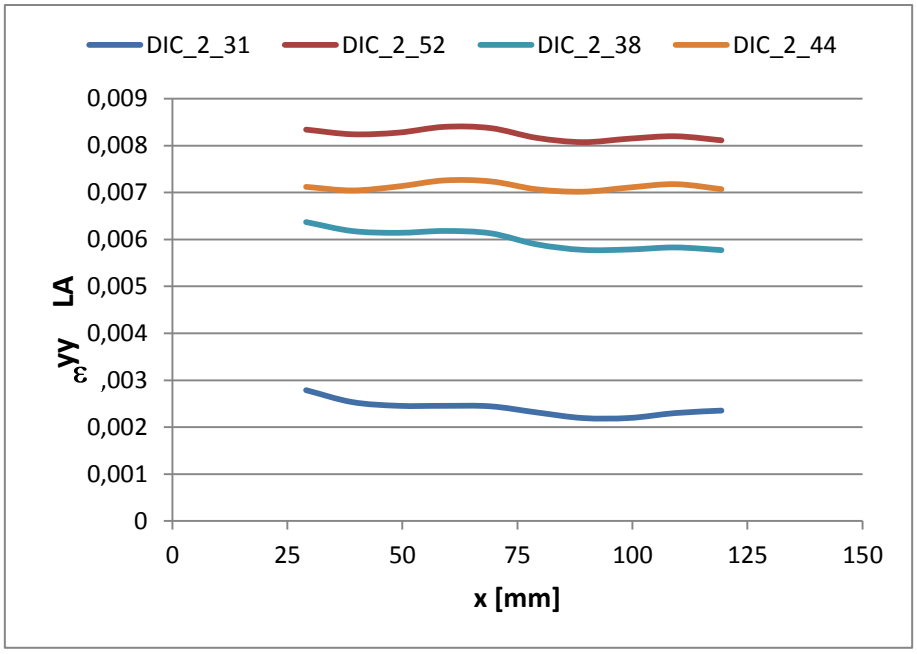

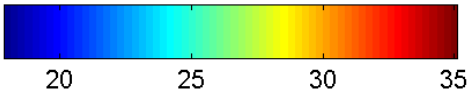

DIC _ Displacement modulus (after "lissage")

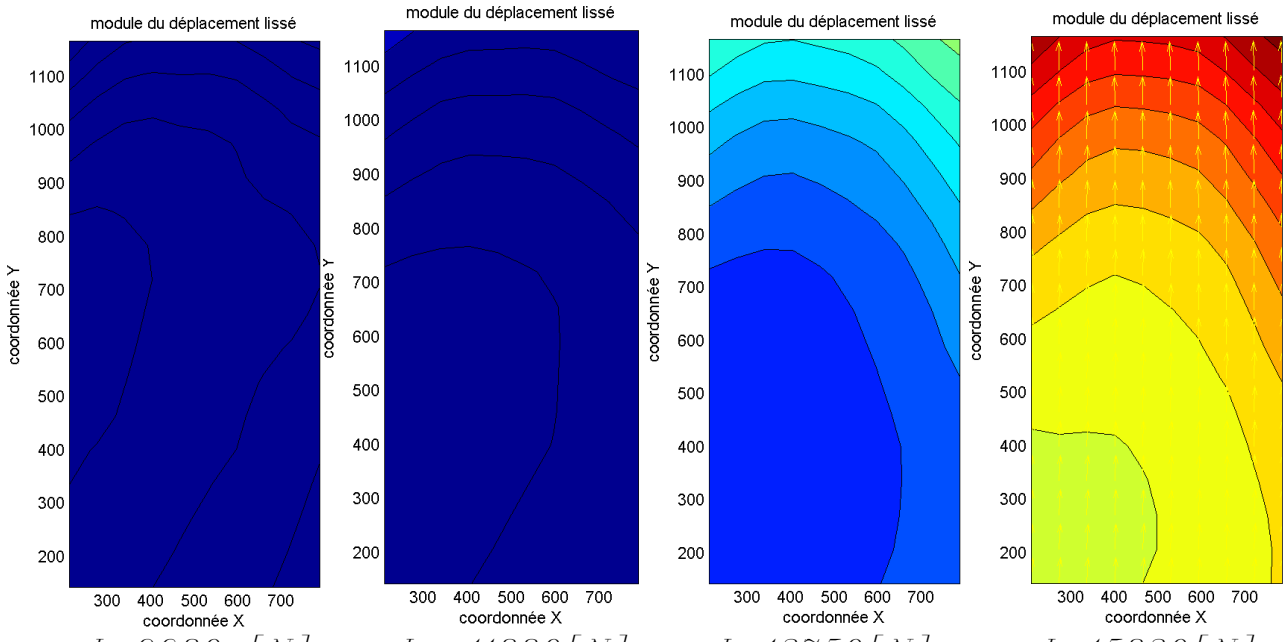

L=9680 [N] *L= 11880[N]* *L=13750[N]* *L=15830[N]*

DIC _ Strain ε_{yy} (after "lissage")

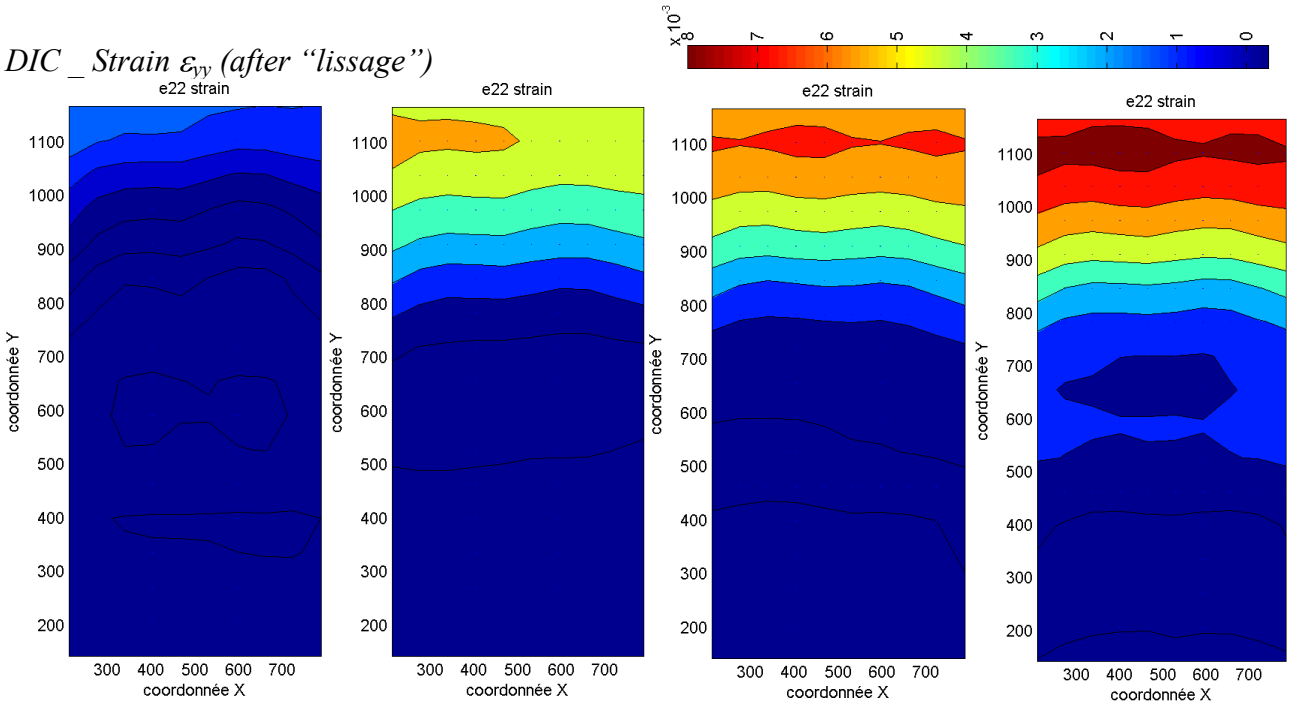

L=9680 [N] *L= 11880[N]* *L=13750[N]* *L=15830[N]*

DIC _ Strain ε_{xx} (after "lissage")

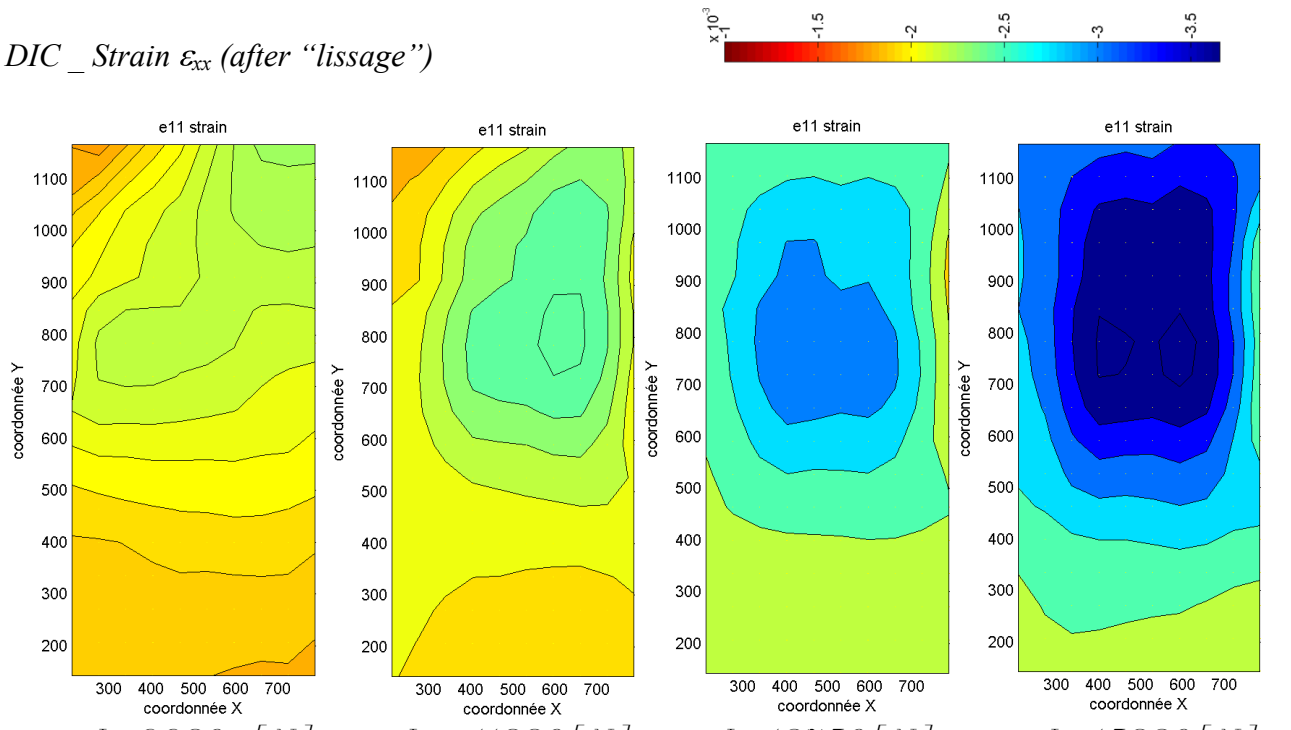

L=9680 [N] *L= 11880[N]* *L=13750[N]* *L=15830[N]*

4.2.5 Series T2_40_V

The tests of series T2_40_V are described by curves of figure *4.nn*. In the graph is possible to note that the rupture has occurred whit a brittle failure after the peak P2, or a brittle failure after the peak P3. The average of peak registered are 11,87 for P_1, 19,98 for P_2 and 13,73 for the peak P_3. The average value of P_2 is 61,65 % bigger than that of T0. All the sample of this series are characterized by an approximately equal stiffness, it is shown by curves of figure 4.nn. This stiffness value is the same of that registered in specimens of series T0. The comparison between the master curve (MC) of series T2_40_V and T0 is shown in figure *4.oo*. The MC of series T2_40_V has been realized by interpolation of experimental curves of fig. *4.nn* neglecting that of sample T2_40_V_2.

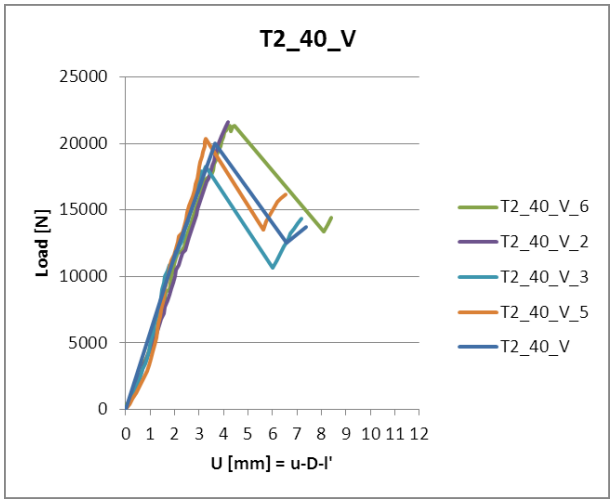

fig. 4.nn - The curves U-L registered during test of series T2_40_V

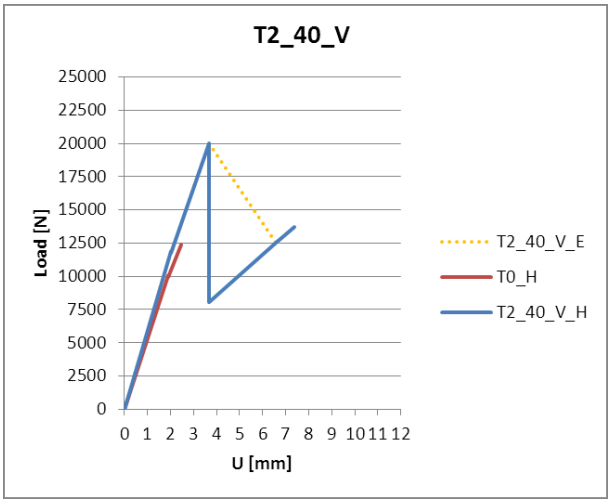

fig. 4.oo - The master curve of specimens T2_40_V compared with that of T0; in dotted the experimental master curve, in red the MC

The partial amounts of dissipated energy are shown in the bar graphs of *fig. 4.pp*. The value of are respectively 10.53 J, 25.99 J and 11.02 J. The average value of Γ_{End} is the 153% more higher than that registered in series T0.

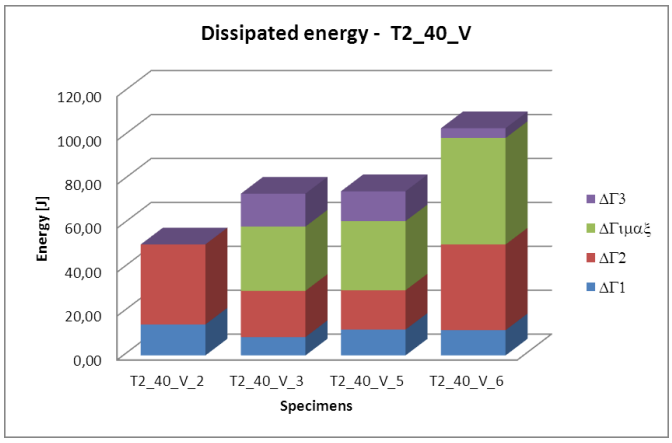

fig. 4.pp - The energy dissipated during the tests of series T2_40_V

The *table 4.X* collects all the numerical values of peaks and energy.

	U_1	P_1 [kN]	$\Delta\Gamma_1$ [J]	U_2	P_2 [kN]	$\Delta\Gamma_2$ [J]	Γ_{imax_1}	U_3	P_3	$\Delta\Gamma_3$ [J]	Γ_{End}[J]
T2_40_V_2	2,44	11,99	14,12	4,17	21,60	36,46	0,00	NO	NO	0,00	50,58
T2_40_V_3	1,78	10,84	8,36	3,26	18,22	21,06	29,26	7,20	10,57	15,00	44,41
T2_40_V_5	2,19	13,04	11,74	3,29	20,35	17,91	31,50	6,52	16,19	13,61	43,25
T2_40_V_6	2,15	11,74	11,50	4,45	21,36	39,01	48,51	8,40	14,42	4,46	54,97
average	2,04	11,87	10,53	3,66	19,98	25,99	36,42	7,37	13,73	11,02	47,55

fig. 4.X - Peaks and energy registered during the tests of series T2_40_V

Several failure modes have been observed during the tests execution. Three specimens fail in the same manner with a cohesive fracture after P2 (point C of the characteristic curve) and a prismatic brittle failure after P3 (point E of the characteristic curve) (*tab. 4.X* and *fig. 4.qq*). Two experiments, the T2_40_V_2 and the T2_40_V_3, allow to a cohesive fracture contemporary to a brittle prismatic failure. Finally, the test on specimen T2_40_V_1 is characterized by a cohesive failure in C and an anchor splay debonding in E.

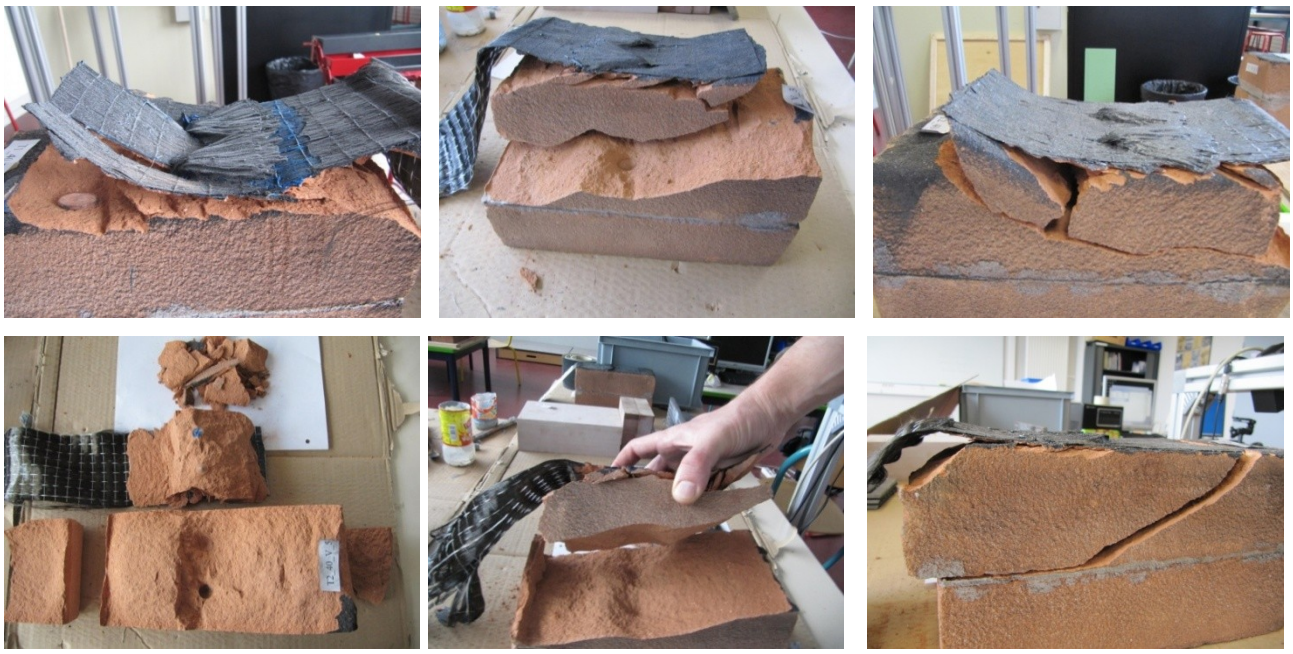

fig. 4.qq - The samples of series T0 after the test (in order T2_40_V_1, T2_40_V_2, T2_40_V_3, T2_40_V_4, T2_40_V_5, T2_40_V_6)

Specimen	*Fracture in C*	*Fracture in E*
T2_40_V_1	CF	DSA
T2_40_V_2	CF - PF	-
T2_40_V_3	CF	PF
T2_40_V_4	CF - PF	-
T2_40_V_5	CF	PF
T2_40_V_6	CF	PF

Tab. 4.XI - The failure modes of specimens T2_40_V

The DIC shown that during the test the deformed zone moves from the loaded to the unloaded side. The anchor allows to a concentration of stress and deformation in the surface within the fan and the loaded side. In the *par.4.2.4.14.2.4.1* a results sheet shown the displacement and strain field obtained in the indicative case of specimen T2_40_V_5.

T2_40_V_5

Specimen's imperfections:
Not remarkable

Speckle pattern quality:
Homogeneous size spot. Good quality

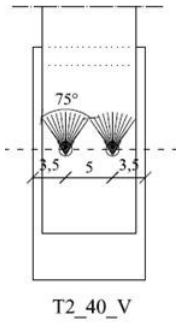

Alignment in the steel apparatus:
Distance between the steel lock and the fabric range between 3-5 mm.

Light:
Natural light

Remarks:
The fibers of the left side of fabric was strength more than the others.

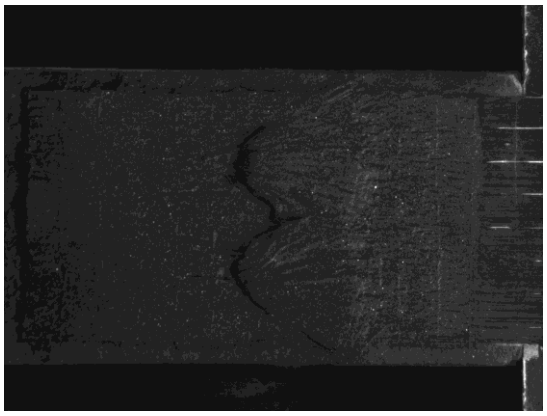

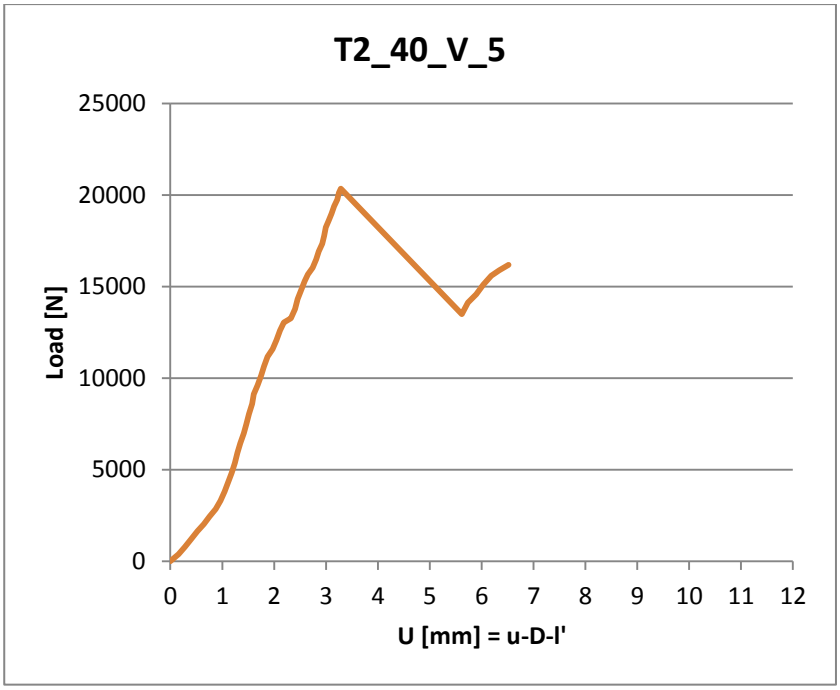

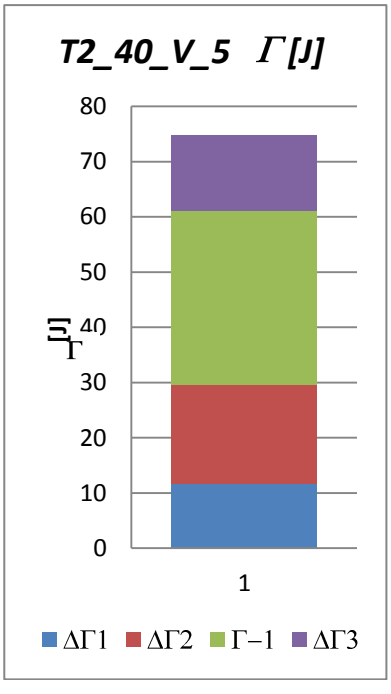

U_1	P_1 [kN]	$\Delta\Gamma_1$ [J]	U_2	P_2 [kN]	$\Delta\Gamma_2$ [J]	Γ_{imax_1}	U_3	P_3	$\Delta\Gamma_3$ [J]
2,19	13,04	11,74	3,29	20,35	17,91	31,50	6,52	16,19	13,61

Specimen	*Fracture in C*	*Fracture in E*

T2_40_V_5	CF	PF

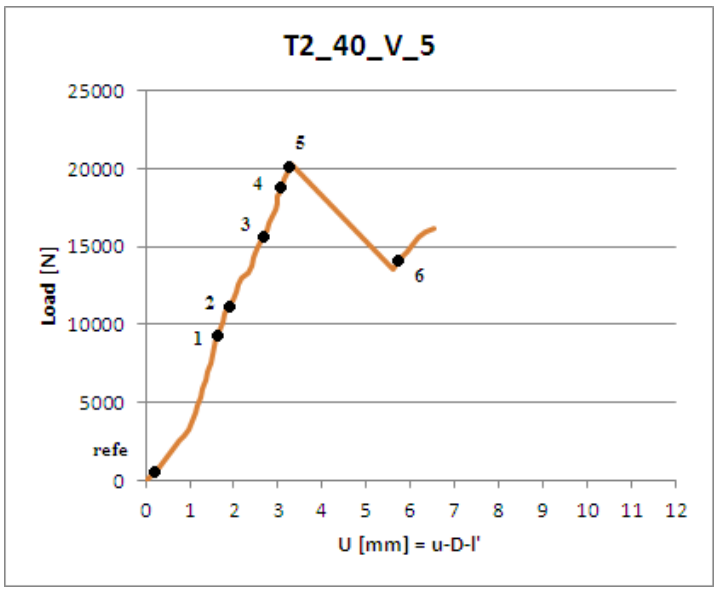

STEP DIC	L [N]	photo
refe	800	2
1	9620	28
2	35	11600
3	51	15670
4	61	18670
5	71	20130
6	72	14120

Rz	*0,16*	*[mm/pixel]*
ZOI	*128,00*	*pixel*
ZOI	*20,06*	*mm*
dx	*64,00*	*pixel*
dx	*10,03*	*mm*

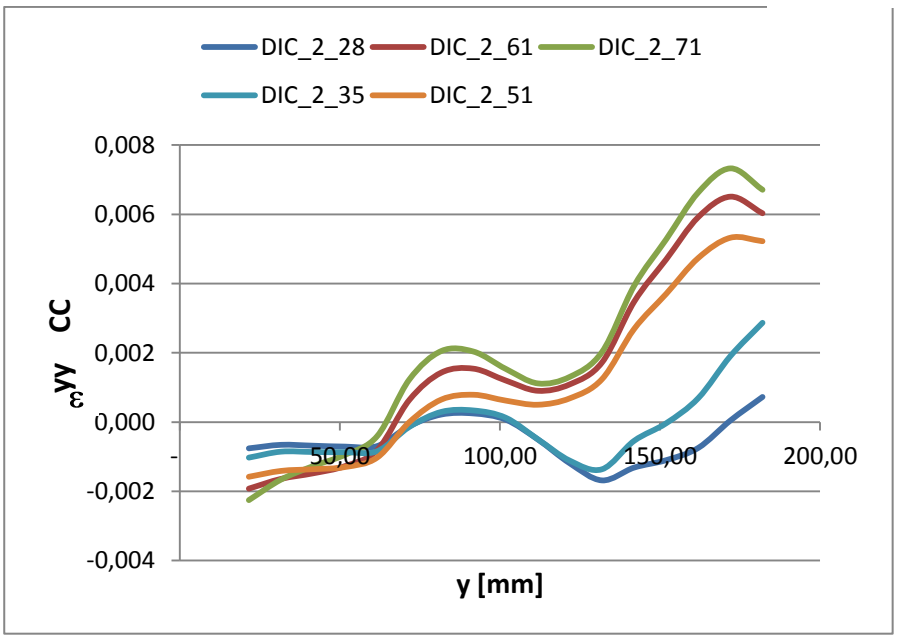

Fig….The grid of ZOI center used in the DIC analyzes

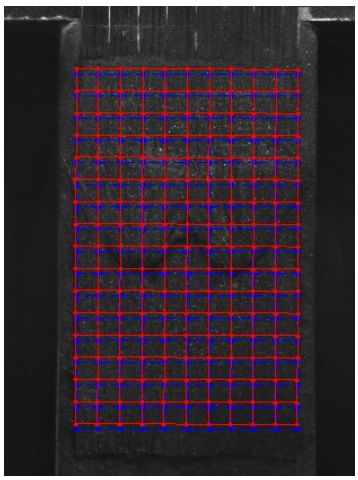

Fig. The Strain eyy in the central column of the grid varying the y value

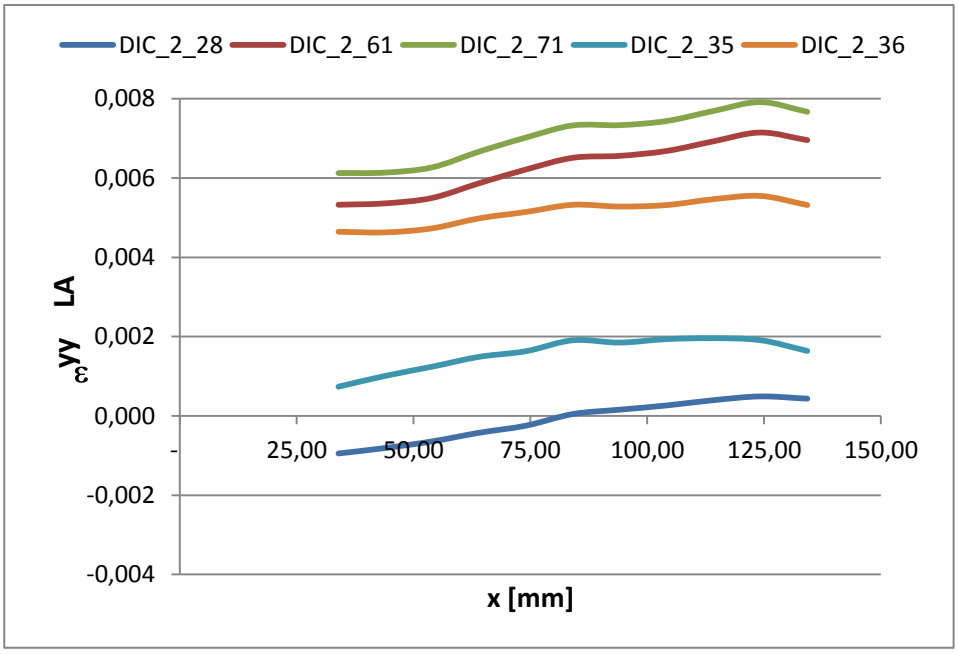

Figure…the deformed shape of the grid amplified by a factor 30 in the step 4

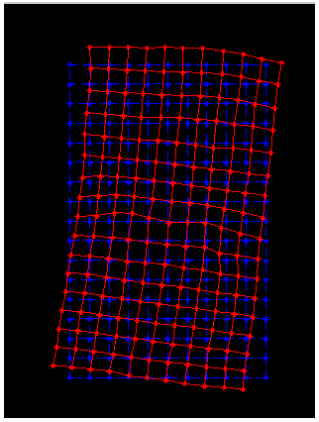

Figure…: the strain ε_{yy} in the line A of the grid, varying the value of x.

DIC _ Displacement modulus in pixel (after "lissage")

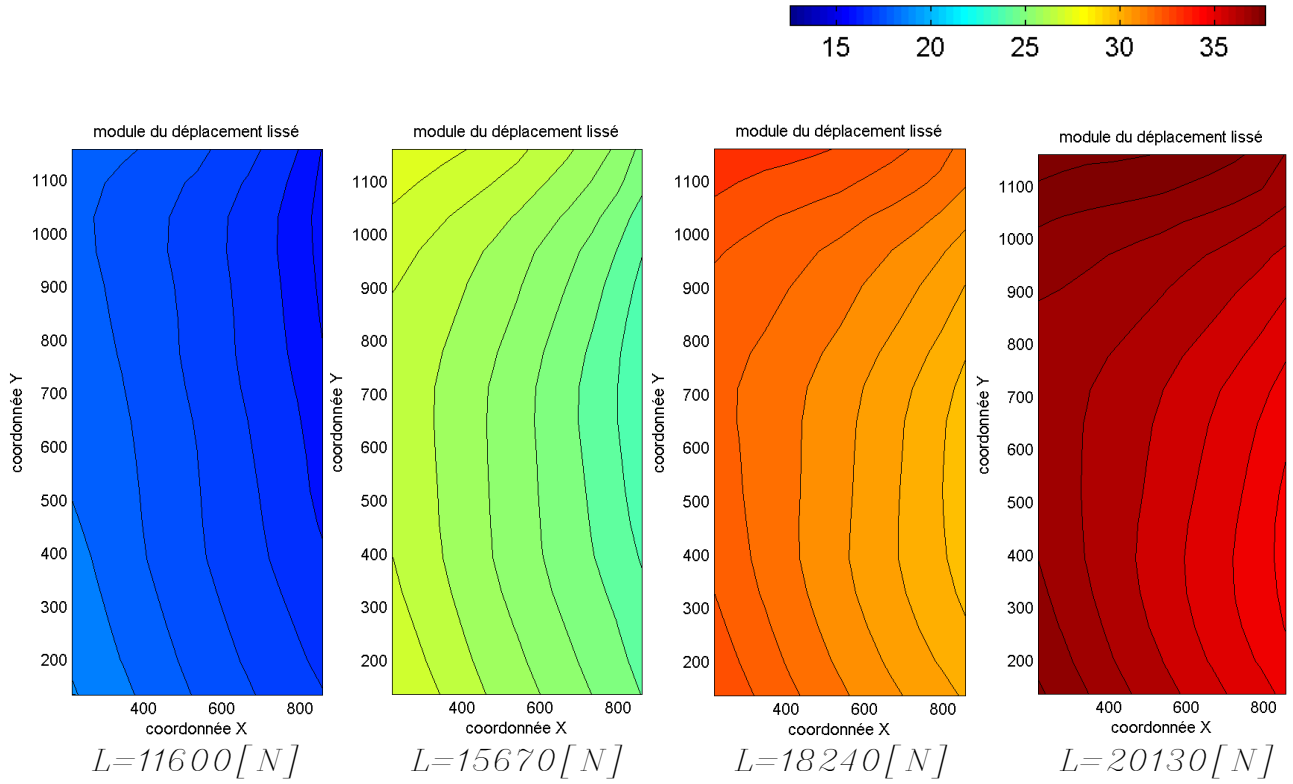

DIC _ Strain ε_{yy} (after "lissage")

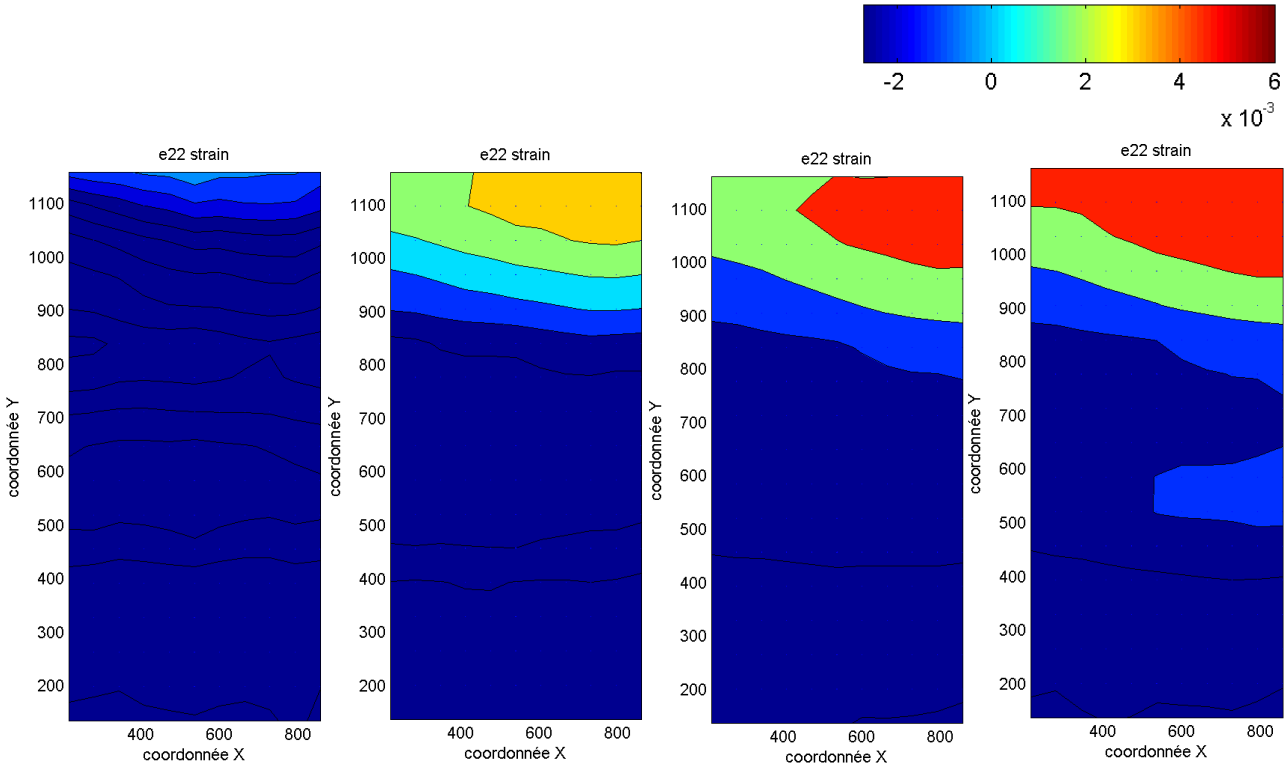

L=11600[N] *L=15670[N]* *L=18240[N]* *L=20130[N]*

DIC _ Strain ε_{xx} (after "lissage")

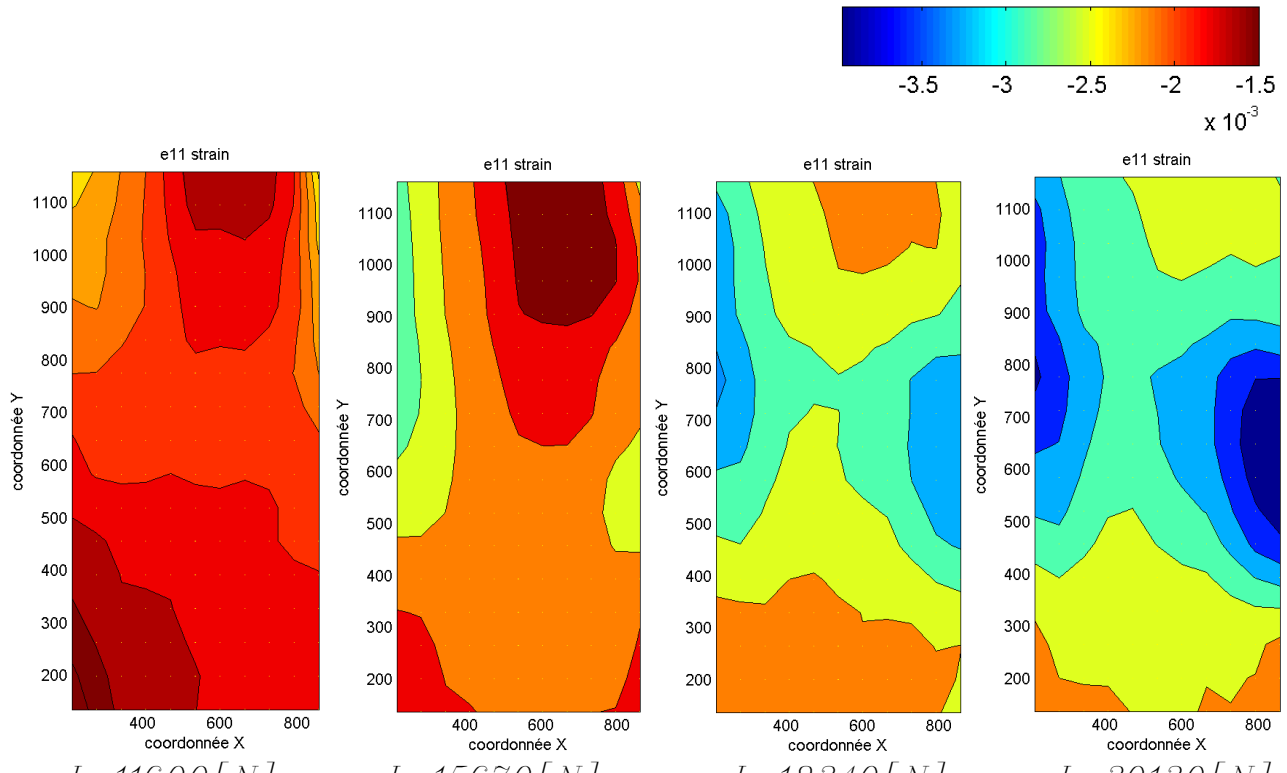

L=11600[N] *L=15670[N]* *L=18240[N]* *L=20130[N]*

4.2.6 - Series T3_25_V

The curves that describe the tests T3_25_V are shown in *fig 4.rr*. The graphs U-L underline the achievement of high maximal peaks and a successive failure. The anchor loading phases, defined by stroke DE of fig. *4.a*, occurred only two times. Two experiments of the series has been invalidated because a technical problem in the lock steel apparatus occurred.

The average peaks P1 and P2 are respectively 9,67 kN and 23,01 kN. The average maximal peak is the 86,15 % more higher than that of the series T0. The peaks P3 registered during the tests T3_25_V_3 and T3_25_V_6 are respectively 18,77 kN and 16,71 kN.

It is interesting to note that the stroke slopes AB of the test curve T3_25_V is approximately equal to that of series T0. As well shown in *figure 4.ss* the stiffness of the reinforced system T3_25_V is approximately equal to that of T0. The master curve realized for the series T3 neglected the of anchor loading phase, occurred only two times.

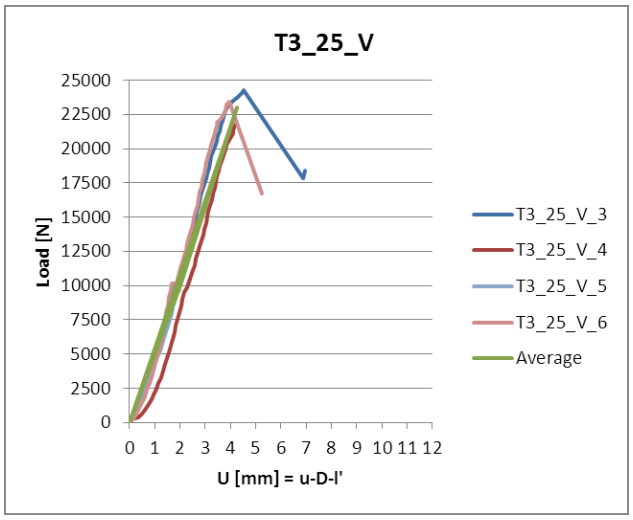

fig. 4.rr - The curves U-L registered during test of series T3_40_V

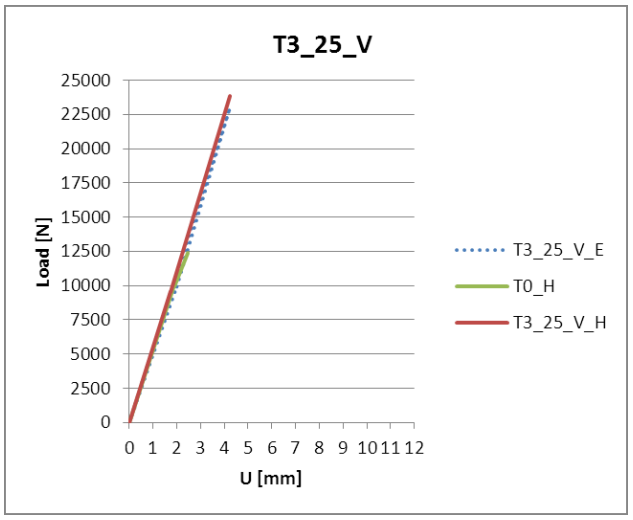

fig. 4.ss - The master curve of specimens T3_40_V compared with that of T0; in dotted the experimental master curve, in red the MC

The energy dissipated during the tests are described by the bar graphs of *figure 4.tt*. The average value of energy necessary to achieve the maximal peak ($\Delta\Gamma_1+\Delta\Gamma_2$) is equal to 47,50 J. This value is the 153% more higher than that registered during the T0 series. A representation of the dissipated energy is presented in *fig. 4.tt*.

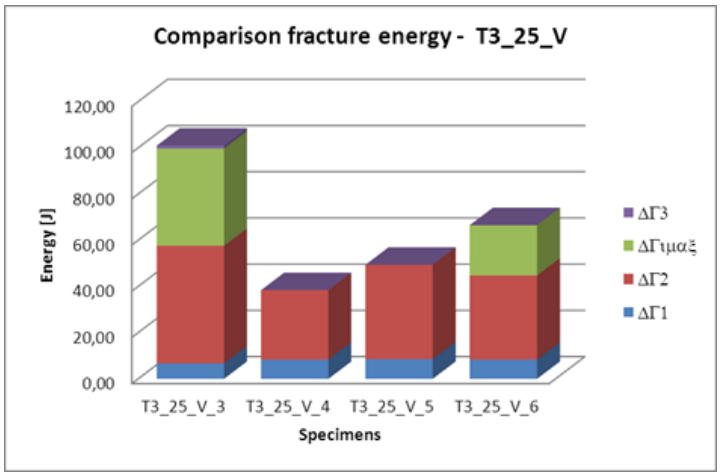

fig. 4.tt - The energy dissipated during the tests of series T3_40_V

The *table 4.XII* collects all the numerical values of peaks and energy.

	U_1	P_1 [kN]	$\Delta\Gamma_1$ [J]	U_2	P_2 [kN]	$\Delta\Gamma_2$ [J]	Γ_{imax_1}	U_3	P_3	$\Delta\Gamma_3$ [J]	$\Delta\Gamma_{End}$[J]
T3_25_V_3	1,63	9,06	6,69	4,52	24,29	50,87	42,11	6,95	18,39	1,25	58,81
T3_25_V_4	2,28	9,85	8,32	4,17	21,73	30,08					38,40
T3_25_V_5	1,94	9,63	8,48	4,37	22,58	40,87					49,36
T3_25_V_6	1,87	10,13	8,29	3,95	23,42	36,41	21,79	5,26	16,71	0,01	44,71
average	1,93	9,67	7,95	4,25	23,01	39,56					51,76

tab. 4.XII - Peaks and energy registered during the tests of series T3_40_V

The failure modes registered during this series are shown in *figure 4.uu* and defined in *table 4.XIII*. Two specimens failed with the development of a cohesive fracture between the sheet and the support after the achievement of P2, and with a brittle prismatic failure after a short anchor loading phase. The remaining samples, reached the P_2, failed with a brittle prismatic failure.




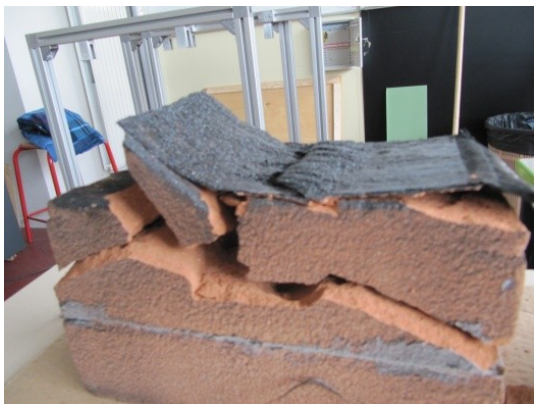

fig. 4.uu - The samples of series T0 after the test (in order T3_40_V_3, T3_40_V_4, T3_40_V_5, T3_40_V_6)

Specimen	*Fracture in C*	*Fracture in E*
T3_25_V_1	*1	
T3_25_V_2	*2	
T3_25_V_3	CF	PF
T3_25_V_4	PF	-
T3_25_V_5	PF	-
T3_25_V_6	CF	PF

tab. 4.XIII - The failure modes of specimens T3_40_V

The DIC shown that during the test the deformed zone moves from the loaded to the unloaded side. The anchor allows to a concentration of stress and deformation in the surface within the fan and the loaded side. In the *par.4.2.5.1 4.2.4.1* a results sheet shown the displacement and strain field obtained in the indicative case of specimen T3_25_V_.

4.3 Discussion about the global results

The results analyze of each test has permitted to define the representative values (P_1, P_2, $\Delta\Gamma$…) of each series. As shown in the graphs U-L presented above, almost all the specimens belonged to the same group have a similar behavior. The exceptions registered are correlated to several main causes: 1) the mechanical property of each firebrick (par. 2.2.2.1.1), 2) the imperfect alignment of the specimen in the test apparatus due to the geometrical imperfection of each firebrick. 3) the amount of epoxy resin used in the manufacturing process. The characterization study executed in Florence shown that the main value of compressive strength of the fire brick have a coefficient of variation that range between 5,13% and 9,02%. Since the cohesive fracture occurred inside the support the mechanical features of the brick influence the results. When the surfaces of the specimen in contact with the steel lock are characterized by imperfections is possible that the correct alignment of the sample is impossible to achieve. In this case a load peeling component could be developed easing the premature debonding of anchor splay from the support. It is probably that all the specimens presented a mixed failure had been subjected to peeling. Since the failure of the system sheet-anchor occurs frequently with a simple debonding (DSA), the amount of epoxy resin utilized to bond the anchor fan to the CFRP sheet influence the value of peak P_3 and the correlate modality of failure.

A geometrical average of the test results has been utilized to define one representative Master Curve (MC) for each series. This last permits to make the comparison between the different specimen's configurations. The graph U-L of *figure 4.m* groups the master curve calculated of all the series.

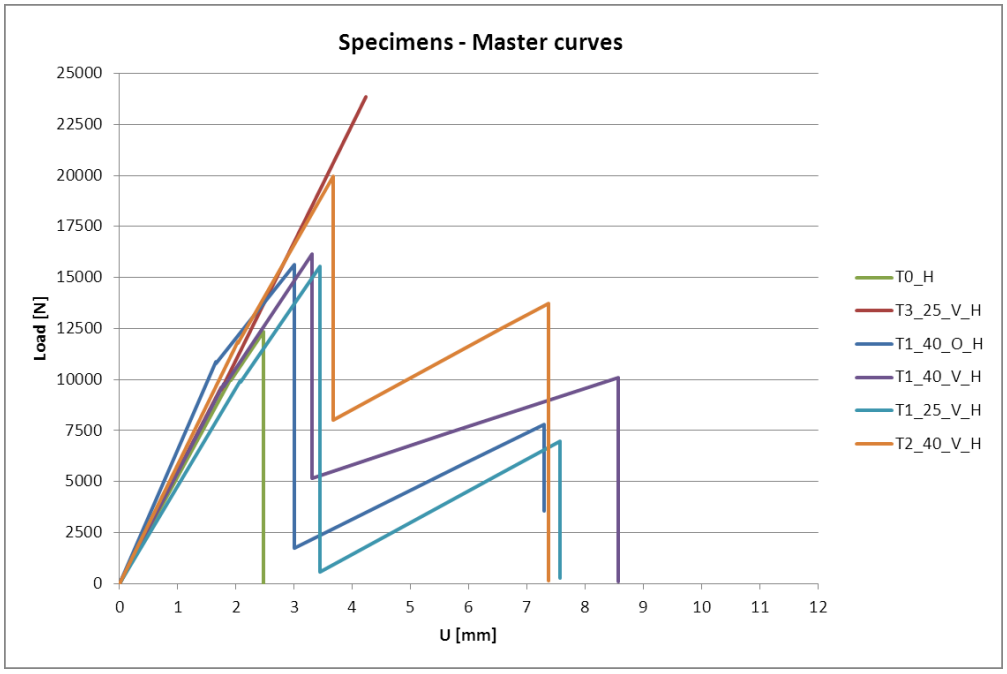

fig. 4.vv - The comparison between the master curve of the six series.

Analising the curves of fig. 4.mm it is possible to observe that:

1) All the series characterized by the application of one or more fiber anchor have an average peak load bigger than that of series T0.
2) The specimen fastened with anchors have a residual resistance.
3) The stiffness of the specimen without anchor is approximately equal to that of the samples with one or more anchors. This is shown by the stroke slopes of the first part of the curves.

The average value of the peak P_1 is shown in *fig. 4.ww*. This value is correlated to the apparition of the first crack in the fire brick. The results shown an almost uniformly behavior of the different series tested.

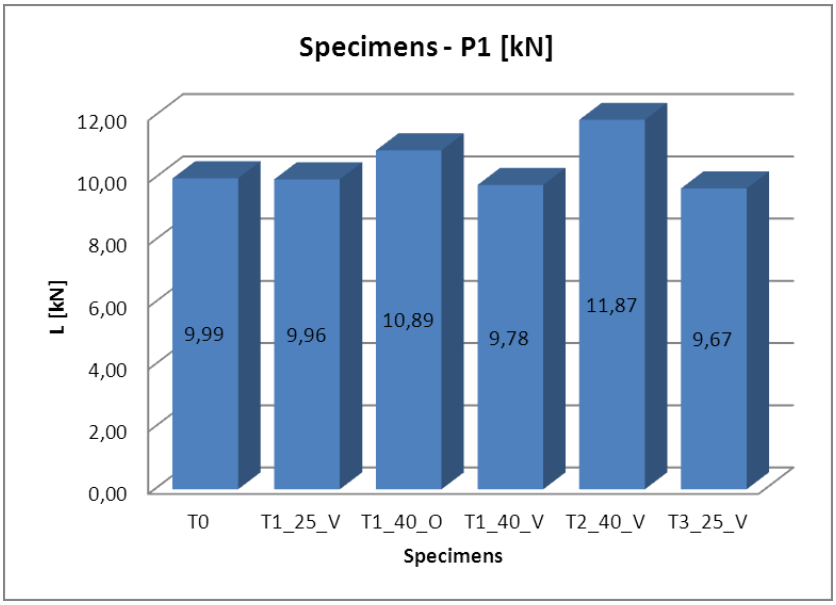

fig. 4.ww - The average peak P1 registered in the different series

The bar graph of figure 4.xx presents the average values of P_2. This last is the load registered at the end of the crack advancement phase. The tests executed shown that the maximum load achieved is linked to the number of anchors. The typology of anchor splay not affect the value of P2; in fact the bars that represented the peak load of specimen T1_25_V, T1_40_O and T1_40_V have the same value. Therefore the experiments underline that the crack advancement is influenced by the number of anchor dowel fastened inside the fire brick. In this context, the "nail" diameter and the amount of fiber used to realize the anchor have a central role.

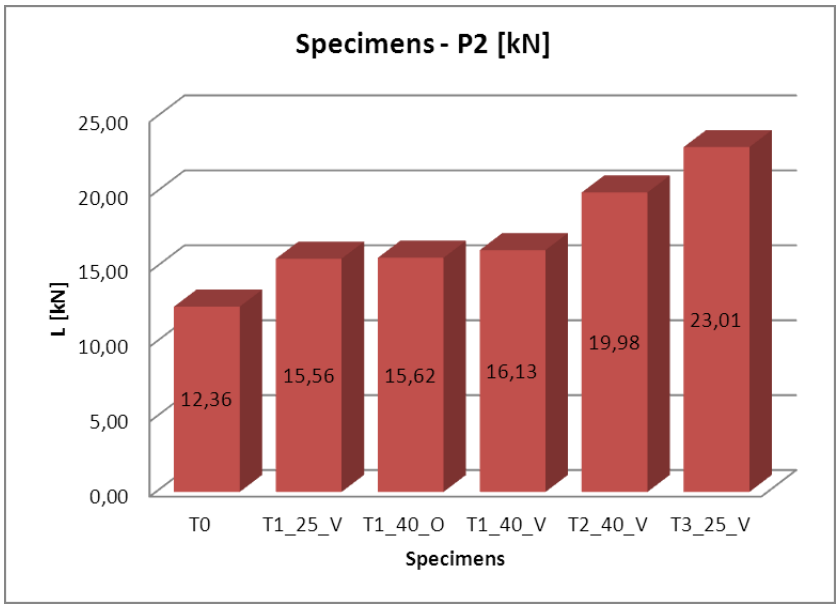

fig. 4.xx - The average peak P2 registered in the different series

The rate of the maximal load increase has been obtained comparing each series of specimen fastened with the reference series T0 (tab. 4.XIV). It is interesting to underline that the percentage increase almost linearly with anchor number (+ 30% each step).

	$P2_{average}$	
T0	**12,36**	**[kN]**
T1_25_V	+ 25,91	%
T1_40_O	+ 26,39	%
T1_40_V	+ 30,54	%
T2_40_V	+ 61,65	%
T3_25_V	**+ 86,15**	**%**

tab. 4.XIV - The % of increase of the maximum load P2

The peak P3 has been registered for almost all the tests of the series T1_25_V, T1_4O_O and T1_40_V. In those experiments the failure of the system CFRP sheet – fiber anchor has occurred with an adhesive debonding. The peak P3 is registered also in 4 experiment of the series T2_40_V. In three of these the failure is not linked to the detachment of the fan anchor but to a prismatic failure. The peak P3 registered during two of 6 tests T3_25_V have been not considered in this study. The value of the average peaks P3 are shown in *fig. 4.yy*.

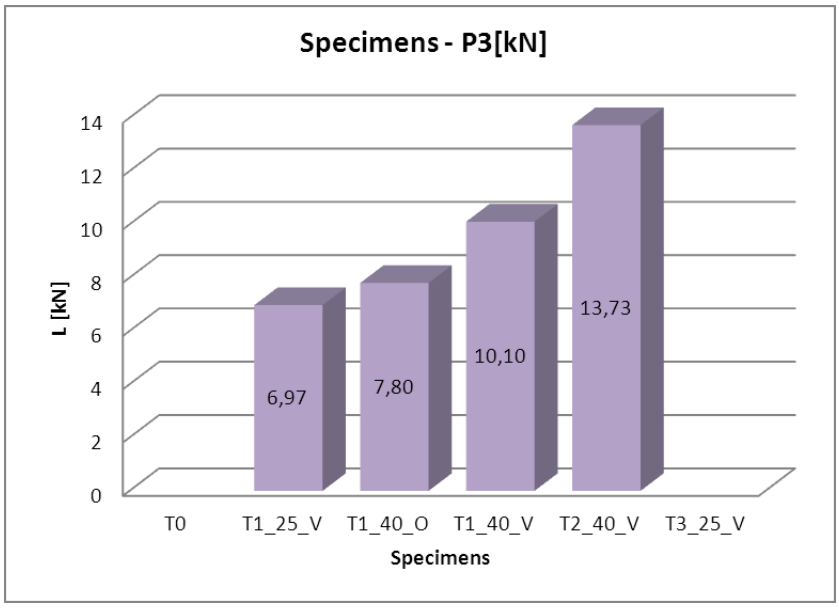

fig. 4.yy - *The average peak P_3 registered in the different series*

Between the series T1, the specimens of T1_40_V are the most ductile. It is important underline that the average value of P3 of the series T2_40_V is higher than the P_2 of series T0.

The dissipated energy has been calculated to measure the ductility of the different reinforced system. The Γ_{END} average values of the different series have been compared with the Γ_{end} of the T0 (*tab. 4.XV*). The increment of dissipated energy is considerable; it's range between + 86,11 % (series T1_25_V) and +175,78 % (series T3_25_V). The high ductility of the series T1_40_V is confirmed by a big amount of Γ_{END}.

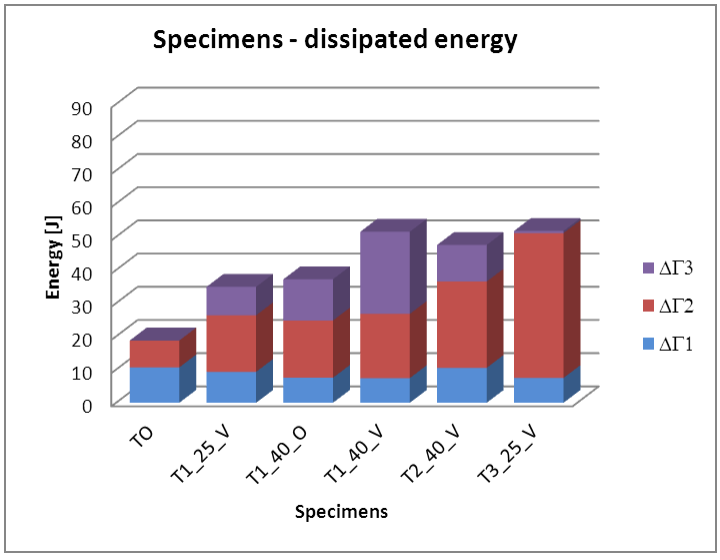

	$\Gamma_{end\_average}$	
T0	**18,77**	**[J]**
T1_25_V	+ 86,11	%
T1_40_O	+ 98,32	%
T1_40_V	+ 174,55	%
T2_40_V	+ 153,33	%
T3_25_V	+ 175,78	%

fig. 4.XV - The graphs and the % of increase of the dissipated energy Γ_{end}

Chapter 5

Conclusions and perspectives

5 Conclusions

This chapter collects the conclusions made after the analyses of the experimental results. The preliminary questions that have encouraged this thesis work have found some responses. These last are relative to the NES single shear tests executed and, at the same time, permit to have a general idea of the fiber anchors potentialities when the CFRP "nail" are applied to support different to concrete. Specifically this thesis research represent a first step of a numerical and experimental study on CFRP to masonry bonded joint fastened with carbon anchors.

The experimental analyzes shown that the CFRP anchors applied onto a CFRP to support bonded joint permit to achieve two main advantages:

1) The increase of the maximal load peak
2) The attribution of a resistance post peak, and therefore, the increase of the ductility of the reinforced system.

The series of reference used to measure the increase of resistance is the T0 one. The specimens of this last, subjected to a Near End Single Shear test, fail in a brittle manner reached the peak P_2. The average value of P_{2T0} registered during the T_0 tests is 12,36 kN. The average of energy dissipated to achieve this maximum load is 18,77 J.

The experimental analyze proves that the application of fiber anchors generate a considerable enhancement of the maximal peak P_2. The maximal loads registered in each series permit to conclude that the increment of the P_2 range between +26% and +86% (these limits are average values corresponding to series T1_25_V and T3_25_V).

Fifteen out of eighteen tests executed on specimens fastened by only one anchor, shown a reserve of resistance after the achievement of P_2. A further loading phase has been registered until the achievement of a peak P_3. The average values of P_3 of the series T1_25_V, T1_40_O and T1_40_V are respectively equal to the 56%, 63% and 81% of the P_{2T0}. The characteristic failure observed in P3 during these series is a debonding between the anchor fan and the CFRP sheet. The specimens with more than one nail have a different characteristic behavior. The series T2_40_V shown a reserve post peak during four tests; only one time the failure registered in P_3 is a DSA, in the others three experiments the CFRP sheet remains attached with the anchor to the support and the failure occurred inside the fire brick by a prismatic fracture. The average value of P_3 achieved after the PF

is equal to the 110% of the P_{2T0}. In the series T3_25_V no specimen fail by a debonding of splay anchor. The two specimen that are characterized by a post peak reserve fail by a prismatic fracture after the achievement of peak P_3. The average of P3 measured in the tests T3 is equal to the 148% of the P_{2T0}. Therefore the experimental tests shown that when the anchors are more than one, disposed and designed in the geometrical configurations of series T2_40_V and T3_25_V, the reinforced system fail because the firebrick fail; the CFRP remain attached to the anchor and, consequently, also to the support.

In the experimental study the highest value of P_2 has been obtained for the specimens of series T3_25_V, however the tests shown that this configuration of reinforce is frequently exposed to a brittle failure. The tests prove that the series T2_40_V ensures high performances and a lower probability of brittle failure. It's interesting to underline that the value of P_3 reached by the specimens with two anchors is bigger than P_{2T0}.

Within the test configurations with one nail the most efficient is the series T1_40_V because it is characterized by the longest ductile phases (the bigger value of $\Delta\Gamma_3$) and the highest value of P_3.

The displacement and strain fields onto the surface reinforced of the specimens have been defined using the Digital Image Correlation (DIC). This method, for the first time used to study the CFRP reinforcement fastened with anchors, has led to a description clear and accurate of the "strain transfer zone" during the tests. The DIC shown that this last moves from the loaded to the unloaded side in agreement with the literature studies realized by strain gouges. Using the Digital image Correlation also the anchor fan surface and his closer zone have been studied. A concentration of strain have been observed in the neighborhood of the splay anchor.

The efficiency of the different configuration has been measured analyzing the dissipated energy. This parameter has permitted to better determinate a most important property of the specimens: the ductility acquired by the CFRP reinforced system when one or more anchors are fastened.

The research presented in this thesis lay the ground work for a study of the CFRP to masonry bonded joint fastened by fiber anchors. The second step of the research provides the realization of NES single shear tests on pillars, composed by fire bricks and mortar. The specimen will be reinforced bonding a CFRP sheet onto a surface and applying the anchors reproducing the configuration T2_40_V and T1_40_V. The study will be carry out using the same methodology and the same steel apparatus projected and realized in this research work. The successive step will be the realization of the flexural tests on masonry reinforced walls.

The experimental analysis will be executed in parallel with a numerical analysis. This last will be based to the damage mechanics; indeed it permit to study the development of the cohesive fracture in the continuum using several internal variables.

Bibliography

[1] CNR-DT 200/2004, "*Istruzioni per la Progettazione, l'Esecuzione ed il Controllo di Interventi di Consolidamento Statico mediante l'utilizzo di Compositi Fibrorinforzati-Materiali,strutture in c.a. e in c.a.p., strutture murarie*", Versione Sottoposta ad Inchiesta Pubblica, Roma-CNR 13 luglio 2004.

[2] Morphy R. D., "Behaviour of fibre reinforced polymer (FRP) stirrups as shear reinforcement for concrete structures", Thesis, University of Manitoba, 1999

[3] Liberatore D., Gambarotta L., Beolchini G.C., Binda L., Magenes G., Cocina S., Lo Giudice E., Scuderi S., "*Tipologie edilizie in muratura del comune di catania*", estratto dal sito dell'istituto di I.N.G.V.

[4] D.M. 14 gennaio 2008, "*Norme Tecniche per le costruzioni", Cap. 11 "materiali e prodotti per uso strutturale", January 2008*

[5] Chen J.F., Teng J.G., *"Anchorage strength models for FRP and steel plates bonded to concrete"*, Journal of structural engineering, luglio 2001

[6] Yao J., Teng J.G., Chen J.F., "*Experimental study on FRP-to-concrete bonded joints*", Composites: Part B 36 (2005) 99-113

[7] Jongsma J. E., "*Etude de Structures Adhésives de Polymères en Couches Minces*", Thèse de doctorat, Ecole Doctoral « Mécanique, Thermique et Génie Civil » de Nantes, Année 2008

[8] Cottone A., Giambanco G., "*Minimum bond length and size effects in FRP-substrate bonded joints*", Engineering fracture mechanism, May 2009

[9] Fedele R., Milani G., "*A numerical insight into the response of masonry reinforced by FRP strips. The case of perfect adhesion*", Composite Structures, March 2010

[10] Briccoli Bati S., Fagone M., "*An analysis of CFRP-brick bonded joints*", XVIII Conference of the Italian Group of Computational Mechanics (GIMC) – Siracusa 22-24 September 2010

[11] S. Briccoli Bati, M. Fagone "*Caratterizzazione della modalità di rottura di elementi in laterizio fibrorinforzati: test sperimentali e simulazioni numeriche*". Conference "Materiali e Metodi innovativi nell'Ingegneria Strutturale", Catania 4-6 July 2007

[12] Capozzucca R., "*Experimental FRP/SRP-historic masonry delamination*", Journal of Composite Structures - 92 (2010)

[13] Giacquinta C., "Analisi sperimentale sotto carichi ciclici di pannelli murari rinforzati in CFRP", Phd thesis, University of Catania (Italy), december 2005

[14] Milani G., "*3D FE limit analysis model for multi-layer masonry structures reinforced with FRP strip*", International Journal of Mechanical Sciences 52 (2010), 784-803

[15] Ha Lee J., Lopez M. M., Bakis C. E., "Slip effects in reinforced concrete beams with mechanically fastened FRP strip", Cement & Concrete Composites, April 2009, pagg. 496-504

[16] Martin J. A., Lamanna A. J., «*Performance of mechanically fastened FRP strengthened concrete beams in flexure*», Journal of composites for construction ASCE, Maggio/Giugno 2008

[17] Bramblett, R. M. "Flexural Strenghtening of reinforced concrete beam using carbon fiber reinforced composites", Master of Sciences thesis, The University of Texas at Austin, 2000

[18] Orton, S. L., Jirsa, O. J., Bayrak, O. (2008). "Design considerations of carbon fiber anchors." J. Compos. Constr. November/December 2008, 608-616

[19] Le Tuan Pham, « Development of a quality control test for Carbon Fiber Reinforced Polymer Anchors » Thesis of master of Sciences in Engineering, University of Texas at Austin, May 2009

[20] Niemitz C.W., « Anchorage of carbon fiber reinforced polymers to reinforced concrete in shear application », thesis of master of Science, University of Massachusetts, February 2008

[21] H.W. Zhang, S.T. Smith, S.J. Kim: "Optimisation of carbon and glass FRP anchor design", Construction and Building Materials, article in press (2011)

[22] American Concrete Institute (ACI). (2002). "Guide for design and construction of externally bonded FRP systems for strengthening concrete structures" ACI 440.2R-02, Farmington Hills, Mich

[23] S. T. Smith, S. Hu, S.J. Kim, R. Seracino, "*FRP-strengthened RC slabs anchored with FRP anchors*", Engineering Structures 33 (2011) 1075-1087

[24] BASF Construction Chemicals Italia SPA, technical sheet "MBrace Primer: Primer a base epossipoliamminica del sistema MBrace FRP (Fiber Reinforced Polymer)", December 2009

[25] BASF Construction Chemicals Italia SPA, technical sheet "MBrace Adesivo: adesivo a base epossidica del sistema MBrace FRP (Fiber Reinforced Polymer)", January 2011

[26] BASF Construction Chemicals Italia SPA, technical sheet "MBrace fibre CFRP: rinforzo fibroso unidirezionale in fibra di carbonio del sistema MBrace FRP (Fiber Reinforced Polymer)", June 2009

[27] BASF Construction Chemicals Italia SPA, technical sheet "*MBrace fibre: rinforzo fibroso a base di tessuti unidirezionali in fibra di carbonio, aramide e vetro del sistema MBrace FRP (Fiber Reinforced Polymer)*", December 2009

[28] OTUA (Office technique pour l'utilisation de l'acier) « *Dossier technique OTUA* »; internet web link *www.otua.org/Prop_Physiques/FicheOTUA/OTUA1.html*

[29] Henan BEBON international, internet web link *www.steel-plate-sheet.com*

[30] Sikadur

[31] Chevalier L. "Mécanique des systèmes et des milieu déformables: course, exercise et problèmes corrigès", Ediption Ellipses

[32] Peters W.H., Ranson W.F., 1981. "*Digital image techniques in experimental stress analysis"* Opt. Eng. 21, 427–441.

[33] Chu T.C., Ranson W.F., Sutton M.A., Petters W.H., 1985. "Applications of digital-image-correlation techniques to experimental mechanics". Exp. Mech. 3 (25), 232–244.

[34] Hild F., Roux S., Guerrero N., Marante M. E., Flòrez-Lòpez J. "*Calibration of constitutive models of steel beams subject to local buckling by using digital image correlation*", Europeab Journal of Mechanics A/Solids 30 (2011) 1-10

[35] Hild F., Périé J.N., Coret M., 1999. « *Mesure de champs de déplacements 2D par intercorrélation d'images : CORRELI^{2D}* », Internal report 230, LMT-Cachan

[36] Chevalier L., Calloch S., Hild F., Marco Y., "*Digital image correlation used to analyze the multiaxial behavior of rubber-like materials*" Eur. J. Mech. A/Solids 20 (2001) 169-187

[37] Hild F., "CORRELI^{LMT}: a software for displacement field measurement by digital image correlation" Rapport interne n°254 LMT-CACHAN, January 2002

[38] Besnard G., Hild F., Roux S., "*Finite-element" displacement fields analysis from digital images: application to Portevin-Le Chatelier bands*", ?

[39] Hild F., Roux S., "Digital image correlation: from displacement measurement to identification of elastic properties – a review", Strain [in press] 2006

[40] Corr D., Accardi M., Graham-Brady L., Shah S., "Digital image correlation analysis of interfacial debonding properties and fracture behavior in concrete", Engineering Fracture Mechanics 74 (2007) 109-121

[41] Carloni C. , K. V. Subramaniam, "Direct determination of cohesive stress transfer during debonding of FRP from concrete", Composite Structures 93 (2010) 184-192

[42] Carloni C., Subramaniam K. V., Savoia M., Mazzotti C. "Experimental determination of FRP-concrete cohesive interface properties under fatigue loading", Composite Structures 94 (2012) 1288-1296

[43] Ali-Ahmad M., Subramaniam K. V., Ghosn M. *"Experimental investigation and fracture analys of debonding between concrete and FRP*", J Eng Mech, ASCE 2006; 132 (9): 914-23

[44] W. S. Boyle, G. E. Smith (April 1970). "Charge Coupled Semiconductor Devices". Bell Sys. Tech. J. 49 (4): 587–593

[45] P. Martinez, A. Klotz, "*A practical guide to CCD astronomy*", Cambridge University Press, 1998

[46] http://www.matbase.com/material/polymers/elastomers/styrenebutadiene-rubber/properties